Universitat Politècnica de València
Departamento de Máquinas y Motores Térmicos

RADIATION HEAT TRANSFER IN DIRECT-INJECTION DIESEL ENGINES

Doctoral Thesis
Presented by:
David Villalta Lara
Directed by:
Dr. Antonio García Martínez

Valencia, November 2018

Doctoral Thesis

RADIATION HEAT TRANSFER IN DIRECT-INJECTION DIESEL ENGINES

Presented by: David Villalta Lara
Directed by: Dr. Antonio García Martínez

Examining Board:

President: Prof. José Vicente Pastor Soriano
Secretary: Prof. Octavio Armas Vergel
Examiner: Dr. Michele Bardi

Reviewing Board:

Dr. Francesco Concetto Pesce
Dr. Michele Bardi
Prof. Pedro A. Rodríguez Aumente

Valencia, November 2018

Abstract

In the last two decades engine research has been mainly focused on reducing pollutant emissions and increasing efficiency. These facts together with growing awareness about the impacts of climate change are leading to an increase in the importance of thermal efficiency over other criteria in the design of internal combustion engines (ICE). To achieve the objective, there are different strategies to apply. The heat transfer to the combustion chamber walls can be considered as one of the main sources of indicated efficiency diminution. In particular, in modern direct-injection diesel engines, the radiation emission from soot particles can constitute a significant component of the efficiency losses. In this context, the main objective of the thesis is framed: to contribute to the understanding of the radiation heat transfer in DI diesel combustion together with the improvement of the knowledge in the soot formation-oxidation processes. The work has been based on experimental results through the optical technique application in different types of engine and on simulated results from validated one-dimensional models.

In the first part of experimental results, the amount of energy lost to soot radiation relative to the input fuel chemical energy has been evaluated by means of the optoelectronic probe application (based on the 2-Color technique) in both an optical engine DI and a production 4-cylinder DI engine. In this study, the values of soot spectral intensity emitted have been obtained and later, the total radiation emitted by the soot particles in the whole spectrum.

As mentioned above, soot particles are the main responsible for the radiation heat transfer, in addition to one of the important concern in meeting emissions regulations. Soot emissions are the result of two competing processes: soot formation and soot oxidation. Mechanisms of soot formation are discussed extensively in the literature. However, there are deficiencies in the knowledge of soot oxidation. Therefore, the objective of this section has been to evaluate the impact of mixing process and bulk gas temperature on late-cycle soot oxidation process under real operating conditions.

Finally, based on the results and knowledge acquired, a model able to predict heat losses by radiation for a spray diesel has been developed. The model is based on three sub-models: spray model, which analyzes and characterizes the internal spray structure in terms of mixing and combustion process with temporal and spatial resolution. A soot model, in which the results have been justified according to soot formation and oxidation processes. The link of these two sub-models has been used to obtain the input values to the radiation model. The radiation model simulates the temporal evolution of the spectral intensity, and consequently, the total soot radiation losses from the simulated soot concentration results as well as the spatial temperature distribution.

Resumen

En las últimas décadas, la investigación en motores de combustión ha estado enfocada fundamentalmente en la reducción de las emisiones contaminantes y la eficiencia de los mismos. Estos hechos junto con un aumento de la concienciación sobre el cambio climático han llevado a un aumento en la importancia de la eficiencia térmica respecto a otros criterios en el diseño de motores de combustión interna (MCIA). Para alcanzar este objetivo, existen diferentes estrategias a aplicar. En concreto, la transferencia de calor a las paredes de la cámara de combustión puede ser considerada como una de las principales fuentes de disminución de la eficiencia indicada. En particular, en los modernos motores diésel de inyección directa, la emisión de radiación de las partículas de hollín puede constituir un componente importante de las pérdidas de eficiencia. En este contexto se enmarca el objetivo principal de la tesis: contribuir a la comprensión de la transferencia de calor por radiación en la combustión diésel de inyección directa junto con la mejora del conocimiento en el proceso de formación-oxidación de hollín. El trabajo se ha basado tanto en resultados experimentales mediante la aplicación de técnicas ópticas en diversas tipologías de motor como en resultados simulados a partir de modelos unidimensionales validados.

En la primera parte de resultados experimentales, se ha evaluado la cantidad de energía por radiación respecto a la energía química del combustible mediante la aplicación de una sonda optoelectrónica (basada en la técnica del 2-Colores) tanto en un motor óptico DI como en motor policilíndrico DI de producción. En este estudio se han obtenido valores de intensidad espectral emitida por el hollín y posteriormente, la radiación total emitida por las partículas de hollín en todo el espectro.

Como se ha citado anteriormente, las partículas de hollín son las principales responsables de la transferencia de calor por radiación, además de uno de los principales agentes contaminantes emitidos por los motores diésel. Las emisiones de hollín son el resultado de dos procesos antagonistas: la formación y oxidación del hollín. Los mecanismos de formación de hollín se

discuten extensamente en la literatura. Sin embargo, existen deficiencias en cuanto al conocimiento de la oxidación de hollín. Por lo tanto, el objetivo de esta sección ha sido evaluar el impacto del proceso de mezcla y la temperatura del gas sobre el proceso de oxidación de hollín durante la última parte de la combustión bajo condiciones reales de operación.

Finalmente, y en base a los resultados y conocimientos adquiridos hasta el momento, se ha desarrollado un modelo capaz de predecir las pérdidas de calor por radiación para un chorro diésel. El modelo está basado en tres sub-modelos: modelo de chorro, el cual analiza y caracteriza la estructura interna del chorro en términos de mezcla y combustión en un proceso de inyección con resolución temporal y espacial. Un modelo de hollín, en el que los resultados se justifican en función de procesos de formación y oxidación del hollín. La cohesión de estos dos sub-modelos se utiliza para obtener los valores de entrada al modelo de radiación. El modelo de radiación simula la evolución temporal de intensidad espectral, y consecuentemente, la perdida de radiación total emitida por las partículas de hollín a partir de los resultados simulados de concentración de hollín junto con la distribución espacial de la temperatura.

Resum

En els últims anys, la recerca en motors de combustió ha estat focalitzada principalment en la reducció de les emissions contaminants i la millora de la eficiència. Aquests fets afegits al fet del augment de la conscienciació del canvi climàtic han impulsat el interés per incrementar la eficiència tèrmica per damunt de altres criteris en el disseny de motors de combustió interna alternatius (MCIA). Per aconseguir aquest objectiu, existixen diferents estratègies a aplicar. Concretament, la transferència de calor a les parets de la càmera de combustió pot ser considerada un dels principals focs de reducció de eficiència indicada. En particular, en els moderns motors dièsel de injecció directa, la emissió de radiació de les partícules de sutja pot constituir un component important de les pèrdues de eficiència. En aquest context s'emmarca el objectiu principal de la tesis: contribuir a la comprensió de la transferència de calor per radiació en la combustió dièsel de injecció directa i la millora del coneixement del procés de formació-oxidació de la sutja. El treball esta basat tant en resultats experimentals mediant l'aplicació de tècniques òptiques en diverses tipologies de motor com en resultants simulats a partir de models unidimensionals validats.

En la primera part dels resultats experimentals, s'ha avaluat la quantitat de energia per radiació respecte a la energia química del combustible mediant la aplicació de una sonda optoelectrònica (basada en la tècnica del 2-Colors) tant en un motor òptic DI com en un motor poli-cilíndric DI de producció en serie. En aquest estudi s'han obtingut valors de intensitat espectral emesa per la sutja i posteriorment, la radiació total emesa per les partícules de sutja en tot el espectre.

Com s'ha citat amb anterioritat, les partícules de sutja son les principals responsables de la transferència de calor per radiació, a més de un del principals agents contaminants emès per els motors dièsel. Les emissions de sutja son el resultat de dos processos antagonistes: la formació i la oxidació de sutja. Els mecanismes de formació de sutja es discuteixen àmpliament en

la literatura. No obstant això, existeixen deficiències pel que fa al coneixement de l'oxidació de sutja. Per tant, l'objectiu d'aquesta secció ha sigut avaluar l'impacte del procés de mescla i la temperatura del gas sobre el procés d'oxidació de sutja durant l'última part de la combustió sota condicions reals d'operació.

Finalment, i en base als resultats i coneixements adquirits fins aquest moment, s'ha desenvolupat un model que permet predir les perdudes de calor però radiació per a un raig dièsel. El model esta basat en tres sub-models: model de raig, el qual analitza i caracteritza la estructura interna del raig en termes de mescla i combustió en un procés de injecció amb resolució temporal i espacial. Un model de sutja, en el qual els resultats es justifiquen en funció del procés de formació i oxidació de la sutja. La cohesió d'estos dos submodels s'utilitza per a obtindre els valors d'entrada al model de radiació. El model de radiació simula l'evolució temporal d'intensitat espectral, i conseqüentment, la perduda de radiació total emesa per les partícules de sutja a partir dels resultats simulats de concentració de sutja junt amb la distribució espacial de la temperatura.

A mis padres
A Elena

Agradecimientos - Acknowledgements

La realización de esta tesis no hubiera sido posible sin el apoyo y colaboración de muchas personas a las que me gustaría mostrar mis agradecimientos en las siguientes líneas.

En primer lugar, me gustaría agradecer al grupo directivo del departamento CMT-Motores Térmicos formado por *Francisco Payri* y *José María Desantes* por brindarme la oportunidad de unirme a su grupo de trabajo, así como facilitarme los mejores medios posibles para llevar a cabo la investigación. En particular, mostrar mi gratitud a *Jesús Benajes* por permitirme unirme al grupo de combustión.

En segundo lugar, me gustaría nombrar a la persona más importante para mí dentro de este departamento, mi amigo *Antonio García*. No solo me ha enseñado conocimientos y metodologías en el ámbito profesional, si no que me ha inculcado diferentes maneras de enfocar ciertos aspectos de la vida. El trabajo conjunto durante estos algo más de 4 años me ha hecho crecer científica y profesionalmente, creo que ha sido de gran calidad y gran parte del resultado ha sido gracias a su incansable persistencia y apoyo en todo momento. Me gustaría agradecerle todas las horas de despacho (que han sido muchísimas) en la que gracias a sus discursos y monólogos me ha dado fuerzas y ánimos para seguir adelante. Muchas gracias por todo *sheriff*.

Me gustaría expresar mi más sentido agradecimiento a todo el departamento de combustión con el que he convivido durante estos años, en especial a *José María García*, *Javier López*, *José Vicente Pastor*, *Jaime Martín*, *Raúl Payri* y *Pablo Olmeda* por sus consejos, ayuda encomiable y ante todo por hacerme la vida un poco más fácil durante este tiempo.

Mis agradecimientos también a mis compañeros de despacho *Javier Monsalve*, *Vicente Boronat* y *Rafael Lago* porque siempre habéis estado ahí cuando os he necesitado. Gracias por vuestras ideas y, sobre todo, por hacer cada jornada más amena. Y no puedo olvidarme de todos los compañeros con los que he colaborado a lo largo de este periodo: *Daniel Estepa*, *Eduardo*

Pérez, Mattia Pinotti, Carlos Micó, Darío Pintor y *Leo Pachano*. Vuestra ayuda ha sido clave en la realización de este trabajo. De entre ellos destacar a *Diego Blanco*, ya que además de su apoyo desinteresado, me llevo una gran amistad.

A continuación, mostrar mi gratitud a todo el grupo técnico, en especial a *Vicente Esteve, Daniel Lérida, Toni Peris* y *Gabriel Alcantarilla* por toda la ayuda recibida a lo largo de este periodo y por los buenos momentos pasados en las salas. Mencionar también a *José Yustas*, *Norma Molina*, *Jose Enrique del Rey*, *José Gálvez* y al departamento administrativo por abrirme la puerta de su despacho desinteresadamente cuando lo necesitaba.

I would like to express my gratitude to the Institute for Combustion Engines of the RWTH Aachen University for welcoming me in their laboratories and give me all the support during the internship. Especially, I sincerely appreciate the advice of *Dr. Benedikt Heuser* and *Mr. Marius Zubel* during my stay in Aachen.

Queda mi familia, a la que tengo que agradecer su apoyo incondicional. En especial, gracias a mis padres, *Ángel* y *Mari*, por haberme guiado y ayudado no solo en este período, sino durante todo el transcurso de mi vida. Mucho de lo que soy se lo debo a ellos. Y gracias también a *Elena*, quien ha sufrido de manera directa esta tesis. Gracias por tu paciencia, por tu apoyo, por tu compañía, por ayudarme a salir de los momentos más difíciles y por estar a mi lado celebrando las victorias. Muchas gracias. Te quiero.

Table of Contents

Index of Figures

Index of Tables

Nomenclature

Latin

ACT - Apparent Combustion Time

BMEP - Brake Mean Effective Pressure

CA50 - Crank Angle at 50% mass fraction burned

CAD - Crank angle degree

CI - Compression Ignition

CMOS - Complementary Metal Oxide Semiconductor

CO_2 - Carbon Dioxide

CRT - Continuous Regeneration Traps

DBI - Diffused Back-Illumination

DCN - Derived Cetane Number

DI - Direct-Injection

DPF - Diesel Particulate Filter

ECN - Engine Combustion Network

EGR - Exhaust Gases Recirculation

EoC - End of Combustion

EoI - End of Injection

ET - Energizing time

EVC - Exhaust Valve Close

EVO - Exhaust Valve Open

FSN - Filter Smoke Number

FWHM - Full Width at Half Maximum

GIE - Gross Indicated Efficiency

HCCI - Homogeneous Charge Compression Ignition

HDSI - High Speed Direct Injection

HPHT - high pressure and high temperature test chamber

HRL - Heat Release Law

HSIP - High Speed Imaging Pyrometer system

HT - Heat Transfer

ICE - Internal Combustion Engines

IVC - Inlet Valve Close

LHV - Lower Heating Value

LII - Laser Induced Incandescence

LOL - Lift-off length

LTC - Low Temperature Combustion

KL - Optical Thickness

NOx - Oxides de Nitrogen

O_2 - Oxygen

OP - Optoelectronic Probe

PID - Proportional, Integrative and Derivative

PM - Particulate matter

POC - Point of Combustion

POI - Point of Injection

PPC - Partially Premixed Combustion

RCCI - Reactivity Controlled Compression Ignition

RoHR - Rate of Heat Release

SCE - Single Cylinder Engine

SCR - Selective Reduction Catalysts

SI - Spark Ignition

SoC - Start of Combustion

SoI - Start of Injection

SR - Swirl Ratio

SY - Soot Yield

$t_{1/2}$ - Half-life time

t_r - residence time

TDC - Top Dead Center

TGV - Turbine Geometry Variable

Greck

α - Absorptivity Coefficient

ε - Emissivity

θ - Spray Cone Angle

σ - Scattering coefficient

λ - Wavelenght

μ - Viscosity

ρ - Density

ϕ - Equivalence Ratio

Ω - Solid Angle

Subscripts

a - relative to air

b - relative to black body

exh - relative to exhaust conditions

f - relative to fuel

in - relative to intake conditions

inj - relative to injection

O2 - relative to oxygen

rad - relative to radiation

soot - relative to soot

Chapter 1

Introduction

Content

1.1 Introduction

The objective of this first chapter has been split into two different parts:

- On the one hand, the historical framework and the technological context on which the research study has focused. A historical description of the internal combustion engines (ICE) has been presented, focused mainly on compression engines. Next, a discussion on the importance of ICE in different aspects such as the economy and the impact on the environment and the challenges that society must face in the near future.
- On the other hand, the general structure of the document has been presented, developing in detail the content of each of the different chapters, with the aim of providing a global view of the study.

1.2 Technological framework of the internal combustion engines

During the last century, the energy paradigm focused on the production of energy, such abundant quantity and good quality. It is clear that the main sources of energy have favored global economic growth and achieve the current quality of life. Much of the progress made in the fields of health, medicines, communications and food production is mainly due to the extensive use of energy sources.

In reference to the previous paragraph, Figure 1.1 shows the evolution of the values of energy consumption in Europe during the last 25 years, from 1990 to 2015 [1]. In addition, each graph is divided according to how the energy source was obtained. As it is possible to observe, the total consumption energy sustains small variations depending on the year

(maximum variations of 8%). However, it is possible to observe different trends depending on the source of energy production. In the case of solid fuels, it is observed that the energy consumption has decreased around 40% since 1990. Regarding electricity and renewable energy, these energy sources show an upward trend mainly up to the year 2005 promoted by subsidies of the European administration. Another important reduction in terms of energy supply is observed in the demand for oil. During the last 5 years, it has experienced a significant reduction below the levels reached during the 90's. Therefore, the most relevant conclusion of this evolution is that energy sources have been redistributed since it is possible to achieve the same level of energy consumption.

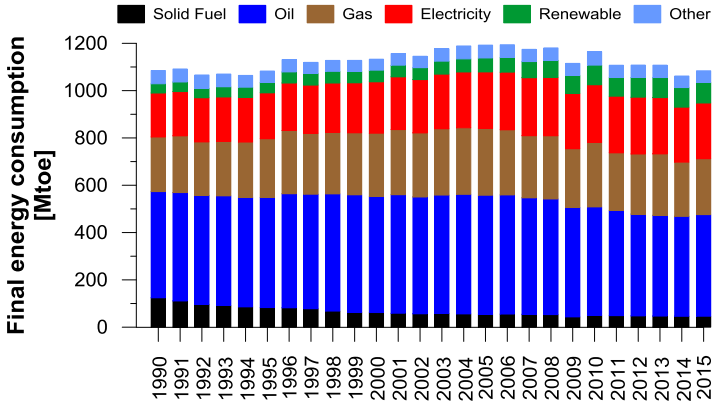

Figure 1.1. Evolution of final energy consumption by sources in Europe from 1990 up to 2005 [1].

Figure 1.2 shows the distribution of energy consumption by sector in Europe during 2015 [1]. According to the figure on the left, energy consumption in transport occupies 33% of the total energy consumed, being the sector with the highest energy consumption. Regarding the figure on the right, the distribution of 33% of the energy consumed by transport is shown. In this sense, the goods and people transport by road is clearly the most used mode of transport (82%). The second most used mode is air transport followed by rail and navigation, both with 3% in total. It can be considered

that most of the energy consumed in this sector comes from oil. In fact, compression ignition engines dominate road transport.

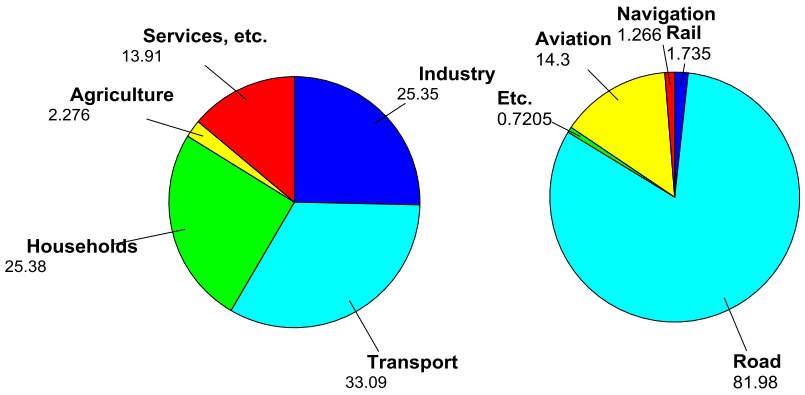

Figure 1.2. Left) Final energy consumption by sector in Europe in 2015 and Right) transport energy consumption in Europe in 2015 by modes in % [1].

One way or another, what is currently indisputable is that engines, whether gasoline or diesel, occupy an undeniable leadership position in terms of the propulsion of road vehicles.

The question is *why is the diesel engine the best option for this type of application?* Commercial success with respect to diesel engines has grown rapidly since the early 1990s to the present. In particular, the growth of this type of engine has increased by around 50% in the European Union [2], as shown in Figure 1.3. More than half of the vehicles dedicated to the goods and passengers transport, which have been sold in recent years in Europe, have been diesel engines [3][4].

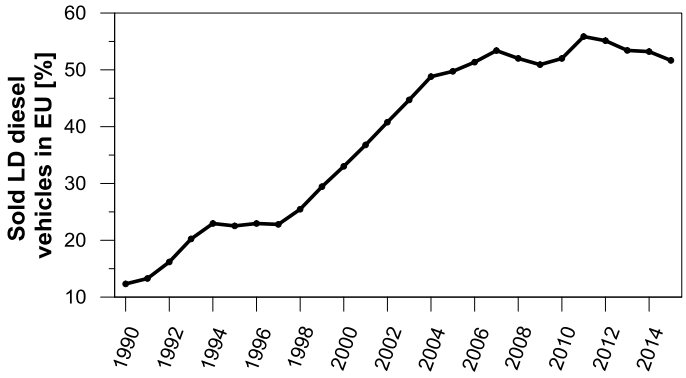

Figure 1.3. Evolution of the sold light duty diesel vehicles in Europe between 1990 and 2015.

Compared to other types of engines, the diesel engine produces a more useful torque per unit than the Otto engine or the gas turbine. In addition, diesel engines are more efficient, reliable and durable than other ICEs. In summary, the vehicles (mainly destined to the goods and passengers transport) equipped with diesel engines are the most economical to operate. In general, the success of diesel engines is due to the unique combination of low fuel consumption, high reliability and durability, and a competitive cost that makes the diesel engine especially attractive to the user.

However, despite the high efficiency of compression ignition engines, these are considered one of the main sources of environmental pollution. The main pollutants associated with their operation are described below:

- *Nitrogen oxides (NOx):* these emissions are mainly responsible for phenomena such as acid rain environment or photochemical smog. Nitrogen oxides are formed mainly by nitric oxide (NO) and nitrogen dioxide (NO_2), although a smaller proportion also includes nitrous oxide (N_2O). In addition, these pollutants can reduce the concentration of ozone in the stratosphere or produce respiratory illness [5]. The majority of NOx emissions are mainly due to the reaction produced between oxygen and

nitrogen at elevated temperatures, and it depends on the characteristics of the fuel and the air-fuel mixing process.

- *Particulate matter (PM)*: particulate matter is the name given to these solid and/or liquid particles, and are defined by their size. If the particles are more than 100 microns in size, they do not remain suspended in the air. Two grades of PM are regulated: PM10, which are "thick" particles between 10 and 2.5 microns in size. PM2.5 particles are "fine" particles of 2.5 microns or less and really small particles are known in various ways as "ultra-fine" or "nano" particles, but there is no universally recognized term for them [6]. The transport sector, monopolized by ICE, is responsible for 11% of particles with a diameter of 10 µm or less (PM10) and 16% of PM2.5 emitted into the atmosphere [7].
- *Carbon monoxide (CO)*: the CO molecule is an intermediate product of the oxidation process of a hydrocarbon. In internal combustion engines, the majority of CO emissions are due to the equivalence ratio: the leaner air-fuel mixing regions can not burn quickly and the very rich regions can not burn completely due to lack of oxygen. Carbon monoxide emissions are also higher in gasoline engines mainly due to the richer equivalence ratio during engine operating conditions.
- *Hydrocarbons (HC)*: hydrocarbons are the product of incomplete combustion of injected fuel due to the rich conditions and low temperatures that can be achieved locally inside the cylinder. Partially oxidized HC and unburned HC are generally included within this group. As in the case of carbon monoxide, HC emissions are less important than those of NOx and PM in diesel engines.

Despite their advantages, diesel engines generate intrinsically high levels of nitrogen oxides (NOx) and particulates, which are emitted into the atmosphere as a constituent part of the exhaust gases. However, diesel

engines emit very low amounts of CO and HC emissions under engine conditions, so these pollutants are not a problem for diesel engines.

During the 1940s, pollutants emissions emitted by engines became a social concern, as a result of the usual appearance of photochemical smog in important cities such as Los Angeles (California). For that, the first pollutant regulations applicable to the emissions of the engines appeared in the United States in 1974, establishing limits for the four main pollutants (NOx, PM, CO and HC). In the European Union, the emission limitation of the EURO I standard started in 1992 and regulated the emissions of these four pollutants.

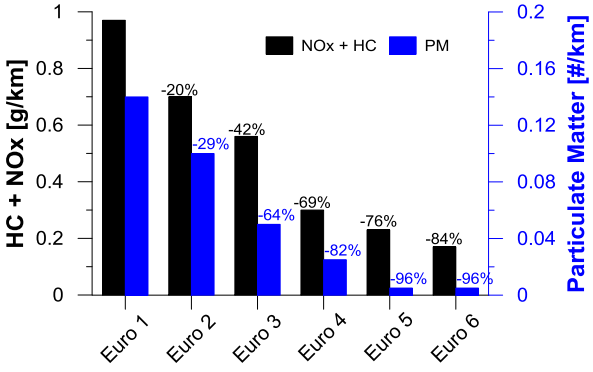

Figure 1.4. Evolution of the sold light duty diesel vehicles in Europe between 1990 and 2015.

Figure 1.4 shows the evolution of the EURO standard emission limitations applied in the European Union for NOx and PM (since these pollutants are the most representative emissions), for light duty diesel engines, evaluated in stationary conditions. As can be seen in this figure, governments have responded to the growing social concern about the problem of environmental pollution, imposing a gradual reduction of the permitted emission limits to extremely low levels. In particular, the maximum level of NOx emissions has been reduced by 84%, the PM by 96%.

In order to fulfill the European pollutant regulations, certain technologies have been developed to apply them to the engine and considerably reduce the pollutant emissions. These technological developments can be divided into two groups: active and passive solutions.

Regarding the *active solutions*, these strategies are applied in-cylinder engine to reduce polluting emissions. These solutions focus on the air management systems and the injection system, mainly to modify the combustion process. Regarding the solutions associated with the air management system, improvements in the performance of the turbocharger with fixed turbine, the turbine geometry variable (TGV), the use of coolers and, more recently, two-stage turbochargers. In addition, the management of exhaust gas recirculation (EGR) and its subsequent evolutions (EGR cooling, low pressure EGR), as well as the introduction of variable valve systems that increase the flexibility of the air management process. According to the solutions of the injection system, these include the increase of the injection pressure, the reduction of the nozzle diameter, the increase of the number of orifices and the strategies of multiple injections. With these solutions, the flexibility of the injection system is improved. It implies greater control of the air-fuel mixture process and, with it, the combustion process and emissions.

Regarding the *passive solutions*, the objective is to eliminate or reduce the concentration of pollutant particles, which have been generated inside the combustion chamber by means of the after-treatment devices. After-treatment devices have been placed in the exhaust line of the engine and can be classified according to the reduced pollutant. On the one hand, the particulate elements are eliminated by means of a particle filter (DPF) and continuous regeneration traps (CRT). On the other hand, selective reduction catalysts (SCR) and/or passive catalysts (DeNOx) reduce NOx emissions. The main drawbacks of these passive solutions are the increase in fuel consumption (regeneration of the filter and the total weight of the vehicle), and in the total cost due to the installation of additional technology and a greater maintenance service. Due to the fact that the after-treatment systems

are not an element of this work, it is possible to find several studies on the subject [8][9]], which are developed in the Máquinas y Motores Térmicos Department in the Universitat Politècnica de València.

Recently, new combustion concepts are being investigated with the aim of improving the NOx-soot *trade-off*, since this is the main disadvantage of diesel diffusion combustion. These new concepts are based on low temperature combustion (LTC) and are based mainly on the modification of the reactivity in the combustion chamber using low cetane content fuel (or fuel mixtures), dual fuel injection or the use of gasoline in a compression ignition engine. Derived from all these studies, new modes of combustion have appeared (HCCI [10], PCCI [11], RCCI [12], etc.) during the last five years. Although these new combustion concepts present important improvements, their implementation and development are still complicated. It is still necessary to continue with the research due to the need for a better basic knowledge (injection process, mixing, autoignition) and intrinsic problems, such as difficulty in ignition control, control of the combustion process and mechanical stress in high load conditions.

Considering the previously described, it seems reasonable to study different active strategies to improve the efficiency of diesel engines, as well as to keep the levels of polluting emissions below the values established by the standard emission regulations.

1.3 Approach and content of the document

The document is divided into seven chapters including the present introduction. Next, a brief summary of the contents of each chapter is presented:

I. **Introduction**: The first chapter aims to provide an overview of the entire document.

II. **Phenomenology of Late-cycle Soot Oxidation Process and its implication on Radiation for diesel diffusion**

combustion: The second chapter explains the structure of a diesel spray and the processes involved in it, such as atomization, evaporation, autoignition, etc. In addition, a review of the phenomena related to soot emissions has been presented, since it is one of the most important pollutant. Finally, the emission of radiation from the soot particles and their influence on the efficiency of combustion has been described. According to that, the objectives, justification and methodology of this investigation are defined.

III. **Experimental and theoretical tools**: The third chapter provides a complete description of the tools used to collect the information for this research work. The test facilities in which the experiments have been carried out, the optical techniques that have been used and the numerical models that have been used to analyze the combustion process and the evolution of the spray diesel have been described in detail.

IV. **Experimental study of the Radiation Heat transfer in diesel flames**: Following the objectives and approach of the study, the fourth chapter will present the results obtained from the heat transfer by radiation in the direct combustion of diesel. An in-depth analysis of the impact of different controlled thermodynamic conditions on the radiation in the combustion chamber of an optical DI engine will be carried out, as well as the evaluation of the amount of energy by radiation with respect to the chemical energy of the fuel in real operating conditions in a multi-cylinder production engine DI.

V. **Analysis of soot oxidation process in a production DI engine**: The fifth chapter focuses on the effects of different parameters of the engine in relation to soot oxidation process. For that, this chapter is divided into two result sections. In the first part, the objective is to evaluate the soot oxidation process by varying the parameters related to the air thermodynamic conditions and the injection process. In the second section, an

assessment of the swirl ratio and an appropiate injection strategy will be carried out to optimize the mixing controlled combustion process and finally, both strategies will be compared and the best option will be selected.

VI. **Soot Radiation Model in Diesel Flames**: Chapter 6 aims to develop a soot radiation model for diesel spray capable of predicting heat losses in the chamber walls due to radiation. For this, three sub-models have been implemented: spray model, soot model and radiation model.

VII. **Conclusions and Future work**: In the last chapter the results obtained have been summarized and the main conclusions of this work have been extracted. In addition, suggestions have been presented for future research work.

The line of argument followed to define and reach the objectives of this thesis is shown in Figure 1.5.

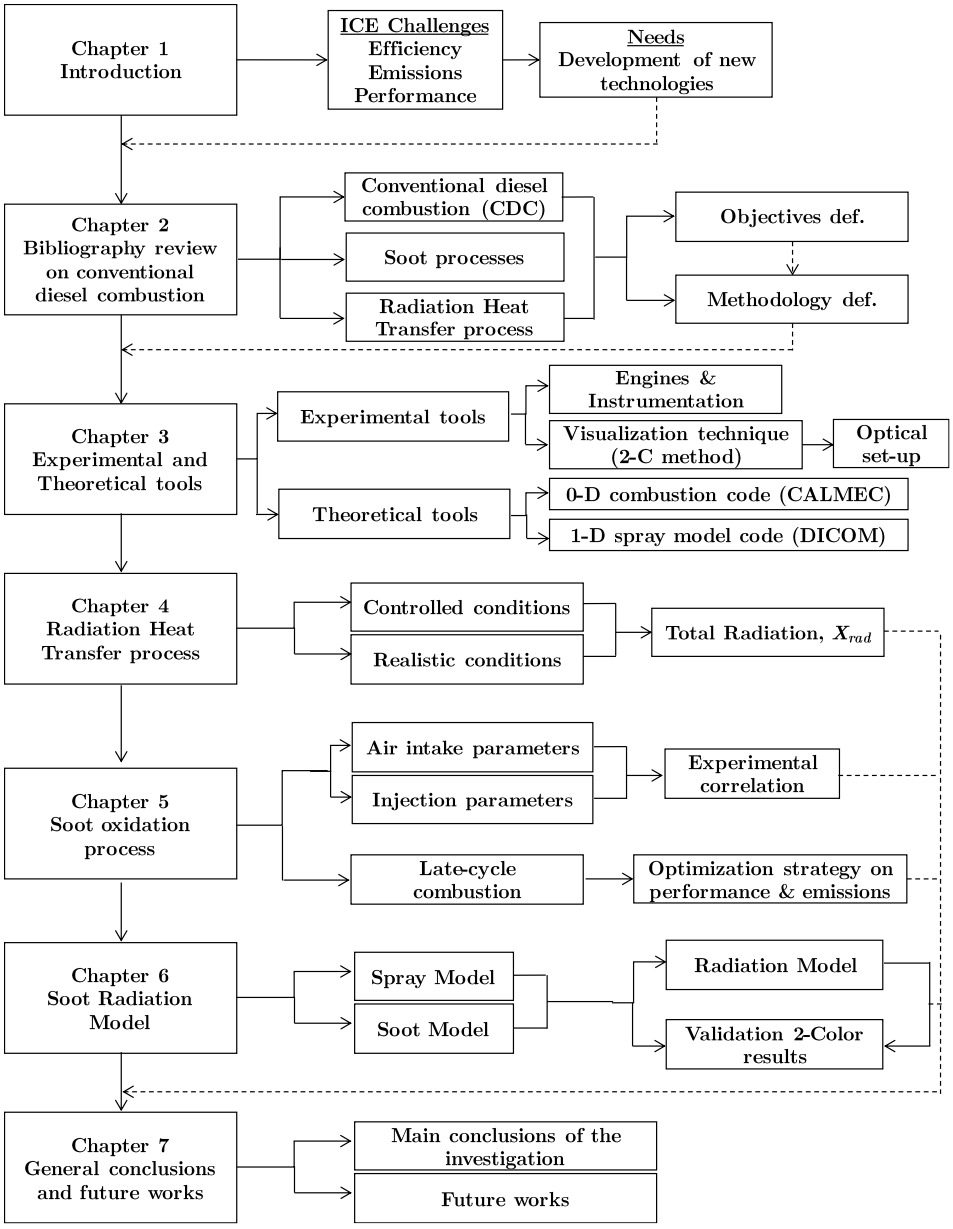

Figure 1.5. Flow chart followed in this thesis.

1.4 Bibliography

[1] European Commission. Transport. Statistical pocketbook, 2017. https://ec.europa.eu/transport/facts-fundings/statistics/pocketbook-2017_en.

[2] Diesel car salet set to overtake petrol in europe. Price Watrhouse Coopers, 2015.

[3] New passenger car registrations in Western Europe. http://www.acea.be, 2015.

[4] DieselNet: Diesel Emissions Online http://www.dieselnet.com/standards/eu/fuel_automotive

[5] Environmental Protection Agency. "Nitrogen Oxides (NOx), Why and How They Are Controlled". Technical report, 1999.

[6] Environmental European Agency. "Emissions of primary PM2.5 and PM10 particulate matter". Technical report.

[7] Wallace W. E., Keane M. J., Murray D. K., Chisholm W. P., Maynard A. D. y Ong T.-M. "Phospholipid lung surfactant and nanoparticle surface toxicity: Lessons from diesel soots and silicate dusts". Journal of Nanoparticle Research, Vol. 9 nº 1, pp. 23-38, 2007.

[8] Payri F., Desantes, J.M. "Motores de combustión interna alternativos". Editorial Reverté, 2011.

[9] García A., Piqueras P., Monsalve-Serrano J., Lago R. "Sizing A Conventional Diesel Oxidation Catalyst To Be Used For RCCI Combustion Under Real Driving Conditions". Applied Thermal Engineering, Vol. 140, pp. 62-72, 2018.

[10] Desantes J.M., López J.J., García J.M., López D. "A Phenomenological Explanation Of The Autoignition Propagation Under HCCI Conditions". Fuel, Vol. 206, pp. 43-57, 2017.

[11] Torregrosa A.J., Broatch J.A., García A., Mónico L. "Sensitivity Of Combustion Noise And NOx And Soot Emissions To Pilot Injection In PCCI Diesel Engines". Applied Energy, Vol. 104, pp. 149-157, 2013.

[12] Benajes J., García A., Monsalve-Serrano J., Villalta D. "Benefits Of E85 Versus Gasoline As Low Reactivity Fuel For An Automotive Diesel Engine Operating In Reactivity Controlled Compression Ignition Combustion Mode". Energy Conversion and Management, Vol. 159, pp. 85–95, 2018.

[13] Benajes J., García A., Monsalve-Serrano J., Villalta D. "Exploring The Limits Of The Reactivity Controlled Compression Ignition Combustion Concept In A Light-Duty Diesel Engine And The Influence Of The Direct-Injected Fuel Properties". Energy Conversion and Management, Vol. 157, pp. 277–287, 2018.

[14] Inagaki K, Fuyuto T, Nishikawa K, Nakakita K, Sakata I. "Dual-fuel PCI combustion controlled by in-cylinder stratification of ignitability". SAE technical paper, 2006-01-0028, 2006.

[15] Kokjohn S, Hanson R, Splitter D, Reitz R. "Fuel reactivity controlled compression ignition (RCCI): a pathway to controlled high-efficiency clean combustion". Int JEngine Res., 12, 209–226, 2011.

Chapter 2

Phenomenology of Late-Cycle Soot Oxidation Process and its implication on Radiation for diesel diffusion combustion

Content

2.1 Introduction

Specifically, the main objective of this chapter is to explain to the reader the fundamental concepts to understand the justification of the study that has been carried out.

The methodology used to achieve the main objective is divided into the following steps. In the first hand, a conceptual, qualitative and detailed description of the main physical chemical phenomena involved in the diesel combustion will be carried out. Specifically, the injection/combustion process was described in a diesel spray and a review of the phenomena involved in one of the most important pollutants: soot. Finally, the effect of heat transfer on engine efficiency has also been analyzed. In particular, the radiation emission from the soot particles and their influence on combustion efficiency has been described, which is directly related to the in-cylinder soot temperature and concentration.

In the last part of this chapter, a series of conclusions have been obtained, whose current deficiencies continue to exist in the study that justify the objectives of the current work. Once the objectives have been defined, the general methodology aimed at achieving the aforementioned objectives has been described.

2.2 Phenomenology of the DI Diesel combustion

In this section, the main physical-chemical phenomena related to the diesel diffusion combustion process have been described conceptually. First, the traditional temporal definition of the diesel injection/combustion process based on the injection rate and the heat release law is presented. Then, the different phenomena that occur in each stage of the combustion process have been defined qualitatively. That is, the processes of air/fuel mixture formation, autoignition and diffusion flame have been detailed.

2.2.1 Temporal description of injection/combustion process

The typical methodology used to study the temporal evolution of the combustion process in diesel engines is the comparison between the fuel injection rate and the heat release curve (heat release rate) obtained as a function of the in-cylinder pressure. This last calculation is carried out using the first thermodynamic law to the in-cylinder volume closed for each instant [1]. Figure 2.1 shows the comparison between the temporal evolution of the heat release rate and the injection rate. In this figure, it is possible to see the different main stages in the diesel combustion process:

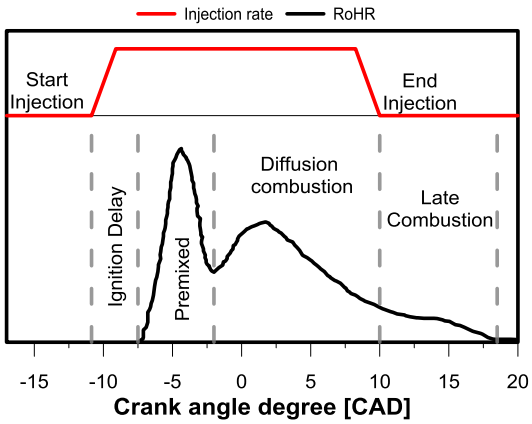

Figure 2.1. Different phases occurring during conventional diesel combustion.

- *Ignition delay phase*: as shown in the previous figure, this phase is between the start of the injection (SoI) and the start of combustion (SoC), although the rigorous definition is taken, this stage begins when the first fuel particle is injected by the nozzle until the rate of heat release increases substantially. In this phase, the air/fuel mixes in the chamber and, therefore, with the oxygen. The air/fuel mixture process is controlled by the amount of in-cylinder air movement generated by the injection pressure differential and the gas within the combustion

chamber. As a result, low-intensity chemical pre-reactions occur prior to the breakdown of the fuel molecules into shorter-chain hydrocarbons and free radicals. Consequently, these processes consume the spontaneous autoignition of the mixture that indicates the end of this stage.

- *Premixed combustion phase*: this stage is included from the start of the autoignition process to the first relative minimum in the rate of heat release graph. In this phase, the fuel (which has been previously mixed with the air in the chamber) burns and is within the limits of flammability but could not react before because the chemical reactions could not reach the optimal conditions for autoignition. Therefore, the physical-chemical processes that govern this phase are closely related to the processes carried out in the process of autoignition. During premixed combustion, energy release is very high and occurs in a relatively short time, achieving a maximum peak in the heat release velocity curve (Figure 2.1).
- *Diffusion combustion phase*: during this stage, it is assumed that the rate of heat release is controlled by the air/fuel mixture process inside the combustion chamber [2][3]. During the injection process, the mixture is governed by the amount of in-cylinder spray movement. The flame reaches quasi-stationary conditions until the end of the injection. Therefore, the duration of this phase is established from the end of the premixed combustion phase until the end of the injection process.
- *Late-cycle diffusion combustion phase*: this last phase includes from the end of the injection process until the disappearance of the flame. Once the injection process is finished, the contribution of the mass and the momentum to the combustion process ceases. This causes the almost stationary structure of the diffusion combustion flame to acquire random structures. At this stage, a decrease in the rate of heat release is observed, as shown in Figure 2.1, so that combustion loses intensity until it ends.

2.2.2 Formation of the air-fuel mixture

In the injection process, different processes are initiated that cause the formation of the mixture between the injected fuel and the in-cylinder ambient air. In recent years, the formation process has been extensively analyzed theoretically and experimentally, reaching different approaches depending on the conditions considered within the combustion chamber. As examples, the work developed by Arrègle [4] and López [5], in which an integral study of the physical mixing phenomena in an isothermal liquid fuel spray in a non-reactive environment (lack of oxygen) was carried out. On the other hand, García [6] went further, and did the same analysis, but in this case for a diesel spray in evaporative and reactive conditions.

The injection process originates due to the difference between the in-cylinder pressure and the fuel injection pressure. The in-cylinder pressure is around 50 to 100 bar at the instant in which the fuel is injected, depending on the boundary conditions (intake pressure and temperature, compression ratio, etc.). On the other hand, currently the injection pressure is located in a pressure range between 200 (minimum value for the needle of the injector to rise) and 2500 bars [7]. The maximum injection pressure increases with the development of new technologies. This high injection pressure causes the fuel to enter as a liquid spray with a high velocity in the combustion chamber. In addition to speed, fuel spray is associated with a large amount of movement which, in contrast to the low air velocity within the chamber, converts the fuel spray into a turbulent spray.

Next, the two most important physical phenomena have been described that take place during the formation of air/fuel mixture and serve as a background for the autoignition process.

2.2.2.1 Atomization

After the discharge of the spray fuel through the nozzle, the first physical phenomenon occurs: atomization. Atomization is called a process in

which the liquid core (continuous medium) of the nozzle stops and begins to disintegrate into drops of different sizes. With this, the area in contact between the fuel and the air increases and that favors the physical processes between them (air entrainment and evaporation). In the literature, this first phase is also called primary atomization.

For the turbulent flow (direct diesel injection), the primary atomization process takes place from a certain axial length with respect to the nozzle orifice. From this distance, the liquid core begins to disintegrate and there are only drops of fuel around the air entrainment. This distance is called *intact length* and depends on the conditions (fuel type, injection pressure, nozzle size, ambient density, etc.). According to Arrègle [4], under the current configurations of a DI diesel engine, sprays under non-evaporative (and non-reactive) conditions are always in a single atomization flow: complete atomization flow. In this flow, the intact length does not vary for different conditions.

After primary atomization, secondary atomization takes place. In this, the fuel droplets disintegrate into smaller droplets, which infers an increase in air entrainment. In addition, it is important to note that, simultaneously with secondary atomization, the coalescence phenomenon occurs. The drops generated in the primary atomization interact with the ambient air and other drops produce a considerable increase in the average diameter of the drops.

2.2.2.2 Evaporation

Taking into account that the atomization process implies uniqueness between the gaseous spray and the diesel spray, the physical phenomenon of evaporation should differentiate both types of spray, since it only occurs in the second type of spray. Once the atomization and air entertainment processes have been carried out, the fuel drops exchange energy with the high temperature gas. This exchange of energy produces an increase in energy from the fuel drop. In this way, the droplets become gaseous and the diameter is considerably reduced.

This phenomenon has been studied by several researchers [8][9], concluding that the liquid phase does not exceed a certain limit from a certain distance, called the maximum liquid length. From this length, the drops disappear and, therefore, the fuel becomes a gaseous state.

On the basis of the above results, the length of the liquid is influenced by different boundary conditions: nozzle diameter [10], ambient gas temperature and density [11] and fuel properties [12]. However, the injection pressure does not reveal a significant influence on the maximum liquid length [13]. With this, Siebers [13] concluded that the evaporation phenomenon in engine conditions is controlled by the mixing process. This nomenclature is used to specify that the fuel droplets evaporate as the surrounding environment transmits the necessary enthalpy by turbulent mixing.

The phenomenon of fuel evaporation is completed when it reaches the maximum liquid length, which is usually about 100 times the nozzle diameter. As a conclusion, according to García [6], *the hypothesis of mixing control indicates that the evaporation process, despite only taking place in the diesel spray, does not establish important differences between it and the gaseous stream, it is a global phenomenon of air-fuel mixing.*

2.2.3 Autoignition process

In the previous section, the phenomena related to the evolution of a fuel spray in an environment lacking oxygen were described. However, the objective of an ICE is to oxidize the fuel of a chemical reaction to produce work and energy, and for this, the presence of oxygen is necessary. Oxygen, together with the appropriate temperature and pressure conditions and the air/fuel mixture, produces the start of the chemical reaction, called autoignition. During this stage, physical processes are linked to chemical processes, since the rate of heat associated with chemical reactions alters the local thermodynamic conditions of the spray.

.

The autoignition phenomenon is understood as the beginning of the heat release process. This start is taken at the instant when an increase in the pressure (or temperature) caused by the combustion process is detected, or the moment when the rate of heat release begins to grow considerably.

From advanced optical techniques, Dec and Espey [14][15] show results that confirm that autoignition is not a point-in-time process. Therefore, this phenomenon must be studied as a continuous process that must be studied as in temporally and spatially. In this way, the following paragraphs describe the sequence of events that occur during the continuous autoignition process of the fuel, which is proposed by Higgins [16], and which is divided into three stages:

From advanced optical techniques, Dec and Espey [14][15] show results that confirm that the autoignition is not a point-in-time process. Therefore, this phenomenon must be studied as a continuous process that must be studied as temporally and spatially. In this way, the following paragraphs describe the sequence of events that occur during the continuous autoignition process, which is proposed by Higgins [16], and which is divided into three stages:

- *Physical ignition period*: this phase extends from the beginning of the injection process until an instantaneous increase in pressure in the combustion chamber occurs or until an emission related to chemiluminescence is detected. During this temporal interval, the fuel injected enters the combustion chamber and is governed by the physical processes described in the previous section (atomization, evaporation and mixing of air and fuel). As the fuel evolves and physical processes occur, in a given spray area the appropriate conditions (mainly temperature and pressure) are reached for the autoignition process to begin. This start of reaction would mark the end of the physical ignition phase. The physical processes of evaporation and mixing of air/fuel are still important for the following stages.

- *First ignition stage*: this stage begins at the instant when an increase in pressure is detected until the rate of heat release (also called combustion phase premixed) is initiated. In this phase, the ignition reactions extend to the front of the spray. In this area, the mean relative equivalence ratio is rich in values between 2 and 4. According to Kosaka [17], the low intensity radiation contemplated in the first ignition stage is associated with the chemiluminescent radiation that originates mainly in the chemical species of CH and formaldehyde CH_2O that appears during this pre-reaction phase. As the temperature increases due to the air/fuel mixture and the heat release of the autoignition, the dissociation reactions inhibit the development of the chain reactions, which clarifies the reduction in the rate of heat release observed before of the start of the second ignition stage (premixed combustion phase). This phenomenon is related to the appearance of cold flames. These are typical of autoignition process of hydrocarbons in low temperature. conditions
- *Second ignition stage*: this phase starts when the fuel that was mixed during the ignition delay phase is completely burned. During this phase, the heat is released at a much lower rate, as it is controlled by the availability of the new mixture formed to burn, hence the name of mixing controlled combustion [18]. The air and fuel have been perfectly mixed within the limits of flammability during the ignition delay stage until autoignition, but has not yet been able to burn. This causes a very high rate of heat release in a short time interval, and this is the reason why important pressure gradients are produced inside the combustion chamber. When the autoignition delay is longer, the mixture progresses progressively and the equivalence ratio is poorer. Otherwise, when the shortest delay in autoignition is low, the process is governed by the incandescence of the soot [15][16].

2.2.4 Concept model of diesel diffusion flame

Throughout the years and demanded by the complexity of the processes involved, the knowledge of the structure of the diesel diffusion flame in quasi-stationary conditions has been studied by a multitude of scientific studies. To do this, numerous tools and computational models have been developed to analyze this complex phenomenon and establish an adequate conceptual model. According to Dec [20], *a precise conceptual model provides a global framework for interpreting experimental measures, guides the development of the numerical model, and provides a mental image that guides the thinking of engine designers.*

The most common conceptual model, which is widely accepted by the scientific community to describe the diesel diffusing flame under quasi-stationary conditions, is the one developed by Dec [20] and Flynn [18], shown in Figure 2.2. It is important to note that the model is only valid in the temporal interval from the beginning of the diffusion phase until the end of the injection process, which is the temporal interval in which the flame is quasi-stationary.

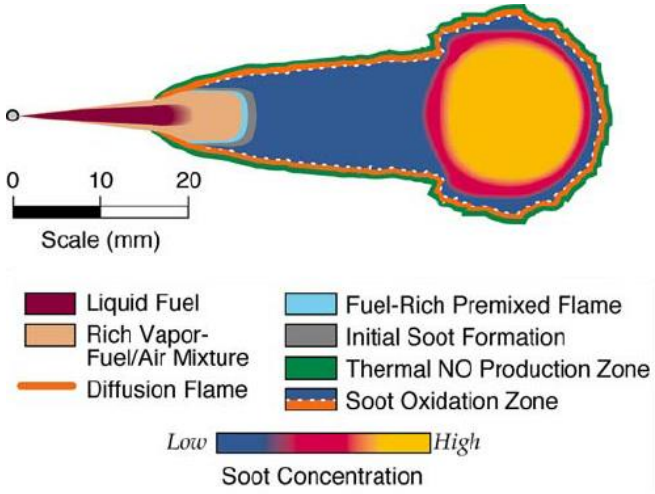

Figure 2.2. The structure scheme of the diesel flame during the quasi-stationary phase of the diffusion combustion stage presented by Dec [20]

Qualitatively, three zones are distinguished in the following scheme:

- *Zone 1*: this zone is comprised between the injector nozzle and the lift-off length. In this first part, chemical reaction does not occurs. The liquid fuel injected and the different physical processes explained in the previous section are performed in the stage: atomization, air entrainment and evaporation.
- *Zone 2*: from the lift-off length, the spray take places to reactive conditions. In this area, Dec establishes the existence of a premixed reaction zone, which burns down the included oxygen in zone 1. Consequently, the products of the premixed combustion, which develop in a rich equivalence ratio, are formed by partially oxidized hydrocarbons and are attributed the function of soot precursors.
- *Zone 3*: this zone is established from zone 1 and surrounding zone 2. In it, the flame reaches the characteristic diffusion flame structure and it is compound by two zones: an internal zone, in which they accumulate the unburnt products (mainly hydrocarbons) and formed soot in zone 2 and an external zone, that surrounds the internal zone and in which the unburned fuel reacts.

  Although soot formation process begins in zone 2, the soot concentration growth is more important in zone 3. As shown in Figure 2.2, the maximum soot concentration is reached in the flame front (low velocity part). The residence time is the main factor responsible for the formation and growth of soot. When the soot reaches the outer edge of the flame (reaction zone), it is oxidized completely by the presence of OH radicals (that is generated in the diffusion flame) plus the available oxygen.

  Regarding nitrogen oxides, the Dec and Canaan studies [21] analyze the NO species. They form on the outside of the flame because the conditions are very favorable, mainly in terms of temperature and oxygen availability. Finally, this model shows how the most favorable areas for soot oxidation are also ideal conditions for the formation of NO radicals.

Next, the conceptual diffusion flame model has been completed with a qualitative description of the spatial and temporal evolution of a fuel package longitudinally from the injector outlet through the different diffusion flame. This description is supported in Figure 2.3.

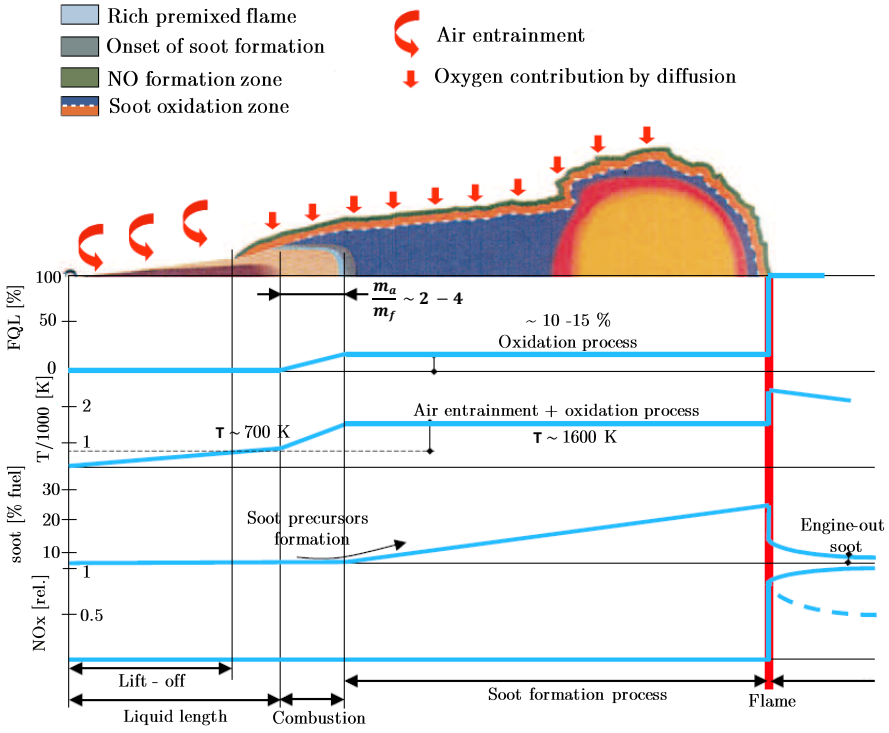

Figure 2.3. Spatial and temporal description of a package of mass injected during the stationary part of the diffusion combustion phase. Source: García [22]

The injected fuel package is atomized and mixed with the air ambient, due to the high-pressure injection and temperature. The high temperature and the air entrainment cause the change of liquid state to the vapor state of the fuel, reaching the maximum liquid length. The evaporated fuel continues to mix up to the reaction zone, where the equivalence ratio is between 2 and 4 and the temperature reaches 700 K. The fuel package is

burned through the reaction zone and the fuel energy is released between 10 and 15% of the total [18]. The temperature rises to around 1600 K and gives rise to partially oxidized products, where carbon monoxide and short chain unsaturated hydrocarbons predominate [23] (the latter are considered the precursors of soot formation). In addition, local temperatures and soot concentration are too low for the formation of NO species by the thermal route.

After the premixed reaction zone, the fuel package enters the internal area of the diffusion flame in which, although the fuel continues to mix, there is an absence of oxygen due to the premixed zone and the external reaction zone that prevents the introduction of oxygen. In the absence of oxygen flow, it is difficult to produce a significant heat release in the internal flame. In the inner part of the flame periphery, where the flame front is located, there is an increase in temperature which, together with the soot precursors, causes the appearance of the first soot particles. These particles increase in size until they reach the flame front, in which their size and concentration are maximum. On the front surface of the flame, the partially oxidized products and the soot formed together with the diffused oxygen burn out, releasing most of the fuel energy (85-90%). In the front of the flame, the equivalence ratio is very close to the stoichiometric and therefore, the temperatures reached are very similar to the adiabatic temperature. With these temperatures, the soot formed is almost completely oxidized. On the contrary, the rate of nitrogen oxide formation increases considerably. Finally, the combustion products are diluted in the rest of the gases in the combustion chamber.

2.3 Characterization of soot formation and oxidation processes

The most important drawback of diesel engines is the emission of pollutants into the atmosphere. Specifically, nitrogen oxides (NOx) and soot particles (PM). Focusing on the soot particles, they are produced as a result

of two simultaneous and antagonistic processes: soot formation and oxidation. The first of these is preceded by the precursors formation in the premixed combustion zone with rich equivalence ratio within the diffusion flame (as described in the previous section). Due to the presence of these precursors together with the absence of oxygen and high local temperatures, the soot particles are generated. At this stage, the dominant process in the soot concentration is formation with respect to oxidation. Once these particles reach the periphery of the flame, v practically all of the soot particles formed within the spray oxidize when they reach the edge of the diffusion flame. In this area, the presence of oxygen and high temperatures (similar to the adiabatic flame temperature) favor the soot oxidation process. The soot formation process begins to be less important, with the oxidation process being the dominant process. It is also worth noting that only a fraction of the soot formed inside the cylinder is emitted in the exhaust [2].

Next, both processes have been described more widely, in addition to the influence of various parameters on them.

2.3.1 Soot formation. General description.

Several researchers have shown that the soot formation is directly related to the lift-off length. This phenomenon is based on the flame displacement from the injection nozzle for a diffusion diesel flame. The reaction zone starts at a certain distance from the injection nozzle.

In the literature, there are numerous works dedicated to analyzing the lift-off. Among them, it is worth mentioning Higgins and Siebers [24][25], in which they analyze the effect of different conditions and operating parameters on the lift-off length and its relationship with the soot formation in a constant-volume combustion chamber. These investigators studied the lift-off length by means of OH chemiluminescence [24]. The air/fuel mixture characteristics are determined by the amount of oxygen available in the diesel spray upstream of the lift-off length. Next, the fuel begins to evaporate and oxidize in the rich premixed reaction zone where the soot is initially formed.

Due to the higher available oxygen in the diesel spray downstream of the lift-off, the equivalence ratio is lower in the reaction zone and, therefore, in the soot formation. Siebers and Higgins [25] established an experimental relationship between the light intensity from soot and the relative equivalence ratio. For an increase in the lift-off length, the soot is not visible for a relative equivalence ratio between 2 and 2.5. From this range, the soot particles are imperceptible. Therefore, it is possible to establish that the parameters that control the lift-off length are also governed by the soot formation. It is important to note that although the diesel flame consists of two stages (rich premix combustion and diffusion combustion), the first controls the soot formation process.

2.3.1.1 Influence of physical parameters

Next, the role of the different engine parameters in the soot formation process is analyzed, such as the unburned temperature, the injection pressure, the ambient density, the nozzle diameter and the oxygen concentration. It is important to note that the following conclusions are valid for free sprays and quiescent ambient mainly. These conclusions are not directly applicable to the conditions in which the liquid part of the spray interacts with the combustion chamber walls or with other sprays or in high turbulence environments (high swirl):

- *Unburned temperature*: several authors [6][25][26] have studied the effect of temperature on soot formation. In general, the temperature has a large non-linear influence on the lift-off length and, consequently, on the soot formation. As the temperature increases, the lift-off length is shortened and, therefore, the amount of ambient gas entrainment upstream of the spray. As a result, the equivalence relation in the take-off length becomes richer, which causes a greater soot formation. Siebers and Higgins [25] attributed this effect to the increase in temperature and reactivity in the air/fuel mixture and then

generated a shorter lift-off length. In addition, an increase in unburned temperature implies an increase in the temperature of the flame. Although changes in the temperature of the adiabatic flame can not be directly related to the lift-off length, this has a direct effect on the formation and growth of the soot precursor formation [27].

- *Injection pressure*: as the injection pressure increases, the spray velocity increases, which causes the reaction zone to move downstream and, therefore, extend the lift-off length [6][25][28]. With the injection pressure, the air entrainment phenomenon benefits upstream of the lift-off length, decreasing the equivalence ratio in the reaction zone and the soot formation process. In addition, changes in injection pressure affect the residence time of soot (or precursors) formed at lift-off [29][30]. The decrease in residence time is mainly justified for two reasons: the first hand, due to the residence time, is inverse to the injection pressure. In addition, to increase the injection pressure, the length of the flame remains constant, but the lift-off length increases, so that the distance to be covered by the soot (or precursors) formed between the reaction zone and the periphery of the flame is shorter. Therefore, the time required for the soot particles to cross the flame decreases.
- *Ambient density*: the ambient density has two opposite effects with respect to the lift-off length. On the one hand, a higher density implies a shorter lift-off length [6][25][26], which means that there is less distance at which air can include fuel in the mixing process. On the other hand, a higher density infers a higher air mass for a lift-off length. The balance between both effects, the first of them takes a small advantage over the second and results in a small decrease in the air inclusion rate [31], which results in an increase in the equivalence ratio and, therefore, soot formation [29][30]. Finally, Picket and Siebers show that if the environmental density is low, the equivalence

ratio at lift-off is less than 2 and, therefore, the soot formation process is considered negligible [30].

- *Nozzle orifice diameter*: if the nozzle diameter decreases, the lift-off length also decreases slightly [6][25][26]. By reducing the nozzle diameter, the amount of fuel injected is less. However, the rate of air entrainment remains practically constant. This causes an increase in the percentage of stoichiometric air and a poorer equivalence ratio at lift-off and the premixed reaction zone, resulting in a reduction in soot formation. Like the ambient density, there is a minimum diameter that is considered the minimum threshold at which soot formation disappears [28][32].
- *Ambient oxygen concentration*: a reduction in oxygen concentration implies an increase in the lift-off length [33]. Like the ambient density, there are two opposite effects: in the first hand, a longer lift-off length should improve the air entrainment process. However, on the other hand, the concentration of oxygen for this air entrainment is reduced. Siebers [34] shows that both effects are counteracted and, therefore, the amount of oxygen in the lift-off is independent of the oxygen concentration in the ambient air. Although, a reduction in oxygen concentration does not have a significant effect on the equivalence ratio of the lift-off length (and in the formation of the soot precursor), it does have a significant effect on the adiabatic flame temperature, reducing the growth of soot precursors. In addition, reducing the soot concentration means a longer residence time of the precursors inside the flame, which results in an increase in the growth rate. Like other parameters, the soot formation is negligible at a minimum oxygen concentration.

2.3.2 Soot oxidation. General description

During the soot formation process, soot oxidation, nucleation and particle stages can occur. The soot particles formed in the reaction zone of the diffusion diesel flame, a large part of the soot is oxidized inside the cylinder before the exhaust process begins.

Figure 2.4 shows a sequence of images for a single spray combustion. In this, it shows a cloud of soot particles surrounded by a diffusion flame that arises from the luminosity of the high-temperature soot particles consumed in this flame.

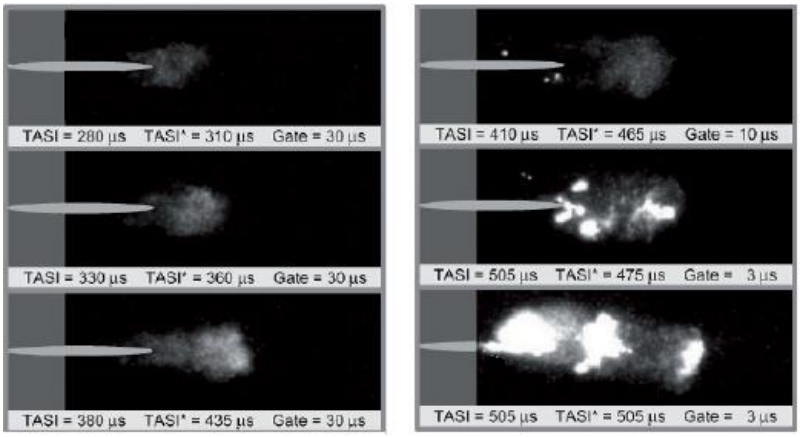

Figure 2.4. A sequence of images for a DI diesel combustion in a single spray. Source: García [6]

In general, the rate of heterogeneous reactions, such as soot oxidation, depends on the diffusion of reactants and products on the surface, as well as the kinetics of the reaction. For particles less than about 1 µm in diameter, diffusion resistance is minimal. The soot oxidation process in the diesel cylinder is kinetically controlled, since the particle sizes are smaller than this limit. There are many species in or near the flame that could oxidize the soot: examples are O_2, O, OH, CO_2 and H_2O. Recent reviews of soot formation [35] have concluded that at high oxygen partial pressures, soot oxidation can be

correlated with a semi-empirical formula based on pyrographite oxidation studies. However, for fuel-rich and almost stoichiometric combustion products, oxidation by OH has been shown to be more important than O_2 attack, at least at atmospheric pressure.

Taking into account the structural similarities that the oxidation rates of soot and pyrographite, the semi-empirical formula of Nagle and Strickland-Constable (NSC) has been used [36]. The NSC oxidation model is based on the correlation of pyrographite oxidation for oxygen partial pressures p_{O2} <1 atm and temperatures between 1100 and 2500 K. In this model, carbon oxidation is produced by two mechanisms whose rates depend on the chemistry of the surface that involves more A reactive sites and fewer reactive B sites. The chemical reactions are:

(2.1) $$A + O_2 \leftrightarrow A + 2CO$$

(2.2) $$B + O_2 \leftrightarrow B + 2CO$$

(2.3) $$A \leftrightarrow B$$

The NSC soot oxidation rate implemented in equation (2.4) is given by:

(2.4) $$\frac{dm_{SO}}{dt} = \frac{M_C}{\rho_s d_s} m_s w$$

where m_{SO} is the soot mass, M_C is the carbon molecular weight (12 g/mole), ρ_s is the soot density (2.0 g/cm^3), and d_s is the soot diameter (4.5×10^{-9} m). The term w in previous equation is the net reaction rate of reactions (2.1), (2.2), and (2.3) and is defined as:

(2.5) $$\frac{w}{12} = \left(\frac{k_A p_{O2}}{1+k_z p_{O2}}\right) x + k_B p_{O2}(1-x)$$

where p_{o2} is the oxygen partial pressure in atm. The proportion, x, of A sites is given by:

(2.6) $$x = \frac{p_{ox}}{p_{ox} + \left(\frac{K_T}{K_B}\right)}$$

The rate constants used in the NSC oxidation model are given in Table 2.1.

Rate Constant	Units
$K_A = 20 \cdot \exp(-15100/T)$	$g \cdot C/cm^2 \cdot s \cdot atm$
$K_B = 4.46 \cdot 10^{-3} \cdot \exp(-7640/T)$	$g \cdot C/cm^2 \cdot s \cdot atm$
$K_T = 1.51 \cdot 10^5 \cdot \exp(-48800/T)$	$g \cdot C/cm^2 \cdot s$
$K_Z = 20 \cdot \exp(-15100/T)$	Atm^{-1}

Table 2.1. Rate constants for NSC soot oxidation model [2]

According to this mechanism, the reaction is of first order at low oxygen partial pressures, but approaches zero order at higher pressures. At a given oxygen pressure, the rate initially increases exponentially with temperature. Beyond a certain temperature, the rate decreases as the thermal rearrangement favors the formation of less reactive B sites. When, at a sufficiently high temperature, the surface is completely covered with B sites, the rate is first order in the oxygen partial pressure and increases again with temperature [37].

Park and Appleton [38] compared this formula with the oxidation rate data obtained from pyrographite samples, carbon black particles and with the available flame soot oxidation data. Figure 2.5 shows the soot oxidation rate predicted by the equations (2.5) and (2.6) as a function of temperature and oxygen partial pressure. In diesel engine conditions, the partial pressure of O_2 can be high (~ several atmospheres), as can the temperatures of close-to-stoichiometric mixtures (2800 K).

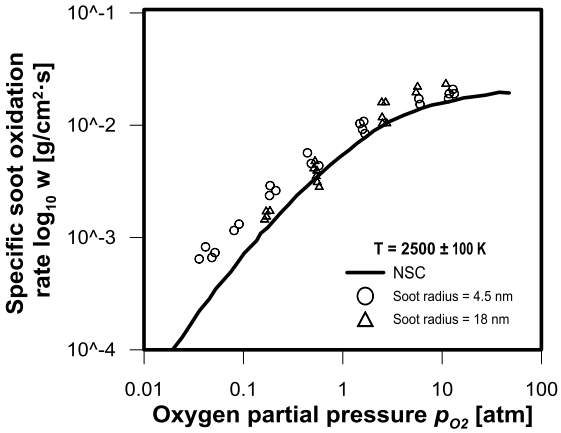

Figure 2.5. Specific soot oxidation rate measurements and predictions as a function of temperature and oxygen partial pressure. Image adapted from [2]

The agglomeration has an indirect influence on the amount of soot oxidized through its effect on the surface area. In the limit case of a spherical cluster, n monodisperse spherules can be imagined as compacted into a single solid sphere of equal volume. Alternatively, the same n spherules can be imagined compacted in a cylinder of equal diameter to that of the original spherules. Since oxidative attack is essentially an outer surface phenomenon, the surface/volume ratio is the appropriate measure of the effect of the particle shape on the rate of soot mass burning. It can be shown that the surface/volume ratios for the single sphere, the cylinder and the individual sphere are in the ratio $n^{-1/3}$, 2/3 and 1 respectively. Thus, the agglomeration will decrease the relative oxidation rate. In the limit, spherical groups are less desirable than a chain: the larger the cluster, the greater the relative reduction in the surface area.

In operating conditions in which the environment is rich and close-to-stoichiometric combustion products where the O_2 molar fractions are low, the oxidation by the attack of the OH radical is more significant than the oxidation by O or O_2. The OH radical can be important in the soot oxidation of the flame area in close-to-stoichiometric conditions.

2.3.2.1 Influence of the physical parameters

Then, as described in the previous subsection for the phenomenon of soot formation, the role of different engine parameters in soot oxidation has been analyzed: temperature and ambient density, injection pressure and oxygen concentration.

- *Temperature*: temperature is considered an important factor that affects chemical reactions. In the case of soot processes, a higher temperature increases the rate of soot oxidation faster than the rate of soot formation [39]. A change in the in-cylinder gas temperature does not have a significant impact on the temperature of the flame compared to a variation in the oxygen concentration in the intake air. However, it is expected to benefit the phenomenon of soot oxidation and, therefore, improve the levels of exhaust soot. Rooster [40] has analyzed the effect of temperature on the soot oxidation process. For this, he has made experimental measurements on an optical motor using the laser extinction method. When the temperature at the top dead center was modified from 900 K to 1100 K, which results in an increase in the rate of soot oxidation. This improvement in the rate of soot oxidation does not appear to have an effect on the amount of soot particles in the exhaust. One possible explanation is that the rate of soot formation is also affected and counteracts the improvement in soot oxidation. Although it is not possible to give a strict answer to explain these observations, however, it can be concluded that the temperature at the top dead center has a limited impact on the soot oxidation.
- *Density*: the in-cylinder gas density must positively affect the soot oxidation, increasing the number of oxidizing molecules per unit volume. It is difficult to isolate the effect of density and temperature, since both variables are closely related. Pickett [30] studied the effect of density on the soot concentration. The

experimental measurements were made from the laser extinction technique in a wide range of operating conditions. This work concluded that a reduction in the in-cylinder gas density causes a significant decrease in soot concentration due to the increase in the duration of combustion.

- *Injection pressure*: the soot oxidation, mainly in the late-cycle diffusion part, is a process controlled by mixing. Therefore, increasing the energy of the turbulent kinetic gas in the combustion chamber has a positive influence on the soot oxidation process. Dembinski [41] studied the impact of injection pressure on the soot oxidation process. The experimental measurements were made on an optical motor. The measurements made at high injection pressure show higher values of soot concentration in the combustion process, but lower soot emissions in the exhaust. If a comparison is made between the injection condition of 500 bar and that of 1500 bar, it is observed that the exhaust emissions decrease from 1.22 FSN to 0.19 FSN. It is also observed that the maximum soot concentration is 50% higher for the case of 1500 bar compared to the 500 bar measurement. For that, the soot formation process is less important than the soot oxidation process. Arrègle [42] analyzed different subsequent injection strategies to mitigate soot emissions in direct injection diesel engines. For this, he made an extensive parametric experimental study of the post-injection for a wide range of operations, concluding that the soot emissions are reduced when the post-injection conditions are added.
- *Oxygen concentration*: when the available oxygen concentration in the combustion chamber decreases, the soot oxidation process worsens due to the low oxygen availability. In addition, the combustion temperature is reduced due to the higher inert concentration and the lower oxygen content in the inlet gas directly, which affects the soot oxidation process. Rooster [40] demonstrated a reduction in the rate of soot oxidation when the

oxygen concentration decreases. They also provide an experimental correlation between soot oxidation and exhaust soot emissions, concluding that the oxidation rate shows a strong relationship with exhaust emissions.

2.4 Heat transfer process in ICE

Heat losses have a strong influence on the engine efficiency [2]. The energy lost through the walls of the cylinder is not available to produce mechanical work, which results in the reduction of the indicated efficiency. In the intake ports, the heat transfer from the walls to the intake air increases the charge temperature, decreasing the volumetric efficiency. In the exhaust ports, the heat losses from the exhaust gases reduce the amount of energy that can be recovered in the turbocharger. In addition, heat transfer is related to combustion anomalies, such as flame quenching and lubrication problems due to oil degradation at high temperatures. Heat transfer is also relevant because it affects gas and surface temperatures, which have an important influence on the formation of pollutants such as NOx [43], CO [44] or unburned hydrocarbons [45]. Therefore, the general objective of this section is to increase the knowledge related to heat transfer within the cylinder with the purpose of contributing to the efficiency improvement.

Wall temperatures are a good indicator of heat transfer. Convective heat transfer is proportional to the difference between the fluid and the wall temperatures. Conductive heat fluxes also depend on the distribution of wall temperature. Finally, the radiation heat transfer is proportional to the temperature difference at the fourth power. Another point of view is that if the boundary conditions (such as refrigerant, oil, intake air and ambient temperatures) are kept constant, the variations in wall temperatures will depend only on the conditions of the combustion chamber.

Next, the phenomenon of heat transfer has been described in depth, in addition to the different modes in which it manifests itself.

2.4.1.1 Phenomenology of heat transfer in an engine

The peak burned gas temperature in the cylinder of an internal combustion engine is of order 2500 K. Maximum metal temperatures for the inside of the combustion chamber space are limited to much lower values by a number of considerations. These conditions lead to heat fluxes to the walls of the chamber that can reach up to 10 MW/m^2 during the combustion period. However, during other parts of the operation cycle, the heat flow is essentially zero. The flow varies substantially with the location: the regions of the chamber that come into contact with the high-temperature burned gases that move rapidly experience the highest flows. In regions with high heat flux, thermal stresses should be kept below levels that could cause fatigue cracking (so temperatures should be below 400 °C for cast iron and 300 °C for aluminum alloys). The gas-side surface of the cylinder wall must be kept below about 180 °C to prevent deterioration of the lubricating oil film. Solving these heat transfer problems of the engine is obviously an important design task.

Heat transfer affects engine performance, efficiency and emissions. For a given mass of fuel inside the cylinder, a higher heat transfer to the combustion chamber walls will decrease the pressure and the mean temperature gas, and will reduce the work per cycle transferred to the piston. Therefore, the specific power and efficiency are affected by the magnitude of the engine heat transfer. The most important parameter is the heat transfer from the exhaust valve and the piston to the exhaust gases. Changes in gas temperature due to the heat transfer impact on the processes of emission formation, both inside the cylinder and in the exhaust system where the subsequent combustion of CO and HC occurs. The exhaust temperature also governs the power that can be obtained from the exhaust energy recovery devices, such as a turbocharger turbine. The friction is affected by the engine heat transfer and contributes to the refrigerant charge. The temperature of the cylinder liner governs the temperature of the lubricating oil film of the piston and the ring, and therefore its viscosity. Piston distortion and coating due to non-uniformity of temperature has a significant impact on the piston

component of the engine friction. Part of the mechanical energy dissipated due to friction must be rejected to the atmosphere by the cooling system, which eventually leads to an engine efficiency loss. The importance of the engine heat transfer is clear.

To examine the heat transfer in depth, it is useful to divide the engine into its subsystems. The intake system consists of intake manifold and inlet ports and valves. The heat transfer to the intake flow charge reduces the volumetric efficiency. Inside the engine cylinder, the charge temperature in relation to the wall temperature and the flow field vary profoundly throughout the cycle. Both variables have a great influence on heat transfer. During the admission process, the admission charge is usually cooler than the walls and the flow rates are high. During compression, the charge temperature increases above the wall temperature and the gas velocities decrease. The heat transfer is now from the cylinder gases to the chamber walls. During combustion, the gas temperatures increase substantially and the gas expansion produces an increase in gas movement. This is the period in which the rates of heat transfer to the walls are higher. In addition, as the cylinder pressure increases, a small fraction of the cylinder charge is forced into the crevice regions, resulting in additional heat transfer. During the expansion, the gas temperatures decrease, thus decreasing the heat transfer rates. However, when the exhaust valve is opened, the purge process produces high speeds inside the cylinder, and beyond the exhaust valve and in the exhaust port. During the exhaust process, there is a substantial heat transfer from the exhaust gas to the valve, the port and (to a lesser extent) the manifold. Figure 2.6 shows an example of how the rate of heat transfer to the walls of the total combustion chamber varies throughout the four-stroke operation cycle of a compression ignition engine. The heat transfer rate was estimated from the cylinder pressure, the burned temperatures and unburnt gas, the surface area of the combustion chamber and the wall temperature, assuming that the gas velocities were scaled with the average piston speed. The ability to predict the magnitude of the heat transfer between the working fluid, the walls of the intake system, the combustion chamber and the exhaust system and the coolant is of obvious importance to the engine designer.

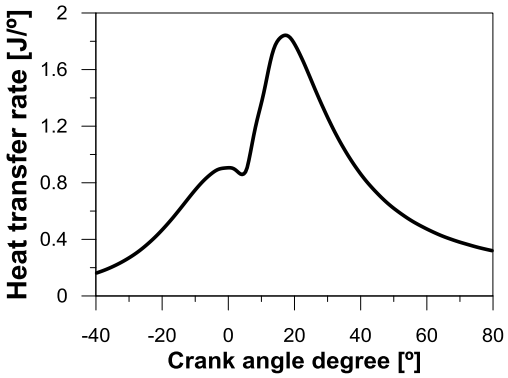

Figure 2.6. Temporal evolution of heat transfer rate in a compression ignition engine.

The heat transfer in the engine is presented in three different ways: conduction, convection and radiation. The main characteristics of the conduction and convection modes are described below, while the radiation phenomenon is discussed in more detail in the following subsection.

Conduction

Conduction is the transfer of energy associated with random molecular motions, from the most energetic particles to the smallest energetic particles, as a result of their mutual interactions. Since the temperature is a measure of the molecular energy, when the molecules collide with each other, an energy transfer occurs in the direction of the temperature decrease. This type of heat transfer is the only possible in opaque and fluid solids at rest, so that the engine is only isolated in the solid parts, since the fluids (gases, lubricants and coolants) that circulate through the engine are in constant movement. The flow of heat $\dot{Q}$ transmitted in conductive processes can be expressed by an empirical law due to Fourier [2]:

$$\dot{q} = -k\Delta T \tag{2.7}$$

where k is the thermal conductivity of the material. Therefore, the conductive heat flow depends on the contact surface, the material and the

temperature gradient. In one-dimensional situations, the above equation is simplified, such as:

$$\dot{q} = \frac{\dot{Q}}{A} = -k\frac{dT}{dx} \tag{2.8}$$

Heat is transferred by conduction through the cylinder head, cylinder walls and piston; through the piston rings to the cylinder wall; through the engine block and manifolds.

Convection

This heat transmission mode occurs between fluids and solids in which there is both a difference in temperature (a fundamental fact for the existence of a thermal transfer process) and a movement of the fluid. Considering how this movement occurs, two kinds of convection are differentiated: free and forced. The first one occurs when the movement of the fluid is caused exclusively by the density difference produced in the fluid's core by the temperature difference. On the other hand, forced convection is used when the movement of the fluid is caused by an external element such as a fan or a pump.

The convective heat transfer process between a surface and a fluid includes the conduction and advection mechanisms. Advection is defined as the transport of energy associated with the macroscopic movement of the fluid. Within the layer of fluid adjacent to the surface, and therefore, at rest with respect to it, the heat is transmitted by conduction, whereby the heat flow can be written as:

$$\dot{Q} = -k_f A \frac{\partial T}{\partial x}\Big|_{x=0} \tag{2.9}$$

where k_f is the thermal conductivity of the fluid and x is the normal coordinate to the wall (positive direction towards the wall).

Between that limit layer of the fluid and the mass of the fluid in motion the energy is transmitted by advection. By analogy with the conductive case, the heat flux transmitted is expressed by Newton's cooling law:

(2.10) $$\dot{Q} = hA(T - T_p)$$

where T and T_p are the temperatures of the fluid and the wall, respectively, and h is the coefficient of convective heat transmission (also called the film coefficient). Considering the heat transmitted by conduction in the limit layer equal to the heat transmitted by advection, the convection coefficient can be cleared:

(2.11) $$h = -k_f \frac{\partial T}{\partial x}\Big|_{x=0} (T - T_p)^{-1}$$

This coefficient depends not only on the properties of the fluid and the solid material, but also on the conditions existing in the limit layer due to the fluid velocity field, the thermodynamic properties and the fluid transport, and the geometry of the fluid surfaces, so that its determination is only viable in some simple cases. For this reason, semi-empirical correlations based on analysis are used, which indicates that a relation of Nu = f (Re, Pr) must be fulfilled, where Nu, Re and Pr are the numbers of Nusselt, Reynolds and Prandtl, defined as:

(2.12) $$Nu = hL/k_f \quad ; \quad Re = \rho uL/\mu \quad ; \quad Pr = \mu c_p/k_f$$

where L and u are a characteristic length and velocity, respectively, and k_f, ρ, μ and c_p are the conductivity, density, viscosity and specific heat at constant pressure of the fluid, respectively. The functional form used is usually of the following type:

(2.13) $$Nu = a\, Re^m Pr^n$$

where a, m and n are experimentally constants.

The heat transmission by convection in engines can be found at any solid-liquid interface, such as between the gas and the walls of the combustion chamber (piston, cylinder head and liner), between the solid parts of the engine and the fluid coolant (where the possible cooling function of the lubricating oil is also included), between the intake air or the exhaust gases and the walls of their respective manifolds, and finally between the external surface of the engine and the environment. In addition, convection is also present in the heat exchangers and their auxiliary circuits. When the engine is running, convection is forced in practically all cases.

2.4.1.2 Characterization of the radiation

There are two sources of radiative heat transfer within the cylinder: the high temperature burned gases and the soot particles in the diesel engine flame. In a spark-ignition engine, the flame propagates across the combustion chamber from the point of ignition through previously mixed fuel and air. Although the flame front is slightly luminous, all the chemical intermediaries in the reaction process are gaseous. Combustion is essentially complete early in the expansion stroke. In the compression-ignition engine (and in fuel-injected stratified-charge engines), most of the fuel burns in a turbulent diffusion flame as fuel and air mix. There can be many ignition locations, and the flame conforms to the shape of the fuel spray until dispersed by air motion. The flame is highly luminous, and soot particles (which are mostly carbon) are formed at an intermediate step in the combustion process.

The radiation from soot particles in the diesel engine flame is about five times the radiation from the gaseous combustion products. Radiative heat transfer in conventional compression-ignition engines is small in comparison with convective heat transfer. However, radiative heat transfer in diesel engines is not negligible; it contributes 20 to 35 percent of the total heat transfer and a higher fraction of the maximum heat-transfer rate.

Radiation from gases

The gases absorb and emit radiation in narrow wavelength bands rather than in a continuous spectrum as the solid surfaces. The simplest gas molecules such as H_2O and N_2 are essentially transparent to radiation. Of the gases important in combustion, CO, CO_2, and H_2O emit sufficient energy to justified their consideration. In gases, emission and absorption will occur throughout the gas volume. These processes will be governed by number of molecules along the radiation path. For each species, this will be proportional to the product of the species partial pressure p_i, and the path length l. In addition the radiative capacity depends on gas temperature T_g. Thus the emissivity of the gas, ε_g, can be expressed as:

$$\varepsilon_g = \mathrm{f}(T_g, p_1 l, \ldots, p_n l) \tag{2.14}$$

The mean path length for a volume V with surface area A is given with sufficient accuracy by:

$$l = 0.9 \cdot \frac{4V}{A} \tag{2.15}$$

where 4V/A is the mean path length for a hemispherical enclosure.

In recent years, standard methods have been developed for estimating emissivity of the gas for mixtures of CO_2 and H_2O [44]. The estimates for engine combustion gases at peak conditions give ε_g=1 and peak heat fluxes due to gas radiation of order 0.2 MW/m^2. This amounts to 5 percent of the peak convective heat transfer. Since gas radiation is proportional to T_g^4, this radiative flux falls off more rapidly from peak values than convective heat flux and, when integrated over the cycle, can be neglected.

Flame Radiation

Flame radiation is a more complex process because the detailed geometry and chemical composition of the radiating region are not well known. Since the radiation from the optically transparent or nonluminous

flames of engines is small, only the luminous nontransparent flames has been studied where the radiation comes from incandescent soot particles and has a continuous spectrum. Because the particle size distribution, number density and temperature, and flame geometry in a diesel engine are not well defined, flame emissivities can not be calculated from first principles. Direct measurements of flame emissivities are required. Several measurements of the magnitude and spectral distribution of radiation from a diesel engine combustion chamber have been made. The most extensive of these by Flynn [46] in a direct-injection engine used a monochromatic to measure intensity of radiation at seven wavelength. The viewing path cut through the piston crown into the central region of the combustion chamber. As results, Flynn obtained the distribution of energy over the seven wavelengths that was used to reconstruct the complete energy spectrum and to calculate the apparent radiation temperature and optical thickness.

The energy distribution deviated from that of a grey-body model (for which the emissivity is independent of the wavelength), and the monochromatic emissivity was adjusted by the following equation:

$$\varepsilon_\lambda = 1 - \exp\left(\frac{-KL}{\lambda^{1.2}}\right) \tag{2.16}$$

The equation (2.16) combined with the Planck's equation (equation (2.17)) which a spectral emitted by a blackbody is calculated as a result of an apparent radiation temperature and a concentration of particles for the radiant medium, in this case the diesel flame.

$$I_{bb,\lambda} = \frac{2\pi C_1}{\lambda^5\left(e^{\frac{C_2}{\lambda T_R}}-1\right)} \tag{2.17}$$

where $C_1 = 0.59548 \cdot 10^{-16}$ W · m^2 and $C_2 = 1.43879$ cm · K

Figure 2.7 shows sample results for four equivalence ratios at an engine speed of 2000 rpm. The radiation flux has approximately the same shape and time span as the net heat-release rate curve (which was determined from the

cylinder pressure curve). During the period of maximum radiation, the apparent emissivity is 0.8 to 0.9; it then decreases as the expansion process proceeds. In previous experiments on the same engine, instantaneous total heat fluxes had been measured at various locations on the cylinder head [47]. A comparison of radiant and total heat fluxes (both peak and average) showed that the radiation heat flux could be a substantial fraction of the peak heat flux. The average radiant flux is about 20 % of the average total flux: the percentage varies significantly with load.

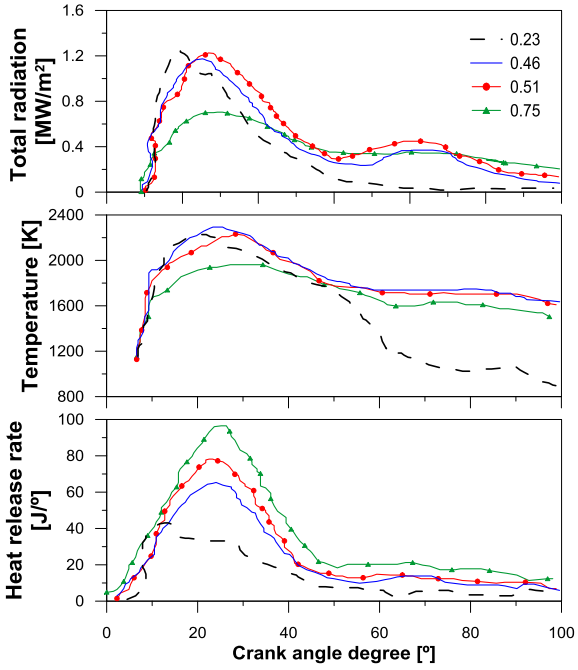

Figure 2.7. Temporal evolution of total radiation, temperature and rate of heat release for DI diesel engine at four different loads.

2.5 Approach of the study

In this section, the thesis approach will be presented. This section is essential to understand the subsequent objectives and studies proposed in the research.

The section begins with an overview about the main problems and challenges that arise from the review of the state-of-art of the soot formation-oxidation process, as well as the contribution of radiation heat transfer phenomenon with respect to the efficiency of the diesel engines. Derived from the challenges of these processes, the justification of the present investigation will be explained.

Once the framework has been justified and clarified, the objectives of this study will be shown along with the general methodology that has been developed to meet the objectives.

2.5.1 Motivation of the study

Internal combustion engines have been very important technology in the development of our society. In 1862, Alphonse Beau de Rochas, a French engineer, described for the first time the basic principle of the four-stroke engine. More than 150 years later, the principle remains the same, although technology has experienced enormous improvements in terms of efficiency, reliability and emissions. Despite the emergence of modern alternative technologies (for example, hybrid and electric engines), spark-ignition and compression-ignition four-stroke engines dominate the transport market, with a slight predominance of diesel in Europe with 53% of the new diesel passenger registered in 2015 [50].

A partial explanation for the dominance of diesel technology comes from one of the inherent properties of the principle of engine operation. In 1892, Rudolf Diesel, its inventor, specifically designed the engine to extract as much power as possible per unit of fuel. In other words, the compression-

ignition engine is, by design, more efficient than the spark-ignition engine. The characteristic that leads to lower fuel consumption, combined with favorable taxes on diesel fuel in most European countries leads customers to prefer compression-ignition engines to spark-ignition engines [50].

Regarding the pollutant regulations from alternative internal combustion engines, there are five legislated emissions for diesel engines: particles matter (PM), nitrogen oxides (NOx), unburned hydrocarbons (uHC), carbon monoxide (CO) and carbon dioxide (CO_2). They are strictly regulated by regulations that vary according to the region in which they apply and condition the market release of road vehicles. Under current trends (Euro 6), diesel combustion is produced with sufficient excess air, so emissions of uHC and CO are typically low. However, the high gas temperatures together with the high compression ratios promote the formation of NOx and its corresponding emission to the atmosphere. In addition, due to the rich local regions of fuel in the combustion chamber, soot particles are emitted.

In diesel engines, there is a "*trade-off*" between the soot and NOx emissions. Reducing emissions of one causes the increase of the other's emissions. A reduction in temperature during combustion, for example with exhaust gas recirculation (EGR), limits the formation of NOx and reduces emissions. However, the soot particle emission increases. After the development and extensive use of diesel particulate filters (DPF), the focus was initially on reducing NOx by reducing the combustion temperature. This resulted in an increase in soot exhaust levels that were counteracted by the efficient after-treatment device. More recently, stricter NOx regulations have led to the widespread use of NOx after-treatment in Europe. The EGR has been reduced to increase the temperatures of the exhaust gases that is beneficial for the operation of the after-treatment and this leads to a new "trade-off" between the soot and the NOx emissions.

There are new concepts for low temperature combustion (LTC), such as homogeneous charge compression ignition (HCCI) or partially premixed combustion (PPC). They focus on reducing NOx and soot emissions through

a higher load premix and a lower oxygen content. However, these new concepts have significant drawbacks in terms of operating range, which is why a better understanding of conventional diesel combustion (CDC) is required.

For most of the operating conditions found in diesel engines, large amounts of NOx are formed at the beginning of the cycle, while soot is characterized by the formation and oxidation process. The soot is generated during the combustion process in those zones with equivalence ratio is very rich and absence of oxygen with high pressure and temperature conditions. The hydrocarbon chain begins to fracture and dehydrogenate, and then it is converted into carbon particles. The sequence of phenomena related to the soot formation: pyrolysis, nucleation and agglomeration. On the other hand, oxidation is a conversion process of a carbon or hydrocarbon in products of combustion such as CO, CO_2 and H_2O. It takes place on the flame surface and can occur during all stages of soot formation. In addition, the temperature must be above 1100 K, because if there is no thermal blockage and the particles formed are not longer oxidized. According to various investigations [40], soot formation is poorly correlated with soot exhaust levels; the quality of the soot oxidation process seems to have a strong impact on the soot emissions emitted into the atmosphere. For this last reason, special attention is needed to the soot oxidation process in DI diesel engines.

Regarding the heat transfer phenomenon in engines, soot is the main responsible for the heat transfer by radiation. Radiation is a heat transfer phenomenon based on the emission of energy by particulate matter that at determinate temperature. The radiation heat transfer, together convection phenomenon, is an important mode of heat transfer in diesel engines. In addition to soot, carbon dioxide and water vapor molecules also radiate energy. However, it is focused on a narrow spectral bands and, therefore, its magnitude is assumed to be smaller than the radiation emitted by the soot particles. In addition, radiation can also be emitted by several intermediate species formed during the combustion process, but as in the case of carbon dioxide and water vapor molecules, their concentration levels are very small

and their effect on the heat transfer by radiation is less important. Therefore, it is the soot radiation which can be considered as a loss of efficiency in modern diesel engines by heat transfer.

In this sense, the heat transfer problem in diesel engines is a phenomenon that has been studied in recent decades. Depending on the operating conditions, the radiation loss values vary widely from 0.5-1% [48] to 5-10% [13] of the total fuel energy can be considered as radiation losses. Not only there is uncertainty in the fraction of radiation of the total energy delivered, but also the contribution of radiation to the total heat transfer also varies. In this case, the range of uncertainty that is ranged from 11% to 40% [13]. The significant differences between authors depend fundamentally on the characteristics of the engine (dimensions of the combustion chamber, injection system, etc.) as well as the operating conditions. In summary, there is currently a knowledge gap in terms of the relationship between the characteristics of the engine together with the operating conditions and the transfer of heat by radiation.

To conclude, the scientific community has not fully understood the complex phenomenon of radiation heat transfer and its contribution to the efficiency of compression ignition engines. Therefore, the research work is focused on contributing to the understanding of heat radiation transfer in DI diesel combustion and, therefore, establish the strategy to optimize the efficiency of the compression-ignition engines, maintaining the emission levels below the limits established by the current pollutant regulations.

2.5.2 Objectives of the study

Considering the limitations found in previous works regarding the contribution of soot particles on the heat radiation transfer in diesel combustion, this research work intends to carry out an extensive analysis whose main objective is *to contribute to the understanding of the radiation heat transfer in DI diesel combustion together with the improvement of the*

knowledge in the soot formation-oxidation processes. In order to achieve this general objective, the following particular objectives are proposed:

- ***Analyze** the **impact** on the **radiation** under **different thermodynamic controlled** conditions in an optical direct injection engine.*
- ***Evaluate** the amount of **radiation energy** respect to the total chemical fuel energy under **real operating conditions** in an HSDI engine.*
- ***Evaluate** the **soot oxidation** process under **real operating conditions** in an HSDI engine obtaining a quantification estimator. In addition, it is intended to compare different engine strategies in order to **improve** the mixture controlled combustion process during the **late-cycle diffusion combustion** and, therefore, improve the soot oxidation process while maintaining constant the indicated efficiency.*
- ***Develop** a **soot radiation model** for DI diesel flames able to predict the heat losses to the chamber walls due to radiation.*

To achieve these objectives, a general methodology has been designed to achieve the suggested objectives.

2.5.3 General methodology of the study

The achievement of the proposed objectives in the previous section requires the implementation of an adequate methodology. This methodology has been ordered in different stages:

Based on a review of the diesel combustion process, in Chapter 2 the processes involved in the soot concentration inside the combustion chamber have been described. To finish, a detailed description has been made of the different mechanisms of heat transmission in the combustion engines, putting special attention to the phenomenon of radiation heat transfer by soot particles.

Once a literature review has been made, in Chapter 3 a detailed description has been performed about the experimental facilities and the theoretical tools used to develop the results of the subsequent result chapters.

In the first chapter of experimental results, Chapter 4, the characterization of the soot radiation process was carried out. For this analysis, an optical direct injection engine has been used. By means of the high speed imaging pyrometer system (HSIP), experimental measurements of spectral intensity emitted by soot has been obtained and subsequently, the total radiation emitted by the soot particles has been calculated. This first study is taken as the basis for the tests carried out on a 4-cylinder GM1.9L light-duty DI engine defined in Chapter 3. The experimental information has been obtained by means of the VisioFEM probe and the procedure to follow is very similar to that carried out in the optical engine, to finally reach the specific radiation results, since for metallic engines without optical access it is not possible to calculate the area of the flame.

Chapter 5 is divided into two results sections: in the first part, the soot oxidation process has been analyzed during the late-cycle diffusion combustion modifying different operating parameters related to the air thermodynamic conditions and the injection process. The experimental measurements have been made in the 4-cylinder GM1.9L light-duty DI engine. In addition to evaluating the effect of the different parameters on the soot oxidation, an experimental model based on the previous experimental measurements has been adjusted in order to evaluate the soot oxidation from two experimental parameters. Regarding the second part of this chapter, the effect of the swirl and an appropriate injection strategy have been evaluated in order to optimize the diffusion combustion process. In this case, the tests have been carried out on the single-cylinder DI engine derived from the GM 1.9L 4-cylinder engine.

In Chapter 6, a model able to predict heat losses by radiation for a spray diesel has been developed. The model is based on three sub-models: spray model, which analyzes and characterizes the internal spray structure

in terms of mixing and combustion process with temporal and spatial resolution. A soot model, in which the results have been justified according to soot formation and oxidation processes. The link of these two sub-models has been used to obtain the input values to the radiation model, which the radiation heat transfer values for a diesel flame are obtained. The adjustment of the constants for the spray and soot model have been made based on experimental results of different optical techniques. However, the radiation simulated by the radiation model has been compared with experimental values from the 2-color method for the same operating conditions.

Finally, in Chapter 7, the main conclusions of the proposed study have been enumerated, highlighting the experimental contributions described throughout the document, as well as the experimental evidences that respond to the proposed objectives for this study. In the same way, from the most relevant points and the uncertainties found in the investigation, a set of future works have been listed.

2.6 Bibliography

[1] Payri F., Olmeda P., Martín J., Carreño R. "A New Tool to Perform Global Energy Balances in DI Diesel Engines". SAE Int. J. Engines 7(1):43-59, 2014.

[2] Heywood J. "Internal combustion engines fundamentals". Estados Unidos: McGraw-Hill Inc.

[3] Micó C. "Development of measurement and visualization techniques for characterization of mixing and combustion processes with surrogate fuels". Doctoral Thesis. Universitat Politècnica de València, 2015.

[4] Arrègle J. "Análisis de la estructura y dinámica interna de chorros Diésel". Doctoral Thesis. Universitat Politècnica de València, 1997.

[5] López J.J. "Estudio teórico-experimental del chorro libre Diesél no evaportivo y de su interacción con el movimiento del aire". Doctoral Thesis. Universitat Politècnica de València, 2003.

[6] García J. M. "El proceso de combustión turbulenta de chorros diésel de inyección directa". Doctoral Thesis. Universitat Politècnica de València, 2004.

[7] Xu Q., Xu M., Hung D., Wu, S. "Diesel Spray Characterization at Ultra-High Injection Pressure of DENSO 250 MPa Common Rail Fuel Injection System". SAE Technical Paper 2017-01-0821, 2017.

[8] Julía J. E. "Analisis de chorros Diesel mediante fluorescencia inducida por láser". Editorial Reverté, S.A., Barcelona, 2006.

[9] Martínez S. "Desarrollo de una instalación experimental para el estudio de chorros diesel evaporativos en atmósfera inerte y reactiva". Doctoral Thesis. Universitat Politècnica de València, 2003.

[10] Browne K. R., Partridge I. M., Greeves G. "Fuel property effects on fuel/air mixing in an experimental Diesel engine". SAE Paper 860223, 1986.

[11] Higgins B.S., Mueller Ch.J., Siebers D. "Measurements of fuel effects on liquid-phase penetration in DI sprays". SAE Paper 1999-01-0519, 1999.

[12] Espey Ch., Dec J.E. "The effect of TDC temperature and density on the liquid-phase fuel penetration in a DI Diesel engine". Transactions of the SAE, Vol. 104 nº 4, pp. 1400-1414, 1995. SAE paper 952456.

[13] Siebers D. "Liquid-phase fuel penetration in Diesel sprays". SAE Paper 980809, 1998.

[14] Dec. J.E., Espey C. "Ignition and early soot formation in a DI diesel engine using multiple 2-D imaging diagnostics". SAE Paper 950456, 1995.

[15] Dec. J.E., Espey C. "Chemiluminescence imaging of autoignition in a DI diesel engine". SAE Paper 982685, 1998.

[16] Higgins B., Siebers D., Aradi A. "Diesel-spray ignition and premixed-burn behavior". SAE Paper 2000-01-0940, 2000.

[17] Kosaka H., Drewes V. H., Catalfamo L., Aradi A. A., Iida N., Kamimoto T. "Two-dimensional imaging of formaldehyde formed during the ignition proces of a diesel fuel spray". SAE paper 2000-01-0236, 2000.

[18] Flynn P. F., Durret R. P., Hunter G. L., Loye A. O., Akinyemi O. C., Dec J. E., Westbrook Ch. K. "Diesel Combustion: An Integrated View Combining Laser Diagnostics, Chemical Kinetics and Empirical Validation". SAE Paper 1999-01-0509, 1999.

[19] Briceño F. "Aportaciones al estudio de la evolución transitoria de llamas de difusion diésel". Doctoral Thesis. Universitat Politècnica de València, 2015.

[20] Dec J. E. "A conceptual model of DI diesel combustion based on laser-sheet imaging". SAE Paper 970873, 1997.

[21] Dec J. E., Canaan R. E. "PLIF imaging of NO formation ina DI diesel engine". SAE Paper 980147, 1998.

[22] García A. "Estudios de los efectos de la post inyección sobre el proceso de combustión y la formación de hollín en motores diésel". Doctoral Thesis. Universitat Politècnica de València, 2011.

[23] Pickett L. M., Siebers D. L. "Soot formation in diesel jets near the lift-off length". International Journal of Engine Research, Vol. 7 nº 2, pp. 103-130, 2006.

[24] Higgins B., Siebers D. "Measurement of the Flame Lift-Off Location on DI Diesel Sprays Using OH Chemiluminiscence". SAE Paper 2001-01-0918, 2001.

[25] Siebers D., Higgins B. "Flame Lift-Off on Direct Injection Diesel Under Quiescent Conditions". SAE Paper 2001-01-0530, 2001.

[26] Musculus M. "Effects of the In-cylinder Environment of Diffusion Flame Lift-Off in a DI Diesel Engine". SAE Paper 2003-01-0074, 2003.

[27] Yan J. Borman G. "Analysis and In-Cylinder Maesurements of Particle Radiant Emissions and Temperature in a ÇDirect Injection Diesel Engine". SAE Paper 881315, 1988.

[28] Siebers D.L., Pickett L.M. "Injection Pressure and Orificie Diameter Effects on Soot in DI Diesel Jets". THIESEL 2002: Conference on Thermo- and Fluid Dynamic Processes in Diesel Engines.

[29] Pickett L.M., Siebers D.L. "Non-Sooting, Low Flame Temperature Mixing-Controlled DI Diesel Combustion". SAE paper 2004-01-0139, 2004.

[30] Pickett L.M., Siebers D.L. "Soot in diesel fuel jets: effects of ambient temperature, ambient density and injection pressure". Combustion and Flame, Vol. 138, pp. 114-135, 2004.

[31] Tree D.R., Svensson K.I. "Soot processes in compresion ignition engines". Progree in Energy and Combustion Science, Vol. 33, pp. 272-309, 2007.

[32] Pickett L.M., Siebers D.L. "An investigation of diesel soot formation process using micro-orifcies". Proceedings of the Combustion Institute, Vol. 29, pp. 655-662, 2002.

[33] Singh S., Reitz R., Musculus M. "2-Color Thermometry Experiments and High-Speed Imaging of Multi-Mode Diesel Engine Combustion". SAE Paper 2005-01-3842, 2005.

[34] Siebers D.L., Higgins B., Pickett L.M. "Flame Lift-Off on Direct-Injection Diesel Fuel Jets: Oxygen Concentration Effects". SAE paper 2002-02-0890, 2002.

[35] Smith O. I. "Fundamentals of Soot Formation in Flames with Application to Diesel Engine Particulate Emissions". Prog. Energy Combust. Sci., Vol. 7, pp. 275-291, 1981.

[36] Nagle J. and Strickland-Constable R. F. "Oxidation of Carbon between 1000-2000 °C". Fifth Carbon Conference, Pergamon, Oxford, Vol. 1, pp. 154-164, 1962.

[37] Haynes B. S., Wagner H.G. "Soot formation". Prog. Energy Combust. Sci., Vol. 7, pp. 229-273, 1981.

[38] Park C., Appleton J.P. "Shock-Tube Measurements of Soot Oxidation Rates". Combustion and Flame, Vol. 20, pp. 369-379, 1973.

[39] Glasman I. "Soot formation in combustion processes". Proceedings of the 22nd international symposium on combustion. The combustion Institute, 1988. p. 295-311.

[40] Gallo Y., Li Z., Richter M., Andersson O. "Parameters influencing soot oxidation rates in an optical diesel engine". SAE Int. J. Engines 9 (4), 2016.

[41] Dembinski H., Angstrom H. "Swirl and Injection Impact on After-Oxidation in Diesel Combustion, Examined with Simultaneous Combustion Image Velocimetry and Two Colour Optical Method". SAE Technical Paper 2013-01- 0913, 2013.

[42] Arrègle J., Pastor J.V., López J.J., García A. "Insights on postinjection-associated soot emissions in direct injection diesel engines". Combustion and Flame 154, 448–461, 2008.

[43] Torregrosa A.J., Olmeda P., Martín J., Degraeuwe B. "Experiments on the influence of inlet charge and coolant temperature on performance and emissions of a DI Diesel engine". Experimental Thermal Fluid Science, Vol. 30, pp. 633-641, 2006.

[44] Broatch A., Luján J.M., Ruiz S., Olmeda P. "Measurement of hydrocarbon and carbon monoxide emissions during the starting of automotive DI Diesel engines". International Journal Automotive Technology, Vol. 9, pp. 129-140, 2008.

[45] Soid S., Zainal Z. "Spray and combustion characterization for internal combustion engines using optical measuring techniques. A review". Energy, Vol. 36, pp. 724-741, 2011.

[46] Flynn P., Mizuszwa M., Uyehara O.A., Myers P.S. "Experimental Determination of Instantaneous Potential Radiant Heat Transfer

within an Operating Diesel Engine". SAE paper 720022, SAE Trans., vol. 81, 1972.

[47] LeFeuvre T., Myers, P.S., Uyehara, O.A. "Experimental Instantaneous Heat Fluxes in Diesel Engine and Their Correlation". SAE paper 690464, SAE Trans., vol. 78, 1969.

[48] Skeen S., Manin J. and Pickett L. "Quantitative Spatially Resolved Measurements of Total Radiation in High-Pressure Spray Flames". SAE Technical Paper 2014-01-1252, 2014.

[49] Flynn, P., Mizusawa, M., Uyehara, O., and Myers, P. "An Experimental Determination of the Instantaneous Potential Radiant Heat Transfer within an Operating Diesel Engine". SAE Technical Paper 720022, 1972.

[50] European Commission. Transport. Statistical pocketbook, 2017. https://ec.europa.eu/transport/facts-fundings/statistics/pocketbook-2017_en.

Chapter 3

Experimental and theoretical tools

Content

3.1 Introduction

Once the context that frames the research developed in this work has been described, this chapter accurately describes the facilities, the measurement equipment and the theoretical models that are used to carry out the current research work. The main results obtained are presented in Chapters 4, 5 and 6, responding to the main problems raised as a research topic.

The chapter begins with a description of the experimental facilities that includes the different systems necessary for its correct operation, data acquisition and instrumentation. In the second part, the theoretical tools and the codes that have been used for the adaptation of the experimental results are described. Finally, in the third and last part of the chapter, the optical assemblies used in this thesis are detailed, which focus on the different cameras and auxiliary systems used.

3.2 Experimental tools

The strong experimental nature of the research involves the use of adequate experimental tools to achieve precise and repetitive results. Therefore, the description of the experimental equipment provided in this section gives the reader the exact information about the different systems and procedures used in the experimental testing campaign.

The chapter has been divided into three subsections. The first describes the fuel mass flow measurement system. The second subsection details the main characteristics of the engines used during the research work. The third subsection presents all the systems, auxiliary equipment and instrumentation necessary for the control and operation of the engines and the acquisition of data in the test bench.

3.2.1 Fuel mass flow measurement. Mass flow rate meter.

The equipment used in the present work to determine the instantaneous mass flow is a mass flow rate meter. In particular, the commercial model EVI of the company IAV. The principle of measurement is based on the Bosch method [1]. The selection of this measurement method is based on the comparative analysis carried out by Plazas [2] between the different methods or equipment currently available to measure the injection rate. According to Plazas, the long tube method is the one that offers the best performance in terms of dynamic response and, therefore the most adequate method to measure the relevant temporary gradients that are intrinsically generated at the injection rate, especially at the beginning and at the end.

Figure 3.1 shows an illustration of the mass flow rate meter used. The operation of the system is described as follows. The injector is placed in the cavity at the mass flow rate meter, so that when injecting it fills with fuel the total volume, the pipe plus the tank of the mass flow rate meter circuit. By means of a regulating valve, the fuel is maintained at the desired discharge backpressure, which aims to simulate the backpressure that the fluid finds when it is injected into the combustion chamber and avoids the possible formation of bubbles in the tube. When the injector starts the injection process, it generates a pressure wave that moves at the speed sound from the injector nozzle, right up to the reservoir where it is damped. A piezoelectric sensor records the pressure variation caused by this wave. This main wave can cause secondary waves. Hence, the long tube tries to attenuate the eventual reflected waves so that they do not modify the signal of the main wave as indicated by Payri *et al.* in [3].

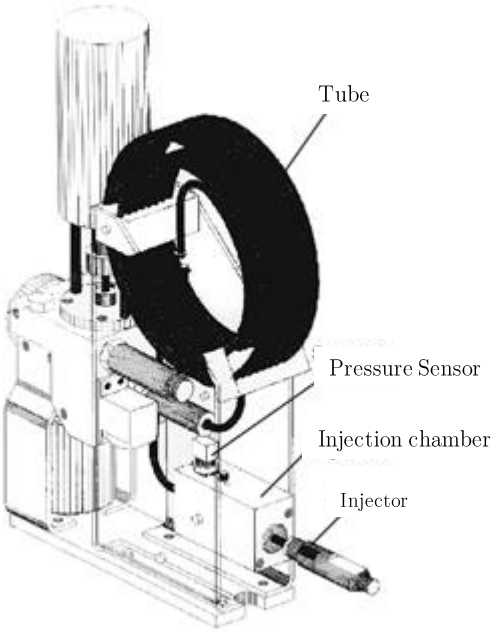

Figure 3.1. Fuel mass flow rate meter developed by Bosch [1]. Long tube method

The theoretical base has been deeply explained by Gimeno [5], but it can be simplified in the following equation:

(3.1) $$\dot{m} = \frac{A_t}{a} \cdot \Delta P$$

The section of the tube is known A_t, the speed sound of the fluid a and ΔP instantaneous from the pressure sensor allow to obtain the injection rate. Finally, in order to obtain a more accurate injection rate, fuel mass flow signal is adjusted by making coincident the integer of the fuel flow mass signal with the fuel mass injected in one injection event. Fuel mass is obtained by using a fuel balance meter located downstream the fuel flow rate meter, following the procedure described by Payri *et al.* [4].

3.2.2 Test bench and engines

Engines and test cell are the most relevant elements of the present investigation. In addition, these elements present a huge complexity from the technological and structural standpoint. The facilities and their auxiliary elements allow the performing of the different tests conducted during the research work.

3.2.2.1 Production 4-cylinder engine

A production-type GM 1.9L Diesel engine was used for the study. The 4-cylinder engine uses a Common-Rail fuel injection system, variable geometry turbocharger (VGT), an exhaust gas recirculation system and an intake throttle valve. The engine has four valves per cylinder, centrally located injectors, and a re-entrant type combustion chamber. The swirl number is variable from 1.4 up to 3 and can be adjusted by a dedicated valve. The engine stock calibration allows meeting the EUROIV standard regulation. Main characteristics of the engine are shown in Table 3.1.

Characteristics	
Type	CI 4-stk, DI
Capacity [cm^3]	1900
Stroke [mm]	90.4
Bore [mm]	82
Compression ratio [-]	17.5
Output Max Power [kW]	110 @ 4000 rpm
Max. Torque [Nm/min^{-1}]	320 @ 2000-2750 rpm
Injection system	Common-Rail Bosch
Injector type	Solenoid
Max. Injection Pressure [bar]	1600
Nozzle diameter [mm]	0.141 (7 orifices)

Table 3.1. Main characteristics of the GM 1.9 L engine.

The engine is directly coupled to a dynamometer, which controls the engine speed as well as the engine load. The dynamometer actuates as an engine when it drives the engine (no combustion operation) or how a generator when it is driven by the engine (during combustion operation). Most relevant characteristics of the dynamometer are summarized in Table 3.2.

Type	dynamometer
Manufacturer	Schenck
Nominal Power [kW]	2200
Nominal Torque [Nm]	562
Max. Speed [rpm]	9000
Min. Speed [rpm]	250

Table 3.2. Main characteristics of the dynamometer.

The in-cylinder pressure is measured with a Kistler 6125C piezoelectric transducer associated to a Kistler 4603B10 amplifier. The crank angle degree resolution is 0.5 CAD and the signal is registered by using a DRIVVEN [6] acquisition system.

Through a low sampling frequency acquisition system are recorded, which are those variables whose instantaneous values during an engine cycle are out of interest.

The system configuration consists of a commercial acquisition software provided by National Instruments and an in-house developed software named as *Samaruc.*

3.2.2.2 Research single-cylinder engine

The research single-cylinder engine (SCE) used during this investigation is a compression ignition (CI) engine fitted with a direct diesel injection (DI) system. The SCE is based in the GM 1.9L commercial engine,

which is fully described in the previous subsection. The engine uses a *Common-Rail* identical to the stock engine configuration. Indeed, the SCE is equipped with two swirl valves at the intake pipes, allowing to vary the swirl effect from 0 to 5. Main SCE characteristics are presented in Table 3.3.

Characteristics	**Values**
Type	CI 4T, DI
Displacement [cm^3]	477
Stroke [mm]	90.4
Bore [mm]	82
Compression ratio [-]	17.1
Output maximum power [kW]	27.5 @ 4000 rpm
Maximum torque [Nm/min^{-1}]	80 @ 2000-2750 rpm
Injection system	Common-Rail Bosch
Injector type	Solenoid

Table 3.3. Main SCE characteristics.

Figure 3.2 presents the scheme of the test cell used to carry out the test campaign on the SCE.

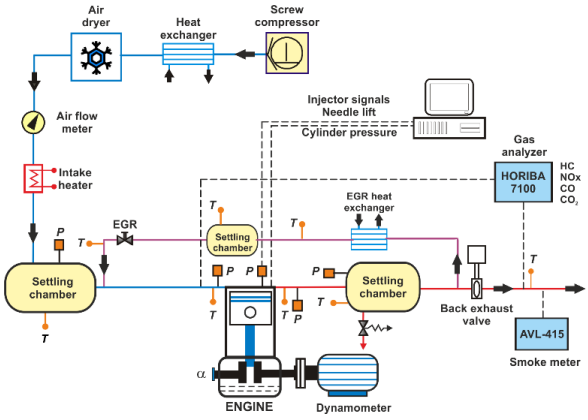

Figure 3.2. Test cell scheme. Auxiliary systems, measurement devices and main sensors location.

As it is possible to observe in Figure 3.2, the test cell is equipped with the SCE, the auxiliary systems such as torque and engine speed control system, air management equipment control, EGR loop and measurement equipment installed. Moreover, the figure shows the general layout of these systems and the main sensors location at the experimental setup, the next subsections describe in detail the different equipment present at the test cell.

3.2.2.3 Single-cylinder optical engine

The optical engine is a two-stroke direct diesel injection SCE (Jenbach JW50), which is fully described in [7]. The displacement of the engine is 3 liters with a stroke of 170 mm and a bore of 150 mm. The SCE was usually operated at 500 rpm. Intake and exhaust pipes are machined at the engine block and the cylinder head is specially designed to provide optical access to the combustion chamber. The cylindrical combustion chamber design avoids the impact between the spray and the chamber walls and contains an orifice at the upper section where it is placed the injector and englobes 4 lateral access sections. One of the access sections is dedicated to the in-cylinder pressure sensor location. The other three sections contain quartz windows with 88 mm in length, 37 mm in width and 28 mm in thickness, as it can be observed in Figure 3.3. Coolant temperature of the cylinder head and the engine block is controlled by using an auxiliary coolant circuit. In this sense, the coolant temperature was set to 353 K for all tests, to ensure good lubricant oil performance.

Equipped with thermoresistances and large volumetric compressors, the installation regulates the intake gas temperature and pressure. Under these conditions, the intake gas can go from air for fundamental combustion studies [8](reactive environment) through nitrogen for studies of the mixing process in the absence of combustion (non-reactive environment)[9][10]. Several investigations are carried out related to the influence of the EGR rate on the combustion process (reactive environment) [11][12].

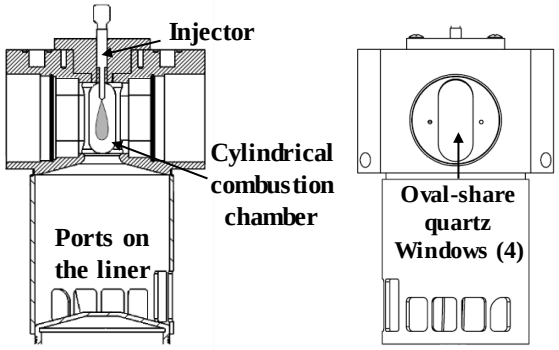

Figure 3.3. Cylinder head and cylinder scheme. a) front view; b) lateral view.

In order to keep in-cylinder conditions constant (pressure and temperature), the engine was operated under *"skip-fire (1/30)"* mode. One injection event takes place every 30 cycles, which guarantees that in-cylinder conditions are not influenced by residual gases from previous combustion cycle.

A *common-rail* Bosch injection system was used, together with a piezoelectric injector and a single-hole 140 μm outlet diameter nozzle. The injected mass was relatively small compared to the volume of air utilized. Hence it can be assumed that the thermodynamic conditions inside the combustion chamber were barely affected by the fuel evaporation. Due to the low injection frequency used during tests, the temperature of the injected fuel can be considered constant during the tests.

3.2.3 Measurement equipment and instrumentation

In the context of experimentation in internal combustion engines (ICE), a test cell is an enclosure equipped with the necessary auxiliary systems and instrumentation. The test cell is in charge of driving the engine into a several of perfectly controlled tests. These tests are performed in order to investigate the different physical-chemical phenomena that occur during the work

(scientific approach), optimize its operation (technological approach) or make a diagnosis about its state (technical approach).

Once the engines are described, the objective of the present subsections is to explain briefly the main instrumentation and the measurement equipment used.

3.2.3.1 Intake and exhaust lines

Before to start the description of both systems, it is very important to note that the intake and exhaust system detailed below is only found in the single-cylinder engine test cells (metallic and optical), since the 4-cylinder engine has a turbocharger, which is in charge of the air charge renewal.

The intake system used in the SCE facility is external. This is aimed to obtain higher flexibility due to this type of facility is dedicated for research purposes. Hence, the desired conditions can be obtained in each of the tests in the most efficient way possible. The purpose of the intake system is to condition the air that is introduced into the engine during the intake process.

Regarding the test facility used in this work, the air intake supply by using a screw compressor (roots) to the desired intake pressure up to 3 bar. The air is conducted into the filter in order to remove impurities that could affect the mixture composition at the combustion chamber causing damage to the different elements such as intake pipes or intake valves. Then, the air moves into a cooler and a dryer in spite of maintaining steady the air conditions through the different tests. Finally, before the air enters the settling chamber that mitigates the oscillations produced by the SCE, the air temperature is adjusted by using a heater governed by a PID (Proportional, Integrative and Derivative) regulator.

The settling chamber is set before the intake manifold and it has a 500 liters volume. This volume is required to avoid the pulsation of the air flow provoked by the pulsation nature of the engine.

The volume of the intake settling chamber must be sufficient to attenuate the pressure waves that are generated due to the strongly pulsating nature of the intake process. In this case, the volume of the settling chamber is 500 liters, which is a value above the minimum admissible calculated both by the Kastner method [13] (477 liters) and by the SAE method J244 [14] (418 liters). In this sense, the pressure waves caused during the air charge renewal process are attenuated, which depending on the engine speed and the geometry of the manifolds, would hinder the filling of the cylinder. The pressure and intake temperature are controlled in the settling chamber by means of a resistive pressure sensor and a thermocouple respectively.

Likewise the intake system, the exhaust system is also an external system. This system aims to expulse the exhaust gases generated during the combustion process. In the same way that the intake system, it has a settling chamber to attenuate the pressure pulses generated during the process of renewal of the air charge, additionally, the pressure can be maintained constant by increasing 0.2 bar the intake pressure. These conditions simulate the backpressure that would generate the turbine of a conventional turbocharged compression ignition engine.

3.2.3.2 Exhaust gas recirculation system

This equipment is usually found at the SCE test facility. The main reason is that 4-cylinder engines have their exhaust gas recirculation (EGR) loop and the optical engines simulates the air mixture with air/nitrogen.

The SCE test cell has an EGR system that extracts gases from the exhaust line and cools them by means of an air-water heat exchanger. Once the EGR flow is cooled, it is introduced into a settling chamber in order to avoid pressure waves. As in the intake system occurs, the average temperature of the EGR gases is controlled by means of a PID acting on a heater. Finally, a pneumatic valve that allows adjusting the percentage of EGR with a precision $\pm$ 0.2% controls the EGR mass flow manually.

For driving the exhaust gases through the intake manifold, it is required that the exhaust pressure is higher than the intake manifold pressure. Therefore, in order to make possible the EGR flow during the engine tests, the pressure differential minimum is 0.2 bar between exhaust and intake pressure.

A scheme of the different elements that form the EGR system is depicted in Figure 3.2.

3.2.3.3 Cooling and lubrication system

In this case, as it has been previous described, the 4-cylinder engine contains the oil and coolant circuits.

Due to the characteristics of the SCE used in the study, the use of systems where the oil and water pumps are driven by the engine will provide an unacceptable increase in mechanical losses taking into account the power delivered by the only combustion cylinder available. On the other hand, the heat generated by a single cylinder is much lower than that which is dissipated in the equivalent 4-cylinder engine and, therefore, it is more difficult to warm the coolant and the lubricant fluid until reaching the appropriate working temperature.

In both SCE, metallic and optical, is needed to use external coolant and lubrication systems. Lubrication system consist of two circuits. Primary one pumps the lubricant (oil) to the engine, actuating as a coolant fluid as well. Secondary circuit sends the oil to the heat exchanger in order to decrease the temperature. At the same time, the oil pressure is controlled in order to guarantee the proper functioning of the lubrication system.

The refrigeration system consists of two circuits with similar operation than the lubrication system. This case uses water as a coolant fluid. Through a PID regulator, it is ensured that the water temperature at the inlet of the

engine is constant in order to have the same temperature conditions in the walls for all the operating points.

In addition, both circuits have specific heaters for liquids conditioning and, during the startup process, they are used to preheat both the coolant and the lubricating oil accelerating the thermal transient until the optimum test conditions are reached. Heaters provide the possibility of warming up the refrigerant fluid and lubricating oil to the working temperature before running the engine, avoiding the problems associated with cold start.

3.2.3.4 Flow mass meter

Before moving to the equipment used to measure the air mass flow description, it should be noted that the measurement of this parameter is absolutely relevant, since from this measurement other derived parameters are calculated, such as volumetric efficiency or equivalence ratio, whose reliability to the extend is imperative for the purpose of this thesis.

The air mass flow measurement is made through a hot wire meter, Sensyflow, marketed by the company Sensycom with an operating range between 0 to 400 kg/h and an accuracy of ± 1% over the measured value [15].

The fuel flow mass is measured by using an AVL 733s gravimetrical balance [16]. Measurement is performed through a capacitive sensor that generates an electrical signal that is function of the instantaneous fuel mass quantity content in a given volume at the AVL equipment (1 liter in this case). The operating range of goes from 0 to 20 kg/h with an accuracy of ± 0.2% of the measured value. In addition, the fuel mass measurement can be obtained by using the air/fuel ratio provided by the exhaust gas analyzer that takes into account the exhaust gases composition and with the fresh air mass flow measurement.

3.2.3.5 Exhaust gas analyzer

Achieving high accuracy and reliability at the exhaust gases measurement is a key point for the present investigation.

Therefore, the experimental set up is equipped with a Horiba MEXA 7100 DEGR model measuring equipment [17]. This device allows to measure the volumetric concentration (molar fraction) of NO plus NO_2 (NOx), CO, total unburned hydrocarbons (uHC), CO_2 and O_2. Although it is evident that O_2 is not a pollutant, knowing its concentration in exhaust gases is important for the analysis of the combustion process and the formation processes of emissions that are contaminants, such as soot.

As it can be observed in Figure 3.2, the exhaust measurement device extracts the exhaust gases by using a probe placed downstream the backpressure valve. This probe drives the exhaust gas sample to the equipment at a constant temperature of 192 °C in order to avoid unburned hydrocarbons condensation.

On the other hand, the intake system equips a second probe at the intake manifold allowing that a small sample of gases could be driven to the measuring equipment. Hence, the volumetric concentration of CO_2 at the intake is measured. Then, together with the measurement of CO_2 at the exhaust, the EGR rate is calculated. In order to homogenize (at least partially) the mixture between the exhaust and intake gases and avoid errors in the measurement of EGR as much as possible, turbulence is generated on the flow by means of a plate finned located at the manifold cross section before taking the sample at the intake. In addition, the intake gas sensor is designed in the form of a cross-arranged transversely to the manifold section and to the flow direction. This probe has ten equally spaced holes in each arm, thus taking the samples radially at different points from the center to the periphery of the manifold.

Table 3.4 present the main characteristics of the exhaust gases analyzed by the HORIBA equipment. More detail is provided in [18][19].

Emission gases	Principle of measurement	Accuracy
CO y CO_2	Non-dispersive infrared analyzer	± 4%
NO y NO_2	Chemiluminescence analyzer	± 4%
THC	Flame ionization analyzer	± 4%
O_2 (exhaust)	Paramagnetic analyzer	± 4%

Table 3.4. Emissions measurement from the HORIBA Mexa 7100DEGR analyzer.

The analyzer is calibrated prior to the tests every new test session starts by using reference gases whose composition is known.

HORIBA equipment calculates the ratio A/F and lambda parameter (λ) by means of an exhaust gas composition method [20].

NO_x, CO y CO_2 concentrations are corrected in order to take account of the ambient humidity that is introduced in the engine with the air intake. These corrections, as well as the volumetric concentration conversion (ppm) to mass flow units (g/h) have been carried out according to the European Directive 2007/46/EC [21], which is in the current directive.

3.2.3.6 Smokemeter

The smokemeter measurement is performed by means of an AVL 415 smokemeter [22].

The measurement principle of the smokemeter consist of passing a simple of exhaust gas through a white paper filter whose reflectance index is known. Then, a photoelectric cell detects the blackening of the paper produced by the exhaust gas flow. Hence, the measurement is based in the reflectance index comparison. The end of scale is between 0 FSN, completely

white case, and 10 FSN, the paper is totally black. The unit used is FSN (Filter Smoke Number).

On the other hand, the aforementioned sample used to perform the measurement is extracted from the exhaust line practically at atmospheric pressure. Thus, the equipment according to the mode of use that is selected (constant time) directly regulates the volume of said sample.

It is possible to convert the opacity (in FSN) into soot mass (in mg/m^3) by using the correlation proposed by Christian *et al.* [23]. This correlation correspond with the equation (3.2).

(3.2) $$Soot\ [\frac{mg}{m^3}] = \frac{1}{0.405} \cdot 4.95 \cdot FSN \cdot e^{(0.38 \cdot FSN)}$$

Finally, another conversion is made between volumetric concentration and soot mass (in mg/kg) at the exhaust gas considering a constant density of 1.165 kg/m^3.

3.2.3.7 Blow-by measurement

During the closed cycle, part of the gases encapsulated in the combustion chamber escapes through the gap between the piston segments and the cylinder walls, which is known as *blow-by*[1]. Having this measure allows to calculate the instantaneous in-cylinder mass with greater precision, which represents a great advantage for the theoretical model application for the combustion process diagnosis.

The blow-by flow rate (in m^3/h) is measured by using a commercial equipment AVL 442 [24]. The operation principle of this equipment is based on the pressure difference generated by the blow-by flow as it flows through a calibrated orifice. For each test, the volumetric measurement flow is

[1] Blow-by: the leakage of gas past the piston of an engine at maximum pressure

converted to units of mass flow (in kg/h) considering the corresponding atmospheric pressure and temperature conditions. The accuracy of this equipment is ± 1.5% of the measured value and allows a maximum flow of 4.5 m^3/h.

The blow-by flow measurement is also used to detect tightness problems in the cylinder related to the wear of the segments, because if this occurs the blow-by increases drastically. In these engines, this control is necessary since the maximum pressure in the cylinder reaches values above 160 bar, which supposes important mechanical stresses.

3.3 Theoretical tools

Although this is an experimental research mainly and the information obtained in the experimental facilities is relevant, it is important to note that a post-treatment of experimental results is needed to better understand and evaluate them. In addition, it is necessary to use codes that allow to increase the information obtained from experimental tests or that simulate processes that are difficult to uncouple in an experimental process.

Therefore, it is necessary to resort to tools that allow the processing of experimental information in order to improve the quality of it or generate additional information through the theoretical tools. Thus, in this section, the different theoretical tools, which have helped in the treatment of experimental information, have been described.

3.3.1 Combustion diagnosis code. CALMEC.

In thestud field of the combustion process in compression ignition engines, it is practically essential to have a suitable thermodynamic diagnostic model that obtain, among other parameters, the heat release law (HRL) and its derivative (RoHR) from the measurement of instantaneous pressure in the combustion chamber.

These models are usually zero dimensional (from a zone especially for the case of diesel engines). The theoretical basis is the application of the first principle of thermodynamics to the control volume constituted by the combustion chamber during the closed cycle, which is the time between the closing angles of the intake valves and the opening angle of the exhaust valves. The most important differences in terms of results are related to the degree of accuracy of the assumed assumptions and to the greater or lesser number of simplifications made during its development.

The diagnostic model used for the present analysis is called CALMEC [25][26][27]. The general starting hypotheses on which this model has been developed are briefly described below, together with a brief discussion on its validity:

- The in-cylinder pressure is assumed uniform. The validity of this condition is generally accepted since the in-cylinder flow velocities and the propagation of the flame are much lower than the speed of sound.
- The fluid in the chamber is considered as an air mixture, gaseous fuel and products burned in stoichiometric conditions. Although this model assumes the uniformity of composition and temperature of the mixture, it is important to note that up to a maximum of three species (air, gaseous fuel and stoichiometrical-burned products) are considered when evaluating the thermodynamic properties of the enclosed mass in the combustion chamber. Considering stoichiometric burned gas as a species is a correct hypothesis when the flame is purely diffusive but arguable when the combustion process takes place in premixed conditions. However, it is considered acceptable to maintain this hypothesis.
- The in-cylinder gas is assumed perfect. Accepting this assumption for air and burned products is reasonable, however, this hypothesis may initially seem debatable when applied to the fuel in a gaseous state. In the study carried out by Lapuerta *et al.* [28], the results generated by a diagnostic model similar to the one used in the present work are

compared assuming different state equations for the gaseous fuel. The results confirm that the differences in average temperature and HRL are relatively small, although they may be relevant if the results are used to predict the formation of polluting emissions.

Assuming this set of hypotheses, the CALMEC model proposes the resolution of the first principle of thermodynamics applied to open systems, since it is thus possible to consider the fuel flow and blow-by. In this way, the equation (3.3) is solved in calculation intervals determined by the angular resolution of the instantaneous pressure measurement.

$$\Delta HRL = m_{cil} \cdot \Delta U_{cil} + AQ_w + p \cdot \Delta v - \left(hf_{iny} - u_{f,g}\right) \cdot \Delta m_{f,evap} + R_{cil} \cdot T_{cil} \cdot \Delta m_{bb} \quad (3.3)$$

Next, the different energy terms considered by the diagnostic model in each interval have been described:

ΔHRL: This term corresponds to the thermal energy released by the fuel, assuming constant heat power throughout the combustion process.

$m_{cil} \cdot \Delta U_{cil}$: This term is the one corresponding to the internal energy variation experienced by the gas enclosed in the control volume, which as detailed in the work of Lapuerta *et al.* [27] is calculated using specific correlations for each species. In each calculation interval, these correlations are solved according to the average temperature inside the control volume at each moment and weighted by the mass fractions of each species.

AQ_w: This next term represents the heat transmission between the gas enclosed in the control volume and the surfaces of the piston, the cylinder, the cylinder head and the valves (the model does not contemplate the possibility of fuel liquid adhering to the walls). The instantaneous heat transfer coefficient between the gas and the walls is based on the classic Woschni proposal [29]. For the calculation of the wall temperatures a nodal heat transfer model is used [30][31][32].

$p \cdot \Delta v$: This term indicates total work performed by the gas enclosed within the control volume during the calculation interval. For the calculation of the instantaneous volume in the combustion chamber, a mechanical deformation model is available which considers both the pressure force exerted by the gas on the piston head and the inertial forces generated by the reciprocating masses.

$\left(hf_{iny} - u_{f,g}\right) \cdot \Delta m_{f,evap}$: This term includes all the energy considerations associated with the fuel injection process [33]. Thus, this term considers the flow work, the heat sensible energy absorbed by the liquid fuel until reaching the evaporation temperature, the heat latent energy due to this evaporation process and the fuel heating in vapor phase until reaching the average temperature of the combustion chamber.

$R_{cil} \cdot T_{cil} \cdot \Delta m_{bb}$: Finally, the energy that loses control volume due to blow-by flow through the segments is considered. The mass flow of blow-by is calculated using an isentropic model to simulate the evolution of the gas as it circulates from the combustion chamber to the crankcase through the segments.

The most important results obtained after processing of CALMEC model are the HRL and its derivative or RoHR (rate of heat release). However, a series of injection-combustion parameters are also calculated, which have an average results, such as, for example, the indicated mean effective pressure, the start of combustion, the CA50[2], among others. All of them allow knowing and studying in a better way the combustion process that is developed in this investigation.

[2] CA50: Crank angle degree at which 50 % of the heat from combustion has been released.

3.3.2 1-D spray modelling. DICOM

Currently there are different fluid dynamic calculation tools that allow describing temporal and spatial internal spray structure of an injection process in order to characterize the mixing process. These tools range from complex computational fluid dynamics models (known as 3D CFD models) to more simplified models where different hypotheses are involved. The choice of the model depends on the complexity of the problem to be solved and the available calculation time mainly.

In the present work of investigation has chosen to use a one-dimensional model Euleriano 1D called DICOM (developed by the department of Máquinas and Motores Térmicos of the Universitat Politècnica de València) to reproduce the evolution of the spray diesel in steady and/or transitory, in inert conditions (evaporative or non-evaporative) as well as reactive.

A deeper description together with the validation of this model for inert conditions can be found in the work by Pastor *et al.* [34], whereas Desantes *et al.* [35] do the same for reactive conditions.

This model is an approach to the problem of a spray fuel injected through a hole inside the chamber where it is mixed with the ambient gas and eventually the combustion process takes place. The spray evolves freely without any spatial restriction and the chamber volume is sufficiently large so that the spray evolution does not modify the air conditions located sufficiently far from it.

In addition to fuel, the model requires the injection rate and the momentum flux obtained from experimental data. Thermodynamic conditions of the air present in the combustion chamber, the number holes and nozzle diameter and spray angle have been evaluated experimentally. They are introduced as input parameters in the DICOM model.

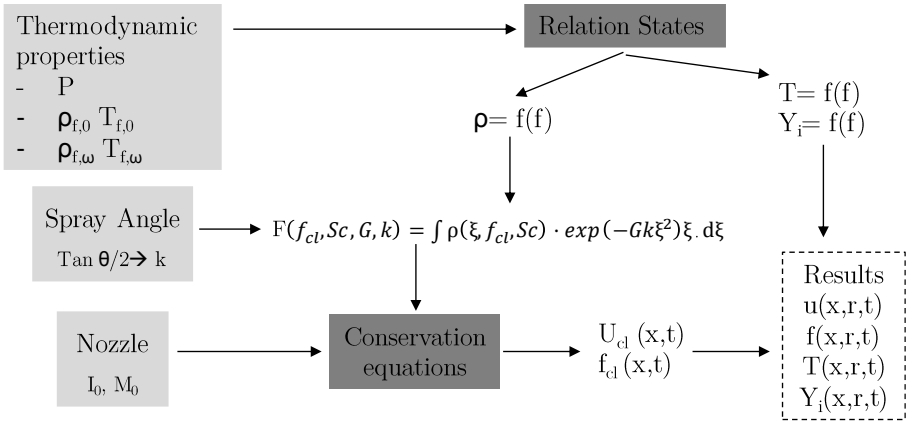

Figure 3.4. Main scheme of the DICOM code

As a conceptual model scheme, Figure 3.4 shows its main inputs and outputs, and the main assumptions that are assumed in this model are listed below. These hypotheses are widely described in García [36].

- The spray is considered axisymmetric. Therefore, it is not considered in any case the swirl movement in the ambient gas.
- The flow is turbulent with the turbulence fully developed. By means of this hypothesis, it is possible to assume self-similar radial profiles of Gaussian type for the conservative variables that define the problem.
- The flow is locally homogeneous.
  As previously mentioned, this hypothesis is reasonable in the current diesel sprays.
- The pressure is constant throughout the domain including the spray. The effects associated with compressibility phenomena are neglected.
- The local density is calculated assuming ideal mixture. The effects associated with compressibility phenomena are neglected.

The main information obtained from this model respect to the proposed objectives consists in the prediction of the total spray penetration, the estimation of the liquid length and the mass fraction of evaporated fuel, together with the temporal evolution of the local equivalence ratio distribution of the spray. In summary, DICOM is an interesting tool to carry out the studies on the phenomenological of the air-fuel mixture process, and how this is influenced by variations in the thermodynamic conditions of the ambient gas.

3.3.3 Chemical kinetic calculation code. CHEMKIN

In the present work, the autoignition process will be evaluated under different conditions, using chemical-kinetics mechanisms available in CHEMKIN tool [37], widely used by the scientific community.

CHEMKIN tool includes several models that can be connected to solve complex chemical kinetics problems. All models need to know the details of the kinetic mechanism that is intended to be used, such as the species considered and their properties (heating value, enthalpy, etc.), as well as the reactions included and their kinetic constants. For this, a preprocessor reads the files of the reaction mechanism and generates an intermediate file that has all the information in a predetermined order so that it can be consulted by the rest of the routines. Both the kinetic mechanism and the associated thermodynamic data must have a certain format, although the use of CHEMKIN is so widespread that its format has become a standard. The data of the kinetic mechanism together with the definition of the problem to be solved, which must be introduced by means of a graphical interface, allow the construction of the differential equations system that describes the problem. Later, this is solved by the appropriate resolution system, and the results of the kinetic problem are stored in compressed files. The post-processor reads these files and shows the user the demanded variables both in graphic format and in data files.

In this research work, a zero-dimensional model has been selected, since it allows simulations with a reasonable calculation time. Indeed, several authors such as Currant *et al.* [38][39] have demonstrated the validity of this kind of models to simulate the kinetics prior to autoignition as well as to predict the ignition delays. However, the use of a zero-dimensional model to predict other variables that are very sensitive to the mixture heterogeneity, such as the rate of heat released, the pollutant emission or the combustion duration. Taking into account that premixed combustion with homogenous load is controlled mainly by the kinetic-chemical phenomena, it is advisable to use reaction mechanisms that describe the oxidation process in detail. The mechanism used has been the Jerzembeck´s [40] that has 203 species and more than 1000 reactions. In addition, the substitute fuel of Diesel has been n-heptane. Figure 3.5 shows a general outline of the chemical kinetics evaluation process using the CHEMKIN code.

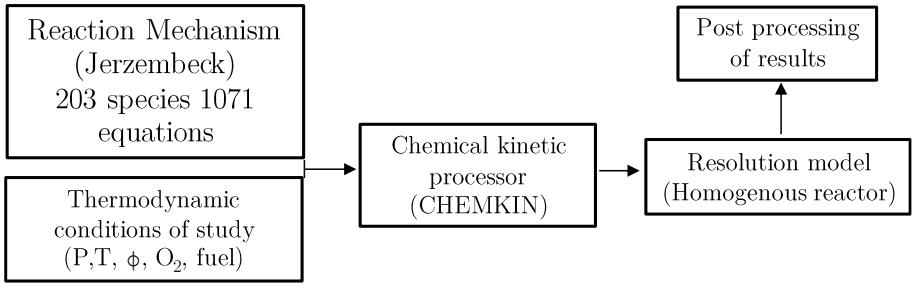

Figure 3.5. General scheme of the CHEMKIN code resolution process

The model used in this work is that of homogeneous reactors that includes the aforementioned program. This model solves the evolution over time of the species concentration and the temperature of a homogeneous mixture contained in a closed reactor. All the executions carried out in this work use this model, for which a constant reactor volume and an adiabatic evolution are considered (the program also allows to consider the constant pressure or to provide a temperature profile and suppose the existence of heat losses). When considering the mass balances, equations similar to the equation (3.4) are obtained where ρ is the density of the blend, Y_i the species

mass fraction, ω_i the species net production rate and MW_i its molecular weight.

(3.4) $$\frac{dY_i}{dt} = \frac{\omega_i \cdot MW_i}{\rho}$$

With the energy balance, the expression (3.5) is constructed, where m_i y u_i represent the mass and the internal specific energy of the specie i, p is the pressure, v the volume of the reactive mixture and Q_w is the heat losses from the wall.

(3.5) $$\frac{d}{dt}\left(\sum_{i=1}^{I} m_i \cdot u_i\right) = -p \cdot \frac{dv}{dt} - Qw$$

When developing the integral and reorganizing terms, the following expression is obtained:

(3.6) $$m \cdot \sum_{i=1}^{I} Y_i \frac{du_i}{dt} = -\sum_{i=1}^{I} u_i \frac{dm_i}{dt} - p \cdot \frac{dv}{dt} \cdot Qw$$

Finally, considering the mixture behavior in the reactor as perfect gas, constant volume and adiabatic process, the equation (3.7) is obtained, where ρ is the density and c_v the specific heat at a constant volume of the mixture.

(3.7) $$\rho \cdot c_v \cdot \frac{dT}{dt} = \sum_{i=1}^{I} u_i \cdot \omega_i \cdot PM_i$$

Therefore, the model is defined with a system with I + 1 equations (composed of I mass balances and one energy), being the boundary conditions necessary to solve the system the composition and initial temperature of the mixture (both introduced through the program interface).

3.4 Visualization techniques. Two-color method

This section describes the experimental optical technique used in the different studies presented in the thesis. The objective is to show the reader in more detail both the assemblies and the technique for a better

understanding of the various studies that will be presented in the subsequent chapters.

3.4.1 Two-color method

Radiation diesel flame from the end of the premixed combustion phase to almost the end of the combustion process is dominated by the phenomenon of soot incandescence. The soot particles that appear inside the flame are at a temperature practically equal to the gas environment them[3], emitting thermal radiation as a body at this elevated temperature. Due to the temperature range that appears inside the flame (700-2800 K according to [36]), the soot radiation is more intense than that in other present species (H_2O, OH, CO_2) that emit by the phenomenon of chemiluminescence. Thus, images taken from the diesel combustion process using conventional visualization techniques, which employ cameras in the visible wavelength range, are radiation images of the soot present in the flame[4].

The starting point of the two-color method is the assumption that the radiation from a soot flame received by a point observer depends on the wavelength, the temperature and the soot concentration present in it. Mathematically, this assumption can be formalized the following equation:

$$I_{soot}(\lambda, T, KL) = \varepsilon(\lambda, KL) I_{bb}(\lambda, T) \tag{3.8}$$

which indicates that the radiance of the soot I_{soot} is proportional to the radiance I_{bb} that would emit a blackbody at the same T and wavelength λ,

[3] Matsui [41] estimates a difference lower than 1 K between the soot and the gas.

[4] The orange color of combustion processes due to diffusion is characteristic due to the range of temperatures in which it is emitted.

weighted by an emissivity ε that depends on the wavelength and the amount of soot. From Planck's Law it follows that, for the black body:

(3.9) $$I_{bb}(\lambda,T) = \frac{1}{\lambda^5}\,\frac{c_1}{\left[exp\left(\frac{c_2}{\lambda T}\right)-1\right]}$$

where c_1 y c_2 are constants with the values $c_1 = 1.1910439 \cdot 10^{-16}$ Wm^2/sr and $c_2 = 1.4388 \cdot 10^{-2}$ mK.

To understand the dependence between emissivity and amount of soot, it is necessary to take into account where this radiation comes from. In a solid body, thermal energy is radiated from the surface of the body. There is a clear location from the starting point of it. The flame can be a continuous distribution of small particles. According to this treatment, the radiation originated in it comes not only from the soot located in the outer part of the flame, but also from the radiation emitted by the soot that is inside of flame, and that tends to come out by the surface after a series of absorption and dispersion processes. It is possible to consider a certain degree of transparency in the flame, which depends on the amount of soot present in the optical path and which determines in what proportion the radiation is influenced by the particles of the flame.

The flame is a semitransparent volume, in which the origin point of the radiation is not known exactly. In this sense there are two interesting limits that should be taken into account. The first is optically thick flame. This occurs if the soot concentration is very high, so that the flame is assimilable to a solid surface, and the soot radiation comes mainly from the particles located on outside of the flame. The other limit is given when the flame has a low soot concentration so that the radiation from the opposite side of the flame crosses it completely and contributes to the one that reaches the receiver. In this case, the optical path traveled by the radiation includes the entire flame thickness. Both limits can be given simultaneously in the same flame, depending on the receiver's point of view.

According to the laws of small particle optics, if the soot distribution (volumetric fraction) and temperature are uniform along the optical path, and the propagation mechanism of the absorption radiation dominates over that of dispersion. The flame emissivity can be quantified by the following expression:

$$\varepsilon\,(\lambda, K_{abs}, L) = 1 - exp(K_{abs}(\lambda) \cdot L) \tag{3.10}$$

where L is the optical path of radiation and K_{abs} is the soot absorption coefficient, which is an explicit function of the wavelength, the average volumetric soot fraction and the optical properties.

In the two-color method, the use of a simple empirical expression for the absorption coefficient is more usual, $K_{abs}\,(\lambda) = (k_{soot} / \lambda^{\alpha})$, obtained by Hottel and Broughton [42], where k_{soot} would be proportional to the volumetric soot fraction along the optical path, and α is an empirical constant. In this way, the emissivity remains the following expression:

$$\varepsilon\,(\lambda, K_{abs}, L) = 1 - exp\left(\frac{k_{soot}}{\lambda^{\alpha}}\right) = 1 - exp\left(\frac{KL}{\lambda^{\alpha}}\right) \tag{3.11}$$

Due to the above-mentioned uncertainties regarding the radiation origin, it is usually used as a variable to define the soot amount $KL = k_{soot} \cdot L$, that would be proportional to the volume soot fraction and the optical path by the radiation. The value of α depends on parameters such as the wavelength, the size of the soot particles or the refractive index. Zhao and Ladommatos [43] collect the values of this parameter proposed by various authors, recommending the use of a value of 1.39, which is valid for most fuels if wavelengths of the visible spectrum are used. It is precisely in this spectral range that the solution is little sensitive to the value of α taken.

Taking into account the expression for emissivity, the soot radiation would be quantified by the expression:

$$I_{soot}\,(\lambda, T, KL) = \left[1 - exp\left(\frac{KL}{\lambda^{\alpha}}\right)\right] \cdot \frac{1}{\lambda^{5}} \frac{c_1}{\left[exp\left(\frac{c_2}{\lambda T}\right) - 1\right]} \tag{3.12}$$

with a dependence of three parameters: wavelength, temperature and soot concentration. The two-color method allows obtaining the two parameters of interest (temperature and soot concentration) from two measurements of radiation at different wavelengths. As can be seen, the foundation is simple, and the instrumentation is not highly complicated either, which is why it has been used for the study of the Diesel flame for decades [44][45].

The implementations of the two-color method can be divided into two groups, depending on the data acquisition system employed:

- First, *point systems*, in which a photodiode is used as a radiation sensor. The optical access is reduced, and the dynamic response of the system is high, allowing to collect radiation data of all cycles. However, the recorded signal is an integration of the radiation. There is no spatial resolution, an aspect of importance to know the structure of the diesel flame.
- In contrast to the previous system, the recording of images allows obtaining information with spatial resolution. A suitable optical system can be used to record two identical images, but with different spectral information, so that they can be processed and obtain temperature and KL maps. Thus, the image is considered as a set of point sensors, in which one picks up a particular radiation signal from a spatial location.

3.4.1.1 High Speed Imaging Pyrometer

This system consists of two high-speed cameras equipped with a lens and a stereoscopic optical system, which allows obtaining two images of the flame with different spectral information. A control system allows a computer to acquire images synchronized with the engine.

The chosen wavelengths belong to the visible range. In particular $\lambda_1 =$ 550 nm (green) y $\lambda_2 = 650$ nm (red). As Zhao and Ladommatos [43] indicate,

in this spectral range, the soot concentration obtained is not very sensitive to the parameter value α, which does not happen if infrared lengths are selected. It is considered that the interference filters allow only the wavelength of interest to pass through. Actually, these filters have a certain bandwidth (10 nm FWHM in this case), an aspect that should be taken into account. Vattulainen *et al.* [46] indicates that taking into account this bandwidth does not improve the results at all. Di Stasio and Massoli [47] show an exhaustive sensitivity analysis of the method. This study show the influence of a 10 nm spectral bandwidth. It is less than 10 K in 2250 K (0.4%) in temperature, and less than 1% in the KL measurement.

Figure 3.6 presents an image of the optical system. The light emitted by the flame pass through a beam splitter, which transmits and reflects 50% of the soot radiation to each of the two High-Speed CMOS cameras employed: a *Phantom V12* for 650 nm and *Photron SA5* for 550 nm. Both cameras were equipped with a 100 mm focal length and f/2 lens. In order to ensure frame-to-frame synchronization, both cameras were connected in a Master/Slave mode. They were set to record at 15000 fps (frame by second), with 5 to 8 µs exposure time for 650 nm and 8 to 12 µs for the 550 nm, depending on test conditions.

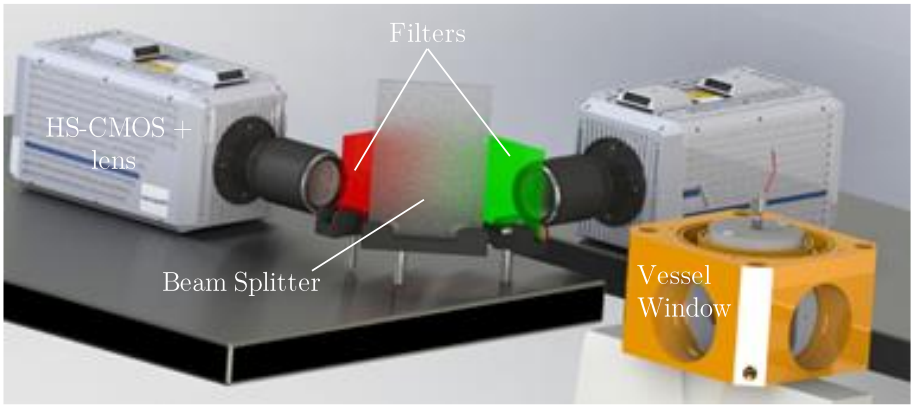

Figure 3.6. High Speed Imaging pyrometer Set-up

Once both images have been registered with both high-speed cameras, it becomes necessary for a post-processing to filter and couple both images as explained in detail in [36]. Once the images have been coupled, by applying the equation (3.12) for each wavelength, results of temperature and soot concentration are obtained. Figure 3.7 shows a color composition for the natural luminosity emitted by the soot, together with the calculated maps of soot concentration and temperature.

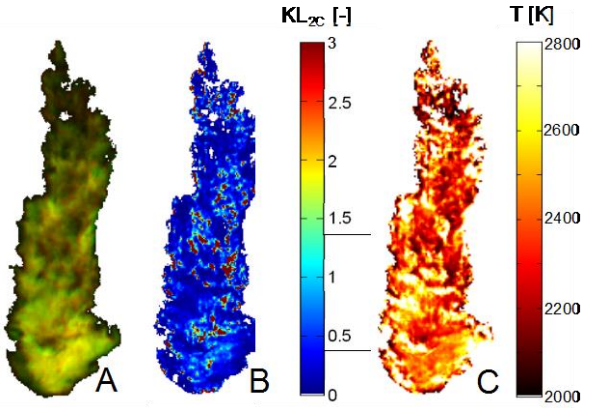

Figure 3.7. Natural luminosity composition emitted by the soot at 550 and 650 nm (A) and their respective KL distribution (B) and temperature (B).

3.4.1.2 Optoelectronic probe

The in-cylinder soot radiation measurements were also performed with an optoelectronic signal converter with a selection of photodiodes and narrow band optical filters adapted to specific applications for combustion engine flame and radiation measurement. This light probe has been developed by AVL and is known as VisioFEM. The operating scheme of the optoelectronic probe is shown in the Figure 3.8. A sapphire lens at the tip of the probe captures the light from the combustion chamber with a view angle of 90°. The soot radiation is conducted through optical fibers and split to two filters at wavelengths of 600 and 950 nm. Then, the photodiodes convert the intensity to a voltage signal. The signals from the photodiodes are amplified

and recorded every 0.5°CAD. From the voltage signal, the spectral intensity emitted by the soot is obtained from the following equation:

$$I_{soot}\left[\frac{W}{m^2 \cdot m \cdot sr}\right] = \frac{Voltage\ signal[V] \cdot Sensitivity\left[\frac{W}{m^2 \cdot m \cdot sr \cdot V}\right]}{Gain \cdot Transmissivity} \tag{3.13}$$

where I_{soot} is the spectral intensity of the soot, the voltage signal is measured experimentally for the wavelengths of 600 and 950 nm, the sensitivity is a constant given by the manufacturer and the gain is selected as a function of the light intensity avoiding the saturation of the signal.

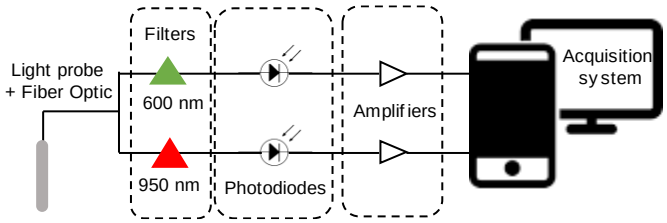

Figure 3.8. Optoelectronic probe operation set-up

Once both voltage signals are recorded, spectral intensity is obtained considering gain, transmission and sensitivity. Thus, once the voltage signal are converted, equation (3.12) is applied for each wavelength and KL and temperature can be obtained at each instant. It is interesting to remark that with the Optoelectronic probe only temporal resolution is obtained for the soot temperature and KL results.

Finally, Figure 3.9 the optical configuration is represented when the optoelectronic probe is used in the optical engine (left) and the metallic engine (right).

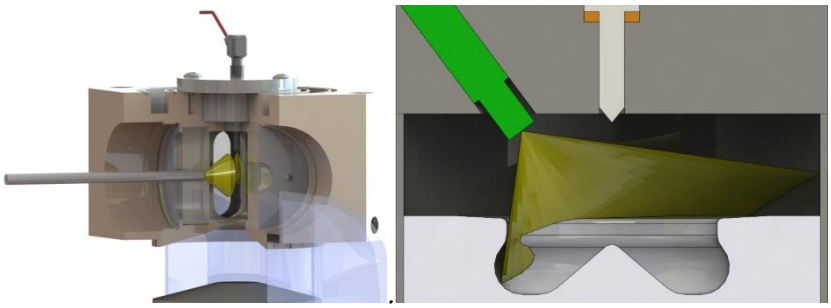

Figure 3.9. Optoelectronic probe implementation at the optical engine (left) and the metallic engine (right)

3.5 Conclusions

In this chapter, the experimental and theoretical work tools have been presented, as well as the optical assemblies that have been used in the investigation.

In the section dedicated to experimental tools, special emphasis has been placed on the characteristics of the different elements that make up the three engines used during this thesis, both production and research, together with the test cells. The instrumentation dedicated to controlling and acquiring the experimental results has been specially detailed.

Regarding the section dedicated to theoretical tools, the main assumptions assumed by the different theoretical models have been emphasized, since these are the ones that establish their main limitations. It has also indicated the application to which it is going to allocate each of them based on their characteristics.

Finally, in a last part, the optical technique and the optical systems used in the research have been developed.

3.6 Bibliography

[1] Bosch, W. "Fuel rate indicator is a new measuring instrument for display of the characteristics of individual injection". SAE Paper 660749, 1966.

[2] Plazas, A.H. "Modelado unidimensional de inyectores common-rail Diesel". Doctoral Thesis. Universitat Politècnica de València, 2005.

[3] Payri, R., Salvador, F.J., Gimeno, J., De la Morena, J. "Effects of nozzle geometry on direct injection diesel engine combustion process". Applied Thermal Engineering, Vol. 29, Issue 10, pp. 2051-2060, 2009.

[4] Payri, R., García, A., Domenech, V., Durrett, R., Plazas,A H. "An experimental study of gasoline effects on injection rate, momentum flux and spray characteristics using a common rail diesel injection system". Fuel, Vol. 97, pp. 390-399, 2012.

[5] Gimeno, J. "Estudio de la inyección Diesel mediante la medida de flujo de cantidad de movimiento". Barcelons: Editorial Reverté S.A, 2011.

[6] DRIVVEN Stand Alone Direct Injector Driver System User's Manual October 2010. Drivven, INC. 12001 Network Blvd, 110. San Antonio, Texas 78249.

[7] Pastor, J., García, J., Pastor, J., and Buitrago, J. "Analysis Methodology of Diesel Combustion by Using Flame Luminosity, Two-Colour Method and Laser-Induced Incandescence". SAE Technical Paper 2005-24-012, 2005.

[8] García J. M. "Aportaciones al estudio del proceso de combustión turbulenta de chorros en motores Diesel de inyección directa". Doctoral Thesis. Universitat Politècnica de València, 2004.

[9] Nerva J. G "An assessment of fuel physical and chemical properties in the combustion of a Diesel spray". Doctoral Thesis. Universitat Politècnica de València, 2013.

[10] Pastor J. V., Payri R., García J. M., Briceño F. J., "Analysis of transient liquid and vapor phase penetration for diesel sprays under

variable injection conditions". Atomization and Sprays, Vol. 21, pp. 503-520, 2011.

[11] Monin, C., "Caracterización del proceso de formación de hollín en una llama de difusión Diesel de baja temperatura". Doctoral Thesis, Universitat Politècnica de València, 2009.

[12] de la Garza O. "Estudio de los efectos de la cavitación en toberas de inyección Diesel sobre el proceso de inyección y el de formación de hollín". Doctoral Thesis, Universitat Politècnica de València, 2012.

[13] Kastner L. "An investigation of the airbox method of measuring the air consumption of internal combustion engines". Proceedings of the institution of mechanical engineers, Vol. 157, pp. 387-404, 1947.

[14] Measurement of intake air or exhaust gas flow of Diesel engines. SAE Standards J244, 1992.

[15] Información técnica de producto Sensyflow. Obtenido de http://www.abb.com.

[16] Información técnica de producto AVL 733 fuel balance. Obtenido de http://www.avl.com

[17] Horiba MEXA 7100 DEGR exhaust gas analyzer. Información técnica disponible en http://www.ats.horiba.com.

[18] Martyr A.J. y Plint M.A. Engine testing: Theory and practice, 3 Ed. Elsevier Science and Technology Books, Butterworth-Heinemann, 2007.

[19] Instrumentation and techniques for exhaust gas emissions measurement". SAE Standards J254, 1993.

[20] Silvis W. M. "An algorithm for calculating the air/fuel ratio from exhaust emissions". SAE Paper 970514, 1997.

[21] "Regulation (EC) No 595/2009 of the European Parliament and of the Council of 18 June 2009 on type-approval of motor vehicles and engines with respect to emissions from heavy duty vehicles (Euro VI) and on access to vehicle repair and maintenance information and amending

Regulation (EC) No 715/2007 and Directive 2007/46/EC and repealing Directives 80/1269/EEC, 2005/55/EC and 2005/78/EC". *Official Journal of the European Union,* Vol. 52 no L275, pp. 1-14, 2009.

[22] Technical information of AVL 415 Smoke meter. Obtained in http//www.avl.com

[23] Christian R., Knopf F., Jasmek A. y Schindler W. "A new method for the filter smoke number measurement with improved sensitivity". MTZ Motortechnische Zeitschift, Vol. 54, pp. 16{22, 1993.

[24] AVL 442 blow-by meter. Información técnica disponible en http://www.avl.com.

[25] Lapuerta M. "Un modelo de combustión fenomenológico para un motor Diesel de inyección directa rápido". Doctoral Thesis, Universitat Politècnica de València, 1988.

[26] Armas O. "Diagnóstico experimental del proceso de combustión en motores Diesel de inyección directa". Doctoral Thesis, Universitat Politècnica de València, 1998.

[27] Lapuerta M., Armas O., Hernández J.J. "Diagnosis of DI Diesel combustion from in-cylinder pressure signal by estimation of mean thermodynamic properties of the gas". Applied Thermal Engineering, Vol. 19 nº 5, pp. 513-529, 1999.

[28] Lapuerta M., Ballesteros R., Agudelo J.R. "Effect of the gas state equation on the thermodynamic diagnostic of diesel combustion". Applied Thermal Engineering, Vol. 26 nº 14-15, pp. 1492-1499, 2006.

[29] Woschni G. "A Universally applicable equation for the instantaneous heat transfer coefficient in the internal combustion engines". SAE Paper 670931, 1967.

[30] Payri F., Margot X., Gil A., Martin J. "Computational study of heat transfer to the walls of a DI diesel engine". SAE Paper 2005-01-0210, 2005.

[31] Degraeuwe B. "Contribution to the thermal management of DI Diesel engines". Doctoral Thesis, Universitat Politècnica de València, 2007.

[32] Torregrosa A.J., Olmeda P., Degraeuwe B., Reyes M.A. "Concise wall temperature model for DI Diesel engines". Applied Thermal Engineering, Vol. 26 nº 11-12, pp. 1320-1327, 2006.

[33] Martín J. "Aportación al diagnóstico de la combustión en motores Diesel de inyección directa". Doctoral Thesis, Universitat Politècnica de València, 2007.

[34] Pastor J. V., Lopez J. J., Garcia J. M. y Pastor J. M. "A 1D model for the description of mixing-controlled inert diesel sprays". Fuel, Vol. 87 no 13-14, pp. 2871-2885, 2008.

[35] Desantes J.M., Pastor J.V., García-Oliver J.M., Pastor J.M. "A 1D model for the description of mixing-controlled reacting diesel sprays". Combustion and Flame, Vol. 156, pp. 234-249, 2009.

[36] García J.M. "Aportaciones del estudio del proceso de combustión turbulenta en chooros en motores diésel de inyeccion directa". Doctoral Thesis, Universitat Politècnica de València, 2004.

[37] Kee R., Rupley F., Miller J., Coltrin M., Grcar J., Meeks E., Moffat H., Lutz A., Dixon- Lewis G., Smooke M., Warnatz J., Evans G., Larson R., Mitchell R., Petzold L., Reynolds W., Caracotsios M., Stewart W., Glarborg P., Wang C., Adigun O., HoufW., Chou C., Miller S., Ho P., Young D. CHEMKIN Release 4.0 & Pro, Rection Design, Inc., San Diego, CA, 2004.

[38] Curran H.J., Gaffuri P., Pitz W., Westbrook C.K. "A comprehensive modeling study of nheptane oxidation". Combustion and Flame, 114, pp. 149–177, 1998.

[39] Curran H.J., Gaffuri P., Pitz W.J.,Westbrook C.K. "A Comprehensive Modeling Study of iso-Octane Oxidation". Combustion and Flame 129: 253-280, 2002.

[40] Jerzembeck S., Peters N., Pepiot-Desjardins P., Pitsch. H. "Laminar burning velocities at high pressure for primary reference fuels and gasoline: Experimental and numerical investigation". Combustion and Flame, Vol. 156, Issue 2, pp.292-301, 2009.

[41] Matsui Y., Kamimoto T., Matsuoka S. "A study on the time and space resolved measurements of flame temperature in a D.I. Diesel engine by the two-color method". SAE Paper 790491, 1979.

[42] Hotel H.C., Broughton F.P. "Determination of true temperature and total radiation from luminous gas flames". Ind. And Eng. Chem., Vol. 4, n°2, pp. 166-175, 1932.

[43] Zhao H., Ladommatos N. "Optical diagnostics for soot and temperature measurement in Diesel engines". Prog. Energy Combustion Science, Vol. 24, pp. 221-255, 1998.

[44] Tan J., Borman G.L. "Analysis and in-cylinder measurement of particulate radiant emissions and temperature in a Direct Injection Diesel engine". SAE Paper 881315, 1988.

[45] Hampson G.J., Reitz R.D. "Two-color imaging of in-cylinder soot concentration and temperature in a heavy-duty DI Diesel engine with comparison to multidimensional modeling for single and split injections". SAE paper 980524, 1998.

[46] Vattulainen J., Nummela V., Hernberg R., Kytölä J. "A system for quantitative imaging diagnostics and its application to pyrometric in-cylinder flame-temperature measurements in large Diesel engines". Meas. Sci. Technol., Vol. 11, pp. 103-109, 2000.

[47] Di Stasio D., Massoli P. "Influence of the soot property uncertainties in temperature and volume-fraction measurements by two-colour pyrometry". Meas. Sci. Technol., Vol. 5, pp. 1453-1465, 1994.

Chapter 4

Experimental study of the Radiation Heat Transfer in diesel flames

Content

4.1 Introduction

Throughout this chapter, the first of the three stages that make up the results of this thesis will be developed.

As it is well known in research community, expanding knowledge for the protection of the environment and the conservation of energy sources has motivated the development of new cleaner and more efficient technologies in reciprocating internal combustion engines (ICE). In order to comply with the strict pollutant regulations, some different strategies have been proposed in the last decades: indicated cycle optimization [1][2]; reduction of friction and auxiliaries losses [3][4]; in-cylinder heat transfer (HT) reduction [5][6]; new combustion concepts [7][8]. In the present work, the research effort has been focused on improving knowledge of in-cylinder heat transfer.

Combustion process in Direct Injection (DI) diesel engines includes different physical and chemical processes. During the turbulent diffusion flame, an important balance between soot formation and oxidation occurs in the spray. During oxidation process, the in-cylinder soot emission is an important source of emission of radiant energy [9]. Carbon dioxide and water vapor molecules also emit radiation, however it is concentrated in some narrow spectral bands and its magnitude is assumed much smaller than soot particles. Moreover, radiation may also be emitted by many intermediate species formed during the combustion process, but since their concentration levels are small, their effect on radiation heat transfer is less important as is described in [10]. Thus, soot radiation can be considered a significant source of the efficiency losses in modern diesel engines [11]. In this sense, there are different studies in the literature which quantify the amount of fuel chemical energy lost by soot radiation. Depending on soot conditions, studies provide very different results. From 0.5-1% [48] up to 5-10% [14] of the total chemical energy released during combustion process can be considered as radiant losses. Not only the amount of radiant heat transfer is a controversy, but also the contribution of radiation to the total heat transfer varies significantly

between different authors as well from 11% up to 40% [9]. The significant differences between authors are directly related with the uniqueness of the radiant emission in each combustion system considering particular engine geometry and the operating conditions tested. Therefore, it could be stated that the relationship between all these combustion and engine parameters and its radiant emission is not fully understood yet.

The objective of this chapter is to contribute to the understanding of heat transfer by radiation in DI diesel combustion. In order to achieve this general objective, the following particular objectives are proposed:

- Analyze the impact of different controlled thermodynamic conditions on the radiation in the combustion chamber in an optical engine DI.
- Evaluate the amount of energy lost by radiation respect to the chemical energy of the fuel under real operating conditions in a production multi-cylinder engine DI.

4.2 General methodology of the study

To carry out the first objective, a specific test plan has been performed to analyze the basic characteristics of the soot radiation process. For this analysis, the optically accessible DI engine has been used due to its greater control of the thermodynamic conditions before, during and after the test. The results obtained have been measured with the High Speed Imaging Pyrometer (HSIP) optical system. For this, the injection pressure, the temperature and the density in the combustion chamber have been modified. First, the soot spectral intensity along the spray and the flame lift-off length have been evaluated spatially and temporally. This is a good starting point regarding the knowledge of the soot formation-oxidation process. The experimental measurements of the soot spectral intensity have been used to calculate the soot temperature and concentration with the two-color method. As a last step, the total radiation emitted by the soot particles in the wavelength spectrum from 300 nm to 3000 nm is calculated for each operating

condition using the Planck equation. In this way, considering the total area of the flame, the energy fraction transmitted by soot radiation is obtained with respect to the chemical energy of the fuel. Finally, validation of the Optoelectronic Probe (Chapter 3) is carried out by comparing the results of soot temperature and concentration obtained with both measurement systems simultaneously.

With respect to the second particular objective, the tests have been carried out in a 4-cylinder GM1.9L engine and the experimental information about soot radiation has been obtained only with the VisioFEM optoelectronic probe. This section has been split into two sub-sections: the effect of the load and the effects of the operating parameters (swirl, EGR and CA50) on the radiation heat transfer. The procedure to follow is very similar to that carried out in the optical engine.

4.3 Spatial-temporal analysis of the radiation under controlled conditions

The objective of this section is twofold. First, the effects of variations in different engine operating parameters on spectral intensity in an optical engine with a completely controlled environment are presented. Second, some experiments were performed with the aim of performing the evaluation of the Optoelectronic Pyrometer (OP) versus a conventional optical set-up, High Speed Imaging Pyrometer (HSIP), in terms of KL and in-cylinder soot temperature. Then, an evaluation of the radiant fraction of the total energy supplied to the chamber is presented.

4.3.1 Test conditions

This study has been carried out in the single-cylinder optical engine, which has been described in Chapter 3. The test matrix consists of eight operating conditions (Table 2.1). The injected fuel mass has been obtained with an injection rate meter [1]. The thermodynamic conditions inside the

combustion chamber have been controlled by the intake gas pressure and temperature at top dead center (TDC). To determine the required values of in-cylinder pressure and temperature at TDC, a thermodynamic characterization of the engine has been carried out as detailed in [15]. The procedure is based on determining thermodynamic conditions inside the cylinder, for a variety of points that covers the entire operating range of the engine. In-cylinder temperature (T_c) and density (ρ_c) are calculated from in-cylinder pressure (p_c), using a thermodynamic analysis and accounting for blow-by, heat transfer and mechanical stress [16][17]. First, the trapped mass is estimated using intake pressure, temperature and volume at exhaust vent closure (EVC). Once the trapped mass is known, T_c and ρ_c are estimated for the whole cycle using the equation of state. The blow-by leakage mass is temporal distributed along the cycle as a linear function of in-cylinder pressure. Once angular-resolved thermodynamic conditions of the set of points are obtained, the exact intake conditions required for a defined test plan can be calculated by interpolating between the values available. The maximum T_c usually presents a linear response to intake temperature (T_{int}), independently of intake pressure (p_{int}). Figure 4.1 shows an example of the temporal evolution of the in-cylinder pressure and temperature in the combustion chamber during the injection event.

TDC Temp. [K]	**TDC Density [kg/m³]**	**Injection Pressure [bar]**	**Injected fuel mass [mg/stk]**	**Equivalence ratio [-]**
800	23.4	500/1000/1500	13.4/20.3/ 25.4	0.05/0.07/0.09
	18.9	1000	20.1	0.08
900	23.4	500/1000/1500	13.4/20.3/ 25.4	0.05/0.07/0.09
	18.9	1000	20.1	0.08

Table 4.1. Experimental conditions optical engine.

Energizing time (*ET*) was set to 2ms for all conditions, which results in an approximate 4.5ms hydraulic injection duration. The injector was triggered at −6.05° after TDC (SoE) and the injection starts at −5.9° aTDC

(SoI), to minimize variations of in-cylinder conditions during injection event. Each test was repeated 20 times to reduce measurement uncertainties due to engine operating variability as well as to improve signal-to-noise ratio.

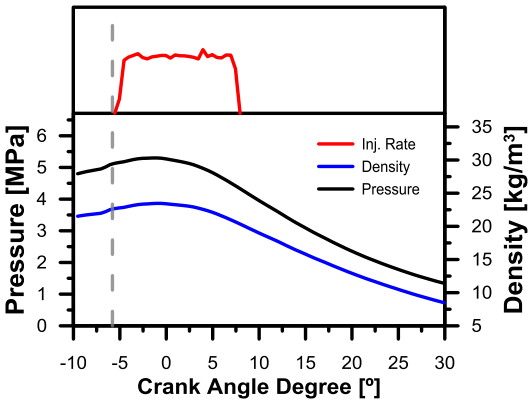

Figure 4.1. Thermodynamic in-cylinder conditions along engine cycle under motored conditions. Injection rate is just shown to clarify the timing and duration of the injection event.

Finally, one blend using two different fuels, n-decane and n-hexadecane, have been employed. In fact, the fuel used is a blend of both single component fuels at a 30%-70% volume fraction, respectively. They have been chosen due to their simplicity (pure fuels) and similarity with diesel fuel in terms of physical and chemical properties. Table 4.2 shows main fuel properties.

Fuel	30% $C_{10}H_{22}$ – 70% $C_{16}H_{34}$		
Density @ 373K [kg/m³]	703.7	**Dynamic Viscosity @ 373K [mPa · s]**	0.667
Derived Cetane Number (DCN)	85.4	**Vapor Pressure @ 373K [kPa]**	7.72
H/C	2.14	**Power Heat. Value [MJ/kg]**	43.995

Table 4.2. Fuel properties at 1 atm y 100°C.

4.3.2 Influence of injection pressure, ambient gas temperature and density on spectral intensity

Figure 4.2 shows the temporal evolution of the spectral intensity (I_{soot}) measurements for High Speed Imaging Pyrometer (HSIP), described in Chapter 3. In particular, sub-figure (a) presents the injection pressure variation effects, sub-figure (b) shows the in-cylinder gas density effects and finally, sub-figure (c) describes ambient temperature effects on I_{soot}. It is interesting to remark that only values in the quasi steady state part of the diffusion combustion process are shown. In each sub-figure, curves represent the average of 20 fired cycles together with their standard deviation for 550 nm and 650 nm. Thus, an average image per instant with spatial resolution is obtained and later, a spatial average of the complete image in each instant was performed.

Independently on the wavelength, it can be stated that when higher injection pressure was used, lower I_{soot} was obtained. In the same way, use of lower in-cylinder gas density and temperature also provided lower spectral intensity. As expected, the longer the wavelength, the higher the I_{soot}. Regarding the measurement scattering, the higher the wavelength, the higher the standard deviation.

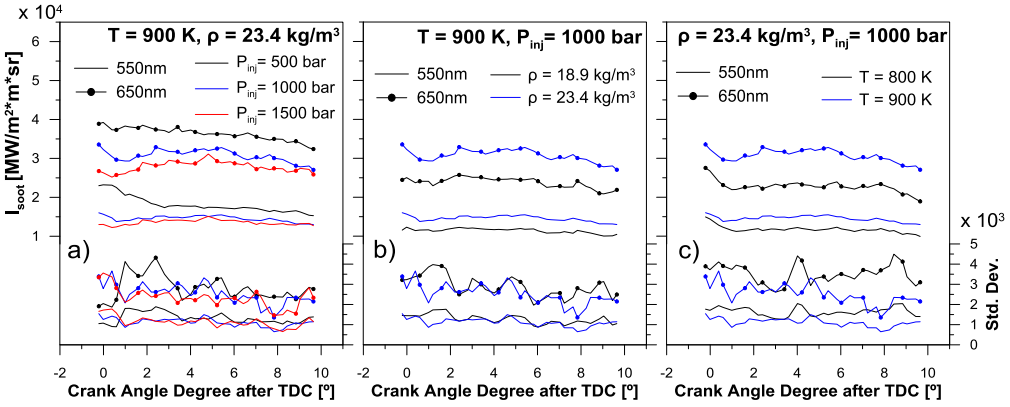

Figure 4.2: Temporal evolution of the spectral intensity for both 550 nm and 650 nm wavelengths, and their corresponding standard deviation, (a)

injection pressure effect; (b) in-cylinder gas density effect; (c) ambient temperature effect.

To provide further insight into the effect of injection pressure, in-cylinder gas density and ambient temperature on I_{soot}, in Figure 4.3, 4.4 and 4.5 is represented the axial evolution of spectral intensity in the centerline of the spray during quasi-steady state of combustion diffusion process along with the maximum spectral intensity at the flame lift-off length, LoL_{FLAME}[5].

Considering Figure 4.3, it can be stated that, independent on the axial position and wavelength tested, the higher the injection pressure, the lower the I_{soot}. Thus, when the injection pressure was reduced, the first occurrences of natural luminosity moved closer to the injector implying a shorter flame lift-off length. Consequently the soot volume fractions increased [18][19]. In this sense, the peak of spectral intensity was also higher when the injection pressure was reduced as shown in Figure 4.3. In fact, when the injection pressure was varied, no significant changes in the mixture fraction field were attained. Nevertheless, it is well-known that the OH lift-off length is reduced due to a different balance between flow and flame velocities [19].

[5] LOL_{FLAME}: the first axial position from the injector orifice where natural luminosity was acquired.

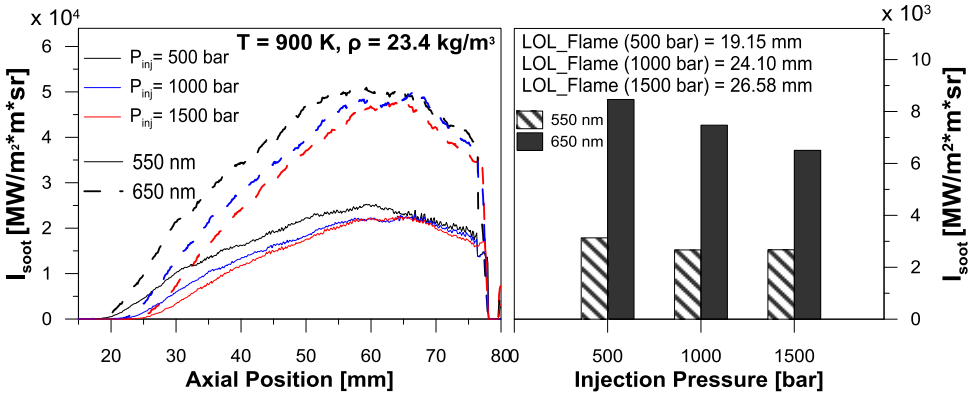

Figure 4.3: Axial evolution of spectral intensity in the centerline of the spray together with the maximum value at the flame lift-off length using three different injection pressures; 500, 1000 and 1500 bar. In-cylinder gas density and ambient temperature were maintained constant.

Figure 4.4 represents the axial evolution of spectral intensity at 550 nm and 650 nm in the centerline of the spray together with the maximum spectral intensity value at the flame lift-off length under two different ambient densities; 18.9 and 23.4 kg/m^3. Ambient temperature and injection pressure were maintained constant at 900 K and 1000 bar respectively. Thus, when in-cylinder gas density was decreased, the spectral intensity was also reduced independent on the wavelength tested as well as the axial position in the spray centerline. The flame lift-off length moved farther from the injector hole and soot and the maximum spectral intensity were also reduced.

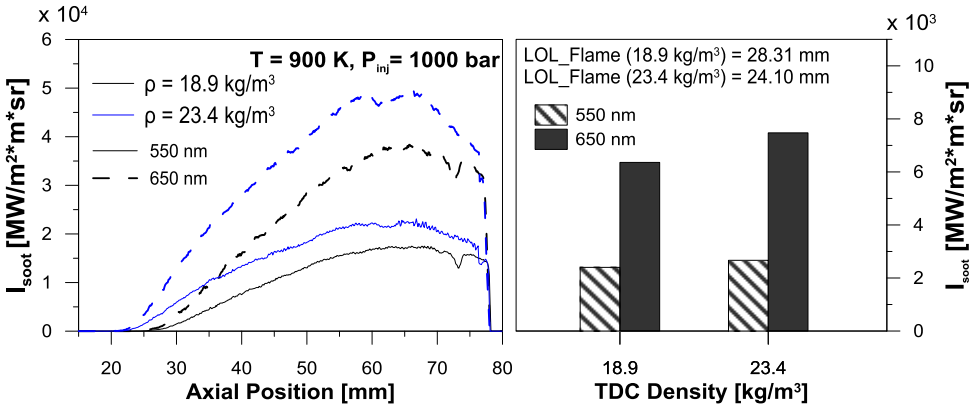

Figure 4.4. Axial evolution of spectral intensity in the centerline of the spray together with the maximum value at the flame lift-off length using two different ambient densities; 18.9 and 23.4 kg/m³. Ambient temperature and injection pressure were maintained constant.

Finally, the ambient temperature have been studied in Figure 4.5 with the aim of examining its effect on I_{soot}. For this, the temperature has been analyzed in two levels: 800 and 900 K. As in the previous cases, the two remaining variables are maintaining constant: 1000 bar and 23.4 kg/m^3. In view of the results shown in the figure, the spectral intensity of the soot decreases when the ambient temperature was reduced, independently of the axial position for both wavelengths tested. In fact, the axial position of the maximum spectral intensity moved closer to the injector hole. This behavior implies a similar result as when the injection pressure was increased or the ambient temperature was reduced, the flame lift-off length was enlarged and therefore the amount of soot decreased as well as its spectral intensity.

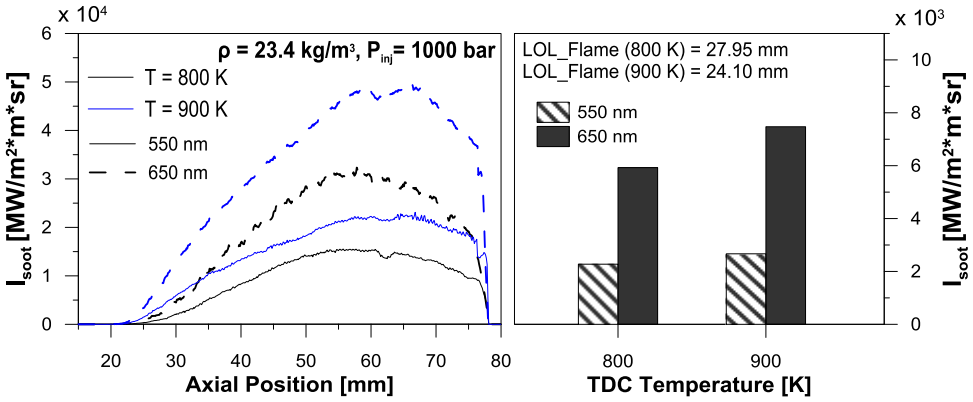

Figure 4.5. Axial evolution of spectral intensity in the centerline of the spray together with the maximum value at the flame lift-off length using two different ambient temperatures: 800 K and 900 K. In-cylinder gas density and injection pressure were maintained constant.

4.3.3 Influence of injection pressure, ambient gas temperature and density on in-cylinder soot temperature and optical thickness (KL)

4.3.3.1 Analysis and discussion

Figure 4.6 shows the temporal evolution of the soot temperature and optical thickness using equation 3.12 for High Speed Imaging Pyrometer (HSIP) along with their corresponding standard deviation. In particular, sub-figure (a) presents the effects of injection pressure variation, sub-figure (b) shows the in-cylinder gas density effects and finally, sub-figure (c) describes ambient temperature effects on KL and in-cylinder soot temperature. Adiabatic flame temperature was also included to compare with soot temperature at each operating point. Thus, adiabatic flame temperature was calculated with the assumption of constant pressure at each step of calculation, adiabatic burning of the stoichiometric fuel/air mixture and

considering a conventional chemical equilibrium model, following the scheme proposed by Way [20].

Considering the results of Figure 4.6, it can be stated that values obtained are from 0.15 up to almost 0.4 independent on the operating condition. Focusing on injection pressure effect it is shown that when the injection pressure is decreased, KL is increased. This behavior can be explained considering Figure 4.3. The lower the injection pressure, the shorter the flame lift-off length and the higher the expected soot. Regarding in-cylinder gas density and temperature effects it is stated that lower in-cylinder gas density and/or temperature, results in lower KL. As in the case of injection pressure, the explanation of effects is possible to observe in Figure 4.4 and Figure 4.5. In this sense, a decrease in the ambient gas temperature and/or density in the chamber produce that the first points of luminosity detected are closer to the end of the injector, so that the lift-off length of the flame is shortened and with this, also the concentration of soot decreases.

The soot temperature values are lower than the adiabatic flame temperature, by around 350 K, This observation agrees with soot thermometry studies reported in the literature for diesel engines [21]. Soot thermometry measures the soot temperature, which is not exactly equivalent to the flame temperature in particular for diffusion flames. This fact does not imply that soot radiation has no influence on the peak flame temperatures. Radiative cooling from soot can reduce the gas temperatures in the sooting area, which are coupled to the high temperature flame by conductive heat transfer [21].

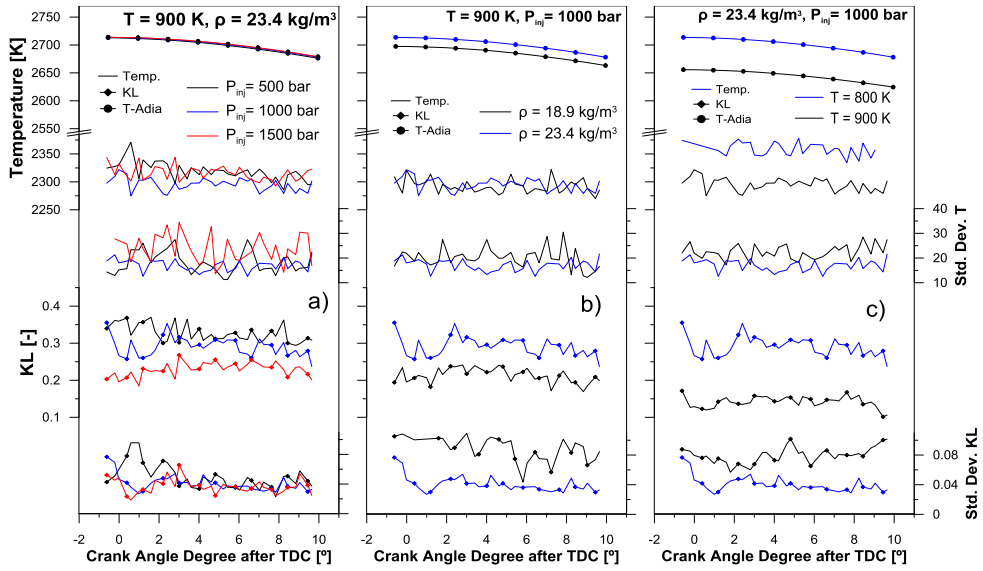

Figure 4.6. Temporal evolution of KL and soot temperature and its standard deviation (a) injection pressure effect; (b) in-cylinder gas density effect; (c) ambient temperature effect

Thus, soot temperature results for the three different injection pressures as well as for the two different ambient densities show quite similar values. This is because these operating conditions are low-radiation environments and consequently the impact of soot radiative heat transfer is similar and relatively minor for these particular conditions. By contrast, when the ambient temperature is increased, the soot temperature is also increased clearly. This behavior is completely expected considering the proportional dependency of the flame temperature on ambient temperature [20].

4.3.3.2 Integration of total radiation

Considering the local soot temperature and optical thickness correspond to a blackbody spectral intensity ($I_{b,\lambda}$) and soot spectral emissivity (ε_λ) at each instant (as described in Chapter 3), the total radiation in Joules, Q_{rad}, is given by equation (4.1):

$$Q_{rad} = \pi \int_t \int_A \int_\lambda \varepsilon_\lambda I_{b,\lambda} \, d\lambda \, dA \, dt \tag{4.1}$$

where t represents the exposure time in which the optical system is registering flame luminosity, and A is the flame area obtained by equation (4.2):

$$A = 2\pi r \int_x dx \tag{4.2}$$

where r is the flame radius, which is determined from a temporal image of the flame and dx, is the axial width. In this case, the axial width corresponds with one pixel.

It is worthy to note that CO_2 and H_2O molecules also emit radiation but it is concentrated in a narrow spectral bands and its magnitude is assumed much smaller than that of soot particles [10]. Thus, as in Musculus [21] and Skeen *et al.* [48], the radiant fraction (X_{rad}) is defined as the fraction of the total chemical energy released during injection that is lost due to radiation heat transfer. This term is expressed by equation (4.3):

$$X_{rad} = {Q_{rad}}\Big/{m_f Q_{LHV}} \tag{4.3}$$

where m_f represents the mass of fuel injected and Q_{LHV} is the lower heating value of 30% Decane and 70% Hexadecane (43.995 kJ/kg).

Figure 4.7 presents the radiant fraction results for the different operating conditions. In particular, sub-figure (a) shows the effect of injection pressure and ambient temperature. Sub-figure (b) presents the effect of in-cylinder gas density variations. Considering soot temperature and KL obtained in previous section, expected trends of radiant fraction were attained. Thus, when the injection pressure was decreased and/or ambient temperature and/or in-cylinder gas density were increased, the radiant fraction was also increased.

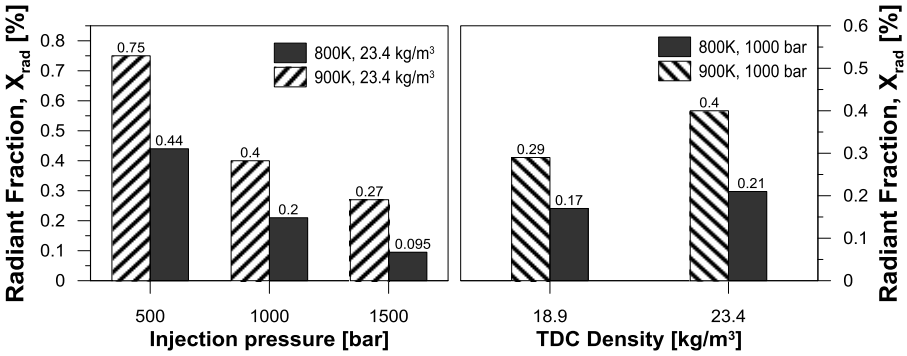

Figure 4.7. Radiant fraction (a) effect of different injection pressures and ambient temperature; (b) effect of different densities and ambient temperature.

In literature, Skeen [12] has presented results in a combustion vessel using an injector with single hole nozzle of 90 µm nominal diameter, n-dodecane as fuel under ECN[6] spray conditions (p_{inj} = 1500 bar; X_{O2} = 15%; ρ = 22.8 kg/m^3) and sweeping the ambient temperature. Thus, some operating conditions are quite similar to the ones presented in this research. For the conditions of Skeen's research, at 850 K ambient temperature the radiant fraction was 0.007% and at 900 K it was 0.068%. Thus, results present similar values compared with those obtained in the present work. In particular, when higher injection pressure was used, the results presented in this study were similar to the ones presented by Skeen. Taking into account the significant differences in the experimental procedure, it is remarkable that there is consistency between the present work and the research performed by Skeen. It should also be remarkable that alkane blends tested were less prone to produce soot compared with a real diesel fuel, which should contain some aromatic compounds. Consequently, some slight underestimations in terms

[6] *ECN*: It is an international group formed by experimental and computational researchers specializing in engine combustion ("*Engine Combustion Network*")

of radiant fraction was attained, although trends obtained under different operating conditions are correct.

Figure 4.8 shows the theoretical maximum radiant fraction for the maximum soot temperature blackbody radiating during the whole injection process, 4.5 ms, for each operating conditions. Thus, the maximum radiant fraction from the spectral data (Figure 4.7) was approximately an order of magnitude less than that expected from the maximum soot temperature blackbody having the same surface area and emitting over the injection event.

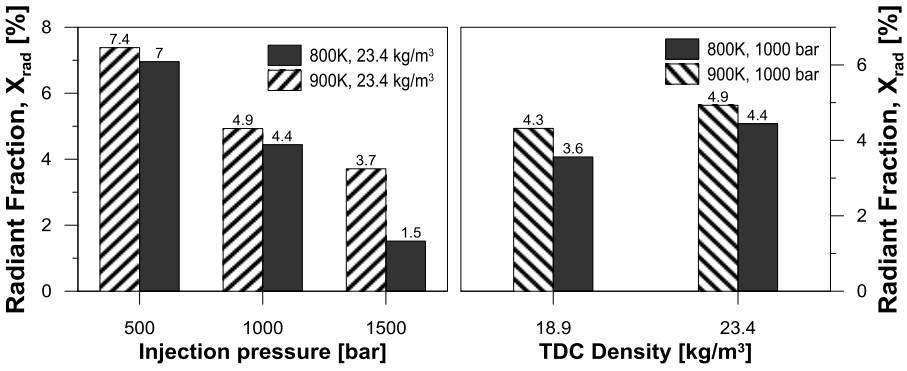

Figure 4.8. Theoretical maximum radiant fraction considering a blackbody flame (a) effect of different injection pressures and ambient temperature; (b) effect of different densities.

Taking into account real soot cloud differences in terms of partial transparency and a probably smaller emitting area due to a considerable spacing between sprays, the differences obtained between spectral data and the maximum soot temperature blackbody radiant fraction seem reasonable [21]. It is worthy to note that other studies of soot radiative heat transfer for higher sooting conditions have reported much higher peak radiant fraction from 5% to 10% [9][13] than the ones showed in the present research. In this sense, it should be considered that in the optical engine very low load with low-sooting conditions are tested.

4.3.4 Comparison of results between different optical configurations. Optoelectronic probe validation (VisioFEM)

Once the effects of injection pressure, in-cylinder gas density and temperature on spectral intensity have been described, it is necessary to evaluate and validate the Optoelectronic Pyrometer (OP) under similar conditions.

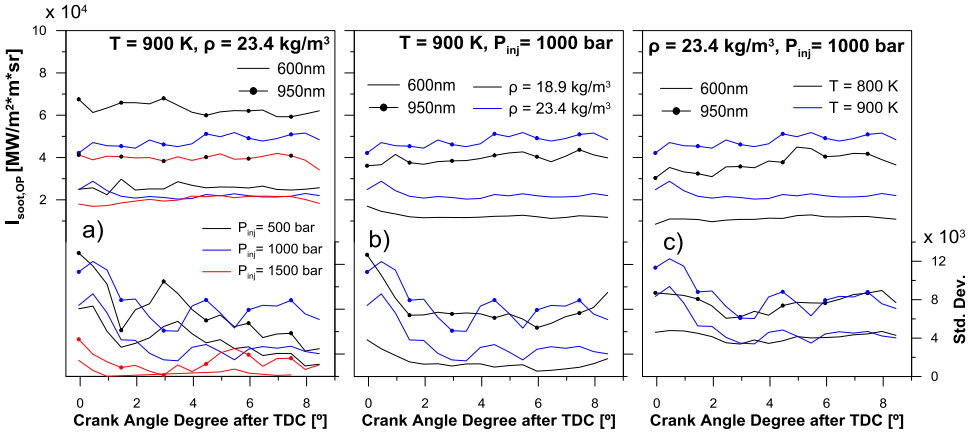

Figure 4.9. Temporal evolution of the spectral intensity for both 600 nm and 950 nm wavelengths, measured with OP configuration (a) injection pressure effect; (b) in-cylinder gas density effect; (c) ambient temperature effect.

Figure 4.9 shows the temporal evolution of the spectral intensity (I_{soot}) measurements for OP. Following similar analysis as the HSIP, three different sub-figures are presented, (a) shows the injection pressure variation effects, (b) presents the in-cylinder gas density effects and finally, (c) is describes ambient temperature effects on I_{soot}. Independent on the sub-figure, the profiles represented are the average of the same 20 fired cycles at each data point. Standard deviation of measured points is also shown in the same figures. The wavelengths used for this system were 600 nm and 950 nm, as detailed in Chapter 3. This fact implied that a direct comparison with HSIP

was not possible. Nevertheless, consistent results were obtained from the two different optical systems. An increase in ambient temperature and/or in-cylinder gas density as well as a decrease in the injection pressure implied higher spectral intensity.

To compare the results measured with both optical systems, it was necessary to complete an additional post-processing in the images obtained with High Speed Imaging Pyrometer. As was mentioned in description of Optoelectronic Pyrometer (Chapter 3), this has a particular field of vision, which is smaller than the one acquired with HSIP. To ensure an appropriate comparison between both methods, the HSIP images are processed considering the particular vision field of the Optoelectronic Pyrometer as it is shown in the Figure 4.10.

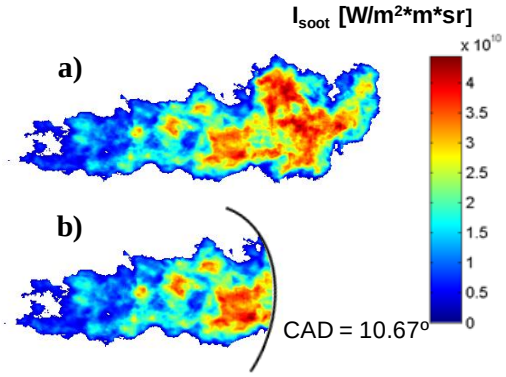

Figure 4.10. a) Raw image obtain from High Speed Imaging Pyrometer (not processed); b) Image post processing to compare properly spectral intensity between High Speed Imaging Pyrometer and Optoelectronic Pyrometer

Figure 4.11 shows the spectral intensity registered by HSIP and OP. In particular, an average value of the spectral intensity during the quasi steady state portion of diffusion combustion is shown along with its standard deviation. Thus, it can be stated that OP results follow similar trend as HSIP for the different operating conditions tested. Moreover, OP 600 nm results presented values quite close to HSIP 650 nm and 550 nm results. It is also

interesting to remark that the dispersion obtained with OP was higher than with HSIP.

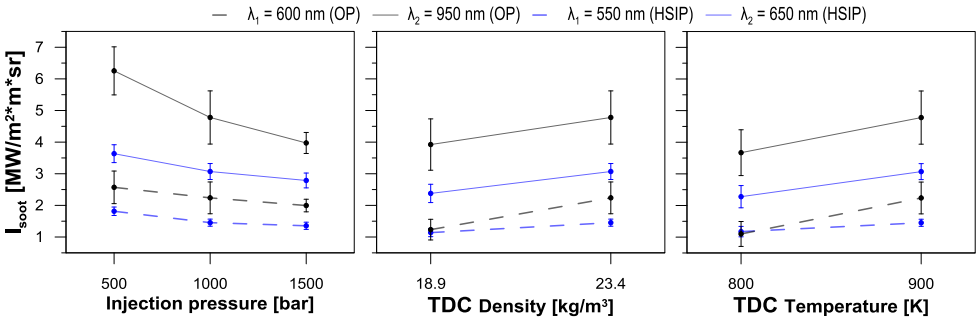

Figure 4.11. Average I_{soot} during the quasi steady state of diffusion combustion and its standard deviation for HSIP and OP in each corresponding wavelengths measured (a) injection pressure effect; (b) in-cylinder gas density effect: (c) ambient temperature effect.

With the aim of comparing directly HSIP and OP, Figure 4.12 presents the temporal evolution of KL and soot temperature differences between both optical systems and its standard deviation (a) injection pressure effect; (b) in-cylinder gas density effect; (c) ambient temperature effect.

Regarding optical thickness, slight differences were attained comparing both optical systems. These discrepancies were higher when the soot generated was lower. Concerning soot temperature, in spite of higher differences between OP and HSIP, it should be clarified that in relative terms, this difference was even lower than in the case of KL. Thus, in general, it can be stated that both systems present a similar response and therefore similar results are expected, consequently the validity of the OP versus HSIP has been demonstrated.

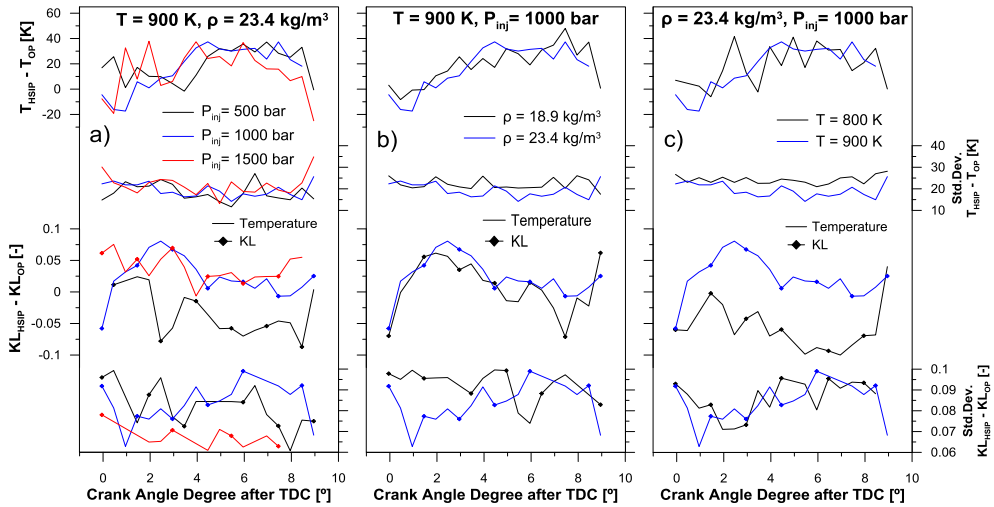

Figure 4.12. Temporal evolution of KL and soot temperature differences between HSIP and OP and its standard deviation for HSIP and OP (a) injection pressure effect; (b) in-cylinder gas density effect; (c) ambient temperature effect.

4.4 Temporal characterization of the radiation under real conditions

In this section, the main objective is to calculate the total radiation heat transfer in a direct-injection 4-cylinder diesel production engine for different operating conditions.

4.4.1 Test conditions

In this section, two different studies have been carried out. In a first step, an evaluation of the load effect on radiation, soot temperature and KL was performed. With this aim, the operating conditions shown in Table 4.3 have been measured in a 4-cylinder engine, which has been described in Chapter 3. The analysis has been carried out for two regimes, 1500 rpm and

2000 rpm. For the speed 1500 rpm, the load conditions analyzed are of medium-high load (8 bar BMEP corresponds to 50% load and 14 bar BMEP, at 85% load). For the speed 2000 rpm, the conditions analyzed are of low load (2 bar BMEP corresponds to 10% load and 5 bar BMEP, to 25%). The tests have performed for keeping constant the parameter CA50 at 13° aTDC and without EGR. Finally, the values represented are the average result of 100 cycles for each operation condition.

Operating condition	**2000rpm @ 2bar**	**2000rpm @ 5bar**	**1500rpm @ 8bar**	**1500rpm @ 14bar**
Torque [Nm]	38	82	133	220
Inj. Pressure [bar]	450	650	735	1037
m_f [g/s]	0.65	1.15	1.33	2.33
CA50 [°aTDC]	13			
T_{in} [K]	315			
P_{in} [bar]	1.16	1.37	1.35	1.73
P_{exh} [bar]	1.29	1.58	1.55	2.19
m_a [g/s]	38.9	43.8	30	38.2
SR [-]	1.4			
EGR [%]	0			
Equivalence ratio [-]	0.244	0.383	0.649	0.893

Table 4.3. 4-cylinder engine operating conditions.

In a second step, the objective is to evaluate the effect of different engine parameters on the soot temperature, concentration and radiation. For this, the operation condition at 2000 rpm@ 5 bar BMEP has been selected as a reference condition and the parametric study is shown in Table 4.4: swirl (SR), EGR and CA50. For the swirl case, the values of 1.4 and 3 have been selected, since they are the minimum and maximum extreme values that can be reached in the 4-cylinder engine, without EGR and maintain CA50

parameter constant at 13° aTDC. On the EGR study, values of 0% and 25% have been selected. The maximum value of EGR has been defined considering an exhaust-soot limit emissions in the FSN = 3. As in the previous sweep, the tests have been measured with a CA50 = 13° aTDC constant and a swirl of 1.4. Finally, for the CA50 sweep, the values of 6 and 16° aTDC have been selected maintaining constant the swirl to 1.4 and without EGR. The limits have been chosen to establish the maximum in-cylinder pressure below 160 bar. The injection pressure, the injected fuel mass and the intake temperature have also maintained constant for the complete study, 650 bar, 1.15 g/s and 315 K respectively. The injection strategy was set in two pilot injections together main injection.

Operating condition	**SR 1.4**	**SR 3**	**EGR 0%**	**EGR 25%**	**CA50 6°**	**CA50 16°**
Torque [Nm]	82	80	82	82	87	82
Inj. Pressure [bar]	650					
m_f [g/s]	1.15					
CA50 [°aTDC]	13	13	13	13	6	16
P_{in} [bar]	1.37	1.35	1.37	1.36	1.36	1.36
P_{exh} [bar]	1.58	1.53	1.58	1.81	1.60	1.52
m_a [g/s]	43.8	41.17	43.83	32.5	42.5	42.83
SR [-]	1.4	3	1.4	1.4	1.4	1.4
EGR [%]	0	0	0	25	0	0
Equivalence ratio [-]	0.38	0.41	0.38	0.52	0.40	0.40

Table 4.4. 4-cylinder engine operating conditions for 2000 rpm@ 5 bar BMEP operating point.

Commercially available European diesel fuel was used in this part of the work. Table 4.5 shows the main characteristics of the fuel used.

Diesel	
Density @ 313K [kg/m^3]	821.5
Derived Cetane Number (DCN)	50.8
H/C	2.15
Dynamic viscosity @ 313K [mm^2/s]	2.7
Molecular weight [kg/kmol]	215.42
Lower heating value [MJ/kg]	44.57

Table 4.5. Fuel properties at 1 atm y 40°C.

4.4.2 Influence of different engine parameters on soot temperature, optical thickness and radiation intensity

4.4.2.1 Effect of load engine

In this section, the Optoelectronic Probe was used to evaluate the radiation intensity, soot temperature and optical thickness in a multi-cylinder engine. In Figure 4.13, an example of the raw data obtained with the Optoelectronic Pyrometer is presented. The temporal evolution of the spectral intensity (MW/m^{3}sr) at both wavelengths, 600 nm and 950 nm is shown for the 2000 rpm and 5 bar BMEP case. Each curve represents the average and the standard deviation of 100 cycles recorded. Thus, under real conditions the results dispersion is higher than the shown in Figure 4.11 for the optically accessible engine. This behavior is mainly due to the fact that the "skip fire[7]" mode provides greater control over the thermodynamic conditions and, therefore, less dispersion.

[7] *Skip-fire mode*: one cycle in combustion for every 30 cycles

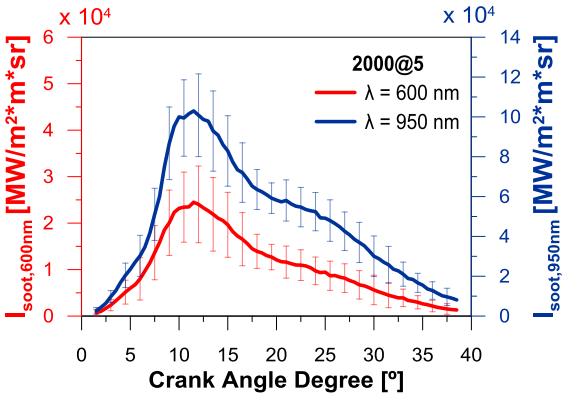

Figure 4.13. Temporal evolution of the spectral intensity using Optoelectronic Pyrometer at 2000 rpm and 5 bar BMEP.

Figure 4.14 shows the temporal evolution of rate of the heat release, radiation intensity, soot temperature and optical thickness KL. Figure (a) shows a comparison between 8 and 14 bar BMEP cases at 1500 rpm. Figure (b) presents a similar comparison but in these cases at low load conditions, 2 and 5 bar BMEP at 2000 rpm. It is interesting to note that these tests were performed maintaining constant the CA50 at 13 CAD aTDC, without EGR and with a constant swirl ratio of 1.4. Different curves represent the average and standard deviation of 100 cycles. RoHR dispersion is completely negligible and therefore only its average value is shown. Injection rate profile was simulated from a particular sub-model included in CALMEC [23] which has been calibrated to the injector and nozzle used in the present research. Thus, the end of injection (EoI) for each test is marked with a vertical straight line. In addition, it should be also noted that radiation intensity is the spectral intensity integrated from 300 nm up to 3000 nm.

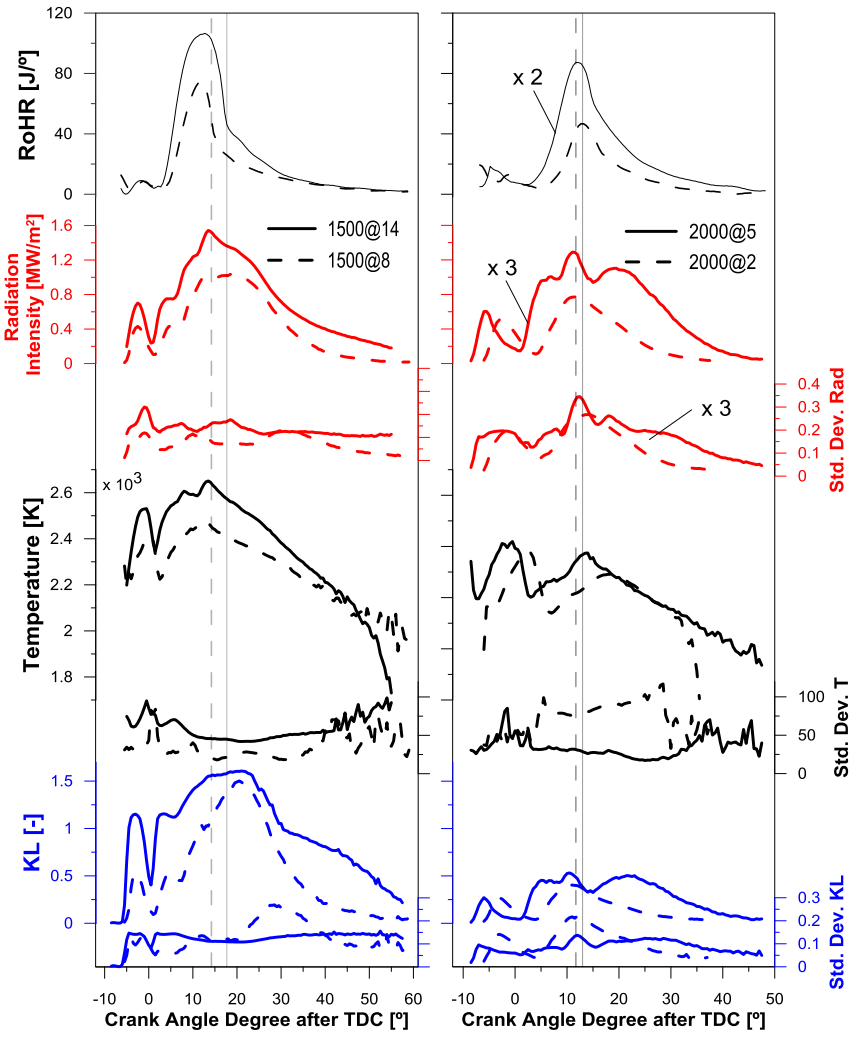

Figure 4.14. Temporal evolution of radiation intensity, soot temperature and KL; (a) 1500 rpm comparing 8 and 14 bar BMEP; (b) 2000 rpm comparing 2 and 5 bar BMEP. For each studied case, the end of injection is marked with a vertical line. CA50, swirl ratio and EGR were constant.

In general, it is possible to state that there were clear differences in radiation intensity profiles considering engine speed and overall load. Nevertheless, there was also some similarity in the temporal evolution of the

different radiation intensity traces. For the same engine speed, shape and slopes were quite similar although the peak was different and higher when the load was increased. The range of the peak values varied from 0.15 MW/m^2 up to 1.6 MW/m^2. Comparing these results with other radiation intensity studies, in particular Soloiu *et al.* [24], radiation intensity peaks found in the literature are in the same order of magnitude that the ones presented in the current work (0.76 MW/m^2), taking account the significant differences in the experimental procedure. Regarding soot temperature curves, for the same engine speed quite similar evolution was attained. In terms of the peak values range for the different operating conditions tested, soot temperature varies from 2600 K up to 2400 K. A clear decrease in the temperature was attained when the engine load was decreased. Moreover, soot temperature values were consistent with other studies in similar conditions [9][21]. KL profiles were quite similar and seem to be governed by the diffusion combustion. In this sense, the greater the diffusion phase in the RoHR, the higher the amount of soot. It could be stated that KL profiles show great similarity with radiation intensity traces. The range of the peak values varied from 0.25 up to almost 1.75. When the injection process ended, a sudden decrease in KL signal was obtained. The maximum peak of the optical thickness traces almost coincided with the end of injection. After the end of injection, the oxidation process governs soot emissions and therefore the soot formation reaches at its maximum value [25]. Thus, when the load was increased the soot formation also increased. This behavior was shown even considering other cross effects. For instance, in the 1500 rpm cases, the CA50 and EGR were constant for both loads tested (8 and 14 bar BMEP). By contrast, the injection pressure was higher when the load was increased (Table 4.3), and therefore reduced soot formation could be expected. Nevertheless, considering in-cylinder measurements, the effect of higher equivalence ratio due to higher load seems to govern the total soot formation and consequently, higher equivalence ratio provides higher soot formation. Considering RoHR traces, it can be stated that the radiation intensity starts with the RoHR and the maximum peak intensity of both curves are almost coincident. The end of radiation traces go to zero at similar crank angle degree as the RoHR.

To provide a direct comparison and with the aim of validating previous discussions, Figure 4.15 presents the total radiation for different load operating conditions. It should be also noted that the total radiation is the radiation intensity integrated during the whole temporal evolution. Thus, an increase in load clearly shows an increase in total radiation.

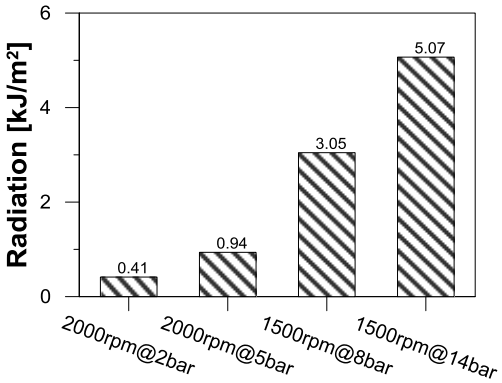

Figure 4.15. Total radiation for different load operating conditions

4.4.2.2 Effect of swirl, EGR and injection parameters

Figure 4.16 presents the temporal evolution of rate of heat release, radiation intensity, soot temperature and optical thickness for the case of 2000 rpm and 5 bar BMEP, which is reference condition. Sub-figure a) shows the isolated effects of swirl ratio maintaining constant the CA50 at 13 CAD aTDC and without EGR. Sub-figure b) presents the EGR effects maintaining constant the SR at 1.4 and CA50 at 13 CAD aTDC. Finally, sub-figure c) presents the effects of CA50 keeping constant SR at 1.4 and without EGR. As previous figures, different curves represent the average and standard deviation of 100 cycles.

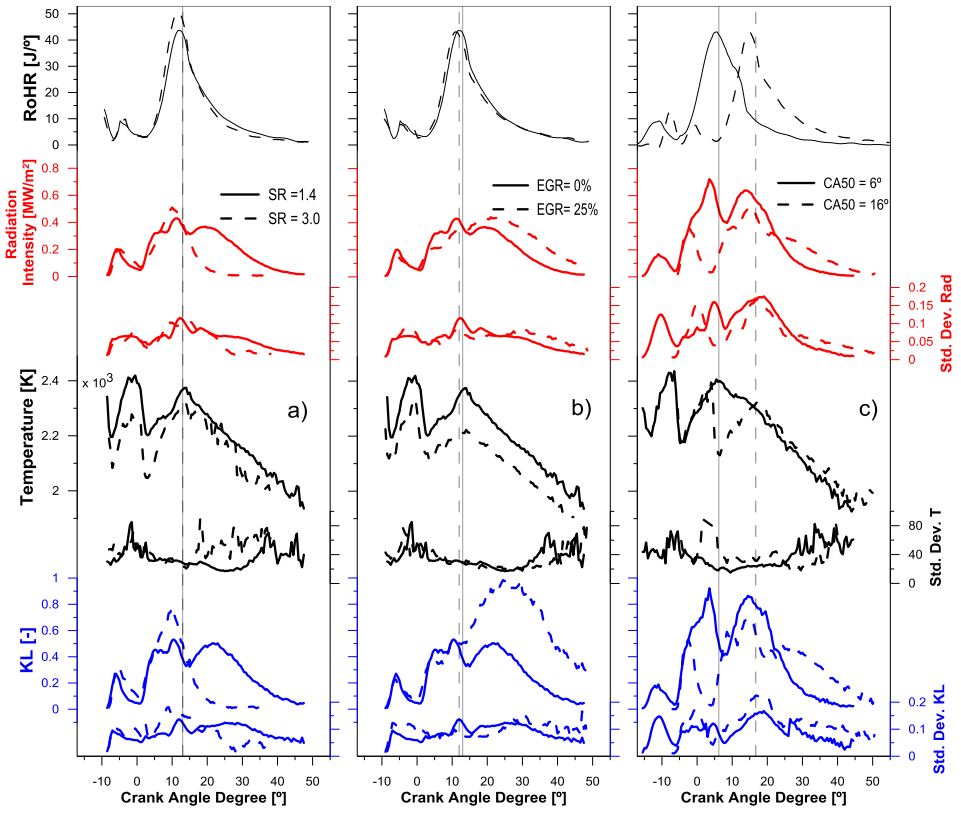

Figure 4.16. Temporal evolution of radiation intensity, soot temperature and KL for 2000 rpm@ 5 bar BMEP; (a) swirl ratio effect; (b) EGR effect and (c) CA50 effect. For each studied case, the end of injection is marked with a vertical line.

Considering the effect of swirl ratio, it is possible to state that an increase of swirl number implies an overall enhancement of fuel air mixing after the end of injection. Consequently there was an acceleration of the flame progression with a higher peak of RoHR and a faster decay after the end of injection [26]. This behavior found in the RoHR was also attained in the radiation intensity. When the swirl ratio was increased, a higher peak of radiation was attained as well as a faster decay after the end of injection. Before EoI, an increase in SR resulted in higher soot formation, maybe due to spray interaction [27]. By contrast, after the EoI, a lower KL was obtained

due to an improvement in mixing process. Regarding soot temperature, quite similar values were attained. A slight increase was obtained when higher swirl ratio was proposed.

Regarding EGR effect, taking into account free spray considerations [28], it can be stated that when EGR was increased, similar equivalence ratios at lift-off length were attained. This fact implies that similar soot formation is expected. Thus, similar soot formation together with lower combustion temperature due to higher EGR should provide lower radiation. By contrast, considering real engine conditions as presented in the current research, it is well known that the higher EGR implies the higher peak of radiation intensity with larger radiation time and therefore higher global radiation. This behavior can be explained considering KL curves. Thus, when the higher EGR rates were used, the higher peaks of KL were obtained. Moreover, more time is available to form soot. Consequently higher soot formation is obtained. This fact seems to have higher impact on radiation than the reduction in soot temperature. Concerning soot temperature, an expected decrease due to the reduction in oxygen concentration was observed.

Concerning combustion phasing effect, when the injection timing is delayed with the aim of delaying CA50, greater part of the combustion process takes place during expansion stroke and therefore lower in-cylinder pressure and temperature are expected. Concerning radiation intensity, it is possible to state that when CA50 is delayed, lower radiation is attained. In particular, lower peak and slower decay is shown during the temporal evolution. Lower in-cylinder temperatures imply more time to attain more premixed combustion process with less rich equivalence ratios and therefore lower soot formation.

To compare directly the effects of swirl ratio, EGR and CA50, Figure 4.17 presents the specific total radiation intensity for the different operating conditions tested (without taking into account the area of the flame). As described in detail in the previous paragraphs, the soot radiation intensity

decreases when the swirl ratio increases and/or EGR rate decreases and/or combustion phasing is delayed.

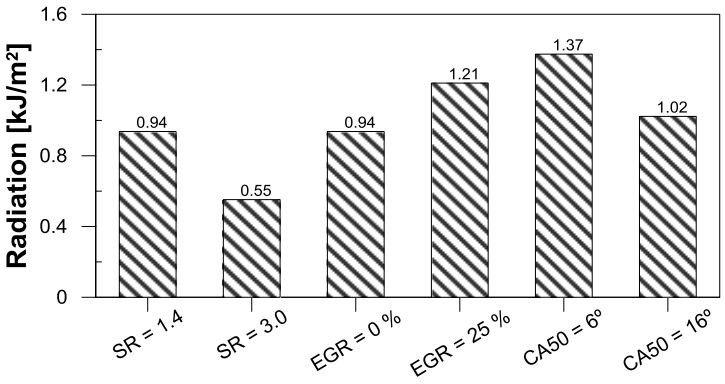

Figure 4.17. Total radiation considering swirl ratio, EGR and combustion phasing effects.

4.5 Conclusions

In this chapter, the main objective has been to evaluate the amount of energy lost by the soot radiation during the combustion process for different operating conditions. For this, the radiation measurements have been based on the two-color method applied on two independent and different optical systems. First, this technique has been used to perform a basic characterization to understand the soot radiation process under simplified and controlled conditions in an optical engine. In addition, these measurements have served to validate both optical systems, Optoelectronic Pyrometer (OP) and High Speed Imaging Pyrometer (HSIP). In a second soot radiation study has been performed in a HSDI production engine simulating real conditions of engine operation. In this case, only the optoelectronic probe has been used to perform the experimental measurements.

Considering results obtained under simplified and controlled conditions, the following conclusions can be stated:

- The temporal evolution of the spectral intensity on the spray axis was characterized showing an increase when the injection pressure was decreased and/or the ambient temperature and in-cylinder gas density were increased. Coupled with this behavior, the lift-off length was also characterized. Thus, larger values were obtained when the injection pressure was increased and/or in-cylinder gas density and temperature were decreased. The larger the lift-off, the lower the soot volume fraction and therefore the spectral intensity. Consequently, an increase in the radiant fraction (i.e. the fraction of energy that is lost by radiation) was obtained when the injection pressure was decreased and/or the ambient temperature and in-cylinder gas density were increased.
- Radiant fraction shows values from 0.1% to 0.75% with respect to the total fuel energy depending on the injection pressure at 800 K. The higher the injection pressure, the lower radiant fraction. For the 900 K cases, the radiant fraction values are between 0.27% and 0.75%. Regarding density, small differences have been obtained, although lower radiation values have obtained with lower ambient density (this behavior seems to be more evident for lower ambient gas temperatures). These values are around an order of magnitude lower than a blackbody with the same area radiating during the whole injection event. In general, the values obtained present consistency with the work performed by Skeen *et al.* [48].
- In spite of several assumptions while analyzing data from the Optoelectronic Pyrometer, information of combustion process is spatially integrated along the line of the probe sight. It provides similar results in terms of soot temperature and optical thickness compared with a conventional High Speed Imaging Pyrometer. Therefore, the optoelectronic probe is considered valid as an optical measurement system.

The main conclusions regarding the results obtained in 4-cylinder engine are summarized below. They can be split depending on the engine parameter sweep:

- Considering load effects, it can be said that maintaining constant engine speed, the radiation intensity peak was higher when the load was increased. In addition, total radiation was defined as the radiation intensity integrated during the completely temporal evolution and as expected, it showed a clear increase when the load was increased. A clear decrease in soot temperature was attained when the engine load was decreased. KL profiles depend directly on the diffusion phase of combustion, the higher the duration of this phase, the higher the amount of soot obtained. In particular, the end of injection determined the evolution of the KL profile in terms of maximum values as well as decay.
- Considering swirl ratio effects, it can be stated that an increase of swirl ratio implied an enhancement of combustion process that seems to be more prominent after the end of injection. Therefore, a higher peak of radiation intensity with a faster decay after the end of injection was attained. Nevertheless, when total radiation was considered, an increase in swirl ratio resulted in lower total radiation. Considering KL temporal evolution results, it seems that end of injection determines an inflection point. Thus, an increase in SR resulted in higher soot formation before the EoI and lower KL after the EoI. Regarding soot temperature, quite similar values were attained independent on the swirl ratio.
- Taking into account EGR effects, it can be demonstrated that higher EGR implies higher peak of radiation intensity with increased radiation time and therefore higher total radiation. Higher EGR rates lead to higher peaks of KL and more time available for soot formation, while soot temperature is decreased. The higher soot formation effect seems to have higher impact on radiation than the reduction in soot temperature and therefore higher total radiation was attained when higher EGR was used.

- Finally, considering the injection timing (combustion phasing) effects it can be stated that when CA50 was delayed, lower peak of radiation intensity was attained. This behavior was due to lower soot temperatures when the CA50 was delayed and lower soot formation since more time to achieve premixed combustion was available.

4.6 Bibliography

[1] Dimopoulos, P., Bacha, C., Soltica, P., Boulouchos, K. "Hydrogen-natural gas blends fuelling passenger car engines: Combustion, emissions and well-to-wheels assessment". Int. J. Hydrogen Energ. 33(23), 7224-7236, 2008.

[2] Osada, H., Uchida, N., Shimada, K., and Aoyagi, Y. "Reexamination of Multiple Fuel Injections for Improving the Thermal Efficiency of a Heavy-Duty Diesel Engine". SAE Technical Paper 2013-01-0909, 2013.

[3] Morawitz, U., Mehring, J., and Schramm, L. "Benefits of Thermal Spray Coatings in Internal Combustion Engines, with Specific View on Friction Reduction and Thermal Management". SAE Technical Paper 2013-01-0292, 2013.

[4] Serrano, J., Olmeda, P., Tiseira, A., García-Cuevas, L. "Importance of Mechanical Losses Modeling in the Performance Prediction of Radial Turbochargers under Pulsating Flow Conditions". SAE Int. J. Engines 6(2):729-738, 2013.

[5] Neshat E., Kloshbakhti R. "Effect of different heat transfer models on HCCI engine simulation". Energy conversion and management 88, 1-14, 2014.

[6] Taymaz, I. "An experimental study of energy balance in low heat rejection diesel engine". Energy 31 (2-3) 364-371 2006.

[7] Benajes J., Pastor J.V., García A., Monsalve-Serrano J. "An experimental investigation on the Influence of piston bowl geometry on

RCCI performance and emissions in a heavy-duty engine". Energy Conversion and Management 103, 1019-1030, 2015.

[8] Benajes J., Molina S., García A., Monsalve-Serrano J. "Effects of Direct injection timing and Blending Ratio on RCCI combustion with different Low Reactivity Fuels". Energy Conversion and Management, Volume 99, 193-209, 2015.

[9] Struwe, F.J. "In-cylinder Measurement of Particulate Radiant Heat Transfer in a Direct Injection Diesel Engine". SAE Technical Paper 2003-01-0072, 2003.

[10] Furmanski P., Banaszek J. and Wisniewski T. S. "Radiation Heat Transfer in a Combustion Chamber of Diesel Engine with Partially Transparent Burnt Gas Zone". SAE Technical Paper 980504, 1998.

[11] Vogelin P. "Experimental investigation of multi-in-cylinder pyrometer measurements and exhaust soot emissions under steady and transient operation of a heavy-duty Diesel engine". SAE Technical Paper 131ICE-0145, 2013.

[12] Skeen S., Manin J. and Pickett L. "Quantitative Spatially Resolved Measurements of Total Radiation in High-Pressure Spray Flames". SAE Technical Paper 2014-01-1252, 2014.

[13] Flynn, P., Mizusawa, M., Uyehara, O., and Myers, P. "An Experimental Determination of the Instantaneous Potential Radiant Heat Transfer within an Operating Diesel Engine". SAE Technical Paper 720022, 1972.

[14] Payri R., Salvador F.J., Gimeno J. and Bracho G. "A new methodology for correcting the signal cumulative phenomenon on injection rate measurements". Experimental Techniques, Vol. 32 no 1, pp. 46-49, 2008.

[15] Nerva J-G. "An assessment of fuel physical and chemical properties in the combustion of a Diesel spray". Doctoral Thesis, Universitat

Politècnica de Valencia, Departamento de Máquinas y Motores Térmicos, 2013.

[16] Bermúdez V., García J.M., Juliá E. and Martínez S. "Engine with optically accessible cylinder head: A research tool for injection and combustion processes". SAE Technical Papers, 2003.

[17] Payri F., Pastor J.V., Nerva J.-G., García-Oliver J.M. "Lift-Off Length and KL Extinction Measurements of Biodiesel and Fischer-Tropsch Fuels under Quasi-Steady Diesel Engine Conditions". SAE International Journal of Engines, Vol. 4 no 2, pp. 2278- 2297, 2011.

[18] Tree D.R, Svensson K.I. "Soot processes in compression ignition engines". Prog. Energy Combustion Science 2007; 33:272–309.

[19] Pickett L.M, Siebers D.L. "Soot in diesel fuel jets: effects of ambient temperature, ambient density, and injection pressure". Combustion and Flame 2004; 138:114–35.

[20] Way RJB. "Methods for determination of composition and thermodynamic properties of combustion products for internal combustion engine calculations". Proc. Inst. Mech. Eng. 1976;190:687–97.

[21] Musculus PBM. "Measurements of the influence of soot radiation on in-cylinder temperatures and exhaust NOx in a heavy-duty DI diesel engine". SAE technical paper 2005-01-0925; 2005.

[22] Manin J, Pickett L.M, Skeen S. "Two-color diffused back-illumination imaging as a time-resolved soot measurements in reacting sprays". SAE technical paper 2013-01-2548; 2013.

[23] Payri F, Olmeda P, Martín J, García A. "A complete 0D thermodynamic predictive model for direct injection diesel engines". Applied Energy 2011;88(12):4632–41.

[24] Soloiu V, Lewis J, Yoshihara Y, Nishiwaki K. "Combustion characteristics of a charcoal slurry in a direct injection diesel engine

and the impact on the injection system performance". Energy 2011;36:4353–71.

[25] Arrègle J, Pastor J.V, López J.J, García A. "Insights on postinjection-associated soot emissions in direct injection diesel engines". Combustion and Flame 2008;154:448–61.

[26] Benajes J, Molina S, García JM, Riesco J.M. "The effect of swirl on combustion and exhaust emissions in heavy-duty diesel engines". Proc. Inst. Mech. Eng., Part D: J. Automobile Eng. 2004; 218.

[27] De la Morena J., Vassallo A. Peterson R.C., Gopalakrishan V., Gao J. "Influence of Swirl Ratio on Combustion System Performance of a 0.4l Single-Cylinder Diesel Engine". THIESEL 2014 Conference on Thermo- and Fluid Dynamic Processes in Direct Injection Engines.

[28] Tao F, Liu Y, Rempelewert B.H, Foster DE, Reitz R.D, Choi D. et al. "Modeling the effects of EGR and injection pressure on soot formation in a high-speed directinjection (HSDI) diesel engine using a multi-step phenomenological soot model". SAE technical paper 2005-01-0121; 2005.

Chapter 5

Analysis of soot oxidation process in a production DI engine

Content

5.1 Introduction

Focusing on soot emissions it is possible to state that soot production in a diesel engine is the result of two competing processes: soot formation and soot oxidation. Thus, spatially the first soot precursors are formed in the fuel-rich premixed burn region in the diffusion flame depending on the local equivalence ratio [1]. Once these precursors appear, particle growth occurs due to high temperature and absence of oxygen in the region covered by the diffusion flame. Now, regarding the soot oxidation process, two different stages in the temporal evolution of the in-cylinder soot concentration need to be considered [4]. In the first stage, from the Start of Injection (SoI) up to the End of Injection (EoI), a quasi-steady state is achieved, and nearly all the soot formed in the spray core is oxidized when reaches the diffusion flame front. In the second stage, from EoI up to the End of Combustion (EoC), the diffusion flame vanishes and soot formation decreases. At these conditions soot oxidation is strongly coupled with the mixing rate and in-cylinder temperature [1]. It is also worthy to note that only a small fraction of the soot formed in cylinder is emitted in the exhaust [3].

Figure 5.1 shows the correlation between the maximum amount of soot formed (peak value of soot concentration, KL) and concentration of PM emissions in the exhaust for different measured engine conditions [4]. Thus, two groups of results are clearly observed: on the one hand, the square symbols points out a group of results in which the PM emissions are similar and low independently on the peak value of soot concentration, KL and therefore independently on the value of in-cylinder soot formed. On the other hand, group of circle symbols indicate other results where the highest concentrations of soot formed, maximum of KL peak value correspond on lowest values of PM emissions, and vice versa. These trends are the opposite of those that would be expected if the PM emissions were explained by the amount of formed soot [5]. Gallo et al. have obtained a similar correlation. In their study [7], different operating conditions were measured in an optical engine and the laser extinction technique was used to evaluate the oxidation

rates during the expansion stroke. They conclude that the amount of in-cylinder soot formed does not explain the engine-out soot emissions. Considering diesel fuel and operating conditions tested, the oxidation process is mainly responsible for the exhaust PM emissions in a CI diesel engine under real conditions.

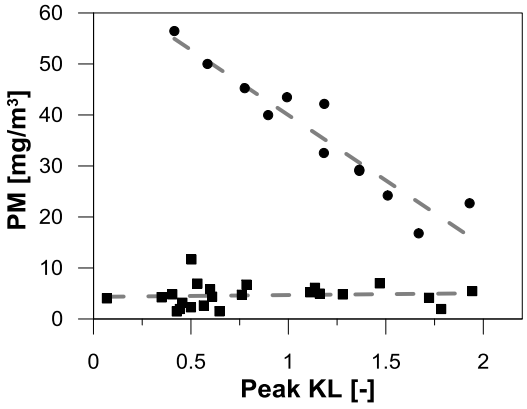

Figure 5.1. Concentration of exhaust PM versus the maximum value of KL for the different engine conditions measured in [4].

The soot formation process has been studied extensively [6], but now we are going to focus on some studies on in-cylinder soot oxidation that can be highlighted. Pickett *et al.* [8] reported that a reduction in the in-cylinder ambient density causes a large decrease in the peak soot volume fraction due to longer combustion duration and slower combustion development. Measurements were made by using laser extinction under a wide range of operating conditions. Gallo *et al.* [7] analyzed the amount of PM emitted by modifying the injection pressure, gas density and temperature at TDC as well as engine speed and nozzle hole size by application of the laser extinction method. These authors concluded that increasing the injection pressure, gas density, and reducing nozzle hole size and the engine speed, the engine-out PM emissions were strongly reduced. Dembinski *et al.* [9] studied the impact of swirl ratio and injection pressure on the soot oxidation process. Experimental measurements were made with two different optical techniques

(Combustion Image Velocimetry and two-color method) in an optical engine. This research stated that the soot oxidation process improved when the swirl ratio and injection pressure were increased due to an enhancement of in-cylinder turbulence. Tree and Svensson [10] studied the effect of different engine parameters on the soot oxidation process, concluding that the ambient temperature had the greatest effect by increasing the reaction rates. O'Connor and Musculus [12] studied the effect of different engine parameters on the soot oxidation process, concluding that a post injection can reduce engine-out soot by up to 45% at high swirl ratios and 30% for low swirl ratios. Finally, Arrègle et al. [42] showed different post-injection strategies for reducing soot emissions in DI diesel engines. In this research, a broad experimental analysis was carried out to explore the behavior of post-injection strategy on exhaust soot emissions under a certain range of operating conditions and with different post-injection timings. These authors concluded that the engine-out soot emissions were reduced when the post-injection event was added.

This chapter is focused on the effects of different engine parameters regarding soot oxidation process. Therefore, the particular objectives are following:

- Evaluate soot oxidation process for different parameters and under real operating conditions and thus, provide a better knowledge of this phenomenon.
- Compare different engine strategies to enhance the late-cycle mixing controlled combustion process and therefore to improve the soot oxidation process while maintaining similar gross indicated efficiency.

5.2 General methodology of the study

To solve the two proposed partial objectives, this chapter is divided into two results sections. In the first place, the aim is to evaluate the soot

oxidation process by varying parameters related to the air thermodynamic conditions and the injection process. These experimental measurements have been made in the production 4-cylinder GM 1.9L direct-injection light-duty diesel engine defined in Chapter 3. In addition, the set of experimental results will be used to adjust an experimental correlation capable of evaluating the soot oxidation from experimental parameters and, in this way, to explain the soot oxidation procedure. In the second section of the chapter, an evaluation of the swirl ratio and an appropriate injection strategy will be carried out in order to optimize the mixing controlled combustion process. Finally, both strategies will be compared and the best option will be selected. These experimental measurements will be made in a single-cylinder direct-injection light-duty diesel engine derived from the 4-cylinder GM 1.9L diesel engine.

Both partial objectives are carried out the same simplified methodology. This methodology analyzed the effect of mixing process on soot oxidation during the late-cycle combustion. This phase has been defined from the end of the injection process (EoI) until the end of the combustion (EoC). As an oxidation process tracer, the soot concentration (KL) measured by the optoelectronic probe (VisioFEM) is used.

To estimate mixing capability an Apparent Combustion Time (ACT) parameter was used. This parameter was calculated as shown in Figure 5.2 (for a particular case with a single injection): it is the dwell time between the instant where a certain percentage of the mass of fuel has been injected (point of injection, POI_i) and the instant where this same percentage is burned (point of combustion, POC_i). On the one hand, this fact does not imply that all the fuel injected in a given instant burns after the ACT_i: this parameter is just representative of the time necessary for a percentage of injected fuel to be ready for combustion. On the other hand, the ACT must not be confused with the ignition delay, because the ACT has a more general meaning: only the ACT corresponding to the first injected fuel coincides with the ignition delay (as shown in Figure 5.2 whereas it has a certain evolution for the rest of the injected fuel. This evolution is shown in Figure 5.3, where the ACT parameter (black solid line) corresponding to the case presented in

Figure 5.3 has been plotted. As it is possible to observe in Figure 5.3, the ACT^{-1} parameter is also plotted. In this sense ACT^{-1} is considered as a mixing capability tracer. Thus, it is possible to observe how the mixing capability remains almost constant while the injection is in progress (up to a mass fraction of 0.43), since it is the momentum flux introduced by the nozzle which governs the mixing process. Nonetheless, once the end of injection is reached, the mixing capability starts to decrease, tending to its lowest value at the end of the combustion process.

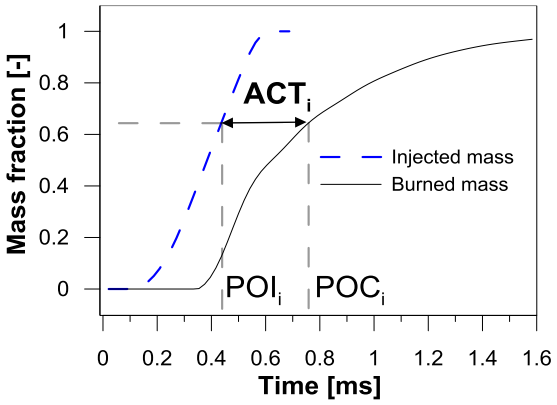

Figure 5.2. Definition for the Apparent Combustion Time (ACT)

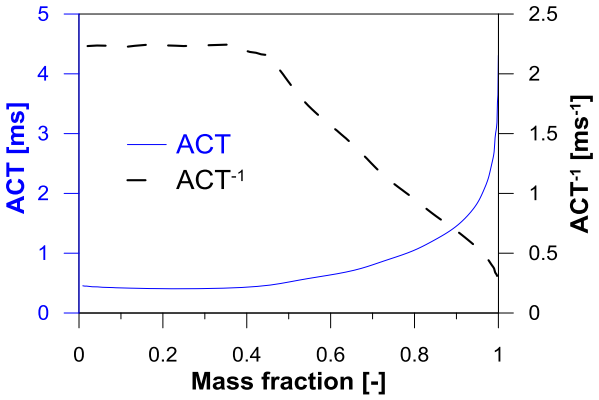

Figure 5.3. Evolution of the ACT and ACT^{-1} parameter for the case shown in Figure 5.2 (single injection pulse)

Assuming that the late-cycle KL and ACT^{-1} curves follow an exponential decay after the main injection, it would be possible to quantify the late-cycle soot oxidation rate by extracting the half-life values of the decay curves.

Figure 5.4 shows the temporal evolution of the experimental average KL together with its standard deviation for the 2000 rpm and 2 bar BMEP case with an injection pressure of 400 bar. In addition, the EoI is marked with a vertical dashed straight line. The KL profile can be split in two parts. The first part consists of the period from SoI up to EoI. It can be checked that during the fuel injection process the soot balance is governed mainly by the formation process and therefore the KL increases. The second part consists of late-cycle combustion, from EoI up to EoC. The fuel injection process is completed and thus, the soot formation phenomenon starts to be mitigated. Then, the soot oxidation begins to be the principal mechanism which rules the soot balance. In spite of significant soot oxidation during the first part, only the second part is considered for calculation of KL half-life time in this study, since the oxidation during this part is the main responsible for the final engine-out soot emissions. This analysis has been done by adjusting the experimental data to an exponential equation, as shown in Figure 5.4.

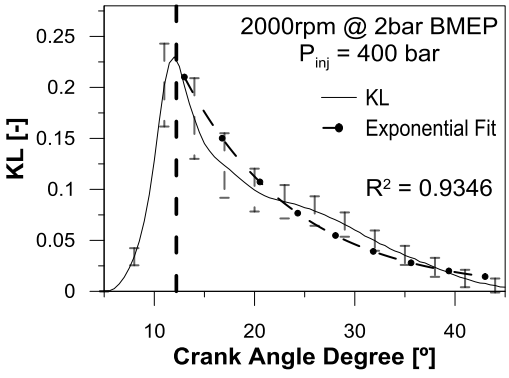

Figure 5.4. KL trace for the P_{inj} = 400 bar case at point 2000 rpm@ 2 bar BMEP and its exponential fit

Once the exponential KL curve is obtained, the half-life time, $t_{1/2}$, is given by equation (5.1):

$$KL = \alpha \cdot e^{\frac{-ln(2)\cdot x_{CAD}}{t_{1/2}}} \quad (5.1)$$

where α is a constant and x_{CAD} is the crank angle position aTDC in CAD. Thus, the half-life time of KL, $t_{1/2\ KL}$, is defined as the time required for the initial soot concentration volume to oxidize to half its value. It is an estimate of the soot oxidation rate: the lower the $t_{1/2\ KL}$, the higher the oxidation rate.

Concerning the mixing process, Figure 5.5 shows the temporal evolution of the experimental ACT^{-1} for the 2000 rpm and 2 bar BMEP case with an injection pressure of 400 bar. The curve represents the average of 100 cycles and its standard deviation. As for the optical thickness analysis, only the late-cycle part of the curve is selected for studying the soot oxidation rate, i.e. from the EoI up to EoC. The experimental ACT^{-1} depends on in-cylinder air density, ρ_a, injection velocity, u_0, and oxygen molar fraction, $[O_2]$, as follows [13]: Thus, ACT^{-1} can be considered as a 'mixing capability' tracer.

$$ACT^{-1} = \frac{\rho_a^{0.5}\cdot u_0\cdot[O_2]^{0.5}\cdot\phi_0^{-1}}{K} \quad (5.2)$$

To quantify the mixing capability related with soot oxidation, exponential decay functions were also used to fit ACT^{-1} curves.

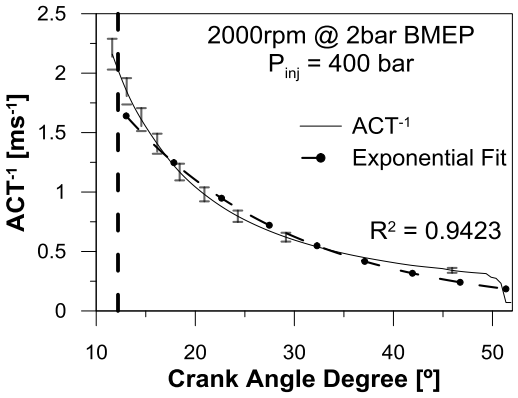

Figure 5.5. ACT^{-1} trace for the P_{inj} = 400 bar case at point 2000 rpm@ 2 bar BMEP and its exponential fit.

By definition, the half-life time of exponential ACT^{-1} curve is given by:

$$ACT^{-1} = b \cdot e^{\frac{-ln(2)\cdot x_{CAD}}{t_{\frac{1}{2}}}} \tag{5.3}$$

where b is a constant and x_{CAD} is the crank angle position aTDC in CAD. Thus, the half-life time of ACT^{-1}, $t_{1/2\ ACT\text{-}1}$, is defined as the time required the mixing capability to be the half of its initial value. It is an estimate of the rate of 'mixing capability'.

5.3 Influence of engine parameters on soot oxidation process.

In this section, soot oxidation process has been studied during late-cycle combustion modifying the intake air characteristics and several parameters of the injection process. For this, the parameters defined in the previous section of methodology will be used.

5.3.1 Test conditions

The engine was operated at different engine speeds and loads. In particular, four operating points at steady-state were selected with the goal to cover a wide operating range of the 4-cylinder engine map. For that purpose, a parametric study has been carried out, which can be classified into two groups: a first group that comprises swirl ratio, EGR rate, ambient density at the TDC and air intake temperature. On the other hand, a second group with the injection pressure and the combustion phasing, involve the characteristics of the injection process.

Starting from the air intake parameters, for the case of the swirl, values have been measured from SR = 1.4 to SR = 3 (minimum and maximum in the 4-cylinder engine). In these conditions, air intake temperature at 318 K, without EGR and ambient density at top dead center of 20.3 and 23.2 kg/m^3 depending on the point of operation. The injection pressure has been adjusted at its reference value depending on the point of operation and the combustion phasing at 13 CAD aTDC. The EGR rate has been varied maintain constant the other variables in their reference values. For the operating condition of 1500 rpm and 14 bars BMEP, the EGR sweep has not been measured since the high load points not allow for a reduction of the oxygen concentration in the intake, which generates a great combustion instability. The maximum EGR for each condition was imposed by taking the limit value of FSN = 3 on the soot emissions in the exhaust. In terms of ambient density, the range has been defined considering the minimum, intermediate and maximum intake pressure that can be generated by the turbine at each operation point. In the case of the air intake temperature, an air intake temperature sweep has been carried out maintaining constant ambient density at the TDC of 22 kg/m^3 for both operating conditions. For this, the intake pressure has been varied to counteract the effect of temperature.

Respect to injection parameter sweeps, the combustion phasing variation has been measured from 6 to 20 CAD aTDC. The range has been selected taking as maximum cylinder pressure limit in 160 bar and minimum

limit value of 3 FSN. Relative to the injection pressure, just as in the cases of intake temperature and density, it has only been possible to measure for low load points, covering a range of injection pressure from 400 to 800 bar. As explained for the previous parameters, the reference values were taken for the rest of the variables. In summary, Table 5.1 shows the different operating conditions.

Operating condition	**2000rpm @ 2bar**	**2000rpm @ 5bar**	**1500rpm @ 8bar**	**1500rpm @ 14bar**
Torque [Nm]	37	87	132	220
Load [%]	10	24	48	84
Inj. Pressure [bar]	450 (400, 600, 800)	650 (400, 600, 800)	735	1037
m_f [g/s]	0.65	1.15	1.33	2.33
CA50 [°aTDC]	13 (6, 11, 16, 20)			
T_{in} [K]	318 (303, 313, 323, 333)		318	
P_{in} [bar]	1.16 (1.03, 1.26, 1.48)	1.37 (1.07, 1.37, 1.65)	1.35	1.73
P_{exh} [bar]	1.29 (1.1, 1.51, 2.41)	1.58 (2.04, 2.49, 3.2)	1.55	2.19
m_a [g/s]	38.9	43.8	30	38.2
SR [-]	1.4 (1.4, 2, 2.5, 3)			
Density [kg/m³]	20.3 (18.1, 22, 25.6)	23.2 (18.5, 23.5, 28.1)		
EGR [%]	0 (0,14,27)	0 (0, 11, 22)	0 (0, 5, 11)	0
Equivalence ratio [-]	0.244	0.383	0.649	0.893

Table 5.1. Experimental engine operating conditions.

Commercially available European diesel fuel was used in this part of the work. Table 4.5 shows the main characteristics of the fuel used.

5.3.2 Effect of air intake characteristics on soot oxidation

This section presents the analysis of soot oxidation results obtained by varying the swirl ratio, exhaust gas recirculation (EGR), ambient density and air intake temperature in a 4-cylinder direct-injection light-duty diesel engine. To simplify the information analyzed in this section, the analysis will be performed for the low load point (2000 rpm and 2 bar BMEP). At last part of this section, a summary will be shown for the rest of the operating conditions.

Effect of swirl on late-cycle soot oxidation

Swirl Ratio (SR) has a well-known effect on the combustion process. An increase in SR implies an improvement in mixing and therefore an acceleration of combustion event [14]. In this sense, a reduction in exhaust soot emissions is also attained when SR is increased [9], Thus, to study the impact of SR on soot oxidation process during the current research two tracers will be used. Considering the work performed by Gallo *et al.* [7] and Huestis *et al.* [11] half-life time for optical thickness is proposed with the aim of evaluating soot reduction after the EoI. On the other hand, to evaluate the mixing capability and its effect on the combustion process and therefore on soot emissions, half-life time for ACT^{-1} is used. Thus, the soot emissions were studied by varying the swirl number from 1.4, 2, 2.5 and 3, while maintaining constant CA50 at 13 CAD aTDC and without EGR. The temporal evolutions of KL and ACT^{-1} were recorded for 400 cycles. Exponential decay functions were used to fit KL and ACT^{-1} after the EoI, as already explained in Section 5.2.

Based on the swirl numbers tested, the crank angle degree intervals to perform the fit are different for each decay curve. These intervals are represented in Table 5.2. Each interval was selected based on a detailed study of the curve shapes. In these tests, the onset of the exponential fits begins at the maximum KL peak which was between 11 - 13 CAD aTDC depending on the SR. End of the exponential fit ranges from 40 - 45 CAD aTDC, where

KL traces approach zero. The R^2-values showed in the Table 5.2 indicate a proper accuracy level of exponential fit, from 0.95 up to almost 0.99.

Swirl [-]	**Interval fitting** [CAD]	**R^2-values** [-]
1.4	11 – 45	0.9515
2	11.5 – 43	0.9803
2.5	11.5 – 42	0.9890
3	13 – 40	0.9795

Table 5.2. Interval used to exponential fit and R^2-values for the swirl sweep KL at point 2000 rpm@ 2 bar BMEP

Figure 5.6 shows the values of half-life time of KL, $t_{1/2\ KL}$, and its standard deviation obtained from the exponential fits of the different swirl numbers tested. As was expected [9], the half-life time decreases with the increase of swirl number. In-cylinder angular velocity in the case of high swirl number (SR= 3) is higher than with low swirl number (SR= 1.4). Thus, an increase in turbulence and vorticity is created due to the higher rotational speed of the airflow. Turbulence and vorticity affect soot oxidation by enhancing the mixing process during the late-cycle period and therefore the soot oxidation rate is increased when swirl number is increased [9].

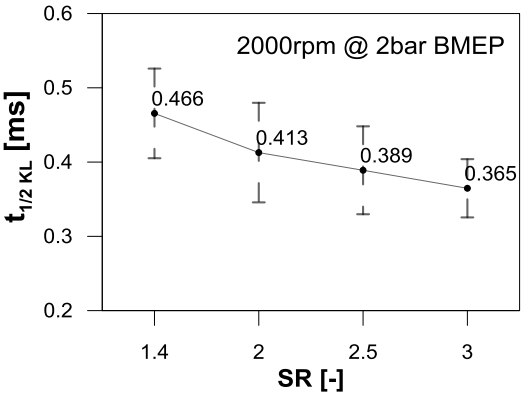

Figure 5.6. The half-life of KL, $t_{1/2\ KL}$, calculated for the swirl sweep at point 2000 rpm@ 2 bar BMEP

Just like in the case of KL, to quantify the mixing capability related with soot oxidation, exponential decay functions were also used to fit ACT^{-1} curves. In these cases, the crank angle degree intervals are similar for each trace, as illustrated in Table 5.3. The onset of the exponential fit for each curve begins after End of Main Injection (EoMI). Profile decay starts between 12 - 13 CAD aTDC and the end of the exponential fits range from 47 - 49 CAD aTDC. The R^2-values indicate reasonable accuracy as it is shown in the Table 5.3 (0.95 - 0.96).

Swirl [-]	**Interval fitting** [CAD]	**R^2-values** [-]
1.4	12 – 47	0.9666
2	12.5 – 49	0.9519
2.5	13 – 48.5	0.9609
3	13 – 48	0.9621

Table 5.3. Interval used to exponential fit and R^2-values for the swirl sweep ACT^{-1} at point 2000rpm@2bar

Figure 5.7 shows the results of half-life times of ACT^{-1} (average value and its standard deviation) for the swirl number sweep. The half-life times of

the ACT^{-1}, $t_{1/2\ ACT\text{-}1}$, decrease when the swirl ratio is increased. The lower the $t_{1/2\ ACT\text{-}1}$ the higher the mixedness. Considering constant in-cylinder ambient density, injection velocity and oxygen concentration between different SR cases, a higher value of swirl number produces an enlargement of the turbulence [9], which is reflected in lower time to burn similar fuel injected comparing different tests. Therefore an improvement in the air/fuel mixing process is confirmed.

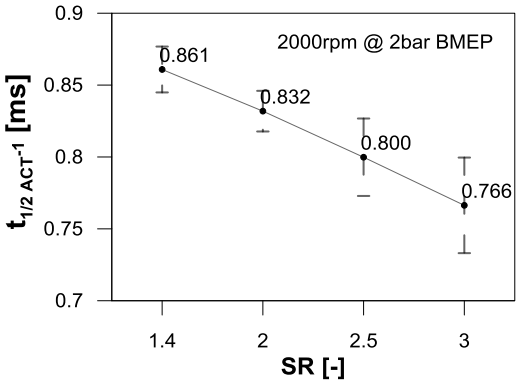

Figure 5.7. The half-life time of ACT^{-1}, $t_{1/2\ ACT\text{-}1}$, calculated for the swirl number sweep at point 2000 rpm@ 2 bar BMEP.

Considering Figure 5.6 and Figure 5.7, it can be stated that similar trends were attained for both half-life times. Thus, the mixedness tracer can be used to explain the soot oxidation process in next sections.

Effect of EGR on late-cycle soot oxidation

In this sub-section, soot oxidation will be analyzed for varying EGR levels, while maintaining the swirl ratio at 1.4 and the CA50 at 13 CAD aTDC. The operating point 1500 rpm and 14 bar BMEP was not tested with EGR as the high load point did not allow for a decrease in the oxygen concentration in the intake without excessive combustion instability (Table 5.1). The maximum EGR percentage in each operating condition was defined considering a limit of FSN = 3 for the exhaust soot emissions. In particular,

for the 2000 rpm and 2 bar BMEP operating point, the maximum EGR rate was 27%. As in the swirl ratio sweep, the temporal evolution of KL and ACT^{-1} were recorded for 400 cycles and similar processing methodology was also followed. Exponential decay functions were used to fit KL and ACT^{-1} after the EoMI.

Figure 5.8 and Figure 5.9 show the half-life time for KL and ACT^{-1}. Average values for both parameters are represented along with their standard deviation. Selected interval for the fitting and the R^2-values are given in Table 5.4.

	KL		**ACT^{-1}**	
EGR [%]	**Interval fitting [CAD]**	**R^2-value [-]**	**Interval fitting [CAD]**	**R^2-value [-]**
0	11 – 45	0.9503	12 – 47	0.9666
14	11.5 – 45	0.9689	12.5 – 49	0.9507
27	12.5 – 48	0.9171	13 – 48	0.9980

Table 5.4. Interval used to exponential fit and R^2-values for the EGR sweep KL and ACT^{-1} at point 2000 rpm@ 2 bar BMEP

As other researchers indicate in the literature [15], the soot oxidation process is worsened with higher EGR rates due to lower oxygen availability. In particular, the half-life time of KL increased when EGR rate was increased. This behavior can be observed in Figure 5.8. In addition, the higher the EGR rate, the lower the combustion temperature due to increased concentration of non-reactive species [10][16].

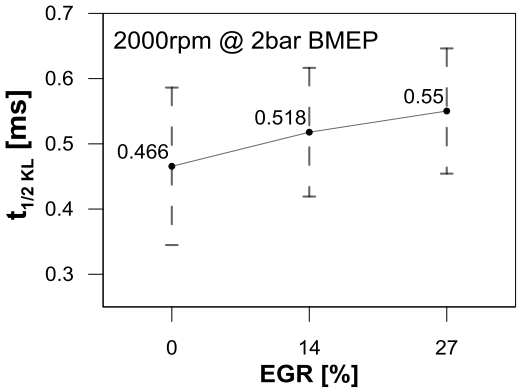

Figure 5.8. The half-life of KL, $t_{1/2\ KL}$ calculated for the EGR sweep at point 2000 rpm@ 2 bar BMEP

Figure 5.9 shows average and standard deviation of the half-life time of ACT^{-1} for the different EGR rates. When the EGR rate was increased the mixedness was worsened implying larger $t_{1/2\ ACT\text{-}1}$.

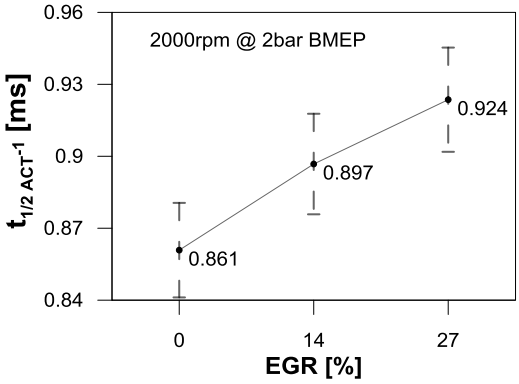

Figure 5.9. The half-life $t_{1/2}$ of the ACT^{-1} calculated for the EGR sweep at point 2000 rpm@ 2 bar BMEP

As in the SR cases, some similarity between both half-life times, $t_{1/2\ KL}$ and $t_{1/2\ ACT\text{-}1}$, were attained. The demonstrated decrease in mixing process due to lower oxygen concentration was directly related with lower soot oxidation.

Effect of ambient density on late-cycle soot oxidation

In this sub-section, soot oxidation will be analyzed for varying ambient density, while maintaining constant the rest of the engine settings. The values of ambient density were defined considering the minimum, middle and maximum intake pressure produced by the turbocharger for each operating point. In particular, for the 2000 rpm and 2 bar BMEP operating conditions, the values of ambient density selected are 18.1, 22 and 25.6 kg/m^3. As in the previous sweeps, the temporal evolution of KL and ACT^{-1} were recorded for 400 cycles, and the same processing methodology was followed. Exponential decay functions were used to fit KL and ACT^{-1} after the EoI.

Figure 5.10 and Figure 5.11 show the half-life time for KL and ACT^{-1}, respectively. The average values for the two tracers are represented together with their corresponding standard deviations. The chosen crank angle degree intervals for the fitting and R^2-values are presented in Table 5.5.

	KL		**ACT^{-1}**	
ρ_{TDC} [kg/m^3]	**Interval fitting [CAD]**	**R^2-value [-]**	**Interval fitting [CAD]**	**R^2-value [-]**
18.1	18 – 45	0.9221	16 – 52	0.9034
22	17 – 42	0.9402	16 – 51	0.9235
25.6	17 – 42	0.9544	17 – 51	0.9654

Table 5.5. Intervals used and corresponding R^2-values for the exponential fits to KL and ACT^{-1} for the ambient density sweep at point 2000 rpm@ 2 bar BMEP

Figure 5.10 shows the average and standard deviation of the half-life time of KL, $t_{1/2\ KL}$. If the ambient density is decreased, the half-life time of KL is larger. A decrease in ambient density produces larger combustion duration and slower decay at the late part of the profile due to slower combustion development [17]. This fact implies poorer soot oxidation and therefore the half-life time of KL increases, as shown in Figure 5.10.

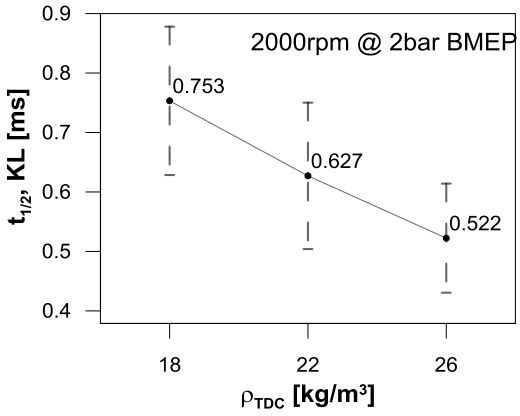

Figure 5.10. Half-life time of KL, $t_{1/2\ KL}$, calculated for the ambient density sweep at point 2000 rpm@ 2 bar BMEP

Figure 5.11 presents the average values and standard deviations of the half-life time of ACT^{-1}, $t_{1/2\ ACT\text{-}1}$, for the different ambient densities sweeps. When the ambient density was increased, the air/fuel mixing process was improved, which implies shorter $t_{1/2\ ACT\text{-}1}$.

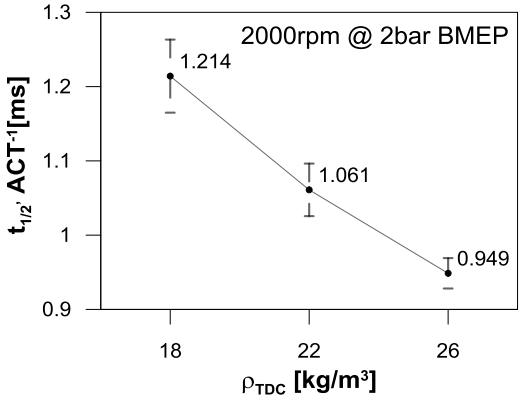

Figure 5.11. Half-life time of ACT^{-1}, $t_{1/2\ ACT\text{-}1}$, calculated for the ambient density sweep at point 2000 rpm@ 2 bar BMEP

Effect of air intake temperature on late-cycle soot oxidation

The effect of intake air temperature variation on soot oxidation will be investigated in this sub-section. Intake air temperature values have been varied maintaining the ambient density at TDC at 22 kg/m^3. The intake air temperature sweep ranged from 303 to 333 K. The lower limit is delimited by the coolant temperature of the intercooler, whereas the upper limited is defined considering the maximum intake air temperature downstream of the compressor (intercooler switched off). As in both previous sweeps, the temporal evolution of KL and ACT^{-1} were recorded for 400 cycles and the same processing methodology was followed. Exponential fits of KL and ACT^{-1} after the EoI were performed. The half-life times for the two parameters are presented in Figure 5.12 and Figure 5.13, and the selected intervals for the fits and the R^2-values are given in Table 5.6.

	KL		ACT^{-1}	
T_{in} [K]	Interval fitting [CAD]	R^2-value [-]	Interval fitting [CAD]	R^2-value [-]
303	16 – 46	0.9482	15 – 45	0.9309
313	15 – 46	0.9601	15 – 45	0.9469
323	15 – 47	0.9832	16 – 47	0.9533
333	16 – 48	0.9508	15 – 49	0.9620

Table 5.6. Intervals used and corresponding R^2-values for the exponential fits to KL and ACT^{-1} for the intake air temperature sweep at point 2000 rpm@ 2 bar BMEP

As other researches indicate in the literature [42][18], the soot oxidation process is improved with higher intake air temperature. In particular, the half-life time of KL, $t_{1/2\ KL}$, decreases when the intake air temperature was increased. This behavior can be observed in Figure 5.12. It is important to note that the half-life times of KL are very similar due to the small variation in the values of intake air temperature (just 40 K of variation, i.e. less than 15%).

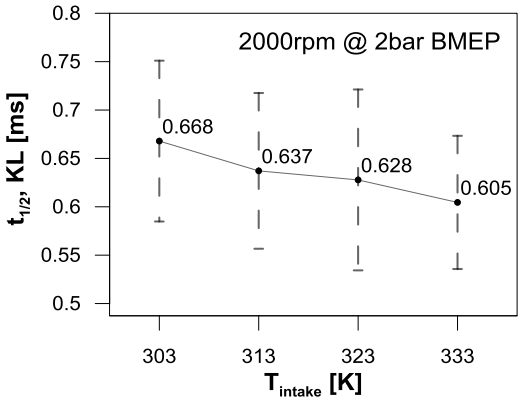

Figure 5.12. Half-life time of KL, $t_{1/2\ KL}$, calculated for the intake air temperature sweep at point 2000 rpm@ 2 bar BMEP

Figure 5.13 shows the average values and standard deviations of the half-life time of ACT^{-1}, $t_{1/2\ ACT\text{-}1}$, for the different intake air temperatures. When the intake air temperature was increased, a shorter $t_{1/2\ ACT\text{-}1}$ was obtained, showing that the mixing capability seems to increase. The authors haven't found any easy explanation to this increase in mixing capability caused by the intake air temperature increase. However, it should be taken into account that the observed variation is quite small.

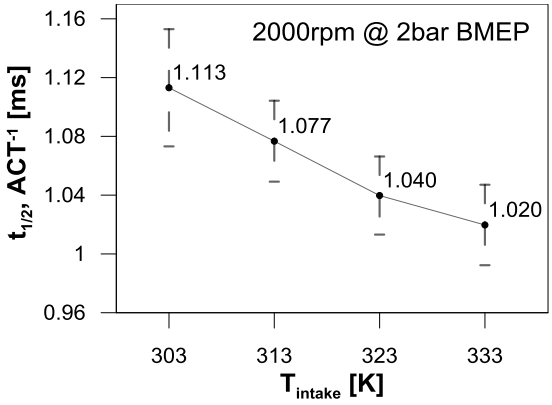

Figure 5.13. Half-life time of ACT^{-1}, $t_{1/2\ ACT\text{-}1}$, calculated for the intake air temperature sweep at point 2000 rpm@ 2 bar BMEP

5.3.3 Effect of injection strategy characteristics on soot oxidation

In this section 5.3.3 the soot oxidation process has been analyzed varying the injection pressure and the combustion phasing, both parameters included in the injection process. Also the experimental measurements were made in the 4-cylinder GM1.9L engine and, as in the previous section, the analysis will be carried out for the point of low load (2000 rpm and 2 bar BMEP) to simplify the information analyzed in this section

Effect of injection pressure on late-cycle soot oxidation

Injection pressure has a well-known effect on the diesel combustion process. An increase in injection pressure produces an increase in the total air entrained into the fuel spray upstream of the lift-off length (LOL), which results in a decrease in the equivalence ratio at the lift-off length (ϕ_{LOL}) and thus, a decrease in soot formation [9]. A reduction in exhaust soot emissions is thereby attained when injection pressure is increased. For this study, as in the sub-section on the air intake characteristics, the half-life time concept has been used to describe the soot oxidation process and as an mixing air/fuel estimator, $t_{1/2\ KL}$ and $t_{1/2\ ACT\text{-}1}$. Thus, in this sub-section, results for variation of the injection pressure from 400, 600 and 800 bar at the 2000 rpm@ 2 bar BMEP operating point are presented, while the rest of engine settings were held constant. As explained previously, the temporal evolutions of KL and ACT^{-1} were recorded for 400 cycles. Exponential decay functions were used to fit KL and ACT^{-1} after the EoI.

Based on the injection pressures tested, the crank angle degree intervals to perform the fit are different for each decay curve. These intervals are represented in Table 5.7.

	KL		ACT^{-1}	
P_{inj} [bar]	Interval fitting [CAD]	R^2-value [-]	Interval fitting [CAD]	R^2-value [-]
400	13 – 43	0.9346	13 – 50	0.9423
600	14 – 43	0.9357	13 – 51	0.9211
800	15 – 43	0.9461	13 – 53	0.9479

Table 5.7. Intervals used and corresponding R^2-values for the exponential fits to KL and ACT^{-1} for the injection pressure sweep at point 2000 rpm@ 2 bar BMEP

Figure 5.14 presents the average half-life times for KL, $t_{1/2\ KL}$, as well as their corresponding standard deviation, for the different injection pressure sweep. The results show smaller values of average half-life time when the injection pressure increases, with the same behavior as the one mentioned in [11]. This means that the soot oxidation process improves. Maintaining constant the ambient density and the oxygen concentration for the conditions measured, the injection pressure produces an increase in the total air entrained into the fuel spray, which improves the soot oxidation process during the late-cycle combustion.

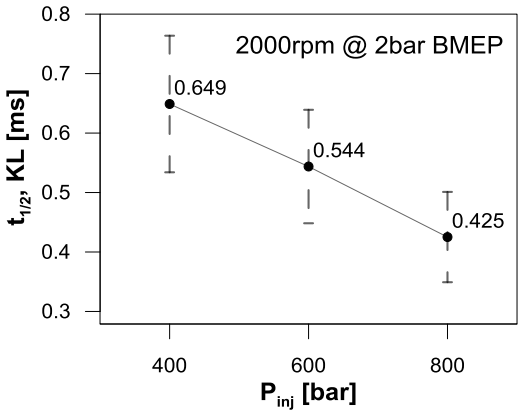

Figure 5.14. Half-life time of KL, $t_{1/2\ KL}$, calculated for the injection pressure sweep at point 2000 rpm@ 2 bar BMEP

Figure 5.15 shows the results of half-life times of ACT^{-1} (average value and its standard deviation) for the injection pressure sweep. The half-life times of the ACT^{-1}, $t_{1/2\,ACT\text{-}1}$, decrease when the injection pressure is increased. Considering constant in-cylinder ambient density and oxygen concentration between the different injection pressure cases, a higher injection pressure produces an increase in the total air entrained into the fuel, which results in an improvement in the soot oxidation process. In addition, the momentum produced by the spray in the case of high injection pressure (P_{inj}= 800bar) is higher than with low injection pressure (P_{inj}= 400bar). Thus, an increase in the movement of the in-cylinder air environment is achieved due to the higher momentum of the spray. The increased air movement affects soot oxidation by enhancing the mixing process during the late-cycle period, and therefore the soot oxidation rate is increased when the injection pressure is increased [11]. All these phenomena translate into a lower time to burn the same amount of injected fuel when comparing the tests with higher injection pressure to those with lower injection pressure.

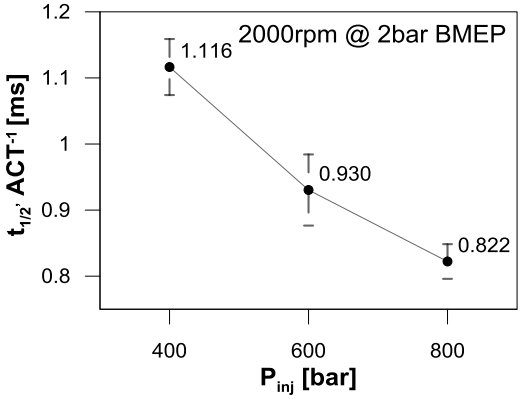

Figure 5.15. Half-life time of ACT^{-1}, $t_{1/2\,ACT\text{-}1}$, calculated for the injection pressure sweep at point 2000 rpm@ 2 bar BMEP

Effect of combustion phasing on late-cycle soot oxidation

To finish with section 5.3.3, the last variable analyzed is the combustion phasing. For the low load condition, the CA50 of the combustion has varied

from 6 to 20 CAD aTDC. This range was selected to keep the maximum in-cylinder pressure below 160 bar. As in both previous sweeps, the temporal evolution of KL and ACT^{-1} were recorded for 400 cycles and similar processing methodology was followed. The half-life time for both parameters are presented in Figure 5.16 and Figure 5.17 and the selected intervals for the fit and the R^2-values are given in Table 5.8.

	KL		ACT^{-1}	
CA50 [°]	**Interval fitting [CAD]**	**R^2-value [-]**	**Interval fitting [CAD]**	**R^2-value [-]**
6	4 – 37.5	0.9355	6 – 37	0.9611
11	9 – 39	0.9986	11 – 41	0.9625
16	13 – 42.5	0.9143	15 – 45	0.9522
20	17 – 45	0.9009	19 – 48	0.9798

Table 5.8. Interval used to exponential fit and R^2-values for the CA50 sweep KL and ACT^{-1} at point 2000 rpm@ 2 bar BMEP

Considering the results in the Table 5.8, it is interesting to underline that for each operating condition the onset is different and this due to the fact that CA50 is delayed and therefore the onset of combustion is also delayed. Combustion duration is quite similar (aprox.≈ 30 CAD) independent on the CA50. The values of R^2 are above 0.9, which indicate good enough accuracy.

Figure 5.16 presents the average and standard deviation of the half-life time of KL. If the combustion phasing is delayed, the half-life time of KL is larger. A delay in CA50 produces larger combustion duration and slower decay at late-cycle due to slower combustion development [17]. This implies poorer soot oxidation and therefore the half-life time of KL increases as it is shown in Figure 5.16.

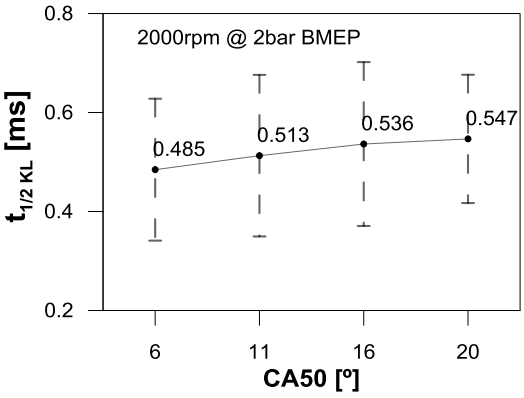

Figure 5.16. The half-life $t_{1/2}$ of the KL calculated for the combustion phasing sweep at point 2000 rpm@ 2 bar BMEP

Figure 5.17 presents the average and standard deviation of the half-life time of ACT^{-1}. When the CA50 was delayed the half-life time of ACT^{-1} was enlarged. In this sense, if the start of injection (SoI) was also delayed, CA50 was also delayed. Thus, the air/fuel mixing and combustion process took place during expansion stroke. The in-cylinder conditions are poorer (in-cylinder pressure and temperature are lower and therefore, density too) which leads to a larger $t_{1/2\ ACT\text{-}1}$.

As in the previous sweeps, both half-life times, $t_{1/2\ KL}$ and $t_{1/2\ ACT\text{-}1}$ present similar trends. The demonstrated decrease in mixing process - larger $t_{1/2\ ACT\text{-}1}$ due to lower in-cylinder density and temperature will be directly related with poorer soot oxidation.

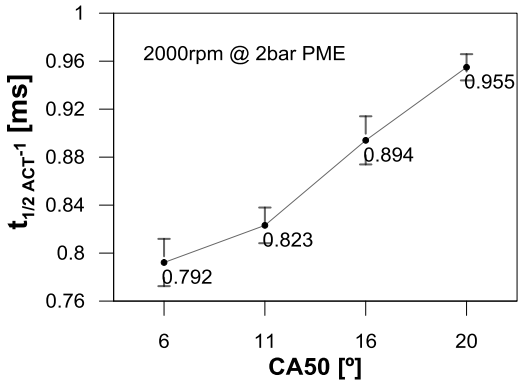

Figure 5.17. The half-life $t_{1/2}$ of the ACT^{-1} calculated for the combustion phasing sweep at point 2000 rpm@ 2 bar BMEP

5.3.4 Discussion $t_{1/2,KL}$ vs $t_{1/2,ACT-1}$

Once the half-life times of KL and ACT^{-1} have been analyzed separately for each parameter sweep at one operating condition (2000 rpm@ 2 bar BMEP), this section aims to relate all parameters under the operating conditions tested. In particular, the relationship between the mixing capability on the soot oxidation process during late-cycle combustion will be analyzed and described.

Figure 5.18 shows the average half-life time of KL versus the average half-life of ACT^{-1} at 2000 rpm and 2 bar BMEP. Results from previous sweeps are presented. For this engine operating point and these parameter sweeps, the R^2-values were already illustrated in the previous subsections (Tables 5.2–5.8), showing an acceptable accuracy. Therefore, the robustness of the methodology is demonstrated. Thus, when the mixing process is inhibited due to a decrease in the injection pressure, ambient density, injection pressure and/or intake air temperature and/or an increase of EGR and/or a delayed of CA50, the soot oxidation is poorer and therefore the $t_{1/2}$ KL is larger. Trying to evaluate how the $t_{1/2\ ACT-1}$ parameter correlates with the soot oxidation process ($t_{1/2\ KL}$), a linear fit was performed to the 20 different cases

obtaining an R^2-value greater than 97%. Finally, in view of the previous results, it can be affirmed that the methodology used is completely appropriate for the analysis performed.

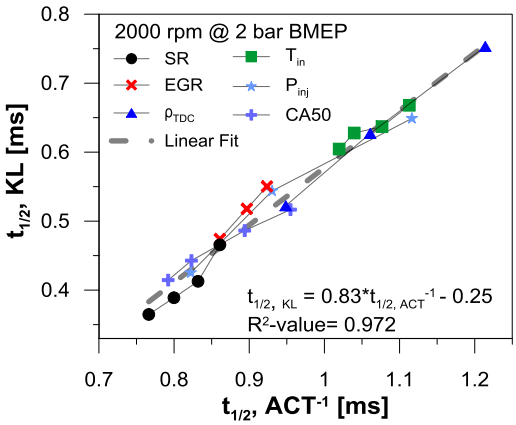

Figure 5.18. Relationship between half-life times of the KL and ACT^{-1} at 2000 rpm@ 2 bar BMEP for the different sweep: swirl ratio, EGR, ambient density, intake air temperature, injection pressure and combustion phasing.

Figure 5.19 shows the average half-life time of KL versus the average half-life time of ACT^{-1} at 2000 rpm and 5 bar BMEP. As in the previous case, all the results from the different sweeps are presented together. The same methodology was followed as in the 2 bar BMEP operating point. Both half-life times trends were similar to those obtained at the 2 bar BMEP point. In general, the inhibition of the mixing process produced a poorer oxidation process. With the objective of quantifying this relationship, a linear fit was performed to the 20 different cases, also obtaining a R^2-value very close to the unit.

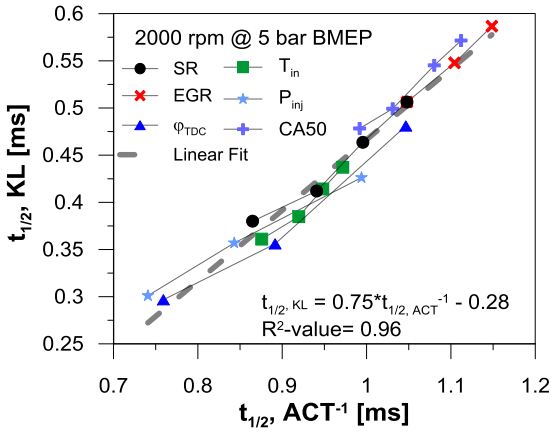

Figure 5.19. Relationship between half-life times of the KL and ACT^{-1} at 2000 rpm@ 5 bar BMEP for the different sweep: swirl ratio, EGR, ambient density, intake air temperature, injection pressure and combustion phasing.

Figure 5.20 and Figure 5.21 show the average values of the average half-life time of the ACT^{-1} versus the average half-life time of the KL for the medium load condition of 1500 rpm and 8 bar BMEP and high load of 1500 rpm and 14 bar BMEP. For these conditions of medium and high load, as shown in Table 5.1, only one swirl sweep, EGR and CA50 have been measured for the case of half load and in the case of high load, swirl and CA50 studies. The trends of both parameters of average half-life time expose a very similar behavior compared to the low load conditions presented above. Regarding the effect of the load, when it increases, the mixing half-life times also increase clearly compared with the values of the low load conditions, moving with it a greater amount of soot and, therefore, a longer average half life time of KL. Finally, as in the case of low load points, a linear adjustment has been applied in order to evaluate the relationship between both half-life times.

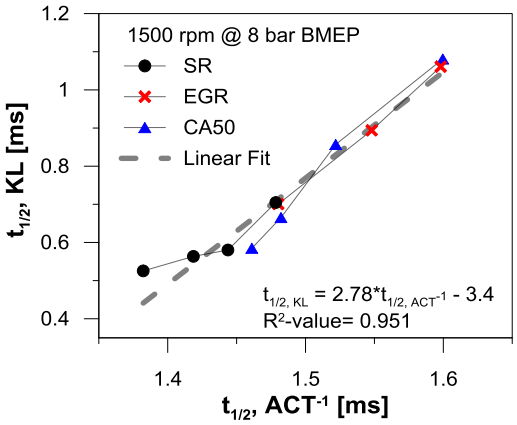

Figure 5.20. Relationship between half-life times of the KL and ACT^{-1} at 1500 rpm@ 8 bar BMEP for the different sweep: swirl ratio, EGR and combustion phasing.

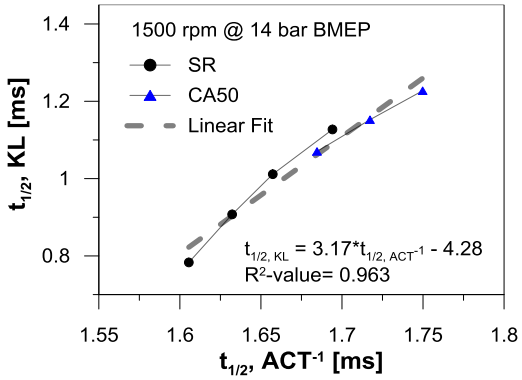

Figure 5.21. Relationship between half-life times of the KL and ACT^{-1} at 1500 rpm@ 14 bar BMEP for the different sweep: swirl ratio and combustion phasing.

To provide a more general approach and considering the reasonable linear agreement between $t_{1/2\,KL}$ and $t_{1/2\,ACT\text{-}1}$ for the two operating conditions tested, both half-life times (for KL and ACT^{-1}) should be related by the equation below:

(5.4) $$t_{1/2,KL} = A \cdot t_{1/2,ACT-1} - B$$

Figure 5.22 presents the experimental half-life time versus the simulated half-life time (from equation(5.4)). The coefficients A and B were adjusted for the four operating conditions separately, using different tests performed at each of them. The values of A and B coefficients are 0.69 and -0.18, respectively. In view of the figure, it can be said that the differences between the experimental and simulated half-life times, even if they are inside acceptable limits, is not perfect. A possible explanation is that soot oxidation is an extremely complex process that might not be governed solely by the mixing process.

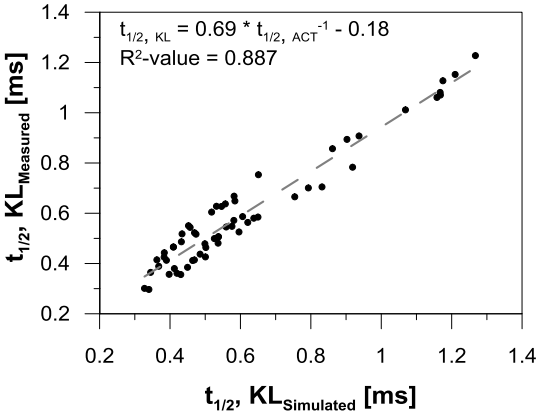

Figure 5.22. Experimental half-life time of KL versus the simulated half-life time of KL (from equation (5.4)) for all the tests performed at the four operating conditions.

Thus, to improve the prediction of the current model (equation (5.4)), additional parameters are surely needed. It is well known that in-cylinder gas temperature should have a considerable impact on soot oxidation [10]. Figure 5.23 presents the KL half-life time error, defined as the experimental results minus the simulated ones, as a function of the average bulk gas temperature. This average was calculated considering the bulk gas temperature values in the crank angle degree range previously used to fit the ACT^{-1} half-life time.

It is worth noting that this way to proceed seems reasonable, since the range considered for computing the average temperature corresponds to the range where soot oxidation is under analysis.

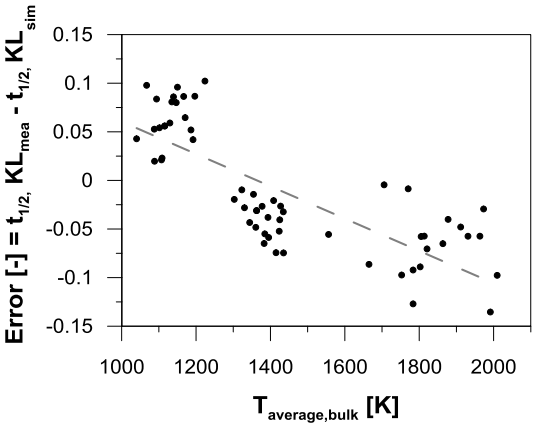

Figure 5.23. Correlation between errors defined as experimental KL half-life time minus simulated KL half-life time (from Eq. (5.4)) and average bulk gas temperature.

Based on this figure, it can be seen that the error of the current model is not at all random, since it correlates quite well with the average bulk gas temperature. Besides, if correctly analyzed, the correlation makes the most sense: on the one hand, when the bulk gas temperatures are high, the model is overestimating the KL half-life time (i.e. the error is negative), which means that it is underestimating the oxidation process. This result illustrates that this underestimation is because the model is not taking into account this higher bulk gas temperature, which enhances the oxidation process. On the other hand, when the bulk gas temperatures are low, the model is underestimating the KL half-life time (i.e. the error is positive), implying that it is overestimating the oxidation process. The reason for this overestimation is that the model is not taking into account the lower bulk gas temperature, which hinders the oxidation process.

Thus, a new model was built, including the two significant parameters previously presented ('mixing capability' and average bulk gas temperature), to better explain the soot oxidation process, which has the form shown in equation (5.5):

$$t_{1/2,KL} = C \cdot t_{1/2,ACT-1}^{D} \cdot (T_{bulk}/10^3)^{E} \quad (5.5)$$

Figure 5.24 shows the experimental KL half-life time versus the simulated one (with equation (5.5)). The coefficients *C*, *D* and *E* were adjusted for the different operating conditions measured. The values of *C*, *D* and *E* coefficients are 0.66, 2.17 and -1.11, respectively. From the figure, it can be observed that this new model is significantly more accurate than the previous one. In this sense, the present study confirms the relevance of the 'mixing capability' and temperature in the soot oxidation process. It is interesting to note that to determine both soot oxidation tracers, 'mixing capability' and average bulk temperature, it is only necessary to have the heat release and the injection rate profiles, which can be obtained quite easily in real engines. In this way, a really complex phenomenon such as soot oxidation is analyzed experimentally.

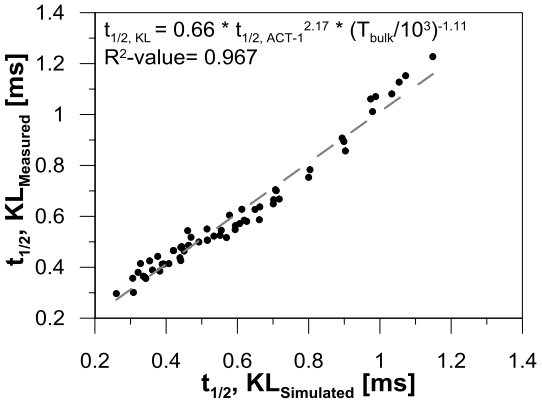

Figure 5.24. Correlation between half-life of the measured KL and the simulated one (from equation (5.5)) for all the tests performed at the four operating conditions.

5.4 Strategies for improve soot oxidation during the late-cycle combustion

The main objective of this work was to compare different engine strategies to enhance the late-cycle mixing controlled combustion process and therefore to improve the soot oxidation process while maintaining similar gross indicated efficiency. For this purpose, a simplified methodology defined in section 5.3 was used. Experimental measurements were made in a single-cylinder direct-injection light-duty diesel engine varying the swirl ratio and the injection pattern.

5.4.1 Test conditions

In this research, a study was carried out for evaluating the potential of swirl ratio and a dedicated injection strategy to enhance the late-cycle mixing controlled combustion. For that, a reference operating condition was selected as baseline case. The engine was operated maintaining constant engine speed at 2000 rpm and low load at 5 bar BMEP. The temperature of the coolant and oil stayed constant for all the measurements at 86°C and 95°C, respectively. For each operating condition, 3 repetitions were measured and the results were averaged in order to minimize the experimental uncertainties.

Baseline case

The experimental engine operating conditions are represented in Table 4.2. These operating conditions were chosen for being representative of typical operating point for the derived production GM 1.9L Diesel engine, which was set up to meet EURO IV emissions regulations.

Operating condition	Baseline (2000 rpm @ 5 bar BMEP)		
Injection pressure [bar]	650	**T_{in} [K]**	318
ET [ms]	0.31 / 0.31 / 0.587	**P_{in} [bar]**	1.306
		P_{exh} [bar]	1.49
m_f [g/s]	0.3	**m_a [g/s]**	11
SoE [°bTDC]	19.5 / 9.9 / 0.3	**EGR [%]**	0
SR [-]	1.5	**CA50 [°aTDC]**	13

Table 5.9. Baseline engine operating conditions

Engine setting sweeps

Table 5.10 presents the text matrix for the two different strategies studied in this section. In the first strategy, the objective was to evaluate the effect of swirl ratio on late-cycle combustion process. For that, the swirl ratio was varied from 0 up to 5, in steps of 1 unit maintaining constant all other engine parameters. The tests were performed with the same trapped mass at the IVC[8]. For that, the intake pressure was adapted in every test. While, the intake air temperature and the exhaust pressure were kept constant. Regarding the injection pattern, all parameters were kept constant except the SoE and ET for the main injection event, which were modified for obtaining the same CA50 and fuel mass in all cases.

[8] IVC: Intake Valve Closed

Operating condition	SR	Injection Strategy Optimization
Injection pressure [bar]	650	800
Number of Injections	3	4
SoE [°bTDC]	19.5 / 9.9 / 0 - 0.5	19.2 / 9.6 / -0.5 / -4.7
ET [ms]	0.31 / 0.31 / 0.582 – 0.590	0.285 / 0.30 / 0.510 / 0.15
m_f [g/s]		0.3
m_a [g/s]		11
P_{in} [bar]	1.30 – 1.41	1.304
T_{in} [K]		318
P_{exh} [bar]		1.475
SR [-]	0 - 5	1.5
EGR [%]		0
CA50 [°aTDC]		13

Table 5.10. Experimental engine operating conditions

The aim of the second strategy was to produce the same Rate of Heat Release (RoHR) for the high swirl case (SR= 3), which implies the highest Gross Indicated Efficiency (GIE). The baseline case was taken as reference point. To achieve the same RoHR, the parameters CA10, CA25, CA50, CA75 and CA90 must be very similar. Thus, some considerable changes of the injection strategy (injection pressure, duration and position of each injection and number of injection) were applied as Table 5.10 shows.

5.4.2 Impact of swirl ratio on late-cycle combustion

An increase in swirl ratio causes an improvement in turbulence and vorticity due to the higher rotational speed of the air flow and therefore, an acceleration of combustion rate [19].

Before the analysis of the impact of the swirl during the late-cycle diffusion combustion, a simplified combustion study has been performed for selecting the most favorable condition regarding the combustion performance. Figure 5.25 shows the apparent combustion time (ACT^{-1}) parameter at 90% of total heat released for the swirl ratio sweep, ranged from 0 to 5. This parameter was used as a mixing capability tracer during the late-cycle (from EoI up to EoC). Thus, it can be said that the values present an increase in mixing capability when the swirl ratio raises up to a maximum and later, a decrease in mixing parameter is produced. From SR= 3, the increase in swirl ratio produces presumably a deterioration of the combustion development due to excessive spray interaction and/or a displacement of the combustion process towards the squish region [20]. In this sense, it is possible to state that SR= 3 is the best condition in terms of mixing capability.

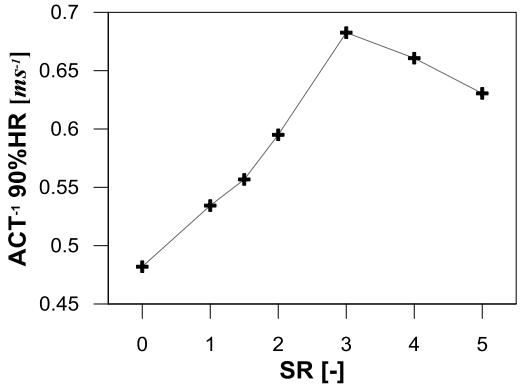

Figure 5.25. ACT^{-1} parameter at 90% of heat release for each swirl ratio measured.

Figure 5.26 (left) represents the maximum values of RoHR for the same swirl ratio sweep in Figure 5.25. When the swirl ratio increases, the peak of RoHR is higher due to a faster mixing process up to the SR= 3 (maximum mixing capability) due to an enhancement in the combustion process. The figure (right) indicates the interval duration (in CAD) from 70 to 80% and 80 to 90% of the total heat release, respectively. These intervals represent approximately the late-cycle part of combustion event. The chart shows a reduction in both interval durations when the swirl ratio is increased. It indicates that there is higher energy released during expansion stroke, resulting a better thermal efficiency.

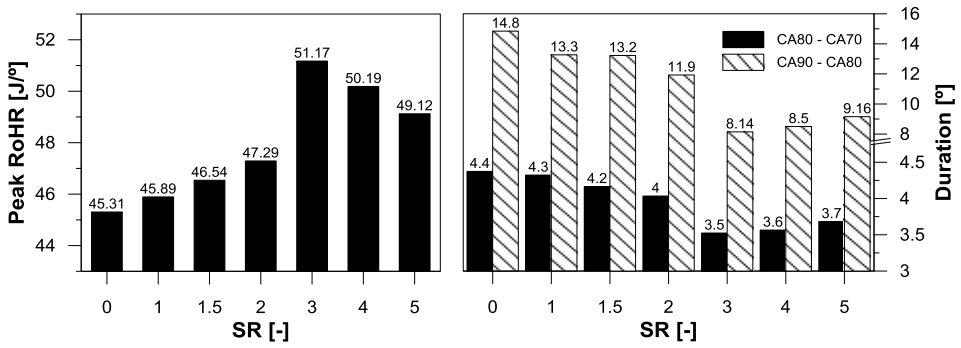

Figure 5.26. Peak of RoHR and interval duration for swirl ratio sweep.

According to the conclusion obtained in the previous figures, it is possible to conclude that, when SR is increases, the GIE should also be increased. Figure 5.27 presents the Gross Indicated Efficiency for seven different swirl ratios. The trend is similar as Figure 5.25 and Figure 5.26. Finally, the SR= 3 condition is selected as optimum point considering that is the best SR condition for swirl sweep in terms of mixing capability, combustion process and GIE.

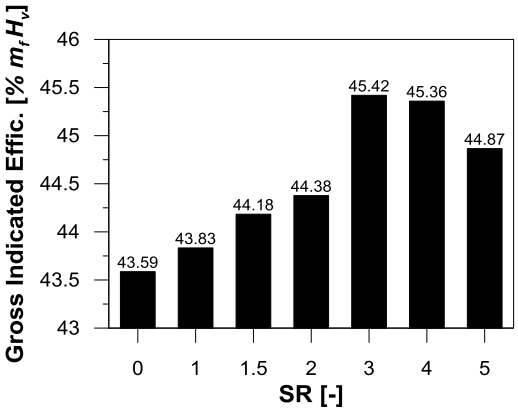

Figure 5.27. Gross Indicated Efficiency for different swirl ratios.

Once the "optimum" SR has been selected, the main goal of this section is to study the impact of SR on the soot oxidation process during the late-cycle combustion, since the oxidation plays the main role in the final engine-out soot emissions. For this, in accordance with the methodology described in section 5.2 of this chapter, the influence of mixing capacity and the average bulk gas temperature on the soot oxidation has been analyzed, comparing the results obtained for the optimum swirl ratio against the baseline condition. To relate the air/fuel mixture capacity and the soot oxidation process, the concept of half-life is going to be used, which has been described extensively throughout the current chapter. The procedure to obtain the average half-life times, both for the ACT^{-1} and KL, is based on the exponential fitting of the temporal evolution for both parameters.

As usual, before beginning with the description of the half-life time of ACT^{-1} results, Table 5.11 indicates the interval in which the ACT^{-1} curves has been fitted and the R^2-values for the experimental fits. The exponential fits start around 13 CAD aTDC (approximately the EoI) up to the point when the profiles approach zero.

Operating condition	Interval fitting [CAD]	R^2-value [-]
Baseline (SR= 1.5)	12.6 – 33	0.9747
SR= 3	12.6 – 33	0.9852

Table 5.11. Interval fitting analyzed and R^2-values for the experimental fits to ACT^{-1} trace at two swirl ratio cases.

Figure 5.28 represents the results of half-life times of ACT^{-1} for the baseline and optimum SR case. When the swirl ratio increases, the half-life time of ACT^{-1}, $t_{1/2\ ACT\text{-}1}$, is reduced and so, the mixing process is improved. Maintaining constant conditions at intake closing (air intake temperature and mass, without EGR) and the injection strategies for both measured points, a higher value of swirl ratio is expected to enhance turbulence and vorticity [7]. These phenomena explain a lower time to burn similar amount of injected fuel. So, an improvement in the air/fuel mixing process was confirmed.

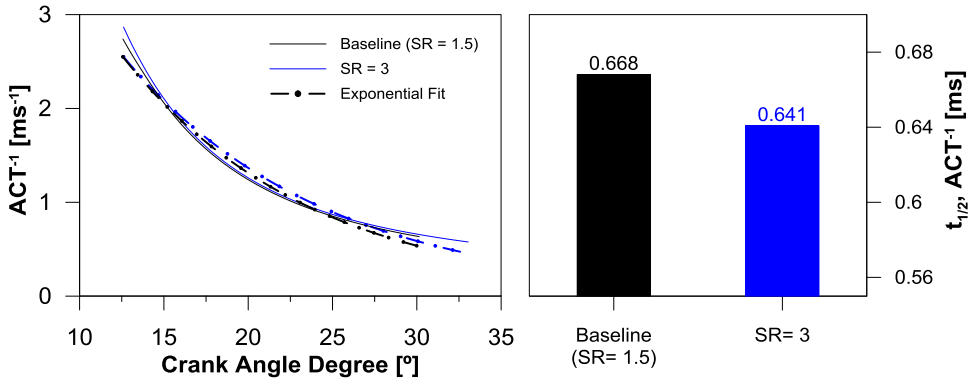

Figure 5.28. Temporal evolution of ACT^{-1} and its exponential fits (left) and half-life times of ACT^{-1} (right) obtained for two swirl ratio cases.

Another parameter to take into account when studying the soot oxidation process is the bulk gas temperature. Figure 5.29 shows the time evolution of gas temperature (left) and average bulk gas temperature (right)

for the baseline and SR= 3 cases. This average was calculated in the same range as previously used to fit the half-life time of ACT^{-1} (Table 5.11). Each curve represents the average of 400 cycles. As other researchers report [10], the bulk temperature has an important effect by increasing the reaction rates. Averaged bulk gas temperature value is higher for the SR= 3 (approximately 100K). At higher temperatures, the soot oxidation process is expected to be enhanced in the flame sheath and then, it leads to a reduction in a both in-cylinder soot and exhaust particulate emissions.

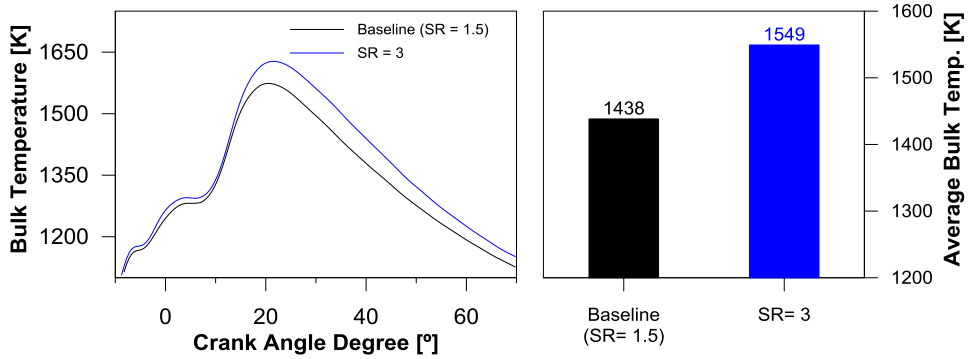

Figure 5.29. Temporal evolution of bulk gas temperature (left) and averaged bulk gas temperature (right) obtained for two swirl ratio cases.

Finally, to evaluate the soot oxidation process, the half-life time of KL has been used, taking into account that the soot concentration curves assume the exponential form after the end of the injection process. Table 5.12 indicates the interval in which the KL curves have been fitted and the R^2-values for the experimental fits. Due to higher swirl, the peak of KL is closer the TDC than to the baseline and therefore, the onset of exponential fit is located at different crank angle intervals.

Operating condition	Interval fitting [CAD]	R^2-value [-]
Baseline (SR= 1.5)	21 – 54	0.9503
SR= 3	11 – 51	0.9786

Table 5.12. Interval fitting analyzed and R^2-values for the experimental fits to KL trace at two swirl ratio cases.

Once the impact of the swirl on the mixing processes and the average bulk gas temperature have been described, the temporal evolution of the KL after the end of the injection is analyzed. For that, Figure 5.30 (left) represents temporal evolution of KL and its exponential fit and the results of half-life times of KL for the baseline and SR= 3 case (right). Each curve represents the average of 400 cycles. The half-life time of KL decreases with the increase of swirl number, maintaining constant the rest of variables. For the optimum SR case, the in-cylinder angular velocity is higher than the baseline. The enhanced turbulence and vorticity produces a higher soot oxidation rate for the SR= 3 case independently on the initial soot concentration [9].

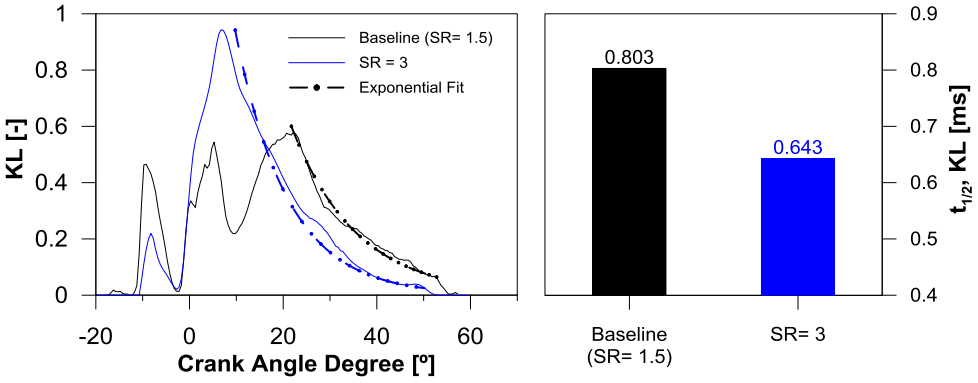

Figure 5.30. Temporal evolution of KL and its exponential fits (left) and half-life times of KL (right) obtained for two swirl ratio cases.

5.4.3 Impact of injection pattern on late-cycle combustion

The post-injection is a shorter injection pulse that follows the main injection, which improves the mixing process and increases the temperature during the late-cycle combustion phase. Thus, the post-injection enhances soot oxidation leading to a reduction in the engine-out soot emissions [21]. The effects of injection pressure and post injections are well-known on the combustion process. An increase in injection pressure causes an equivalence ratio reduction at the lift-off length (LOL) and thus, a reduction in soot formation [22]. In the current section, the aim is to obtain similar RoHR to SR= 3 (optimum GIE case) by using a reduced swirl ratio (baseline SR= 1.5 case) condition by modifying only the injection settings (number of injection, injection pressure and duration and position of each injection event).

The methodology followed to replicate the RoHR is shown in the flow chart of Figure 5.31. Only the injection parameters have been modified. This procedure has been divided into several steps:

- First, the injection pressure was increased in steps of 50 bar. After this, faster RoHR with higher peak has been obtained process.
- In the following step, the Start of Energizing (SoE) times, as well as the Energizing Times (ET), were changed to adjust the CA10, CA25 and CA50 parameter for both operating conditions (SR= 3 and post-injection at SR= 1.5 cases)
- Finally, a post injection event was added to compensate the better mixing process at the late-cycle combustion phase achieved with the optimum SR= 3 case. With this proposal, the differences between CA75 and CA90 were acceptable (less 2° CAD).

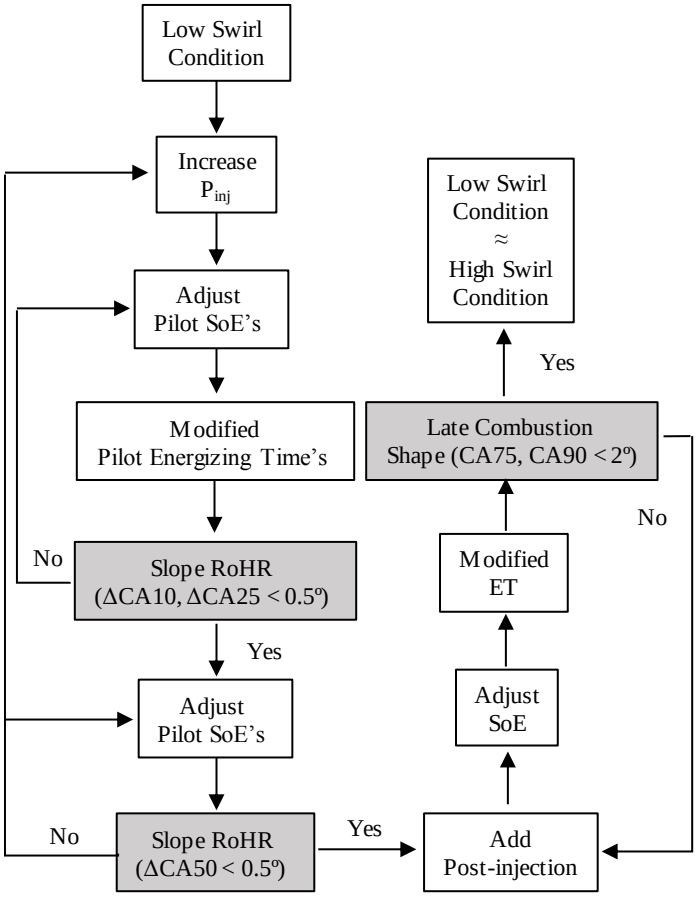

Figure 5.31. Experimental methodology used to get similar RoHR of SR= 3 with baseline condition (SR= 1.5).

As in the previous section of the swirl, the mixing and combustion process for the post-injection condition compared to the reference and SR= 3 are going to be evaluated.

Figure 5.32 shows the apparent combustion time (ACT^{-1}) parameter at 90% of total heat release for baseline, optimum and post-injection cases. It is possible to note that the post-injection case presents a similar mixing capability to the SR= 3 case and, as it has been explained in the previous

sub-section, both operating conditions show an increase in mixing capability when compared to the baseline case.

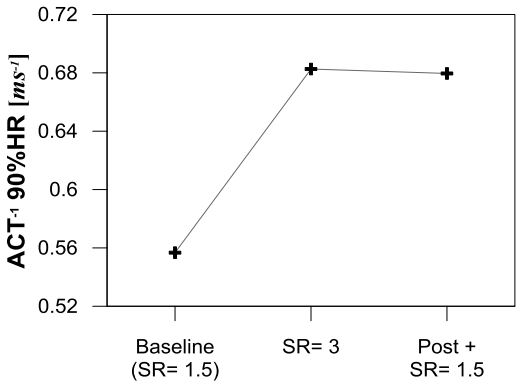

Figure 5.32. ACT^{-1} parameter at 90% of heat release for the baseline, optimum SR and post injection case.

In addition, the peak of RoHR is slightly higher at SR= 3 than the post-injection case (approximately 0.5 J/°) as shown in the Figure 5.33. This fact could be due to the small differences in the RoHR fit. Considering the interval duration from 70 to 80% and 80 to 90 % of the total heat release, the trend follows the same shape. The values of SR= 3 and post-injection case are very similar and the interval durations are shorter compared to the baseline case.

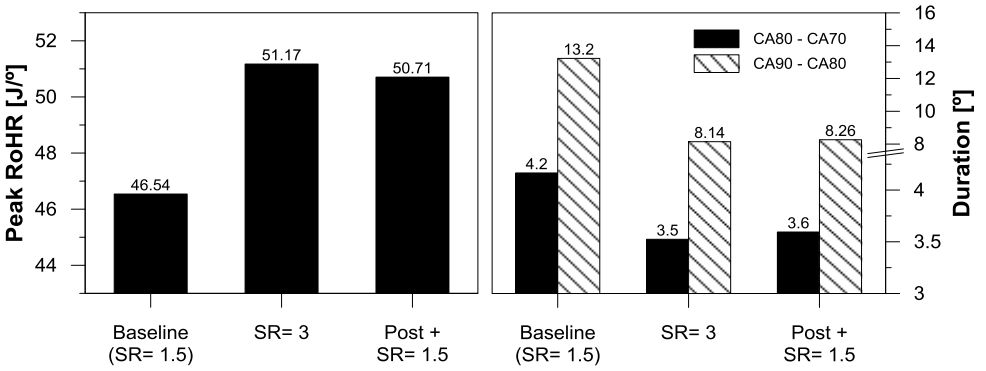

Figure 5.33. Peak of RoHR (left) and interval duration (right) for the baseline, optimum SR and post-injection case.

Finally, Figure 5.34 presents the GIE for the three different operating conditions. According to the conclusion obtained in the two previous figures, SR= 3 and post-injection case present similar values of GIE. It can be therefore concluded that the selected injection strategies replicate the optimum case (SR= 3).

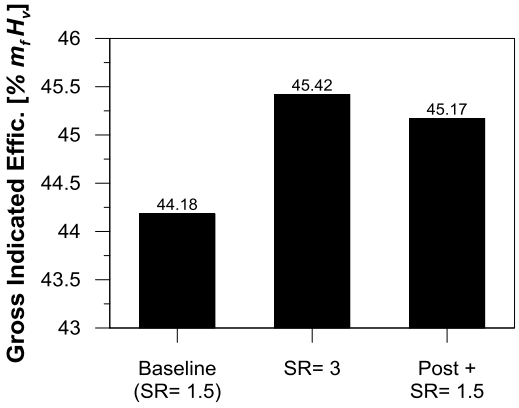

Figure 5.34. Gross Indicated Efficiency for the baseline, optimum SR and post injection case.

Once the post-injection case has been selected, it is necessary to study the impact of the injection pattern on the soot oxidation during the late-cycle

combustion. Following similar work scheme as the swirl ratio section, the relationship of mixing process and bulk gas temperature on the soot oxidation process for post-injection and baseline cases was studied.

Figure 5.35 (left) shows the temporal evolution of ACT^{-1} and its exponential fit (discontinuous line) for the baseline and post-injection conditions. Each curve represents the average of 400 cycles. The crank angle ranges and R^2-values for the exponential fit are presented in Table 5.13. Figure 5.35 (right) presents the half-life times of ACT^{-1} for the baseline and post-injection case. The half-life of ACT^{-1} with the post-injection pulse is lower than the baseline case due to mainly two phenomena: the injection pressure and the post injection event. On the one side, if the injection pressure increases, the half-life time of ACT^{-1} is reduced. A higher injection pressure produces an increase in the movement of the in-cylinder air environment due to the higher momentum of the spray and so, this air movement enhances the air/fuel mixing process during the late-cycle combustion [23]. On the other side, the mixing process is improved by adding the post injection. The post injection redistributes the fuel from the main injection, generating a better-mixed air/fuel distribution [42].

Operating condition	**Interval fitting [CAD]**	**R^2-value [-]**
Baseline	12.6 – 33	0.9747
Post-injection	12.1 – 33	0.9299

Table 5.13. Interval fitting analyzed and R^2-values for the experimental fits to ACT^{-1} trace for the different injection pattern.

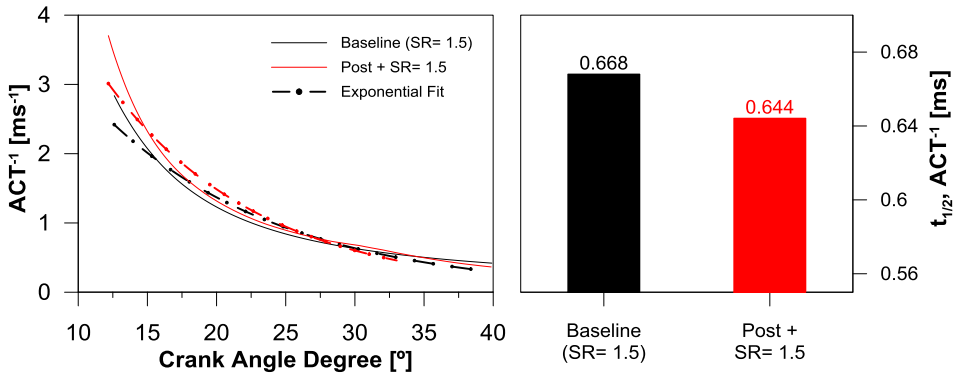

Figure 5.35. Temporal evolution of ACT^{-1} and its exponential fits (left) and half-life times of ACT^{-1} (right) obtained for different injection pattern.

Now, Figure 5.36 shows temporal evolution of bulk gas temperature (left) and average bulk gas temperature (right) during the late-cycle for the baseline and post-injection conditions. Each curve represents the average of 400 cycles. The average bulk gas temperature for the post-injection case is higher than the baseline case (around 100K). As in the previous sub-section, soot oxidation process is enhanced when the bulk gas temperature is higher.

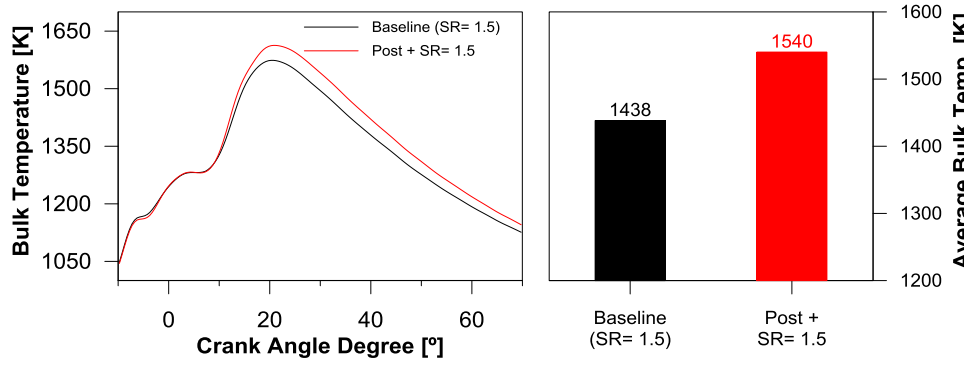

Figure 5.36. Temporal evolution of bulk gas temperature (left) and averaged bulk gas temperature (right) obtained for different injection pattern.

Once the mixing process and bulk gas temperature were studied, it was necessary to evaluate the soot oxidation process.

Figure 5.37 (left) represents temporal evolution of KL and its exponential fit for the baseline and post injection cases. Each curve represents the average of 400 cycles. The selected crank angle ranges for the exponential fit and R^2-values are presented in Table 5.14. Figure 5.37 (right) shows the results of half-life times of KL for the baseline and post-injection case. As expected, the half-life time of KL for the post injection case was lower than the baseline case. An increase in injection pressure enhances the mixing process during the late-cycle combustion and thereby, the soot oxidation process. As other researchers have reported in the literature [24][25], post-injection enhances mixing of soot from the main injection and available in-cylinder air/O_2 and the oxidation of this soot is enhanced due to combustion of the post-injection fuel.

Operating condition	Interval fitting [CAD]	R^2-value [-]
Baseline	21 – 54	0.9503
Post-injection	12 – 51	0.9742

Table 5.14. Interval fitting analyzed and R^2-values for the experimental fits to KL trace for the different injection pattern.

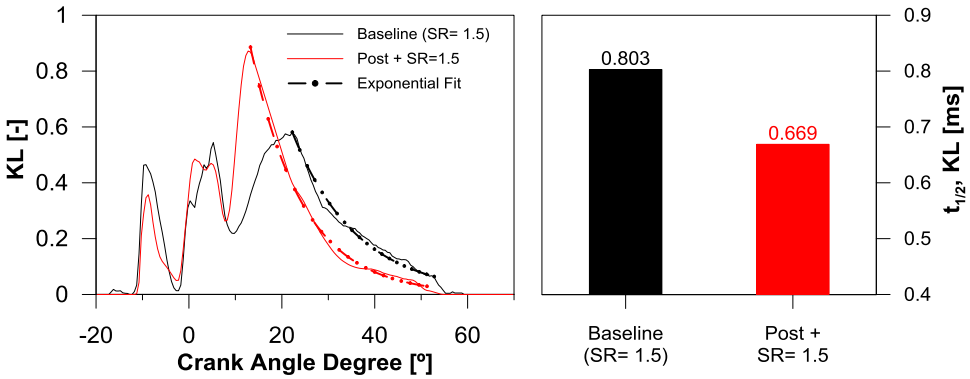

Figure 5.37. Temporal evolution of KL and its exponential fits (left) and half-life times of KL (right) obtained for different injection pattern.

5.4.4 Emissions comparison of optimized swirl ratio and post-injection strategies on late-cycle combustion

Once the soot oxidation has been analyzed independently for the two different strategies versus the baseline case, this section aims to compare the optimum swirl ratio and post-injection cases during the late-cycle combustion. This comparison has been used to identify the best engine strategy.

Figure 5.38 (left) shows the engine-out NOx and soot emissions for baseline, optimum SR and post-injection conditions. The expected soot-NOx trade-off is found. Considering that combustion process between optimum SR and post injection case is quite similar, it is also expected to have similar engine-out emissions. A negligible difference in NOx emission (approximately 0.7 g/kg fuel) was measured. In addition, these conditions present higher values than the baseline case. This fact is maybe due to a faster combustion process and thus higher local combustion temperatures for the maximum GIE cases than the baseline case. Regarding soot emissions, it is interesting to remark that the post-injection soot is quite similar to the SR= 3 case and significantly lower than the baseline case due to an improvement of mixing and oxidation processes.

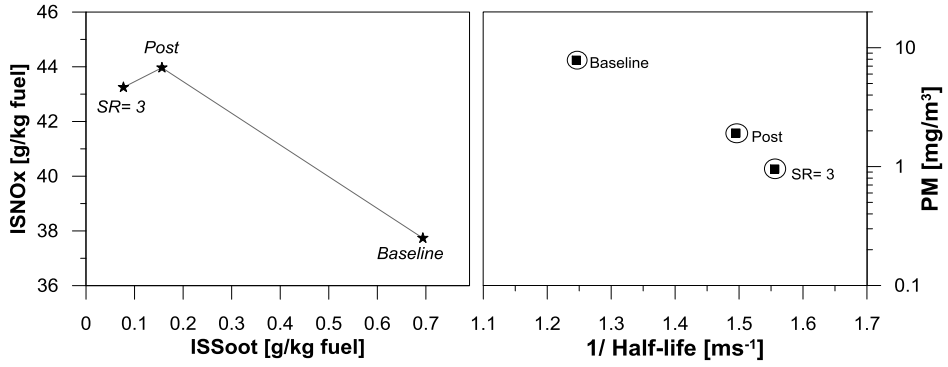

Figure 5.38. Left) The ISNOx vs ISSoot emissions for the 3 different point at 2000 rpm@ 5 bar BMEP. Right) Soot emissions versus half-life time of KL for each swirl ratio at 2000 rpm at 5 bar BMEP

Finally, Figure 5.38 (right) presents engine-out emissions versus the inverse of half-life time of KL ($1/t_{1/2,KL}$) on a semi-logarithmic scale for swirl ratio sweep and post-injection case. The three conditions studied in this research have been marked with black circles. It is observed that the soot emissions are drastically reduced for the SR= 3 and post injection cases, where the soot oxidation rate (and mixing capability) was improved. A linear relationship is stablished between the soot emissions and the oxidation rate. Therefore, engine-out soot emissions are governed mainly by oxidation process. In conclusion, it is possible to improve the late-cycle diffusion combustion (and thus, soot oxidation process) with an appropriate injection strategy for a low SR condition.

5.5 Conclusions

In this chapter, the soot oxidation process has been evaluated mainly during the late-cycle diffusion combustion process (from the end of the injection) for different operating conditions. For this, the chapter has been split into two sections. First, a simplified methodology has been defined to evaluate the soot oxidation process inside the combustion chamber under real engine conditions. In particular, the study has been developed based on two parameters: on the one hand, the oxidation process has been characterized from the half-life time of the KL curves. The concentration of soot has been measured with an optoelectronic probe that has implemented the two-color method. On the other hand, the mixing capacity has been evaluated based on the half-life time of the Apparent Combustion Time (ACT), specifically on the inverse of the ACT (ACT^{-1}). The ACT is obtained with the simulated injection rate and the experimental rate of heat release measures. The experimental measurements have been made in a production engine by varying the properties of the intake air and the characteristics of the injection process. In the second part of the chapter, different engine strategies have been compared to improve the combustion during the late-cycle diffusion combustion, therefore, improve the soot oxidation process while maintaining the indicated performance constant

Considering the results obtained in the first part of the chapter, the following conclusions can be drawn:

- A clear methodology derived has been developed to establish the half-life times using an exponential decay function fit to the late combustion cycle.
- The half-life time of ACT^{-1} was increased, and therefore the 'mixing capability' was poorer, with a decrease in the swirl ratio, ambient density, air intake temperature, injection pressure and/or the EGR rate is increased and/or CA50 is delayed. In the case of SR, when the swirl ratio was reduced the in-cylinder rotational flow decreased and thereby a decrease in turbulence was obtained. Concerning EGR rate, if this parameter was increased, the availability of oxygen was reduced leading to a negative and direct impact on mixing process. Concerning the effect of ambient density and intake air temperature, the mixing process is positively influenced when both parameter increase. In the case of injection pressure, lower values of injection pressure produce lower injection velocity and thus, a worsening in the mixing process. Finally, if CA50 was delayed, the combustion process took place during expansion stroke. This implies that the in-cylinder conditions are worsened (in-cylinder pressure and temperature are lower) therefore the density is lower.
- The half-life time of KL, tracer of soot oxidation, present reasonable similarities with the half-life time of ACT^{-1}, mixing tracer. Thus, when the mixing capability was enhanced due to different variations in engine operating conditions, the half-life time of KL was also increased implying worsened soot oxidation process. This relationship has been demonstrated for all different engine conditions tested in this chapter. A 0D model based on experimental measurements was developed to obtain the half-life time of KL and the half-life time of ACT^{-1}. As expected, the 'mixing capability' cannot fully explain a complex phenomenon such as soot oxidation. In this sense, the average bulk gas temperature has been included as an additional

tracer in the 0D model, significantly improving the accuracy of the soot oxidation process predictions.

The main conclusions regarding the second part of the chapter are summarized below:

- An increase in swirl ratio is not directly related with an increase in mixing process during the late-cycle combustion. Indeed, an excessive SR can lead a deterioration of the combustion development due to excessive spray interaction, which causes a slower and less powerful heat release process reducing the indicated efficiency.
- A proper injection pattern (increase of injection pressure and post-injection addition) coupled with a low SR was showed as a suitable strategy to improve the late-cycle diffusion combustion as well as soot oxidation while maintaining constant GIE.
- According to the emission results obtained, the expected soot-NOx trade-off was found. So, considering that combustion process between optimum SR= 3 and post-injection case was quite similar, it was also expected to have similar engine out emissions. Thus, the soot reduction can be attained with higher swirl ratio and a proper injection strategy. On the contrary, NOx emissions increased appreciably when the mixing process is enhanced (SR = 3 and SR=1.5 adjusted). In addition, a linear relationship was stablished between the soot emissions and the soot oxidation process, which indicates that mainly the soot oxidation process governs the engine-soot emissions.

5.6 Bibliography

[1] Dec J.E. “A Conceptual Model of DI Diesel Combustion Based on Laser-Sheet Imaging”. SAE Paper 970873, 1997.

[2] Arrègle J., Pastor J.V., López J.J., García A. "Insights on postinjection-associated soot emissions in direct injection diesel engines". Combustion and Flame 154, 448–461, 2008.

[3] Heywood J.B. "Internal Combustion Engine Fundamentals". McGraw-Hill Book Co, New York, US, 1988.

[4] López J., Martín J., García A., Villalta D., Warey A. "Implementation of two color method to investigate late-cycle soot oxidation process in a CI engine under low load conditions". Applied Thermal Engineering 113, 878–890, 2017.

[5] Benajes J., Martin J., Garcia A., Villalta D., Warey A. "An investigation of radiation heat transfer in a light-duty diesel engine". SAE Int. J. Engines 8 (5), 2015.

[6] Xiaobei C., Hongling J., Zhaowen W. "A Numerical Modeling and Experimental Study on Soot Formation for a Direct Injection Diesel Engine". SAE Technical Paper 2008-01-1794, 2008.

[7] Gallo Y., Li Z., Richter M., Andersson O. "Parameters influencing soot oxidation rates in an optical diesel engine". SAE Int. J. Engines 9 (4), 2016.

[8] Pickett L.M., Siebers D.L. "Soot in diesel fuel jets: effects of ambient temperature, ambient density, and injection pressure". Combustion and Flame 138, 114–135, 2004.

[9] Dembinski H., Angstrom H. "Swirl and Injection Impact on After-Oxidation in Diesel Combustion, Examined with Simultaneous Combustion Image Velocimetry and Two Colour Optical Method". SAE Technical Paper 2013-01- 0913, 2013.

[10] Tree, D.R, Svensson, K. I. "Soot processes in compression ignition engines". Progress in Energy and Combustion Science 33, 272-309, 2007.

[11] Huestis E., Erickson P., Musculus M. "In-Cylinder and Exhaust Soot in Low-Temperature Combustion Using a Wide-Range of EGR in a Heavy-Duty Diesel Engine". SAE Technical Paper 2007-01-4017, 2007.

[12] O'Connor J., Musculus M. "Post injections for soot reduction in diesel engines: a review of current understanding". SAE Int. J. Engines 6 (1), 2013.

[13] Arrègle J., López J.J., García J.M., Fenollosa C. "Development of a zero dimensional diesel combustion model. Part 1: analysis of the quasi-steady diffusion combustion phase". Applied Thermal Engineering 23, 1301–1317, 2003.

[14] Benajes J., Molina S., García J.M., Riesco J.M. "The effect of swirl on combustion and exhaust emissions in heavy-duty diesel engines". Proc. Instn Mech. Engrs Vol. 218 Part D: Journal Automobile Engineering.

[15] Lequien, G., Andersson Ö., Tunestal P., and Lewander M. "A Correlation Analysis of the Roles of Soot Formation and Oxidation in a Heavy-Duty Diesel Engine". SAE Technical Paper 2013-01-2535, 2013.

[16] Hentschel, W. and Richter, J. "Time-Resolved Analysis of Soot Formation and Oxidation in a Direct-Injection Diesel Engine for Different EGR-Rates by an Extinction Method". SAE Technical Paper 952517, 1995.

[17] P.B.M. Musculus. "Measurements of the influence of Soot Radiation on In-Cylinder Temperatures and Exhaust NOx in a Heavy-Duty DI Diesel Engine". SAE Technical Paper 2005-01-0925, 2005.

[18] López J., Martin J., Garcia A., Villalta D. "Characterization of In-Cylinder Soot Oxidation Using Two-Color Pyrometry in a Production Light-Duty Diesel Engine". SAE Technical Paper 2016-01-0735, 2016.

[19] Li X., Qiao Z., Su L., Liu F. "The combustion and emission characteristics of a multi-swirl combustion system in a DI diesel engine". Applied Thermal Engineering 115, 1203–1212, 2017.

[20] De la Morena J., Vassallo A. Peterson R.C., Gopalakrishan V., Gao J. "Influence of Swirl Ratio on Combustion System Performance of a 0.4l Single-Cylinder Diesel Engine". THIESEL 2014 Conference on Thermo- and Fluid Dynamic Processes in Direct Injection Engines.

[21] Molina S., Desantes J., García A., Pastor J. "A Numerical Investigation on Combustion Characteristic with the use of Post Injection in DI Diesel Engines". SAE Technical Paper 2010-01-1260, 2010.

[22] Benajes J., Martín J., García A., Villalta D., Warey A. "In-cylinder soot radiation heat transfer in direct-injection diesel engines". Energy Conversion nad Management 106, 414–427, 2015.

[23] López J., Martín J., García A., Villalta D., Warey A. "Implementation of two color method to investigate late-cycle soot oxidation process in a CI engine under low load conditions". Applied Thermal Enginnering 113, 878–890, 2017.

[24] Bobba M., Musculus M., Neel W. "Effect of post injections on in-cylinder and exhaust soot for low-temperature combustion in a heavy-duty diesel engines". SAE Int. J. Engines 3 (1), 2010.

[25] Hocine A., Desmet B., Guenoun S. "Numerical study of the influence of diesel post injection and exhaust gas expansion on the thermal cycle of an automobile engine". Applied Thermal Engineering 30,1889–1895, 2010.

Chapter 6

Soot Radiation Model in Diesel flames

Content

6.1 Introduction

Soot formation is a complex process comprising several physical and chemical phenomena, some of which occur simultaneously, and depends largely on local conditions. Computational models fall broadly into betwwen these two categories: the 0D phenomenological thermodynamic models [3] and CFD models [4]. The first of these offers the advantage of simplicity and low computational cost, but with weak information of the physical and chemical processes with respect to the CFD models.

In the literature, several studies provide more information on the soot formation and soot oxidation processes by means of models, which are composed of several sub-models ("*Multi-step models*") [5][6]. These models typically include processes such as precursor formation, particle inception, surface growth and particle oxidation. These multi-step models have typically been developed for use with CFD diesel engine models, but with a lower simulation cost. Regarding its use, soot emissions have been analyzed in different studies: for various injection times [7], different oxygen concentrations in the intake air [8], etc. It is important to know in depth the processes involved in soot particles for two main reasons: on the one hand, soot emissions are regulated by strict pollutant regulations. On the other hand, soot particles are mainly responsible for the total radiation heat transfer in diesel engines [22].

The main objective of this chapter is to develop a radiation soot model for diesel sprays able to predict the heat losses to the chamber walls due to radiation. This study is based on knowing the distribution of soot inside the flame, as well as understanding the processes that affect the radiation heat losses. For that, three sub-models have been used: spray model, which includes all the fundamental knowledge about combusting diesel sprays, a soot model, including both the formation and oxidation processes, and a radiation model.

6.2 General methodology of the study

The structure of the complete radiation model is shown in Figure 6.1. Three sub-models, which are directly connected to each other, compose the whole model: spray model, soot model and radiation model. The spray model (named DICOM) is a one-dimensional model that simulates the axial and radial distribution of a fuel spray for each instant. This model needs input variables such as the temporal evolution of the in-cylinder pressure, ambient density and injection rate. Only one variable, the spray angle, is necessary to adjust it. For this, the experimental results of spray penetration in both inert and reactive environment measured with the Schlieren technique will be used (Section 6.4.3). Once the spray model has been adjusted, these spray model results have been used as input variables for the soot model and thus, axial and radial profiles of soot mass fraction have been obtained for each instant. The soot model is based on soot formation and oxidation processes mainly. As in the spray model, in the soot model is necessary to adjust the optimal values for two constants (K_{soot} and t_0) need to be adjusted from experimental results of soot concentration (Section 6.5.2). These experimental results have been measured with the Diffused Back-Illumination technique (DBI). Next step, the temporal evolution of the spectral intensity will be obtained from the simulated soot concentration results together with the spatial temperature distribution (calculated also in the spray model), and consequently, the total soot radiation losses (Section 6.6.3). Finally, the simulated spectral intensity is integrated for the whole wavelengths spectrum and the radiation heat losses are obtained. As in two previous models, the simulated radiation has been compared with experimental values from the 2-Color method.

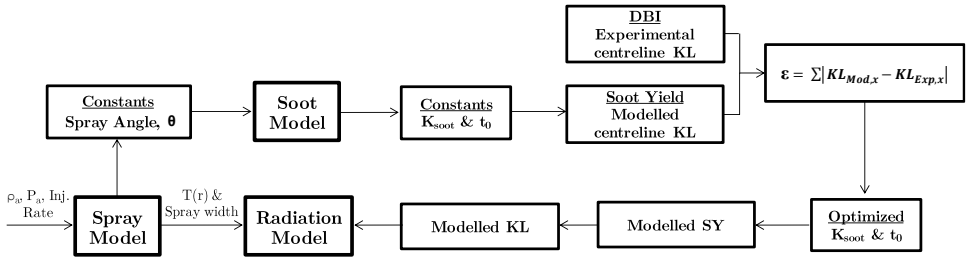

Figure 6.1. Overall model structure

6.3 Experimental database

Throughout this chapter, experimental results have been used to adjust the different constants for each model. The experimental data used in this work are the same as already used in another research [10]. Only, the post-processing has been adapted to be able to compare with the simulated results in the different models. Next, the experimental facility used for the experimental measurements and the test conditions are described.

6.3.1 Installation: High pressure and high temperature vessel

The high pressure and high temperature (HPHT) test chamber is an experimental facility, in which the thermodynamic conditions similar to a diesel engine at the instant of injection can be obtained (Figure 6.2). The vessel is classified as a constant-pressure flow (CPF) facility [11], as the conditions are reached by a continuous flow of high-pressure high temperature gas through the chamber. The vessel is equipped with three large optical accesses (128 mm in diameter) arranged in an orthogonal manner so that there is a full vision of the injection event. The mechanical limits of the vessel are 15 MPa of gas pressure and 1000 K of air temperature, and it is possible to obtain nearly quiescent and steady thermodynamic conditions in the test chamber. In addition, this equipment is also comprised of an injection system that allows changing the fuel injection pressure and the duration of injection.

Figure 6.2. High pressure and high temperature vessel

The pressurized gas is supplied to the vessel by two volumetric compressors working in parallel, providing a continuous feed of 70 Nm^3/h. The rig can work in open or closed loop to test spray evolution either in a standard air atmosphere or in gas mixtures with different O_2 concentrations. The chemical composition of the gas in the chamber is measured and can be adjusted adding either air or nitrogen through a reintegration system.

In order to heat the air, two electrical heaters of 15 kW each are placed upstream the chamber, allowing the mechanical temperature limit of the installation. Also, a secondary heater of 2.5 kW is placed at the bottom of the chamber to help maintain the temperature. Additionally, a 3 kW heating liner is placed in the periphery of the chamber to minimize the heat losses from the in-chamber air to the outside of the vessel.

6.3.2 Previous experimental results [10]

The test matrix is conformed of six selected operating conditions from a previous study [10]. These operating conditions are based on reference conditions of the ECN-Spray A, using n-dodecane as fuel. The injection pressure has swept (500, 1000 and 1500 bar) as well as the O_2 molar fraction

(15 and 21%) keeping the density constant at 22.8 kg/m^3 and the bulk gas temperature at 900 K.

Temperature [K]	**Density [kg/m^3]**	**Injection pressure [bar]**	**Molar fraction O_2 [%]**
900	22.8	500 / 1000 / 1500	15 / 21

Table 6.1. Test matrix measured in the high pressure and temperature vessel

The single-hole piezoelectric injector was used with a nominal diameter nozzle of 90 µm. The energizing time (ET) of the injector was set at 2 ms for all conditions, which results in a 3.5 ms hydraulic opening duration of the injector. Each measurement consisted on 10 repetitions in order to reduce the experimental uncertainties of measurement.

Finally, the operating conditions were measured by three different optical techniques: Schlieren [12], to obtain spray penetration, Diffused Back-Illumination technique (DBI) [13] for the soot concentration and the 2-color method for calculating the soot temperature and concentration (Chapter 3).

6.4 Spray model

Currently, there are several computational models capable of analyzing and characterizing the internal diesel spray structure in an injection/combustion process with temporal and spatial resolution. The set of computational tools ranges from complex models (known as 3D CFD) to more simplified models in which certain assumptions are made. For the analysis that is proposed, a one-dimensional model has been selected, which adapts perfectly to requirements of the analysis and has a short calculation time.

6.4.1 Model description

The spray model is a one-dimensional model capable of simulating the temporal and radial evolution of a fuel spray for inert conditions (evaporative or non-evaporative) and reactive conditions, as well as for steady and transient conditions. This model has been developed by CMT Máquinas y Motores Térmicos group of the Universitat Politècnica de València. This model is described in more detail in Chapter 3, section 3.3 of this thesis and in different previous works [12][15].

The model approaches the analysis of a fuel spray injected through a single hole inside a closed volume, where the process of air/fuel mixing and the combustion processes are reproduced. The spray evolution is considered free of any spatial restriction and the closed volume is considered wide enough so that the air conditions remain constant.

The model requires certain experimental data such as the temporal evolution of the in-cylinder pressure, the ambient density and the injection rate, injector properties (orifice number, diameter, spray angle) and fuel. As output values, the model generates comprehensive results, which describe the air/fuel mixture process with axial and temporal resolution. These results are used as input values in the soot and radiation models.

6.4.2 Spray model adjustment under inert conditions. Spray angle

As mentioned in section 3 (section 3.3.3), the only unknown input of the model is the spray angle; therefore, it needs to be determined by adjusting the results of the modelled vapor penetration to the experimental Spray-A results, defined in the section 6.3.2 of the test matrix for the three injection pressures.

To validate the model and to determine the adequate spray angle for a given set of conditions, a series of calculations were made at small angle

increments (1°); then, the deviation from the experimental curves was determined, and based on that the value for the angle was chosen. Figure 6.3 shows the experimental vapor penetration for the Spray-A standard conditions and the curves for three different values of spray angles as predicted by the model. It can be seen that a wider angle (24°) tends to under-predict the penetration, while a narrower angle (22°) may seem more appropriate at the beginning of the spray, but at the end, it overestimates the penetration values with respect to the experimental case.

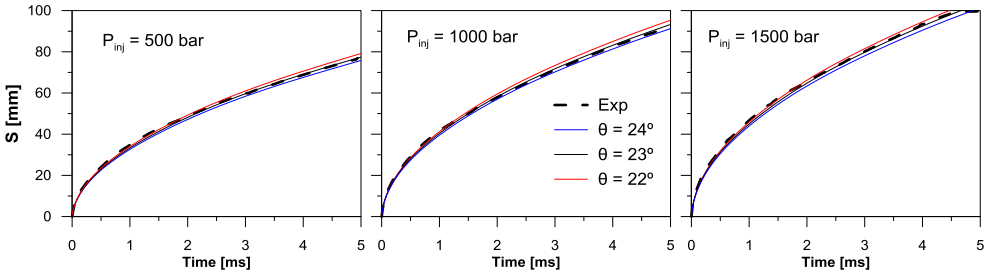

Figure 6.3. Experimental and modeled vapor penetration for the three spray angles tested under different injection pressures

Figure 6.4 shows the temporal evolution of the difference (in absolute values) between the experimental and modelled vapor penetration in the three spray angles tested for the different injection pressures. In this figure, the previous observations are viewed more clearly. In addition, it has been found in the literature [16][17] that the spray angle depends mainly on the density and the injection pressure. In the present tests, only the injection pressure has been varied. Although there are differences depending on the injection pressure, they are small to choose a different spray angle depending on the injection pressure. Therefore, the angle selected was 23° since it presents a good balance between the near and far regions of the spray from the nozzle.

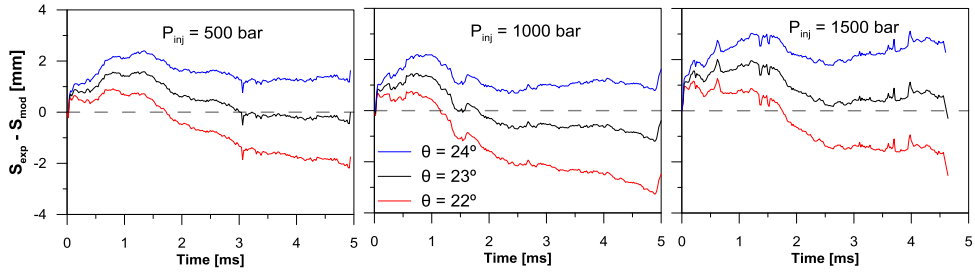

Figure 6.4. Difference between experimental and modeled vapor penetration for the three spray angles tested under different injection pressures

6.4.3 Spray model validation under reactive conditions

To validate the spray model and determine the most suitable angle for the operating conditions measured, the model has calculated the vapor penetration under reactive conditions with the selected angle in inert conditions (23°). The spray penetration in reactive conditions has been analyzed. From there, the results obtained have been compared with the experimental values for determining the most adequacy of the spray angle.

Prior to the comparison it is necessary to describe the methodology used for obtaining the experimental values for the spray penetration from the images. These have been obtained by Diffused Back-Illumination technique (DBI). Each image corresponds to a spatial soot distribution (KL) at a given instant, more specifically every 100 μs. A flame distribution is shown in the top image of Figure 6.5. To acquire the flame penetration, the soot concentration values along the central axis have been represented (bottom image of Figure 6.5), taking as center line the position of the nozzle. Finally, for each image, the first zero value of soot concentration is estimated as the maximum flame penetration. In this way, a temporal evolution of the flame penetration is represented from the experimental images.

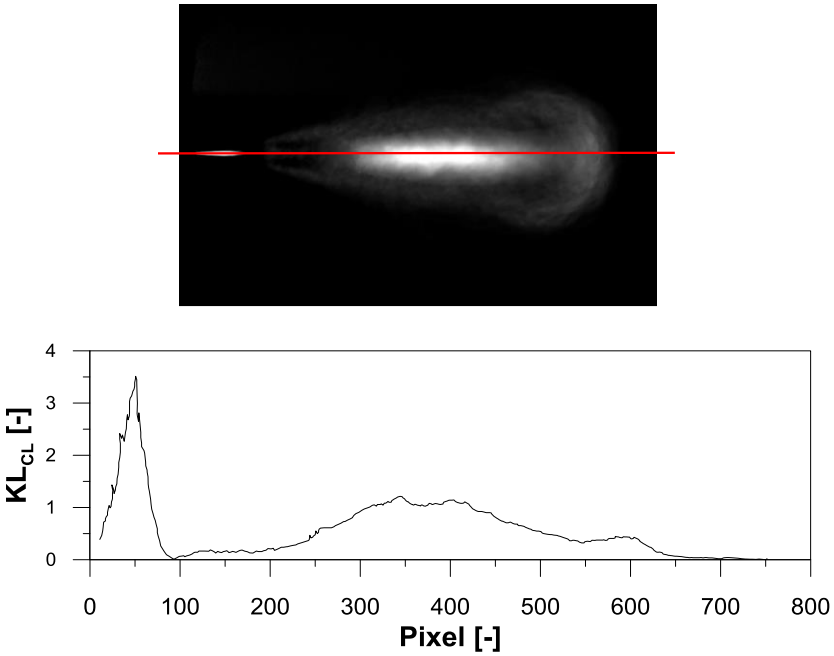

Figure 6.5. Top) Spray image obtained from the Diffused Back-Illumination technique and bottom) the soot concentration profile in the centerline.

Figure 6.6 represents the temporal evolution of the experimental spray penetration (solid line) and modelled (dashed line) for the six operating conditions analyzed. Before to analyzing the spray penetration, it should be noted that there is a field of view limitation caused the optical access of the facility. Therefore, the maximum penetration able to be captured in the experimental measurements was 86 mm. As shown in Figure 6.6, the temporal evolution of the flame penetration is split in two stages. On the one hand, the transient stage, in which the flame penetration increases progressively. In that, it is observed that the modelled and experimental results show small differences (at least until the distance of 86 mm of spatial limitation). On the other hand, the steady stage where the flame penetration maintains a quasi-constant value (the flame front is stabilized). This phase can only be observed in 21% oxygen results, since in the poorer oxygen concentration, stabilized flame penetration extends to approximately 110 mm [19]. The flame

penetration in the steady zone presents small differences (around 5 mm), which is due to a deviation from the acceptable experimental values. Finally, it is possible to conclude that, at least for the whole conditions used in this study, the most suitable spray angle is 23°.

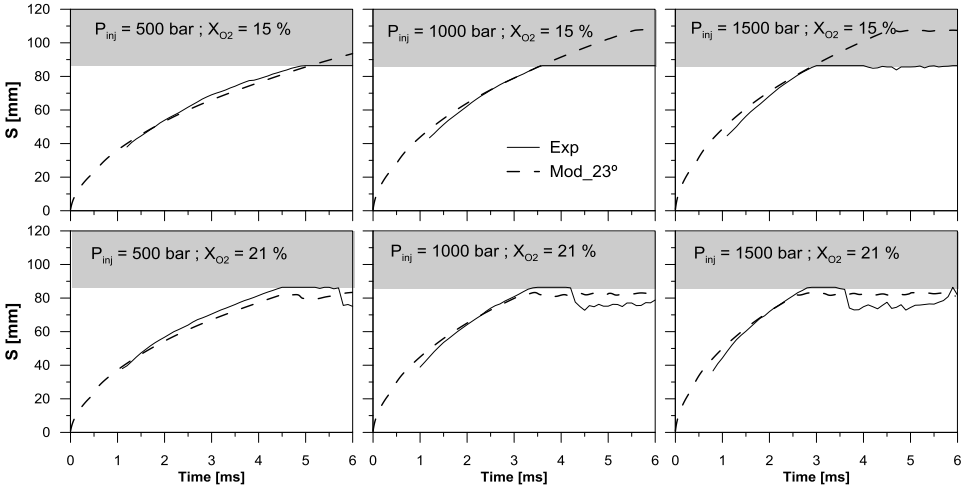

Figure 6.6. Experimental and modelled spray penetration under reactive conditions for the six operating conditions tested.

6.5 Soot Model

In this section a one-dimensional soot model has been developed, which considers the processes of soot formation and oxidation. The model uses the results calculated in the one-dimensional spray model as input variables, thus obtaining axial and radial soot concentration profiles for each instant in a diesel flame. In a first section, the model will be described along with the equations that comprise it. Then, the necessary constants will be adjusted from the experimental results. Finally, the model will be validated.

6.5.1 Model description

The soot model is based on Monin's study [21]. In this work, a parameter was proposed to model the soot formation process easily. The parameter was referred to as "*soot yield*" (SY) and is defined as the ratio between the mass fraction of fuel transformed into soot (Y_{soot}) and the mass fraction of unburned available fuel at that location (Y_{f_nb}):

(6.1) $$SY = \frac{Y_{soot}}{Y_{f\_nb}}$$

It is important to define the available non burned fuel mass fraction parameter for each instant and flame location. This mass includes all the mass coming from the unburned fuel that is available in that location with no distinction of its state (original fuel, cracked fuel, partly oxidized fuel or soot). This parameter is an input value to the soot model from the spray model (mixing/combustion).

Later, López *et al.* [22] proposed a correlation for the SY as follows:

(6.2) $$SY = K_{soot} \cdot max\left(0.5 - \frac{1}{Fr_{LOL}}, 0\right) \cdot t_r \cdot exp\left(\frac{T}{T_{Flame}}\right) \cdot \rho^{2.2}$$

where Fr_{LOL} is the fuel-air equivalence ratio at the lift-off length, t_r is the residence time inside the flame, T_{Flame} is the flame temperature, ρ is the ambient density and K_{soot} and t_0 are constant and their values have been fitting from experimental values (section 6.5.2). Next, the parameters will be explained:

- As many other researchers have observed [23][24] the soot formation process is mainly controlled by the fuel-air equivalence ratio at the lift-off length. Usually, a fuel-air equivalence ratio (Fr_{LOL}) of 2 is the limit to define whether soot is produced (Fr_{LOL} higher than 2) or not (Fr_{LOL} lower than 2) in a combusting diesel spray. For this reason, the soot yield is assumed to be different from this value. Finally, the Fr_{LOL} is an

input variable to the soot model calculated by the spray model (mixing/combustion).

- The soot formation also depends on the residence time of the fuel inside the fuel-rich region of the combusting spray. The residence time parameter is defined as $t-t_{LOL}$, where t is the instant under study and t_{LOL} stands for the time at which the considered fuel reaches the LOL. The SY is proportional to t_r.
- As it is well known, the temperature in LOL influences the soot formation positively. Monin [21] assumed that this parameter affects exponentially the rate of soot formation process: exp (T_0/T_{Flame}), where T_0 is a constant to adjust from the experimental results.
- Finally, Pickett found that the soot formation process is also affected by the in-cylinder pressure (or, for a given temperature, by density) [23]. Based on the data published in this work, the corresponding function is the following: $\rho^{2.2}$, which also should affect the soot yield.

Once the factors, which the SY parameter depends, are defined from the product of equations (6.1) and (6.2) the mass fraction of soot, Y_{soot}, can be obtained. Nevertheless, both of the two most common soot measuring techniques (DBI and two-color method) provide a value for X_{soot} (volume fraction). Consequently, the conversion from one magnitude to the other is required. This conversion can be done as follows:

$$X_{soot} = Y_{soot} \cdot \frac{\rho_a}{\rho_{soot}} \tag{6.3}$$

where ρ_{soot} is the density of the soot particles and ρ_a is the density at the point under consideration (local density). The soot particle density does not have a universal value. However some authors take a value of approximately 1800 kg/m^3 as a representative value [25][26]. For the local density estimation, the local temperature and the mean pressure are considered, assuming that the constant in the equation of state is that of standard air.

Up to now, the soot model is able to predict the evolution of X_{soot} at the spray centerline. As soot radiation takes place at any region where temperature is sufficiently high, the value of the soot volume fraction at any other point of the spray section is needed. There is not much information available in the literature about the shape of the X_{soot} radial profile. For this model, a Gaussian profile has been chosen to simulate the flame section. This profile was proposed by Desantes *et al.* [27], which follows the following equation:

$$\frac{X_{soot}}{X_{soot,CL}} = exp\left[-4.6 \cdot \left(\frac{r}{R_{Flame}}\right)^2\right] \tag{6.4}$$

where r is the radial coordinate and R_{Flame} the flame radius at the section under consideration.

6.5.2 Adjustment methodology. Soot model validation

The purpose of this section has been split in two parts: the two constants adjustment of the model, K_{soot} and T_0, and the soot model validation. For both particular objectives, experimental results of the soot concentration from the Diffused Back-Illumination technique (DBI) will be used.

The methodology used to adjust the constants K_{soot} and t_0 is shown in the flow chart of Figure 6.7. These two parameters have been found by searching the lowest error when comparing the experimental and the modelled soot concentration at each axial and radial position. This procedure has been divided into several steps:

- First, an initial value is assigned to each constant. With them, the parameter "Soot Yield" (SY) is calculated. As described in section 6.5.1, a soot molar fraction value (X_{soot}) is obtained for each flame axial and radial position. Next, the soot concentration values (KL) is calculated from the information of

the soot model and compared it with the experimental values provided by the DBI method. The conversion of X_{soot} to KL is based on the Beer-Lambert equation, which evaluates the light attenuation [20]:

$$\frac{I}{I_0} = exp(-KL) = \tau \quad (6.5)$$

where I is the light intensity, I_0 is the attenuated light intensity and τ, the transmissivity. If it is considered that the flame is divided radially into portions of size dr, the equation (6.5) can be rewritten as follows:

$$\frac{I}{I_0} = exp(-KL) = \tau = \prod_i \tau_i \quad (6.6)$$

where τ_i represents the transmissivity of each portion of the spray. According to Musculus [20], the transmissivity is related to the soot volume fraction in the following way:

$$\tau_i = exp\left(\frac{-g \cdot X_{soot(r)} \cdot dr}{\lambda^{\alpha}}\right) \quad (6.7)$$

where g is a constant equal to 6.3 μm^{-1}, λ is the wavelength in μm and $\alpha = 1.22\text{-}0.245 \cdot \ln(\lambda)$, with λ in μm. If equations (6.6) and (6.7) are considered together, and it is taken into account that the product of an exponential is the exponential of an addition, it can be seen that KL can be related to the local conditions in the following way:

$$KL = \frac{g}{\lambda^{\alpha}} \cdot \int_{-L/2}^{+L/2} X_{soot}(r) \cdot dr \quad (6.8)$$

To finish this first step, the difference of the modelled and experimental soot concentrations for each axial and radial position is calculated.

- The second stage consists on performing the same previous procedure until reaching the sum of the differences, but in this

case varying the values of both constants. In particular, both constants were varied ± 20% of their initial value. This indicates that the first step is repeated with all possible combinations of the constants, that is, four times as many.

- Finally, the constant combination with lower value is chosen from the five error results (initial + 4 combinations). This pair of constants are considered as initial values and the whole procedure is repeated, so that finally a matrix with five accumulated errors corresponding to five constant pairs is obtained again. This step is repeated until the minimum error is achieved twice times consecutively by the same constants K_{soot} and t_0.

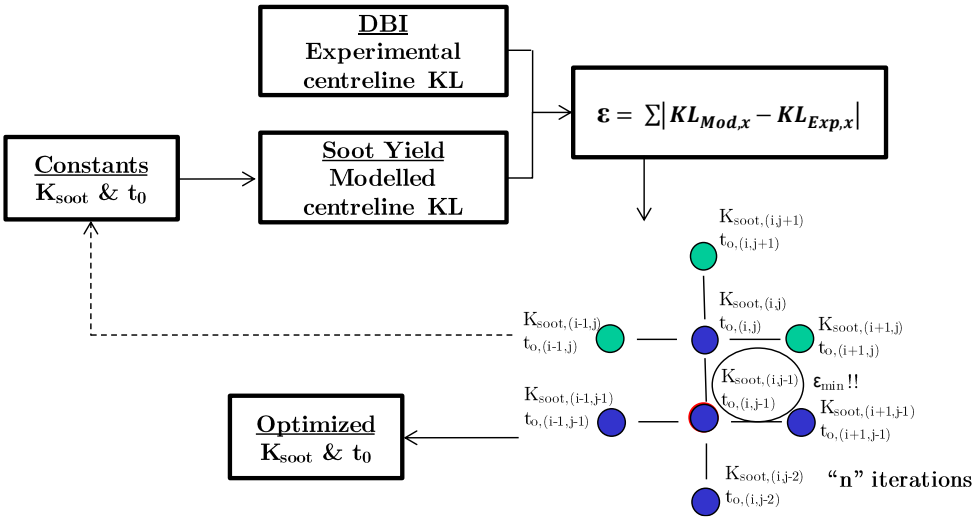

Figure 6.7. Experimental methodology used to fitting the soot model constants (K_{soot} and t_0)

Considering the six operating conditions described in the test plan section, the values obtained for the constants K_{soot} and t_0 are $11.25 \cdot 10^{-4}$ and 4687.5, respectively. Figure 6.8 shows the axial evolution of the experimental and modelled soot concentration along the centerline of the flame at a given instant. The model adjusts the start and end of the flame precisely. There is

a tendency to underestimate the results respect to the experimental results. Qualitatively, the modelled results show good agreement with reality (KL decreases when the injection pressure increases and/or the oxygen concentration increases). Therefore, it is concluded that the soot model is correctly adjusted respect to the experimental data.

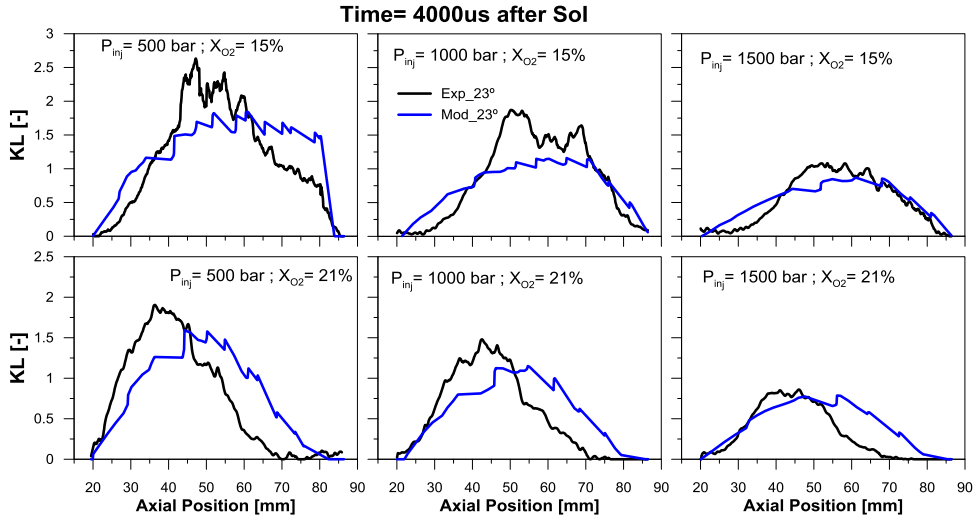

Figure 6.8: Experimental and modelled soot concentration for the six operating conditions tested.

6.6 Radiation model

In this section the radiation model is presented. First, the methodology followed in the model is validated. For that, the spectral intensity of the radiation (I_{soot}) has been calculated and compared to the experimental values measured by the 2-color method. Once the first step has been completed, the total radiation emitted by the soot is calculated. This parameter is the main objective of this chapter.

To begin with, these are the different assumptions taken for modeling the spray radiation:

- The spray/wall interaction will not be taken into account. Consequently, a free spray is considered.
- The swirl existing in the combustion chamber does not modify the spray geometry, which remains axisymmetric.
- The radiation is diffuse. It radiates in the same way in all directions.

6.6.1 Model description

The radiation intensity is the main output variable of the radiation model (as shown in Figure 6.1) and this has been used as a basis to validate the present radiation model. The radiation intensity in the radial direction has been calculated as explained by Payri *et al.* [28].

Figure 6.9 presents the modelled combustion temperature and soot distribution for a particular axial position. The temperature distribution has been obtained from the spray model, as a function of the equivalence ratio distribution at each radial and axial position. In the temperature distribution three different zones can be observed: 1) the flame limits are the stoichiometric surface, where the maximum temperatures are reached; in this location the fuel diffused from the inner part of the flame reacts with oxygen from the outer part. 2) The inner zone, which corresponds to the rich side of the flame; this region consists of partially oxidized fuel, combustion products and soot. 3) The outer part, which is the lean side of the flame; in this region fresh air and combustion products are present. About the distribution of soot concentration, a linear distribution has been considered in which it is assumed that the soot particles are only present in the inner part of the flame, as they are totally oxidized by the OH present on the reaction zone [2].

The flame is divided radially into discrete flame elements with their corresponding values of temperature and soot concentration. To analyze the radiation propagation inside the flame both emission and absorption processes have been considered.

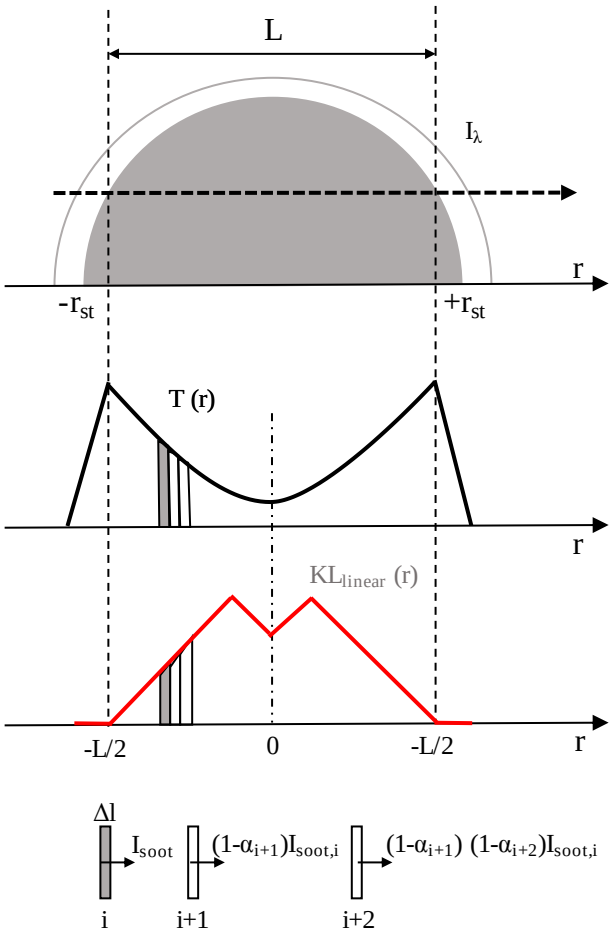

Figure 6.9. Scheme of the diesel spray

Considering the temperature and soot distributions, the radiation propagation process inside the flame is based on the following:

- Radiation is propagated along lines parallel to the flame main symmetry plane.
- The spatial distribution of the local gas temperature is assumed to be equal to the soot temperature. In this case, the spray model calculates the flame temperature.

- Soot is assumed to be completely oxidized at the flame stoichiometric surface.

The radiation path is divided into n elements with the same thickness. Each element i has its temperature T_i and optical thickness KL_i. So, considering the proposed soot distributions it can be stated that:

$$KL = \sum_{i=1}^{n} KL_i \tag{6.9}$$

As indicated in Chapter 3, the radiation emitted by each element can be calculated as:

$$I_{soot,i}(\lambda, T_i, KL_i) = \varepsilon_{\lambda,i} I_{b(\lambda,T_i)} \tag{6.10}$$

where ε indicates soot spectral emissivity and I_b corresponds to a blackbody spectral intensity. The radiation received by the sensor (which is located on either flame limits) at each wavelength is the addition of the $I_{soot,i}$ of each flame element. Considering the attenuation factor between elements, the total soot radiation intensity for each wavelength can be calculated as:

$$I_{soot,i}(\lambda, T_i, KL_i) = \sum_{i=1}^{n} \left[\varepsilon_{\lambda,i} I_{b(\lambda,T_i)} \cdot \prod_{j=i+1}^{n} (1 - \alpha_{\lambda,j})\right] \tag{6.11}$$

where for an element j the absorption ($\alpha_{\lambda,j}$) is defined by the spectral absorptivity ($\varepsilon_{\lambda,j}$) following Kirchhoff's law:

$$\alpha_{\lambda,j} = \varepsilon_{\lambda,j} \tag{6.12}$$

6.6.2 Spectral intensity

Once the radiation model has been defined, the purpose of this section is to evaluate the soot spectral intensity (as an output parameter of the radiation model) versus the experimental results from the 2-color method (defined in Chapter 3).

Figure 6.10 shows the axial evolution of the experimental and modelled soot spectral intensity along the centerline for the six operating conditions. The soot spectral intensity has been calculated for two wavelengths, $\lambda = 550$ and 650 nm. For simplicity, only the results for $\lambda = 550$ nm have been shown. Before starting the analysis, since the experimental spray penetration results for an oxygen mass fraction of 15%, the maximum flame penetration that could be captured is 86 mm. In general, both modelled and experimental results decrease when the injection pressure increases and/or the oxygen mass fraction increases (this was discussed in more detail in Chapter 4). By comparing each graph individually, it can be established that the model provides a good accuracy during the onset of the flame. If the flame length is divided into two parts, in the first one, the model sub-predicts the soot spectral intensity values. This phase is estimated up to 60-70 mm from the inyector. From this, the trend changes and the model over-predicts the results respect to the experimental results.

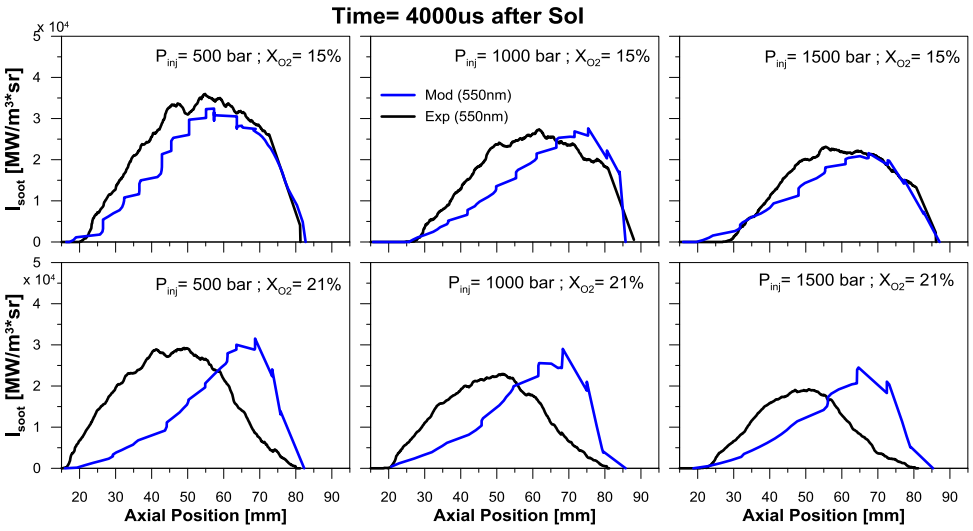

Figure 6.10. Experimental and modelled soot spectral intensity along the centerline for the six operating conditions

6.6.3 Total radiation

The next step in the validation of the radiation model is the calculation of the total radiation emitted by soot particles. Based on the soot spectral intensity, the total radiation was obtained from the integration of the spectral intensity for a particular range of wavelengths using equation (6.13):

$$Q_{rad} = \pi \int_t \int_A \int_\lambda \varepsilon_\lambda I_{b,\lambda} \, d\lambda \, dA \, dt \tag{6.13}$$

where t represents the exposure time in which the optical system is registering flame luminosity, and A is the flame area obtained by equation (6.14):

$$A_t = 2\pi r \int_x dx \tag{6.14}$$

where r is the flame radius, which is determined from a temporal image of the flame and dx is the axial width.

Figure 6.11 represents the temporal evolution of the experimental and modelled total radiation for the six operating conditions studied. For the six cases analyzed, the model predicts total radiation values very similar to the experimental ones. Taking into account the simplifications and assumptions of each model, the results shown in Figure 6.11 can be considered as acceptable results.

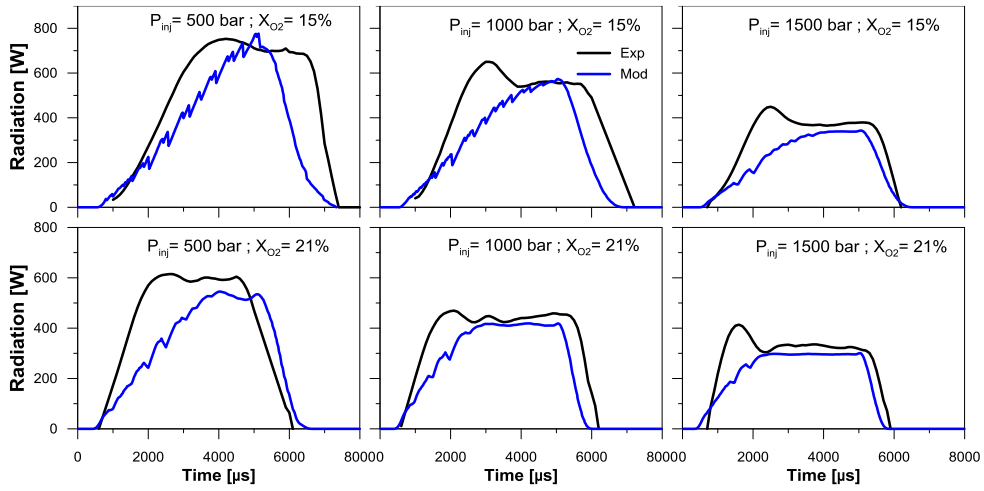

Figure 6.11. The temporal evolution of the experimental and modelled total radiation for the six operating conditions studied.

Finally, in order to better quantify the total radiation, the radiation fraction has been calculated. The radiant fraction (X_{rad}) emitted by soot is defined as the fraction of the total chemical energy released during combustion that is lost due to radiation heat transfer. This term is expressed by equation (6.15):

$$X_{rad} = {Q_{rad}}/{m_f Q_{LHV}} \tag{6.15}$$

where m_f represents the mass of fuel injected and Q_{LHV} is the lower heating value of diesel (44.570 MJ/kg).

Figure 6.12 shows the results of the radiant fraction emitted by soot for the different operating conditions analyzed. Particularly, the sub-figure on the left shows the values of radiant fraction modifying the injection pressure at oxygen molar fraction of 15% and, the figure on the right, at oxygen molar fraction of 21%. Considering the results obtained from soot concentration and spectral intensity in previous figures, the trends of radiation fraction are expected. Thus, a reduction of injection pressure and/or

oxygen molar fraction implies a higher radiant fraction value. In addition, as in the previous graph of the total radiation, the radiation fraction values are slightly lower than the experimental ones. Finally, the modelled radiation fraction values are between 0.11 and 0.43% respect to the total fuel energy. Comparing them with the results obtained from the radiation fraction in section 4.3.3.2 of Chapter 4, the modelled values are in the same order of magnitude. Considering that the operating conditions are similar, the modelled results are coherent with those obtained in Chapter 4. This makes the radiation model a completely suitable tool to predict and study the radiation heat transfer.

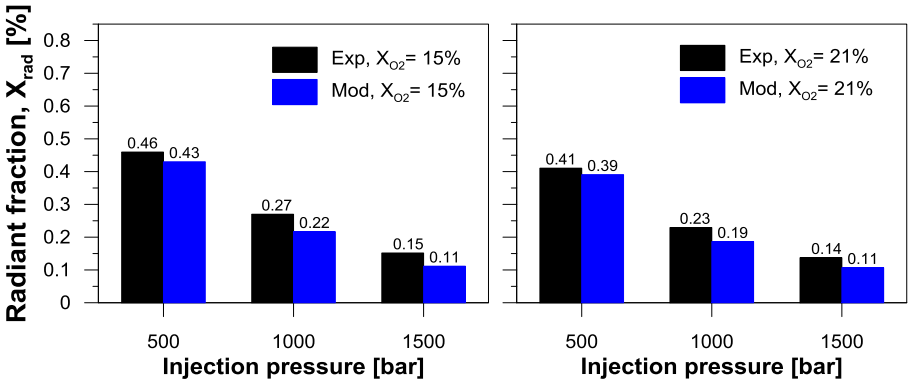

Figure 6.12. Experimental and modelled radiant fraction modifying injection pressure and oxygen molar fraction.

6.7 Conclusions

In this chapter a radiation model has been developed for diesel sprays able to predict the heat losses to the chamber walls due to radiation. The model is based on three sub-models: spray model, which analyzes and characterizes the internal spray structure in terms of mixing and combustion process with temporal and spatial resolution. A soot model, which the results of which are justified according to soot formation and oxidation processes. The cohesion of these two sub-models is used to obtain the input values to

the radiation model, which the radiation heat transfer values for a diesel flame are obtained. The main contributions of this chapter are the following:

- The one-dimensional spray model has been adjusted from the only unknown variable: the spray angle. For the cases analyzed, the most suitable spray angle has been found to be 23° comparing the penetration results in inert conditions. Regarding the validation of the model, penetration values have been used in reactive conditions. The model estimates a penetration very similar to the experimental values, both in the transient and quasi-steady phases.
- The soot model is based mainly on the "*soot yield*" concept, which combines the soot formation and oxidation processes depending on the instant and location. Like the spray model, this model has also been adjusted by means of two unknown constants: K_{soot} and t_0. The values of the constants are $11.25 \cdot 10^{-4}$ and 4687.5, respectively. These constants have been obtained from an experimental methodology, where the soot concentrations are compared with the experimental values measured by Diffused Back-Illumination technique (DBI). The model predicts accurately the start and end of the flame. Although in qualitative terms, the model accurately predicts the experimental values. Depending on the axial position, the model sub-predicts or over-predicts the experimental values. In general terms, the soot model matches correctly with the experimental values.
- Finally, a methodology developed by Payri was used for the radiation model [28]. The methodology has considered both emission and absorption processes for analyzing the radiation propagation inside the flame. From the soot concentration estimated with the soot model and the soot temperature calculated from the spray model, the modelled spectral intensity has been calculated. For the operating conditions used in this study, the radiation model calculates radiation spectral

intensity values very similar to the experimental ones. Taking into account the simplifications and assumptions of each model, it can be accepted as acceptable results. The fraction of radiation shows values from 0.11% to 0.43% respect to the total fuel energy depending on the operating condition. Considering the differences in the operating conditions, these results are consistent with those obtained in Chapter 4 section 4.3.3.2, in which the radiation was characterized under simplified conditions.

6.8 Bibliography

[1] Rolf D. Reitz. "Directions in internal combustion engine research". Combustion and flame, Vol. 160, pp 1-8, 2013.

[2] Dec J. "A Conceptual Model of DI Diesel Combustion Based on Laser-Sheet Imaging". SAE Technical Paper 970873, 1997.

[3] Rao V., Honnery D. "A comparison of two NOx prediction schemes for use in diesel engine thermodynamic modelling". Fuel Vol. 107, pp. 662–70, 2013.

[4] Cheng X, Chen L, Hong G, Yan F, Dong S. "Modeling study of soot formation and oxidation in DI diesel engine using an improved soot model". Applied Thermal Enginnering, Vol. 62, pp. 303-312, 2014.

[5] Kazakov A., Foster D.E. "Modeling of soot formation during DI diesel combustion using a multi-step phenomenological model". SAE paper 982463; 1998.

[6] Tao F., Reitz R.D., Foster D.E., Liu Y. "Nine-step phenomenological diesel soot model validated over a wide range of engine conditions". Int. Jornal Thermal Sciences Vol 48, pp. 1223–1234, 2009.

[7] Jung D., Assanis D. "Multi-zone DI diesel spray combustion model for cycle simulation studies of engine performance and emissions". SAE paper 2001-01-1246; 2001.

[8] Gao Z., Schreiber W. "A phenomenologically based computer model to predict soot and NOx emission in a direct injection diesel engine". Int. Jorunal of Engine Research Vol. 2, pp. 177–88, 2001.

[9] Benajes J., Martín J., García A., Villalta D., Warey A. "In-cylinder soot radiation heat transfer in direct-injection diesel engines". Energy Conversion nad Management 106, 414–427, 2015.

[10] Skeen S., Manin J., Pickett L., Cenker E. et al. "A Progress Review on Soot Experiments and Modeling in the Engine Combustion Network (ECN)". SAE Int. J. Engines 9 (2), 2016.

[11] Baert R.S.G., Frijters P.J.M., Somers B., Luijten C.C.M. and de Boer W. "Design and Operation of a High Pressure, High Temperature Cell for HD Diesel Spray Diagnostics: Guidelines and Results". SAE Technical Paper, nº 2009-01-0649, 2009.

[12] Payri R., Garcia-Oliver J., Xuan T. and Bardi M. "A study on diesel spray tip penetration and radial expansion under reacting conditions". Applied Thermal Enginnering, Vol. 90, pp. 691-629, 2015.

[13] Pastor J., Garcia-Oliver J., Novella R., and Xuan T. "Soot Quantification of Single-Hole Diesel Sprays by Means of Extinction Imaging". SAE Int. J. Engines 8 (5), 2015.

[14] Pastor J. V., Lopez J. J., Garcia J. M. y Pastor J. M. "A 1D model for the description of mixing-controlled inert diesel sprays". Fuel, Vol. 87 no 13-14, pp. 2871-2885, 2008.

[15] Desantes J.M., Pastor J.V., García-Oliver J.M., Pastor J.M. "A 1D model for the description of mixing-controlled reacting diesel sprays". Combustion and Flame, Vol. 156, pp. 234-249, 2009.

[16] Pastor J., Garcia-Oliver J., Pastor J.M., Vera-Tudela W. "One-dimensional diesel spray modeling of multicomponent fuels". Atominzation and Sprays, Vol 25(2), pp. 485-517, 2015.

[17] Siebers D.L. "Scaling liquid-phase fuel penetration in diesel sprays based on mixing-limited vaporization". SAE Technical Paper, nº 1999-01-0528, 1999.

[18] Pastor J., Garcia-Oliver J., Novella R., and Xuan T. "Soot Quantification of Single-Hole Diesel Sprays by Means of Extinction Imaging". SAE Int. J. Engines 8 (5), 2015.

[19] Siebers D., Higgins B. and Pickett L. "Flame Lift-off on direct-injection diesel fuel jets: Oxygen concentration effects". SAE Technical Paper, nº 2002-01-0890, 2002.

[20] Musculus M. "Measurements of the Influence of Soot Radiation on In-Cylinder Temperatures and Exhaust NOx in a Heavy-Duty DI Diesel Engine". SAE Technical Paper, nº 2005-01-0925, 2005.

[21] Monin C. "Caracterización del Proceso de Formación de Hollín en una Llama de Difusión Diésel de Baja Temperatura". Doctoral Thesis, 2009.

[22] López J., Garcia-Oliver J.M., Martin J., Chemisky J.P., Bouet A. "A Soot Radiation Model for Diesel Sprays". SAE Technical Paper, nº 2012-01-1069, 2012.

[23] Pickett L.M. and Siebers D.L. "Soot in diesel fuel jets: effects of ambient temperature, ambient density, and injection pressure". Combustion and Flame, vol. 138, pp. 114-135, 2004.

[24] Benajes J., Martín J., García A., Villalta D., Warey A. "In-cylinder soot radiation heat transfer in direct-injection diesel engines". Energy Conversion nad Management 106, 414–427, 2015.

[25] Matthieu O., Djebaïli-Chaumeix N., Paillard C.E., and Douce F. "Experimental study of soot formation from diesel fuel surrogate in a shock tube". Combustion and Flame, vol. 156 (8), pp. 1576-1586, 2009.

[26] Kronholm D.F. and Howard J.B. "Analysis of soot surface growth pathways using published plug-flow reactor data with new particle size distribution measurements and published premixed flame data". Proceedings of the Combustion Institute, vol. 28, pp. 2555-2561, 2000.

[27] Desantes, J.M., Arrègle, J., López, J.J. and Cronhjort, A. "Scaling laws for free turbulent gas jets and diesel-like sprays". Atomization and Sprays, vol. 16, pp. 443-473, 2006.

[28] Payri F., Pastor J.V., García J.M., Pastor J.M. "Contribution to the application of two-colour imaging to diesel combustion". Measurement Science and Technology, vol. 18, pp. 2579-2598, 2007.

Chapter 7

Conclusions and Future work

Content

7.1 Introduction

The aim of this final chapter is to close this doctoral thesis by listing the main conclusions obtained from the research work, as well as to enumerate a set of research lines that emerge as a continuation of conclusions.

In the first place, the main results obtained for each section in the thesis were synthesized. It also aims to establish a relationship between the objectives based on the literature and the results obtained, as well as justify, interrelate as far as possible, the general methodology that has been carried out for the study and analysis of the work proposed in the development of this investigation.

Once the conclusions are obtained, ideas and studies with potential for the realization of future research work related to what is shown in this thesis are proposed.

7.2 Conclusions

Although the first chapter presents a general justification for the thesis, Chapter 2 presents a bibliographic review of the work done by other previous researchers to define the particular objectives through which the thesis was made along with a general approach to the study. With respect to the review of the literature, the injection/combustion processes involved in the diesel combustion have been described in detail to introduce the review of the phenomena involved in the emission of soot particles as one of the most important pollutants in the diesel engines. In the last part of the literature review, the effect of radiation heat transfer and its influence on combustion performance has been analyzed. Based on the literature reviewed, a lack of knowledge about the efficiency losses due to the phenomenon of radiation heat transfer has been detected. Therefore, the main objective of this doctoral thesis is *to contribute to the understanding of radiation heat transfer in direct*

injection diesel combustion together with the improvement of knowledge in the soot formation and oxidation process.

To achieve this objetive, a methodology was carried out: in a first experimental phase, a basic study was started in which the phenomenology of the radiation process in different thermodynamic conditions in an optical engine is analyzed, which is used as a basis to evaluate the amount of energy by radiation with respect to the chemical energy of the fuel under realistic operating conditions in an HSDI engine. Once the radiation phenomenon has been studied, the soot particles are explored as the main responsible for the radiation phenomenon. In particular, special attention is put to the soot oxidation phenomenon and its involvement in the diesel combustion efficiency. Finally, based on the knowledge acquired in the previous stage, a soot radiation model has been developed for direct injection diesel flames capable of predicting the heat losses by radiation in the combustion chamber.

- **Radiation HT under controlled conditions**

In the first part of Chapter 4, the amount of energy lost by soot radiation during the combustion process under different simplified operating conditions is measured in an optical engine. The soot spectral intensity and the radiant fraction have been the variables analyzed. For this, the radiation measurements have been based on the two-color method applied to two independent and different optical systems. As a result of the soot spectral intensity, it increases when the injection pressure is reduced and/or the ambient temperature and/or the in-cylinder density increases. A higher lift-off length leads to a reduction in the soot concentration and, finally, the soot spectral intensity. With respect to the radiant fraction, the values vary from 0.1% to 0.75% with respect to the total fuel energy depending on the measured operating condition. In addition, these radiation values are around an order of magnitude lower than a blackbody with the same area that radiates during the whole injection event and these values are consistent with the radiation values obtained by other researchers for similar conditions.

- **Radiation HT under realistic conditions**

A second study of soot radiation has been carried out in a 4-cylinder HSDI production engine simulating real operating conditions. In this case, the load, swirl ratio, EGR and combustion phasing have been varied to calculate the soot temperature and concentration together with the soot radiant fraction. Considering load effects, it can be said that maintaining constant engine speed, the peak radiation intensity was higher when the load was increased. A clear decrease in soot temperature was attained when the engine load was decreased. KL profiles depend directly on the diffusion combustion phase, the higher the duration of this phase, the higher the amount of soot obtained. Considering swirl ratio effects, it can be stated that an increase of swirl ratio implied an enhancement of combustion process. However, in terms of radiation, the effect is opposite. The radiation is reduced due to a shorter combustion duration as the swirl increases. As it is well known, the EGR minimizes soot temperature. However, EGR produces higher soot concentration values and combustion duration, which translates into a greater radiant fraction when the EGR rate is increased. Finally, it was stated that CA50 was delayed, lower peak of radiant intensity was attained. This behavior was due to lower soot temperatures when the CA50 was delayed and lower soot formation since more time to achieve premixed combustion was available. Unlike the study carried out in the optical engine, there is great uncertainty about the estimation of the in-cylinder flame area in the metallic engine. For this reason, it has been calculated the specific radiant fraction (units kJ/m^2). Depending on the operating condition, the specific radiant fraction values range between 0.55 and 1.37 kJ/m^2.

As a common conclusion for the radiation study in diesel engines, it is established that radiation losses are a very small energy fraction with respect to the total fuel energy. This statement is consistent with the current diesel engines. With the improvement and development of different strategies on combustion, current diesel engines produce a very low concentration of particle matter.

- **Late-Cycle Soot Oxidation**

As demonstrated in the introduction of Chapter 5, the soot oxidation process is primarily responsible for the soot particle emissions. For this reason, the soot oxidation process has been evaluated by varying parameters related to the air thermodynamic conditions and the injection process in the 4-cylinder diesel engine. The parameter KL has been used as a tracer of the soot concentration in the combustion chamber, which has been measured directly in the engine. A theoretical parameter 0D (ACT^{-1}) has been defined as a mixing tracer based on the experimental heat release and the injection parameters. The results conclude that the mixing process, and therefore the soot oxidation process, improves when the swirl ratio, ambient gas density, air intake temperature, injection pressure and/or decreases the EGR rate and/or an advance the CA50. Thus, when the mixing capacity improves due to different variations in the operating conditions, the average half-life time of KL becomes lower, improving the soot oxidation. In addition, a 0D model based on experimental measurements was developed to obtain the half-life time of KL and the half-life time of ACT^{-1}. As expected, the "mixing capability" can not fully explain a complex phenomenon such as soot oxidation. In this sense, the average bulk gas temperature has been included as an additional tracer in the 0D model, significantly improving the accuracy of the soot oxidation process predictions.

- **Optimized strategies to improve the late-cycle diffusion combustion**

The objective of this section is to compare different engine strategies to enhance the late-cycle mixing controlled combustion process and therefore to improve the soot oxidation process while maintaining similar gross indicated efficiency. For that, a study was carried out for evaluating the potential of swirl ratio and a dedicated injection strategy to enhance the late-cycle mixing controlled combustion.

These experimental measures have been carried out in a single-cylinder engine derived from the 4-cylinder engine. For this, the two estimators of both mixing and soot oxidation processes described previously have been used.

In conclusion, an increase in swirl ratio is not directly related with an increase in mixing process during the late-cycle combustion. Indeed, an excessive SR can lead a deterioration of the combustion development due to excessive spray interaction, which causes a slower and less powerful heat release process reducing the indicated efficiency. Nevertheless, a proper injection pattern (increase of injection pressure and post-injection addition) coupled with a low SR was showed as a suitable strategy to improve the late-cycle diffusion combustion as well as soot oxidation while maintaining constant GIE.

- **Soot Radiation Model**

The last objective of this thesis focuses on developing a soot radiation model. Three sub-models, which are directly connected to each other, compose this model: spray model, soot model and radiation model. The spray model (named DICOM) is a one-dimensional model that simulates the axial and radial distribution of a fuel spray for each instant. This model needs input variables such as the temporal evolution of the in-cylinder pressure, ambient density and injection rate. Only one variable, the spray angle, is necessary to adjust it. For this, the experimental results of spray penetration in both inert and reactive environment measured with the *Schlieren* technique have been used. Once the spray model has been adjusted, these spray model results have been used as input variables for the soot model and thus, axial and radial profiles of soot mass fraction have been obtained for each instant. The soot model is based on soot formation and oxidation processes mainly. As in the spray model, the soot model is necessary to adjust the optimal values for two constants (K_{soot} and t_0) from experimental results of soot concentration. These experimental results have been measured with the Diffused Back-Illumination technique (DBI). Next step, the temporal

evolution of the spectral intensity has been obtained from the simulated soot concentration results together with the spatial temperature distribution (calculated also in the spray model), and consequently, the total soot radiation losses. Finally, the simulated spectral intensity is integrated for the whole wavelengths spectrum and the radiation heat losses are obtained. As in two previous models, the simulated radiation has been compared with experimental values from the 2-Color method. For the operating conditions used in this study, the radiation model calculates radiation spectral intensity values very similar to the experimental ones. Taking into account the simplifications and assumptions of each model, it can be considered as acceptable results. The fraction of radiation shows values from 0.11% to 0.43% respect to the total fuel energy depending on the operating condition. Considering that the operating conditions are similar, the modeled results are coherent with those obtained in first objective of this work, in which the radiation was characterized under simplified conditions.

7.3 Future works

Once the main conclusions and achievements of the doctoral thesis have been described, the next part of the chapter will provide different ways in which the research work could go. The main suggestions are detailed as follows:

- **Improvement on optoelectronic probes for in-cylinder soot characterization of real engines**

The experimental measurements realize during the present doctoral thesis were carried out with the optoelectronic probe VisioFEM (described in Chapter 3). In addition to the capabilities, the equipment presents certain disadvantages during the operation:

- Operability of the equipment: due to small diameter in the quartz window, the probe presented high slenderness and was easy to bend

the whole device with the consequent breaking of it. Once the window is broken, the complete device needed to be replaced with its corresponding delays and cost in the test campaign.

- Optical window fouling: as it is known, the diesel combustion produces a large amount of soot particles (depending on the operating point). This soot was deposited in the window surface (optical access) and blocked the light path from combustion. This fact implies a constant calibration of the device and sometimes, results that needed to be discarded.
- Durability of the access window is very limited: window sealing was not proper designed for diesel application. In this sense, high temperatures provoked glue deterioration and therefore the device futility.

The solution could be to develop a new optical access, which offers the following possibilities:

- To do a removable probe splitting window holder to the rest of the probe. Thus, if the window is damaged, it can be replaced easily.
- To increase the optical access diameter, in this manner the amount of collected light would be higher and therefore the bending problem would be mitigated.
- To improve the heat transfer from the window towards the cylinder head, decreasing the temperature in the critical areas of the optical assembly and so reducing the degradation (irreversible).
- To include electrical resistances in the sapphire window, which prevents the soot deposition.

- Late-cycle soot oxidation

To continue working on late-cycle oxidation process seems to be essential to decrease soot emissions. This subject can be considered as a key point due to new legislations.

In this sense, it is proposed to go deeper in the basic phenomenology which controls the process. For that reason, the use of optical engines with fully combustion access it is completely advisable. In spite of the simplification that optical engines imply, it can also be considered as a possible way to overcome some of the problems previously exposed with the use of probes. Field of vision is not restricted at all as well as 3D resolution is considered.

Thus, in particular is proposed to use a light duty optical single cylinder engine applying laser/light extinction method/imaging to better understand how different engine settings and hardware affect the late-cycle combustion process and therefore the soot production. Once these fundamental tests have been made is proposed to compare with the ones obtained in this thesis to provide a wider overview of the subject.

- **Soot radiation model**

Following the soot radiation model for diesel flames, the next interesting step would be to adapt and validate the model for real engine operating conditions.

- Spray model: to include the influence of the flow dynamics in the combustion chamber (swirl) as well as the wall effect. Up to now DICOM is based on free spray. So, this is an important issue that should be overcome in the future.
- Soot model: to evaluate more elaborated soot models with formation and oxidation processes.

Bibliography

[1] European Commission. Transport. Statistical pocketbook, 2017. https://ec.europa.eu/transport/facts-fundings/statistics/pocketbook-2017_en.

[2] Diesel car salet set to overtake petrol in europe. Price Watrhouse Coopers, 2015.

[3] New passenger car registrations in Western Europe. http://www.acea.be, 2015.

[4] DieselNet: Diesel Emissions Online http://www.dieselnet.com/standards/eu/fuel_automotive

[5] Environmental Protection Agency. "Nitrogen Oxides (NOx), Why and How They Are Controlled". Technical report, 1999.

[6] Environmental European Agency. "Emissions of primary PM2.5 and PM10 particulate matter". Technical report.

[7] Wallace W. E., Keane M. J., Murray D. K., Chisholm W. P., Maynard A. D. y Ong T.-M. "Phospholipid lung surfactant and nanoparticle surface toxicity: Lessons from diesel soots and silicate dusts". Journal of Nanoparticle Research, Vol. 9 nº 1, pp. 23-38, 2007.

[8] Payri F., Desantes, J.M. "Motores de combustión interna alternativos". Editorial Reverté, 2011.

[9] García A., Piqueras P., Monsalve-Serrano J., Lago R. "Sizing A Conventional Diesel Oxidation Catalyst To Be Used For RCCI Combustion Under Real Driving Conditions". Applied Thermal Engineering, Vol. 140, pp. 62-72, 2018.

[10] Desantes J.M., López J.J., García J.M., López D. "A Phenomenological Explanation Of The Autoignition Propagation Under HCCI Conditions". Fuel, Vol. 206, pp. 43-57, 2017.

[11] Torregrosa A.J., Broatch J. A., García A., Mónico L.. "Sensitivity Of Combustion Noise And NOx And Soot Emissions To Pilot Injection In PCCI Diesel Engines". Applied Energy, Vol. 104, pp. 149-157, 2013.

[12] Benajes J., García A., Monsalve-Serrano J., Villalta D. "Benefits Of E85 Versus Gasoline As Low Reactivity Fuel For An Automotive Diesel Engine Operating In Reactivity Controlled Compression Ignition Combustion Mode". Energy Conversion and Management, Vol. 159, pp. 85–95, 2018.

[13] Benajes J., García A., Monsalve-Serrano J., Villalta D. "Exploring The Limits Of The Reactivity Controlled Compression Ignition Combustion Concept In A Light-Duty Diesel Engine And The Influence Of The Direct-Injected Fuel Properties". Energy Conversion and Management, Vol. 157, pp. 277–287, 2018.

[14] Inagaki K, Fuyuto T, Nishikawa K, Nakakita K, Sakata I. "Dual-fuel PCI combustion controlled by in-cylinder stratification of ignitability". SAE technical paper, 2006-01-0028, 2006.

[15] Kokjohn S, Hanson R, Splitter D, Reitz R. "Fuel reactivity controlled compression ignition (RCCI): a pathway to controlled high-efficiency clean combustion". Int JEngine Res., 12, 209–226, 2011.

[16] Payri F., Olmeda P., Martín J., Carreño R. "A New Tool to Perform Global Energy Balances in DI Diesel Engines". SAE Int. J. Engines 7(1):43-59, 2014.

[17] Heywood J. "Internal combustion engines fundamentals". Estados Unidos: McGraw-Hill Inc.

[18] Micó C. "Development of measurement and visualization techniques for characterization of mixing and combustion processes with surrogate fuels". Doctoral Thesis. Universitat Politècnica de València, 2015.

[19] Arrègle J. "Análisis de la estructura y dinámica interna de chorros Diésel". Doctoral Thesis. Universitat Politècnica de València, 1997.

[20] López J.J. "Estudio teórico-experimental del chorro libre Diesél no evaportivo y de su interacción con el movimiento del aire". Doctoral Thesis. Universitat Politècnica de València, 2003.

[21] García J. M. "El proceso de combustión turbulenta de chorros diésel de inyección directa". Doctoral Thesis. Universitat Politècnica de València, 2004.

[22] Xu Q., Xu M., Hung D., Wu, S. "Diesel Spray Characterization at Ultra-High Injection Pressure of DENSO 250 MPa Common Rail Fuel Injection System". SAE Technical Paper 2017-01-0821, 2017.

[23] Julía J. E. "Analisis de chorros Diesel mediante fluorescencia inducida por láser". Editorial Reverté, S.A., Barcelona, 2006.

[24] Martínez S. "Desarrollo de una instalación experimental para el estudio de chorros diesel evaporativos en atmósfera inerte y reactiva". Doctoral Thesis. Universitat Politècnica de València, 2003.

[25] Browne K. R., Partridge I. M., Greeves G. "Fuel property effects on fuel/air mixing in an experimental Diesel engine". SAE Paper 860223, 1986.

[26] Higgins B.S., Mueller Ch.J., Siebers D. "Measurements of fuel effects on liquid-phase penetration in DI sprays". SAE Paper 1999-01-0519, 1999.

[27] Espey Ch., Dec J.E. "The effect of TDC temperature and density on the liquid-phase fuel penetration in a DI Diesel engine". Transactions of the SAE, Vol. 104 nº 4, pp. 1400-1414, 1995. SAE paper 952456.

[28] Siebers D. "Liquid-phase fuel penetration in Diesel sprays". SAE Paper 980809, 1998.

[29] Dec. J.E., Espey C. "Ignition and early soot formation in a DI diesel engine using multiple 2-D imaging diagnostics". SAE Paper 950456, 1995.

[30] Dec. J.E., Espey C. "Chemiluminescence imaging of autoignition in a DI diesel engine". SAE Paper 982685, 1998.

[31] Higgins B., Siebers D., Aradi A. "Diesel-spray ignition and premixed-burn behavior". SAE Paper 2000-01-0940, 2000.

[32] Kosaka H., Drewes V. H., Catalfamo L., Aradi A. A., Iida N., Kamimoto T. "Two-dimensional imaging of formaldehyde formed during the ignition proces of a diesel fuel spray". SAE paper 2000-01-0236, 2000.

[33] Flynn P. F., Durret R. P., Hunter G. L., Loye A. O., Akinyemi O. C., Dec J. E., Westbrook Ch. K. "Diesel Combustion: An Integrated View Combining Laser Diagnostics, Chemical Kinetics and Empirical Validation". SAE Paper 1999-01-0509, 1999.

[34] Briceño F. "Aportaciones al estudio de la evolución transitoria de llamas de difusion diésel". Doctoral Thesis. Universitat Politècnica de València, 2015.

[35] Dec J. E. "A conceptual model of DI diesel combustion based on laser-sheet imaging". SAE Paper 970873, 1997.

[36] Dec J. E., Canaan R. E. "PLIF imaging of NO formation ina DI diesel engine". SAE Paper 980147, 1998.

[37] García A. "Estudios de los efectos de la post inyección sobre el proceso de combustión y la formación de hollín en motores diésel". Doctoral Thesis. Universitat Politècnica de València, 2011.

[38] Pickett L. M., Siebers D. L. "Soot formation in diesel jets near the lift-off length". International Journal of Engine Research, Vol. 7 nº 2, pp. 103-130, 2006.

[39] Higgins B., Siebers D. "Measurement of the Flame Lift-Off Location on DI Diesel Sprays Using OH Chemiluminiscence". SAE Paper 2001-01-0918, 2001.

[40] Siebers D., Higgins B. "Flame Lift-Off on Direct Injection Diesel Under Quiescent Conditions". SAE Paper 2001-01-0530, 2001.

[41] Musculus M. "Effects of the In-cylinder Environment of Diffusion Flame Lift-Off in a DI Diesel Engine". SAE Paper 2003-01-0074, 2003.

[42] Yan J. Borman G. "Analysis and In-Cylinder Maesurements of Particle Radiant Emissions and Temperature in a ÇDirect Injection Diesel Engine". SAE Paper 881315, 1988.

[43] Siebers D.L., Pickett L.M. "Injection Pressure and Orificie Diameter Effects on Soot in DI Diesel Jets". THIESEL 2002: Conference on Thermo- and Fluid Dynamic Processes in Diesel Engines.

[44] Pickett L.M., Siebers D.L. "Non-Sooting, Low Flame Temperature Mixing-Controlled DI Diesel Combustion". SAE paper 2004-01-0139, 2004.

[45] Pickett L.M., Siebers D.L. "Soot in diesel fuel jets: effects of ambient temperature, ambient density and injection pressure". Combustion and Flame, Vol. 138, pp. 114-135, 2004.

[46] Tree D.R., Svensson K.I. "Soot processes in compresion ignition engines". Progree in Energy and Combustion Science, Vol. 33, pp. 272-309, 2007.

[47] Pickett L.M., Siebers D.L. "An investigation of diesel soot formation process using micro-orifcies". Proceedings of the Combustion Institute, Vol. 29, pp. 655-662, 2002.

[48] Singh S., Reitz R., Musculus M. "2-Color Thermometry Experiments and High-Speed Imaging of Multi-Mode Diesel Engine Combustion". SAE Paper 2005-01-3842, 2005.

[49] Siebers D.L., Higgins B., Pickett L.M. "Flame Lift-Off on Direct-Injection Diesel Fuel Jets: Oxygen Concentration Effects". SAE paper 2002-02-0890, 2002.

[50] Smith O. I. "Fundamentals of Soot Formation in Flames with Application to Diesel Engine Particulate Emissions". Prog. Energy Combust. Sci., Vol. 7, pp. 275-291, 1981.

[51] Nagle J. and Strickland-Constable R. F. "Oxidation of Carbon between 1000-2000 °C". Fifth Carbon Conference, Pergamon, Oxford, Vol. 1, pp. 154-164, 1962.

[52] Haynes B. S., Wagner H.G. “Soot formation”. Prog. Energy Combust. Sci., Vol. 7, pp. 229-273, 1981.

[53] Park C., Appleton J.P. “Shock-Tube Measurements of Soot Oxidation Rates”. Combustion and Flame, Vol. 20, pp. 369-379, 1973.

[54] Glasman I. “Soot formation in combustion processes”. Proceedings of the 22nd international symposium on combustion. The combustion Institute, 1988. p. 295-311.

[55] Gallo Y., Li Z., Richter M., Andersson O. “Parameters influencing soot oxidation rates in an optical diesel engine”. SAE Int. J. Engines 9 (4), 2016.

[56] Dembinski H., Angstrom H. “Swirl and Injection Impact on After-Oxidation in Diesel Combustion, Examined with Simultaneous Combustion Image Velocimetry and Two Colour Optical Method”. SAE Technical Paper 2013-01- 0913, 2013.

[57] Arrègle J., Pastor J.V., López J.J., García A. “Insights on postinjection-associated soot emissions in direct injection diesel engines”. Combustion and Flame 154, 448–461, 2008.

[58] Torregrosa A.J., Olmeda P., Martín J., Degraeuwe B. “Experiments on the influence of inlet charge and coolant temperature on performance and emissions of a DI Diesel engine”. Experimental Thermal Fluid Science, Vol. 30, pp. 633-641, 2006.

[59] Broatch A., Luján J.M., Ruiz S., Olmeda P. “Measurement of hydrocarbon and carbon monoxide emissions during the starting of automotive DI Diesel engines”. International Journal Automotive Technology, Vol. 9, pp. 129-140, 2008.

[60] Soid S., Zainal Z. “Spray and combustion characterization for internal combustion engines using optical measuring techniques. A review”. Energy, Vol. 36, pp. 724-741, 2011.

[61] Flynn P., Mizuszwa M., Uyehara O.A., Myers P.S. “Experimental Determination of Instantaneous Potential Radiant Heat Transfer

within an Operating Diesel Engine". SAE paper 720022, SAE Trans., vol. 81, 1972.

[62] LeFeuvre T., Myers, P.S., Uyehara, O.A. "Experimental Instantaneous Heat Fluxes in Diesel Engine and Their Correlation". SAE paper 690464, SAE Trans., vol. 78, 1969.

[63] Skeen S., Manin J. and Pickett L. "Quantitative Spatially Resolved Measurements of Total Radiation in High-Pressure Spray Flames". SAE Technical Paper 2014-01-1252, 2014.

[64] Flynn, P., Mizusawa, M., Uyehara, O., and Myers, P. "An Experimental Determination of the Instantaneous Potential Radiant Heat Transfer within an Operating Diesel Engine". SAE Technical Paper 720022, 1972.

[65] Bosch, W. "Fuel rate indicator is a new measuring instrument for display of the characteristics of individual injection". SAE Paper 660749, 1966.

[66] Plazas, A.H. "Modelado unidimensional de inyectores common-rail Diesel". Doctoral Thesis, Universitat Politècnica de València, 2005.

[67] Payri, R., Salvador, F.J., Gimeno, J., De la Morena, J. "Effects of nozzle geometry on direct injection diesel engine combustion process". Applied Thermal Engineering, Vol. 29, Issue 10, pp. 2051-2060, 2009.

[68] Payri, R., García, A., Domenech, V., Durrett, R., Plazas,A H. "An experimental study of gasoline effects on injection rate, momentum flux and spray characteristics using a common rail diesel injection system". Fuel, Vol. 97, pp. 390-399, 2012.

[69] Gimeno, J. "Estudio de la inyección Diesel mediante la medida de flujo de cantidad de movimiento". Barcelons: Editorial Reverté S.A, 2011.

[70] DRIVVEN Stand Alone Direct Injector Driver System User's Manual October 2010. Drivven, INC. 12001 Network Blvd, 110. San Antonio, Texas 78249.

[71] Pastor, J., García, J., Pastor, J., and Buitrago, J. "Analysis Methodology of Diesel Combustion by Using Flame Luminosity, Two-Colour Method and Laser-Induced Incandescence". SAE Technical Paper 2005-24-012, 2005.

[72] García J. M. "Aportaciones al estudio del proceso de combustión turbulenta de chorros en motores Diesel de inyección directa". Doctoral Thesis, Universitat Politècnica de València, 2004.

[73] Nerva J. G "An assessment of fuel physical and chemical properties in the combustion of a Diesel spray". Doctoral Thesis, Universitat Politècnica de València, 2013.

[74] Pastor J. V., Payri R., García J. M., Briceño F. J., "Analysis of transient liquid and vapor phase penetration for diesel sprays under variable injection conditions". Atomization and Sprays, Vol. 21, pp. 503-520, 2011.

[75] Monin, C., "Caracterización del proceso de formación de hollín en una llama de difusión Diesel de baja temperatura". Doctoral Thesis, Universitat Politècnica de València, 2009.

[76] de la Garza O. "Estudio de los efectos de la cavitación en toberas de inyección Diesel sobre el proceso de inyección y el de formación de hollín". Doctoral Thesis, Universitat Politècnica de València, 2012.

[77] Kastner L. "An investigation of the airbox method of measuring the air consumption of internal combustion engines". Proceedings of the institution of mechanical engineers, Vol. 157, pp. 387-404, 1947.

[78] Measurement of intake air or exhaust gas flow of Diesel engines. SAE Standards J244, 1992.

[79] Techical information of Sensyflow product. Obtain in http://www.abb.com.

[80] Technical information of AVL 733 fuel balance. Obtenido de http://www.avl.com

[81] Horiba MEXA 7100 DEGR exhaust gas analyzer. Technical information in http://www.ats.horiba.com.

[82] Martyr A.J. y Plint M.A. Engine testing: Theory and practice, 3 Ed. Elsevier Science and Technology Books, Butterworth-Heinemann, 2007.

[83] Instrumentation and techniques for exhaust gas emissions measurement. SAE Standards J254, 1993.

[84] Silvis W. M. "An algorithm for calculating the air/fuel ratio from exhaust emissions". SAE Paper 970514, 1997.

[85] "Regulation (EC) No 595/2009 of the European Parliament and of the Council of 18 June 2009 on type-approval of motor vehicles and engines with respect to emissions from heavy duty vehicles (Euro VI) and on access to vehicle repair and maintenance information and amending Regulation (EC) No 715/2007 and Directive 2007/46/EC and repealing Directives 80/1269/EEC, 2005/55/EC and 2005/78/EC". *Official Journal of the European Union,* Vol. 52 no L275, pp. 1-14, 2009.

[86] Technical information of AVL 415 Smoke meter. Obtained in http//www.avl.com

[87] Christian R., Knopf F., Jasmek A. y Schindler W. "A new method for the filter smoke number measurement with improved sensitivity". MTZ Motortechnische Zeitschift, Vol. 54, pp. 16{22, 1993.

[88] AVL 442 blow-by meter. Información técnica disponible en http://www.avl.com.

[89] Lapuerta M. "Un modelo de combustión fenomenológico para un motor Diesel de inyección directa rápido". Doctoral Thesis, Universitat Politècnica de València, 1988.

[90] Armas O. "Diagnóstico experimental del proceso de combustión en motores Diesel de inyección directa". Doctoral Thesis, Universitat Politècnica de València, 1998.

[91] Lapuerta M., Armas O., Hernández J.J. "Diagnosis of DI Diesel combustion from in-cylinder pressure signal by estimation of mean

thermodynamic properties of the gas". Applied Thermal Engineering, Vol. 19 nº 5, pp. 513-529, 1999.

[92] Lapuerta M., Ballesteros R., Agudelo J.R. "Effect of the gas state equation on the thermodynamic diagnostic of diesel combustion". Applied Thermal Engineering, Vol. 26 nº 14-15, pp. 1492-1499, 2006.

[93] Woschni G. "A Universally applicable equation for the instantaneous heat transfer coefficient in the internal combustion engines". SAE Paper 670931, 1967.

[94] Payri F., Margot X., Gil A., Martin J. "Computational study of heat transfer to the walls of a DI diesel engine". SAE Paper 2005-01-0210, 2005.

[95] Degraeuwe B. "Contribution to the thermal management of DI Diesel engines". Doctoral Thesis, Universitat Politècnica de València, 2007.

[96] Torregrosa A.J., Olmeda P., Degraeuwe B., Reyes M.A. "Concise wall temperature model for DI Diesel engines". Applied Thermal Engineering, Vol. 26 nº 11-12, pp. 1320-1327, 2006.

[97] Martín J. "Aportación al diagnóstico de la combustión en motores Diesel de inyección directa". Doctoral Thesis. Universitat Politècnica de València, 2007.

[98] Pastor J. V., Lopez J. J., Garcia J. M. y Pastor J. M. "A 1D model for the description of mixing-controlled inert diesel sprays". Fuel, Vol. 87 no 13-14, pp. 2871-2885, 2008.

[99] Desantes J.M., Pastor J.V., García-Oliver J.M., Pastor J.M. "A 1D model for the description of mixing-controlled reacting diesel sprays". Combustion and Flame, Vol. 156, pp. 234-249, 2009.

[100] García J.M. "Aportaciones del estudio del proceso de combustión turbulenta en chooros en motores diésel de inyeccion directa". Doctoral Thesis. Universitat Politècnica de València, 2004.

[101] Kee R., Rupley F., Miller J., Coltrin M., Grcar J., Meeks E., Moffat H., Lutz A., Dixon- Lewis G., Smooke M., Warnatz J., Evans G.,

Larson R., Mitchell R., Petzold L., Reynolds W., Caracotsios M., Stewart W., Glarborg P., Wang C., Adigun O., HoufW., Chou C., Miller S., Ho P., Young D. CHEMKIN Release 4.0 & Pro, Rection Design, Inc., San Diego, CA, 2004.

[102] Curran H.J., Gaffuri P., Pitz W., Westbrook C.K. "A comprehensive modeling study of nheptane oxidation". Combustion and Flame, 114, pp. 149–177, 1998.

[103] Curran H.J., Gaffuri P., Pitz W.J.,Westbrook C.K. "A Comprehensive Modeling Study of iso-Octane Oxidation". Combustion and Flame 129: 253-280, 2002.

[104] Jerzembeck S., Peters N., Pepiot-Desjardins P., Pitsch. H. "Laminar burning velocities at high pressure for primary reference fuels and gasoline: Experimental and numerical investigation". Combustion and Flame, Vol. 156, Issue 2, pp.292-301, 2009.

[105] Matsui Y., Kamimoto T., Matsuoka S. "A study on the time and space resolved measurements of flame temperature in a D.I. Diesel engine by the two-color method". SAE Paper 790491, 1979.

[106] Hotel H.C., Broughton F.P. "Determination of true temperature and total radiation from luminous gas flames". Ind. And Eng. Chem., Vol. 4, nº 2, pp. 166-175, 1932.

[107] Zhao H., Ladommatos N. "Optical diagnostics for soot and temperature measurement in Diesel engines". Prog. Energy Combustion Science, Vol. 24, pp. 221-255, 1998.

[108] Tan J., Borman G.L. "Analysis and in-cylinder measurement of particulate radiant emissions and temperature in a Direct Injection Diesel engine". SAE Paper 881315, 1988.

[109] Hampson G.J., Reitz R.D. "Two-color imaging of in-cylinder soot concentration and temperature in a heavy-duty DI Diesel engine with comparison to multidimensional modeling for single and split injections". SAE paper 980524, 1998.

[110] Vattulainen J., Nummela V., Hernberg R., Kytölä J. "A system for quantitative imaging diagnostics and its application to pyrometric in-cylinder flame-temperature measurements in large Diesel engines". Meas. Sci. Technol., Vol. 11, pp. 103-109, 2000.

[111] di Stasio D., Massoli P. "Influence of the soot property uncertainties in temperature and volume-fraction measurements by two-colour pyrometry". Meas. Sci. Technol., Vol. 5, pp. 1453-1465, 1994.

[112] Dimopoulos, P., Bacha, C., Soltica, P., Boulouchos, K. "Hydrogen-natural gas blends fuelling passenger car engines: Combustion, emissions and well-to-wheels assessment". Int. J. Hydrogen Energ. 33(23), 7224-7236, 2008.

[113] Osada, H., Uchida, N., Shimada, K., and Aoyagi, Y. "Reexamination of Multiple Fuel Injections for Improving the Thermal Efficiency of a Heavy-Duty Diesel Engine". SAE Technical Paper 2013-01-0909, 2013.

[114] Morawitz, U., Mehring, J., and Schramm, L. "Benefits of Thermal Spray Coatings in Internal Combustion Engines, with Specific View on Friction Reduction and Thermal Management". SAE Technical Paper 2013-01-0292, 2013.

[115] Serrano, J., Olmeda, P., Tiseira, A., García-Cuevas, L. "Importance of Mechanical Losses Modeling in the Performance Prediction of Radial Turbochargers under Pulsating Flow Conditions". SAE Int. J. Engines 6(2):729-738, 2013.

[116] Neshat E., Kloshbakhti R. "Effect of different heat transfer models on HCCI engine simulation". Energy conversion and management 88, 1-14, 2014.

[117] Taymaz, I. "An experimental study of energy balance in low heat rejection diesel engine". Energy 31 (2-3) 364-371 2006.

[118] Benajes J., Pastor J.V., García A., Monsalve-Serrano J. "An experimental investigation on the Influence of piston bowl geometry on

RCCI performance and emissions in a heavy-duty engine". Energy Conversion and Management 103, 1019-1030, 2015.

[119] Benajes J., Molina S., García A., Monsalve-Serrano J. "Effects of Direct injection timing and Blending Ratio on RCCI combustion with different Low Reactivity Fuels". Energy Conversion and Management, Volume 99, 193-209, 2015.

[120] Struwe, F.J. "In-cylinder Measurement of Particulate Radiant Heat Transfer in a Direct Injection Diesel Engine". SAE Technical Paper 2003-01-0072, 2003

[121] Furmanski P., Banaszek J. and Wisniewski T. S. "Radiation Heat Transfer in a Combustion Chamber of Diesel Engine with Partially Transparent Burnt Gas Zone". SAE Technical Paper 980504, 1998.

[122] Vogelin P. "Experimental investigation of multi-in-cylinder pyrometer measurements and exhaust soot emissions under steady and transient operation of a heavy-duty Diesel engine". SAE Technical Paper 131ICE-0145, 2013.

[123] Payri R., Salvador F.J., Gimeno J. and Bracho G. "A new methodology for correcting the signal cumulative phenomenon on injection rate measurements". Experimental Techniques, Vol. 32 no 1, pp. 46-49, 2008.

[124] Bermúdez V., García J.M., Juliá E. and Martínez S. "Engine with optically accessible cylinder head: A research tool for injection and combustion processes". SAE Technical Papers, 2003.

[125] Payri F., Pastor J.V., Nerva J.-G., García-Oliver J.M. "Lift-Off Length and KL Extinction Measurements of Biodiesel and Fischer-Tropsch Fuels under Quasi-Steady Diesel Engine Conditions". SAE International Journal of Engines, Vol. 4 no 2, pp. 2278- 2297, 2011.

[126] Tree D.R, Svensson K.I. "Soot processes in compression ignition engines". Prog. Energy Combustion Science 2007; 33:272–309.

[127] Pickett L.M, Siebers D.L. “Soot in diesel fuel jets: effects of ambient temperature, ambient density, and injection pressure”. Combustion and Flame 2004; 138:114–35.

[128] Way RJB. “Methods for determination of composition and thermodynamic properties of combustion products for internal combustion engine calculations”. Proc. Inst. Mech. Eng. 1976;190:687–97.

[129] Musculus PBM. “Measurements of the influence of soot radiation on in-cylinder temperatures and exhaust NOx in a heavy-duty DI diesel engine”. SAE technical paper 2005-01-0925; 2005.

[130] Manin J, Pickett L.M, Skeen S. “Two-color diffused back-illumination imaging as a time-resolved soot measurements in reacting sprays”. SAE technical paper 2013-01-2548; 2013.

[131] Payri F, Olmeda P, Martín J, García A. “A complete 0D thermodynamic predictive model for direct injection diesel engines”. Applied Energy 2011;88(12):4632–41.

[132] Soloiu V, Lewis J, Yoshihara Y, Nishiwaki K. “Combustion characteristics of a charcoal slurry in a direct injection diesel engine and the impact on the injection system performance”. Energy 2011;36:4353–71.

[133] Benajes J, Molina S, García JM, Riesco J.M. “The effect of swirl on combustion and exhaust emissions in heavy-duty diesel engines”. Proc. Inst. Mech. Eng., Part D: J. Automobile Eng. 2004; 218.

[134] De la Morena J., Vassallo A. Peterson R.C., Gopalakrishan V., Gao J. “Influence of Swirl Ratio on Combustion System Performance of a 0.4l Single-Cylinder Diesel Engine”. THIESEL 2014 Conference on Thermo- and Fluid Dynamic Processes in Direct Injection Engines.

[135] Tao F, Liu Y, Rempelewert B.H, Foster DE, Reitz R.D, Choi D. et al. “Modeling the effects of EGR and injection pressure on soot formation in a high-speed directinjection (HSDI) diesel engine using a multi-step

phenomenological soot model". SAE technical paper 2005-01-0121; 2005.

[136] Benajes J., García A., Pastor J.M., Monsalve-Serrano J. "Effects of piston bowl geometry on reactivity controlled compression ignition heat transfer and combustion losses at different engine loads". Energy 98, 64–77, 2016.

[137] Benajes J., García A., Monsalve-Serrano J., Balloul I., Prade G. "An assessment of the dual-mode reactivity controlled compression ignition/conventional diesel combustion capabilities in a EURO VI medium-duty diesel engine fueled with an intermediate ethanol-gasoline blend and biodiesel". Energy Conversion and Management 123, 381–391, 2016.

[138] López J., Martín J., García A., Villalta D., Warey A. "Implementation of two color method to investigate late-cycle soot oxidation process in a CI engine under low load conditions". Applied Thermal Engineering 113, 878–890, 2017.

[139] Benajes J., Martin J., Garcia A., Villalta D., Warey A. "An investigation of radiation heat transfer in a light-duty diesel engine". SAE Int. J. Engines 8 (5), 2015.

[140] Xiaobei C., Hongling J., Zhaowen W. "A Numerical Modeling and Experimental Study on Soot Formation for a Direct Injection Diesel Engine". SAE Technical Paper 2008-01-1794, 2008.

[141] Huestis E., Erickson P., Musculus M. "In-Cylinder and Exhaust Soot in Low-Temperature Combustion Using a Wide-Range of EGR in a Heavy-Duty Diesel Engine". SAE Technical Paper 2007-01-4017, 2007.

[142] O'Connor J., Musculus M. "Post injections for soot reduction in diesel engines: a review of current understanding". SAE Int. J. Engines 6 (1), 2013.

[143] Arrègle J., López J.J., García J.M., Fenollosa C. "Development of a zero dimensional diesel combustion model. Part 1: analysis of the quasi-

steady diffusion combustion phase". Applied Thermal Engineering 23, 1301–1317, 2003.

[144] Lequien, G., Andersson Ö., Tunestal P., and Lewander M. "A Correlation Analysis of the Roles of Soot Formation and Oxidation in a Heavy-Duty Diesel Engine". SAE Technical Paper 2013-01-2535, 2013.

[145] Hentschel, W. and Richter, J. "Time-Resolved Analysis of Soot Formation and Oxidation in a Direct-Injection Diesel Engine for Different EGR-Rates by an Extinction Method". SAE Technical Paper 952517, 1995.

[146] López J., Martin J., Garcia A., Villalta D. "Characterization of In-Cylinder Soot Oxidation Using Two-Color Pyrometry in a Production Light-Duty Diesel Engine". SAE Technical Paper 2016-01-0735, 2016.

[147] Li X., Qiao Z., Su L., Liu F. "The combustion and emission characteristics of a multi-swirl combustion system in a DI diesel engine". Applied Thermal Engineering 115, 1203–1212, 2017.

[148] Molina S., Desantes J., García A., Pastor J. "A Numerical Investigation on Combustion Characteristic with the use of Post Injection in DI Diesel Engines". SAE Technical Paper 2010-01-1260, 2010.

[149] Benajes J., Martín J., García A., Villalta D., Warey A. "In-cylinder soot radiation heat transfer in direct-injection diesel engines". Energy Conversion nad Management 106, 414–427, 2015.

[150] Bobba M., Musculus M., Neel W. "Effect of post injections on in-cylinder and exhaust soot for low-temperature combustion in a heavy-duty diesel engines". SAE Int. J. Engines 3 (1), 2010.

[151] Hocine A., Desmet B., Guenoun S. "Numerical study of the influence of diesel post injection and exhaust gas expansion on the thermal cycle of an automobile engine". Applied Thermal Engineering 30,1889–1895, 2010.

[152] Rolf D. Reitz. "Directions in internal combustion engine research". Combustion and flame, Vol. 160, pp 1-8, 2013.

[153] Rao V., Honnery D. "A comparison of two NOx prediction schemes for use in diesel engine thermodynamic modelling". Fuel Vol. 107, pp. 662–70, 2013.

[154] Cheng X, Chen L, Hong G, Yan F, Dong S. "Modeling study of soot formation and oxidation in DI diesel engine using an improved soot model". Applied Thermal Enginnering, Vol. 62, pp. 303-312, 2014.

[155] Kazakov A., Foster D.E. "Modeling of soot formation during DI diesel combustion using a multi-step phenomenological model". SAE paper 982463; 1998.

[156] Tao F., Reitz R.D., Foster D.E., Liu Y. "Nine-step phenomenological diesel soot model validated over a wide range of engine conditions". Int. Jornal Thermal Sciences Vol 48, pp. 1223–1234, 2009.

[157] Jung D., Assanis D. "Multi-zone DI diesel spray combustion model for cycle simulation studies of engine performance and emissions". SAE paper 2001-01-1246; 2001.

[158] Gao Z., Schreiber W. "A phenomenologically based computer model to predict soot and NOx emission in a direct injection diesel engine". Int. Jorunal of Engine Research Vol. 2, pp. 177–88, 2001.

[159] Skeen S., Manin J., Pickett L., Cenker E. et al. "A Progress Review on Soot Experiments and Modeling in the Engine Combustion Network (ECN)". SAE Int. J. Engines 9 (2), 2016.

[160] Baert R.S.G., Frijters P.J.M., Somers B., Luijten C.C.M. and de Boer W. "Design and Operation of a High Pressure, High Temperature Cell for HD Diesel Spray Diagnostics: Guidelines and Results". SAE Technical Paper, no 2009-01-0649, 2009.

[161] Payri R., Garcia-Oliver J., Xuan T. and Bardi M. "A study on diesel spray tip penetration and radial expansion under reacting conditions". Applied Thermal Enginnering, Vol. 90, pp. 691-629, 2015.

[162] Pastor J., Garcia-Oliver J., Novella R., and Xuan T. "Soot Quantification of Single-Hole Diesel Sprays by Means of Extinction Imaging". SAE Int. J. Engines 8 (5), 2015.

[163] Pastor J., Garcia-Oliver J., Pastor J.M., Vera-Tudela W. "One-dimensional diesel spray modeling of multicomponent fuels". Atominzation and Sprays, Vol 25(2), pp. 485-517, 2015.

[164] Siebers D.L. "Scaling liquid-phase fuel penetration in diesel sprays based on mixing-limited vaporization". SAE Technical Paper, no 1999-01-0528, 1999.

[165] Monin C. "Caracterización del Proceso de Formación de Hollín en una Llama de Difusión Diésel de Baja Temperatura". Doctoral Thesis, 2009.

[166] López J., Garcia-Oliver J.M., Martin J., Chemisky J.P., Bouet A. "A Soot Radiation Model for Diesel Sprays". SAE Technical Paper, no 2012-01-1069, 2012.

[167] Matthieu O., Djebaïli-Chaumeix N., Paillard C.E., and Douce F. "Experimental study of soot formation from diesel fuel surrogate in a shock tube". Combustion and Flame, vol. 156 (8), pp. 1576-1586, 2009.

[168] Kronholm D.F. and Howard J.B. "Analysis of soot surface growth pathways using published plug-flow reactor data with new particle size distribution measurements and published premixed flame data". Proceedings of the Combustion Institute, vol. 28, pp. 2555-2561, 2000.

[169] Desantes, J.M., Arrègle, J., López, J.J. and Cronhjort, A. "Scaling laws for free turbulent gas jets and diesel-like sprays". Atomization and Sprays, vol. 16, pp. 443-473, 2006.

[170] Payri F., Pastor J.V., García J.M., Pastor J.M. "Contribution to the application of two-colour imaging to diesel combustion". Measurement Science and Technology, vol. 18, pp. 2579-2598, 2007.